

NASA Contractor Report 4636
DOT/FAA/CT-TN93/18

Experimental Water Droplet Impingement Data on Airfoils, Simulated Ice Shapes, an Engine Inlet and a Finite Wing

M. Papadakis, M. Breer, N. Craig, and X. Liu

Document Availability Change Notice

This document was published in December 1994 with a restriction. It was changed March 2005 to Unclassified/Unlimited per DAA modified March 30, 2005.

~~RESTRICTED DISTRIBUTION DOCUMENT~~

~~Distribution limited to U.S. Government agencies and U.S. Government agency contractors only.~~

CONTRACT NAG3-566
DECEMBER 1994



National Aeronautics and
Space Administration



U.S. Department
of Transportation

**Federal Aviation
Administration**

NASA Contractor Report 4636
DOT/FAA/CT-TN93/18

Experimental Water Droplet Impingement Data on Airfoils, Simulated Ice Shapes, an Engine Inlet and a Finite Wing

M. Papadakis and X. Liu
Wichita State University
Wichita, Kansas

M. Breer and N. Craig
Boeing Military Airplanes
Wichita, Kansas

Document Availability Change Notice

This document was published in December 1994 with a restriction. It was changed March 2005 to Unclassified/Unlimited per DAA modified March 30, 2005.

Prepared for
Lewis Research Center
under Contract NAG3-566

~~RESTRICTED DISTRIBUTION DOCUMENT~~

~~Distribution limited to U.S. Government agencies and U.S. Government agency contractors only.~~



National Aeronautics and
Space Administration



U.S. Department
of Transportation
**Federal Aviation
Administration**

DOCUMENT AVAILABILITY CHANGE NOTICE

NASA Contractor Report 4636

**Experimental Water Droplet Impingement Data on Airfoils,
Simulated Ice Shapes, an Engine Inlet and a Finite Wing**

M. Papadakis, M. Breer, N. Craig, and X. Liu

December 1994

This document was published in December 1994
with a restriction.

It was changed March 2005 to Unclassified/Unlimited per DAA modified March 30, 2005.

Per the STI Program Office and Code I at HQ,
you may modify copies in your possession. The restriction notice
on the cover, title page and RDP should be boldly crossed out
and the above statement printed clearly above or below it.

Glenn Research Center
Publishing Services Coordination Office
216-433-3207

Experimental Water Droplet Impingement Data on Airfoils, Simulated Ice Shapes, an Engine Inlet and a Finite Wing

M. Papadakis, M. Breer, N. Craig and X. Liu

ABSTRACT

An experimental method has been developed to determine the water droplet impingement characteristics on two- and three-dimensional aircraft surfaces. The experimental water droplet impingement data are used to validate particle trajectory analysis codes that are used in aircraft icing analyses and engine inlet particle separator analyses. The aircraft surface is covered with thin strips of blotter paper in areas of interest. The surface is then exposed to an airstream that contains a dyed-water spray cloud. The water droplet impingement data are extracted from the dyed blotter paper strips by measuring the optical reflectance of each strip with an automated reflectometer. Experimental impingement efficiency data are presented for a NLF(1)-0414 airfoil, a swept MS(1)-0317 airfoil, a Boeing 737-300 engine inlet model, two simulated ice shapes and a swept NACA 0012 wingtip. Analytical impingement efficiency data are also presented for the NLF(1)-0414 airfoil and the Boeing 737-300 engine inlet model.

ACKNOWLEDGEMENTS

This research was funded by the NASA Lewis Research Center and the Federal Aviation Administration (FAA) Technical Center.

Thanks to Mr. C. Bidwell of NASA Lewis Research Center for assisting with the wind tunnel tests and for reviewing this manuscript, and to the NASA Lewis Icing Research Tunnel personnel for their assistance with the wind tunnel tests.

Thanks also to Dr. G.W. Zumwalt of Wichita State University, Dr. J. T. Riley of the FAA and Dr. R.J. Shaw and J.J. Reinmann of NASA Lewis for their encouragement and support.

TABLE OF CONTENTS

| | |
|--|-----------|
| 1. INTRODUCTION | 1 |
| 2. TRAJECTORY EQUATION AND IMPINGEMENT PARAMETERS | 3 |
| 2.1 Equations of Particle Motion | 3 |
| 2.2 Impingement Parameters | 4 |
| 2.2.1 Liquid Water Content (LWC) | 4 |
| 2.2.2 Cloud Droplet Distribution | 4 |
| 2.2.3 Mean Volumetric Diameter (MVD) | 5 |
| 2.2.4 Local Impingement Efficiency ($\bar{\beta}$) | 5 |
| 2.2.5 Total Impingement Efficiency (\bar{E}) | 6 |
| 2.2.6 Impingement Limits $(s_m/L)_{max}$ | 6 |
| 2.2.7 Local Impingement Rate | 7 |
| 3. EXPERIMENTAL METHOD | 12 |
| 3.1 Test Approach | 12 |
| 3.2 Test Facility | 13 |
| 3.3 Spray System | 13 |
| 3.4 Uniformity Test | 14 |
| 3.5 Reference Collector Mechanism | 15 |
| 3.6 Mass Flow Measurements | 15 |
| 3.7 Droplet Impingement Data Acquisition | 16 |
| 4. TEST MODELS AND CONDITIONS | 26 |
| 4.1 Two-Dimensional Flow Models | 26 |
| 4.1.1 <i>NLF(1)</i> – 0414 Airfoil Section | 26 |
| 4.1.2 Simulated Ice Shapes | 26 |
| 4.2 Three-Dimensional Flow Models | 26 |
| 4.2.1 <i>MS(1)</i> – 0317 Swept Airfoil | 27 |
| 4.2.2 Swept Wing Tip | 27 |
| 4.2.3 Boeing 737-300 Engine Inlet Model | 27 |
| 4.3 Reference Collector Mechanism | 28 |
| 5. DATA REDUCTION METHOD | 45 |
| 5.1 Reflectance Calibration Curve | 45 |
| 5.2 Automated Data Reduction System | 45 |
| 5.3 Data Reduction Process | 46 |
| 5.4 Laser Reflectance Method Error Analysis | 47 |

| | |
|--|-----|
| 6. ANALYSIS METHODS | 51 |
| 6.1 Two-Dimensional Analysis Code | 51 |
| 6.2 Three-Dimensional Analysis Code | 51 |
| 7. RESULTS AND DISCUSSION | 53 |
| 7.1 Test Repeatability Results | 56 |
| 7.2 Two-Dimensional Impingement Data | 56 |
| 7.2.1 <i>NLF</i> (1) – 0414 Airfoil Section | 57 |
| 7.2.2 Small and Large Glaze Ice Shapes | 57 |
| 7.3 Three-Dimensional Impingement Data | 58 |
| 7.3.1 Swept <i>MS</i> (1) – 317 Airfoil | 58 |
| 7.3.2 NACA 0012 Swept Wing Tip | 59 |
| 7.3.3 Boeing 737-300 Engine Inlet | 60 |
| 8. CONCLUSIONS | 137 |
| APPENDIX A - DATA REDUCTION FOR CURVED STRIPS | 138 |
| APPENDIX B - IMPINGEMENT TEST LOG SHEETS | 142 |
| B.1 - Test Variables Recorded | 142 |
| B.1.1 - Run No and Run ID | 142 |
| B.1.2 - Tunnel Conditions | 143 |
| B.1.3 - Spray System Conditions | 143 |
| B.1.4 - Mass Flow Conditions | 143 |
| B.1.5 - Time Recordings | 144 |
| APPENDIX C - NOMENCLATURE | 167 |
| REFERENCES | 169 |

EXECUTIVE SUMMARY

The water droplet impingement characteristics of an aircraft are typically used to determine size and location of ice protection systems. The impingement characteristics have been historically determined experimentally. With the advent of powerful computers, a number of computer codes have been developed capable of predicting the impingement characteristics of aircraft surfaces and performing icing analyses. To insure that these codes are correct, they must be validated against experimental data that must span the range of geometries and flight conditions to which the computer codes will be applied. Until recently, the experimental data base was limited to two-dimensional cylinders, airfoils, several bodies of revolution and a supersonic inlet. These data were generated by the National Advisory Committee for Aeronautics (NACA) in the 1950's using a dye tracer technique and colorimetric analysis.

To provide a more extensive water droplet impingement database, NASA and the FAA began a research program in August 1984 with Wichita State University and Boeing Military Airplanes. The main objectives and accomplishments of this work were presented in NASA CR 4257 published in November 1989. Briefly, experimental and data reduction methods were developed and verified for measuring local droplet impingement efficiency on a variety of aerodynamic surfaces. The data reduction method was based on laser reflectance which is more accurate and considerably more efficient than colorimetric analysis. An automated data reduction system was also developed to make practical the reduction of a large mass of data. Water droplet impingement data were obtained for a 4-inch diameter cylinder, a NACA 65₂015 airfoil, a supercritical airfoil, an axisymmetric inlet and a Boeing 737-300 engine inlet. Experimental data were correlated with analytical results.

The work presented in this report is the conclusion of the research program which was initiated in 1984. The following tasks were accomplished:

1. The design of the collector mechanism for measuring LWC was improved.
2. Water droplet impingement data were obtained for a Natural Laminar Flow airfoil, a swept MS-0317 airfoil, a swept wingtip, a Boeing 737-300 engine inlet and two simulated ice shapes.
3. Experimental data and computational impingement results were correlated for selected geometries and test conditions.

1.0 INTRODUCTION

Aircraft flying at subsonic speeds below about 8000 meters are subject to ice accretion caused by very small supercooled water droplets that freeze upon impact with the aircraft. Ice accretion, which occurs on the forward facing surfaces of an aircraft, can be detrimental when occurring on the leading edge of a wing and/or on engine inlet diffusers. On wing surfaces, ice accretion can lead to an increase in drag, resulting in excessive fuel consumption or flow separation, which results in a decrease in lift. Engine inlet diffusers are more susceptible to the effects of ice accretion, particularly when shedding ice fragments enter the engine inlet and cause mechanical damage to the turbomachinery of the engine. Thus, it is necessary that ice protection systems, for the removal or prevention of ice accretion, are incorporated in aircraft.

Current ice protection systems can be divided into two different categories: de-icing systems and anti-icing systems. De-icing systems periodically shed ice that has already formed by mechanical, thermal or chemical means. Deicing systems have low energy requirements but have higher aerodynamic penalties. Anti-icing systems prevent ice formation by means of thermal energy or a Freezing Point Depressant (FPD). While aerodynamic penalties are held to a minimum with an anti-icing system, the energy requirements are higher than those of a de-icing system.

Of major concern in the design of an anti-icing or de-icing system is the extent and amount of water impingement. The impingement characteristics of an aircraft can be used to determine size and location of ice protection systems. The impingement characteristics have been historically determined experimentally but recent advances in computer speed have allowed the use of trajectory codes to determine them analytically.

With the advent of powerful computers, a number of computer codes have been developed (Ref. 1-5) capable of predicting the impingement characteristics of aircraft surfaces and performing icing analyses. These codes can provide a cost effective means for the design of ice protection systems. To insure that these codes are correct, they must be validated against experiment. The experimental data must span the range of geometries and flight conditions to which the computer codes will be applied. Until recently, the data base was limited to two-dimensional cylinders, airfoils, several bodies of revolution and a supersonic inlet. These geometries were tested by NACA in the 1950's using a dye-tracer technique (Ref. 6-9).

NASA and the FAA began a research program in August of 1984 with Wichita State University and Boeing Military Airplanes to provide a more extensive water droplet impingement data base. The objectives of this program are listed below:

- a . Develop an efficient and accurate method for measuring local droplet impingement efficiency on a variety of aerodynamic surfaces in two and three dimensional flows.
- b . Develop experiments to verify the method.

- c . Test several state-of-the-art airfoil sections as well as wing and engine inlet geometries to produce a comprehensive experimental water droplet impingement data base.
- d . Develop an automated data reduction system that would be practical and efficient for the acquisition and reduction of large quantities of data.

Several two and three dimensional models were tested during the initial phases of this research program (Ref. 10). The current tests represent the completion of data acquisition for the water droplet impingement data base. This report presents the testing of several modern geometries: a Natural Laminar Flow airfoil, a swept MS-0317 airfoil, a swept wingtip, a Boeing 737-300 engine inlet and two simulated ice shapes.

2.0 TRAJECTORY EQUATION AND IMPINGEMENT PARAMETERS

The non-dimensional droplet trajectory equation and impingement parameters which are commonly used in the presentation of theoretical and experimental impingement data are presented in this section. A more detailed discussion of impingement parameters can be found in Ref. 10.

2.1 Equations of Particle Motion

The forces on a small spherical droplet moving in the steady flow of air are droplet drag, weight and buoyancy. The predominant force acting on a droplet is the fluid dynamic drag arising from the relative (slip) velocity of air with respect to the droplet (Ref. 10). The particle equation of motion in non-dimensional form is:

$$\frac{dU_i}{dt} = \frac{C_D(R_v)R_v(V_i - U_i)}{24K} - \frac{(1 - \sigma)g L \delta_{i2}}{V_\infty^2} \quad (2 - 1)$$

where

- C_D = drag coefficient of spherical particle
 - $K = \rho_{particle}U_\infty d^2 / (18\mu L)$, inertia parameter of droplet
 - t = time, dimensionless with L/V_∞
 - $\sigma = \rho/\rho_p$, density ratio of air to particle
 - L = characteristic dimension of body
 - $R_v = \rho_{air}|\bar{V} - \bar{U}|d/\mu$, relative Reynolds number of droplet
 - U_i = i th component of particle velocity, non-dimensionalized by V_∞
 - V_i = i th component of air velocity, non-dimensionalized by V_∞
 - δ_{ij} = Kronecker δ
 - d = particle diameter
 - μ = absolute air viscosity
 - ρ = air density
 - ρ_p = particle density
 - V_∞ = freestream air velocity
- $i = 1$ x - direction, $i = 2$ y - direction, $i = 3$ z - direction

The derivation of equation (2 - 1) is based on the following assumptions:

- Single phase (air) flow about the body (i.e., air flow is not disturbed by the presence of the droplets)

- Quasi-steady-state approximation (i.e., at each instant and position the steady-state drag and other forces act on the particle)
- Compressible or incompressible potential flow field of the gas phase about the body
- Particles of spherical shape
- Viscous flow effects such as thick boundary layer formation and flow separation are not considered

The above mathematical model is a valid approximation for typical icing conditions within the intermittent and continuous maximum icing envelopes of the FAA (Ref. 11). The maximum concentration and mean volumetric diameter (MVD) for these conditions are:

| Intermittent Maximum | | Continuous Maximum | |
|----------------------|----------------------|--------------------|----------------------|
| LWC Max | 3.0 g/m ³ | LWC Max | 0.8 g/m ³ |
| MVD Max | 50 μm | MVD Max | 40 μm |

For the concentrations and sizes of droplets expected to occur within icing clouds, the assumptions of undisturbed airflow and spherical shape (due to surface tension) of droplets are very closely approximated.

Given an expression for $C_D(R_v)$, the drag coefficient of the droplet as a function of the relative Reynolds number of the droplet, equation (2 – 1) can be integrated numerically to find the particle trajectory path. An example of C_D as a function of R_v can be found in Ref. 10.

2.2 Impingement Parameters

Impingement parameters for non-uniform droplet distributions are discussed below.

2.2.1 Liquid Water Content (LWC)

The liquid water content (LWC) of a cloud is the amount of water contained in a given volume of cloud. LWC is usually expressed in grams of water per cubic meter of cloud. Typical LWC_{max} values for icing clouds are listed in section 2.1.

For simulated icing clouds, the LWC is controlled by the water and /or air pressures of the spray system used to create the spray clouds.

2.2.2 Cloud Droplet Distribution

The distribution of droplets in a cloud can be expressed in many various forms (Ref. 10), but for convenience and computational efficiency, a discrete form of cumulative liquid water content versus droplet diameter normalized to mean volumetric diameter is used. The droplet distributions used in this work were obtained experimentally as explained in Ref. 10 and are given in Table 2.1 and 2.2.

A distribution which has been employed in various analytical studies is the Langmuir “D”. This distribution and other similar distributions were established by Langmuir by

matching the data from natural-icing cloud measurements made on Mt. Washington (Ref. 12). Comparisons of Langmuir "D" distribution and droplet distributions produced by the spray system used in the current tests are shown in Fig. 2.1.

2.2.3 Mean Volumetric Diameter (MVD)

By definition, the Mean Volumetric Diameter (MVD) of a droplet distribution is that mean diameter for which half the total liquid water content is contained in droplets larger than the mean and half in droplets smaller than the mean. Given a droplet distribution the MVD can be calculated as follows.

For a continuous distribution if $n(D)$ is the number of particles per unit sampling volume having diameters between D and $D+dD$ (volumes between V and $V+dV$) then D_{MVD} can be calculated from

$$\frac{\frac{\pi}{2} \rho_w \int_{D_{min}}^{D_{MVD}} n(x) x^2 dx}{\frac{\pi}{2} \rho_w \int_{D_{min}}^{D_{max}} n(x) x^2 dx} = 0.5 \quad (2-2)$$

For a discrete distribution if the particle number density is given in N discrete groups such that $n_i(D_i)$ is the number of the particles in group i having diameters between D and $D+dD$ then, equation (2-2) can be written as

$$\frac{\frac{\pi}{6} \rho_w \sum_{i=1}^K n_i(D_i) D_i^3}{\frac{\pi}{6} \rho_w \sum_{i=1}^N n_i(D_i) D_i^3} = 0.5 \quad (2-3)$$

where:

$$D_K = D_{MVD}$$

$$\rho_w = \text{density of water, g/cm}^3$$

2.2.4 Local Impingement Efficiency ($\bar{\beta}$)

Considering a body in a cloud with uniform droplet size distribution the local impingement efficiency β for any point on the body surface is defined as the local droplet flux rate at the body surface normalized to the free stream flux rate. Referring to figure 2.2 β is the ratio of that infinitesimal area dA_∞ to the corresponding impingement area on the body surface dA_s . This definition follows from the continuity of droplet mass flow.

For a continuous non-uniform cloud distribution, the impingement efficiency is given by equation (2-4).

$$\bar{\beta} = \frac{1}{w_t} \int_0^{w_t} \beta dw \quad (2-4)$$

where β is a function of drop size and therefore can be expressed as a function of w , the liquid content for a given drop size.

For a discrete cloud distribution such as the one shown in Fig. 2.1, β is defined as the weighted average of the local impingement efficiency values due to each droplet group in the cloud. Let w_t be the liquid water content of the cloud, Δw_i be the partial liquid water content contained in the droplets of size (d_i), in the group (i) of the distribution, and N be the total number of discrete size droplet groups available. For a body exposed to a cloud with such a droplet distribution, the local impingement efficiency due to a single droplet group of size d_i is β_i , where β is defined in Fig. 2.2. The local impingement efficiency due to all N groups in the distribution over an infinitesimal area of the body is given by equation (2 - 5) below.

$$\bar{\beta} = \frac{1}{w_t} \sum_{i=1}^N \beta_i \Delta w_i \quad (2 - 5)$$

2.2.5 Total Impingement Efficiency (\bar{E})

The total impingement efficiency of a three dimensional body exposed to a cloud of droplet distribution is

$$\bar{E} = \frac{1}{A_f} \int \beta dA_s \quad (2 - 6)$$

where:

A_f is the projected frontal area of the body

dA_s is an infinitesimal impingement area on the surface of the body

In order to integrate equation (2-6), $\bar{\beta}$ must be known as a function of surface location. Such a function can be defined from experimental or analytical results.

2.2.6 Impingement Limits (s_m/L)_{max}

Droplets which start out at a freestream position (y_∞) with respect to a reference line that pass through the highlight (most forward point at $\alpha = 0^\circ$) of a body downstream will impinge at some position on that body. As these initial freestream droplet positions increase in distance from the reference line they will impinge farther back along the surface of the body until a maximum distance ($y_{\infty,max}$) is obtained. This limiting trajectory is defined as the tangent trajectory to the body at point P (Fig. 2.2). Any droplet starting at a freestream position farther from the reference line than ($y_{\infty,max}$) will miss the body entirely. The distance s_m measured along the body surface from the highlight of the body to the point P is called the limit of impingement. This distance is usually expressed in dimensionless form by dividing s_m by the characteristic length (L) of the body.

For two-dimensional flow, there are two impingement limits, an upper and a lower (for external flow, e.g., airfoil section) or an outer and inner (for partly internal flow, e.g., engine inlet). For three-dimensional flow, the limits of impingement may vary spanwise along the surface of a finite wing or circumferentially along the surface of an engine inlet.

For a droplet distribution that varies from d_{min} to d_{max} , the impingement limits can be established for each droplet size. The maximum impingement limits are defined by the impingement limits of the largest droplet diameter of the distribution.

2.2.7 Local Impingement Rate

To calculate the amount of water collected on a small area of the body where the local impingement efficiency value is known, the following equation can be used.

$$\bar{W}_\beta = 0.3296V_\infty w_t \bar{\beta} \quad (2 - 7)$$

where:

\bar{W}_β = Local impingement rate, $lb/hrft^2$

V_∞ = freestream velocity, mph

w_t = Total liquid water content, g/m^3

$\bar{\beta}$ = Local impingement efficiency

TABLE 2.1
DISCRETE CUMULATIVE DISTRIBUTION
FOR 0.80 PRESSURE RATIO

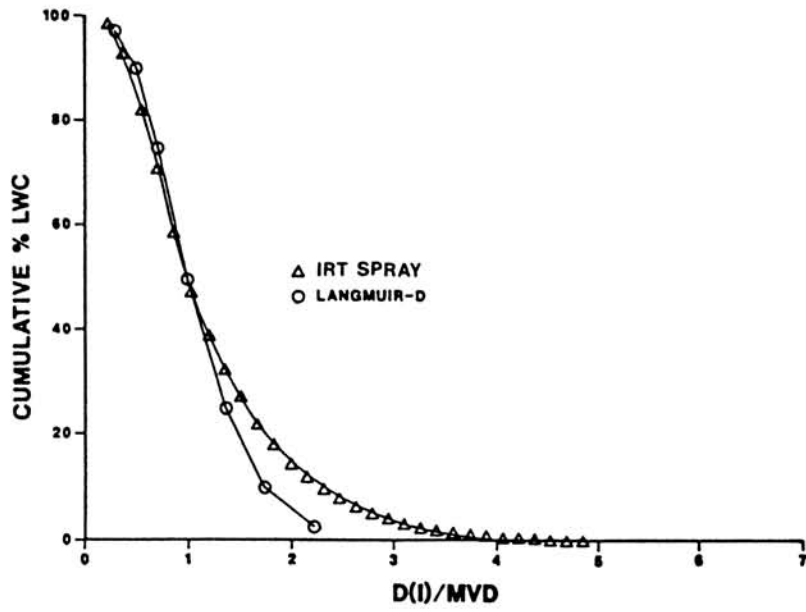
| CUMULATIVE % LWC(I) | % LWC(I) | D(I)/MVD |
|---------------------|----------|----------|
| 97.5 | 5 | 0.3161 |
| 90.0 | 10 | 0.4981 |
| 75.0 | 20 | 0.6872 |
| 50.0 | 30 | 1.0000 |
| 25.0 | 20 | 1.3737 |
| 10.0 | 10 | 1.9614 |
| 2.5 | 5 | 2.8288 |

MVD = 16 MICRONS

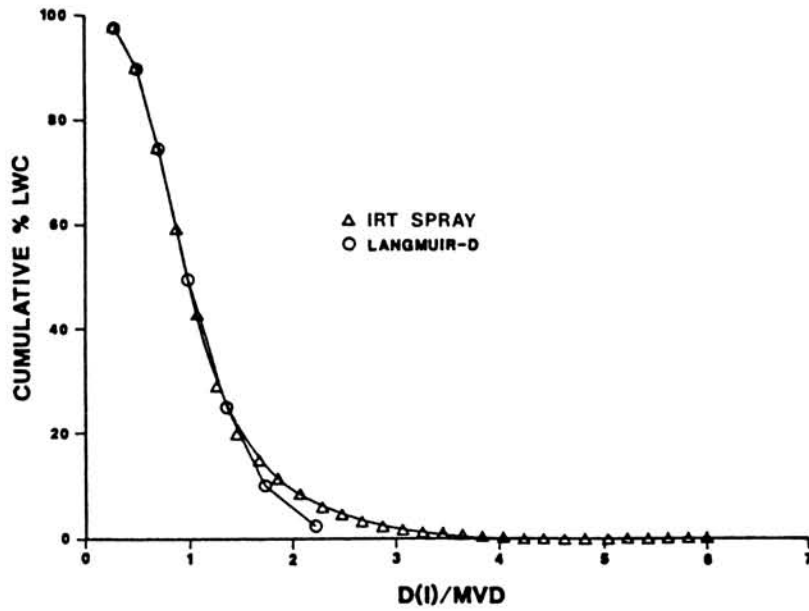
TABLE 2.2
DISCRETE CUMULATIVE DISTRIBUTION
FOR 0.65 PRESSURE RATIO

| CUMULATIVE % LWC(I) | % LWC(I) | D(I)/MVD |
|---------------------|----------|----------|
| 97.5 | 5 | 0.2770 |
| 90.0 | 10 | 0.4460 |
| 75.0 | 20 | 0.6617 |
| 50.0 | 30 | 1.0000 |
| 25.0 | 20 | 1.5865 |
| 10.0 | 10 | 2.2943 |
| 2.5 | 5 | 3.2542 |

MVD = 20 MICRONS



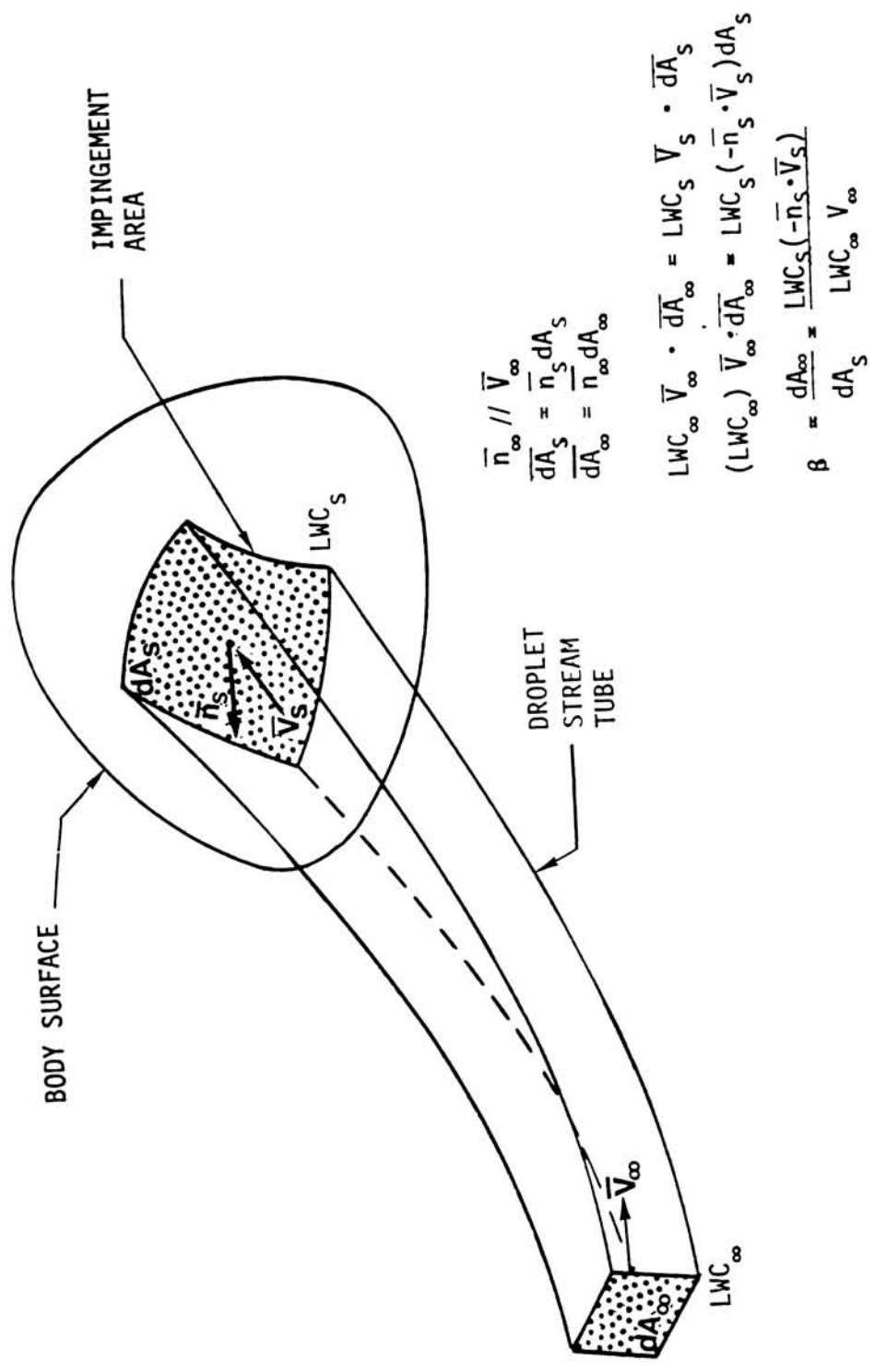
(A) MVD = $16 \mu m$



(B) MVD = $20 \mu m$

FIGURE 2.1

EXPERIMENTAL AND LANGMUIR D CUMULATIVE DROPLET DISTRIBUTIONS



$$\vec{n}_\infty // \vec{V}_\infty$$

$$\frac{\vec{n}_\infty}{dA_\infty} = \vec{n}_s \frac{dA_s}{dA_\infty}$$

$$LWC_\infty \vec{V}_\infty \cdot \vec{n}_\infty = LWC_s \vec{V}_s \cdot \vec{n}_s$$

$$(LWC_\infty) \vec{V}_\infty \cdot \vec{n}_\infty = LWC_s (-\vec{n}_s \cdot \vec{V}_s) dA_s$$

$$\beta = \frac{dA_\infty}{dA_s} = \frac{LWC_s (-\vec{n}_s \cdot \vec{V}_s)}{LWC_\infty \vec{V}_\infty}$$

FIGURE 2.2
 DEFINITION OF LOCAL IMPINGEMENT EFFICIENCY FOR A BODY
 IN A CLOUD OF UNIFORM DROPLET SIZE

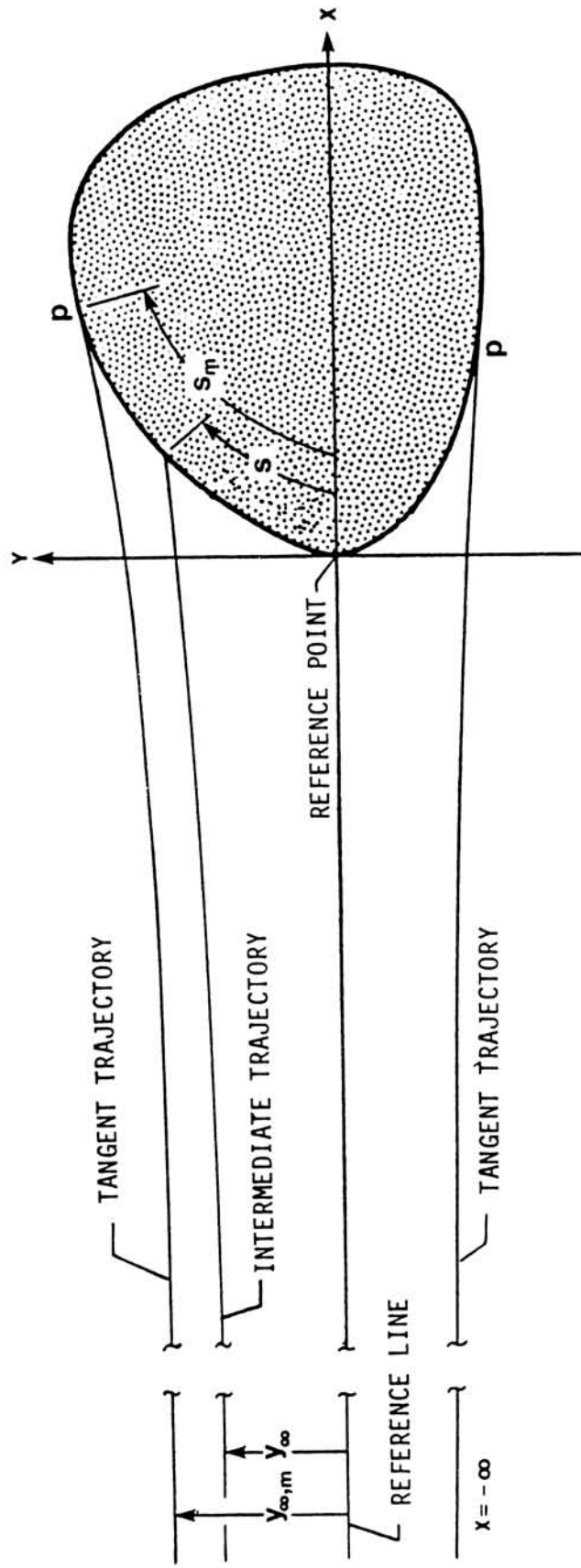


FIGURE 2.3
TWO-DIMENSIONAL DROPLET TRAJECTORIES FOR A BODY
IN A CLOUD OF UNIFORM DROPLET SIZE

3.0 EXPERIMENTAL METHOD

3.1 Test Approach

The dye-tracer technique that was employed in the water droplet impingement tests conducted in September of 1985 was used for the current tests. Details of the experimental approach are given in Ref. 10. Briefly, distilled water containing a known concentration of blue dye was injected into the airstream of a wind tunnel in the form of a droplet spray cloud. The test model was covered with thin strips of blotter paper in areas of interest and was exposed to the spray cloud. The amount of dye-mass per unit area of blotter strip obtained in a given time interval was measured using a laser reflectance method. The water impingement characteristics of a surface was then extracted from the concentration and location of the dye distribution on the blotter paper.

To calculate the local impingement efficiency from the measured dye-mass per unit area, an accurate measurement of the LWC in the spray cloud is required. In reality, a totally uniform spray cloud is very difficult to achieve. During the current tests LWC was measured at each location in the wind tunnel test section where a blotter strip was placed on a model. This was accomplished by using a reference collector mechanism with nine small collector blades. The impingement efficiency of these blades, for the droplet distributions given in tables 2.1 and 2.2, were close to 100 percent. The collector mechanism was placed in the test section of the wind tunnel with its collector blades positioned as close as possible to the blotter strip locations on the test model. A blotter strip was placed on each collector blade and impingement tests were conducted at identical conditions that the model was tested. During all collector tests the test model was removed from the test section. Using the laser reflectance method on the reference collector blotter strips the amount of dye per unit area of freestream at all locations of interest was determined. The local impingement efficiency, $\bar{\beta}$, at a given model location was obtained from equation (3 - 1).

$$\bar{\beta} = \frac{\text{Measured amount of dye/unit surface area/unit time on model at a given location}}{\text{Measured amount of dye/unit surface area/unit time in the freestream for a collector whose } \bar{\beta} = 1} \quad (3 - 1)$$

The reference collector that was used for the current tests is discussed in Section 3.5.

It should be noted that the same blotter paper from the same batch was used for the April 1989 tests as it was in the September 1985 tests. This is also true for the blue dye used in these tests. This is important when validating the laser calibration curve that is used in the data reduction method.

3.2 Test Facility

All of the water droplet impingement tests described in this report were conducted in the NASA Lewis Icing Research Tunnel (IRT). This tunnel has a test section of 6 ft high by 9ft wide and is capable of an airspeed of 300 mph with air temperatures as low as $-30^{\circ}F$. The IRT has a spray system that produces simulated icing clouds with LWC ranging from 0.5 to 2.0 g/m^3 .

All impingement tests were conducted at a temperature of 35 to $70^{\circ}F$ (i.e., no icing) and at a true air speed of 165 mph. The IRT spray system was not used to produce the spray clouds for the impingement tests for reasons explained in Section 3.3. However, the IRT spray system was activated occasionally between test runs to help maintain a high humidity level in the tunnel airstream and keep droplet evaporation low. The spray system designed and used during the 1985 tests was employed in all 1989 impingement tests. This system is briefly described in section 3.3, details of the spray system design can be found in Ref. 10.

3.3 Spray System

To avoid saturation of the blotter strips with the dyed water, a short spray interval was required, typically 2.6 to 4.5 seconds, depending on cloud MVD size. For the larger MVD size shorter spray durations were used. The IRT spray system was not designed for such short spray intervals, so an alternate system was designed that could accurately control the spray time interval.

The spray system used for the 1989 tests used the same principles and components that were used in the 1985 tests. The spray system consisted of a 9 gallon aluminum tank (which contained the dyed water solution), a pressure system and twelve nozzles (Fig. 3.1). Each nozzle assembly consisted of a solenoid valve that controlled the water supply, a nozzle housing that contained the atomizing air inlet, a pressure gauge or pressure transducer to monitor water pressure, and a NASA standard icing spray nozzle (Fig. 3.2).

The dye solution, which was pressurized in the tank to approximately 106 psig, passed through rubber hoses to each individual nozzle assembly. The air supply to the nozzle assemblies was controlled by a single solenoid valve at the main air supply. During testing, the air supply was turned on a few seconds before the water supply to allow the air pressure to stabilize. Next the dyed water supply was turned on and a spray cloud was produced. The mean volumetric diameter (MVD) of the spray cloud was controlled by varying the air-to-water pressure ratio. Two air pressures were used in the current impingement tests. These were 65 psig and 80 psig corresponding to clouds with MVDs of 20 and 16 microns respectively.

The spray system was mounted on the existing spray bars of the IRT spray system located in the plenum chamber of the tunnel. The nozzles were initially set up in the wind tunnel at the same position as they were in September 1985 in an effort to duplicate the spray cloud uniformity in those tests. After checking the uniformity of the spray cloud, the nozzles were relocated until a satisfactory degree of cloud uniformity was obtained (see Section 3.4).

Once uniformity was achieved, more extensive measurements of the nozzle locations were taken. Originally, only the nozzle locations with respect to the spray bars in the IRT were recorded. During uniformity testing it was determined that the spray cloud is sensitive to nozzle orientation with respect to the tunnel floor and tunnel walls. To obtain a better definition of nozzle placement in the IRT, additional measurements were taken. With the tunnel at zero airspeed and with the spray system air supply off, the nozzles were turned on to allow a pressurized stream of dyed water to flow from each nozzle. The stream of water (as opposed to a spray when the air was on) exited from the nozzles and impinged on the tunnel floor near the tunnel bellmouth. The coordinates of the points of impingement were recorded for each nozzle. These additional measurements will allow for a more accurate recreation of the spray cloud should any further testing be required. The nozzle locations with respect to the IRT spray bars and the tunnel floor are shown in Fig. 3.3.

3.4 Uniformity Test

Cloud uniformity was measured using a 6 ft \times 9 ft brass grid with horizontal and vertical increments 6 inches apart. Blotter strips were attached to this grid to cover an area of 2 ft \times 3 ft centered about the tunnel longitudinal axis, as shown in Fig. 3.4. The tunnel was brought up to test speed and the blotters were sprayed. The dye distribution on each blotter (35 blotter strips were used during each test) was determined using the data reduction method, and the nozzles were adjusted to remove dark or light regions of dye distribution.

During the 1985 uniformity test runs, all spray nozzles were activated during each uniformity test and problem areas in the spray cloud were identified by measuring variations in the color of the blotter squares and their perspective locations. In this method it was difficult to determine which nozzles should be moved to correct any light or dark regions in the array of blotter squares. In the current uniformity tests each nozzle of the spray system was tested individually to determine its contribution to the spray cloud. This gave the opportunity to make a more educated guess on how the positions of nozzles should be adjusted to obtain a uniform spray cloud.

It was also decided that a single 2 to 3 ft long 1.25 inch wide strip of blotter paper could be used to replace a row or column of blotter squares (used in the 1985 tests), allowing for a continuous measurement of dye deposit along the row or column instead of measurements at six inch intervals (see Fig. 3.5). To prevent excess flow blockage in the area of the uniformity grid, the test was conducted separately for the five rows of strips and the seven columns of strips.

After a satisfactory cloud distribution was obtained (by visual check), the dye deposits on the blotter strips were measured using the laser reflectance method to verify that the deposits did not vary more than $\pm 10\%$ from the average. Further adjustments were then made to the spray system based on the results obtained from the laser reflectometer to meet the $\pm 10\%$ uniformity requirement. A total of 59 uniformity runs were performed (see Appendix B).

3.5 Reference Collector Mechanism

To calculate the local impingement efficiency, the local LWC of the free stream spray cloud had to be determined by use of a "reference collector mechanism". The reference collector mechanism consisted of an airfoil shaped vertical beam with eight arms spaced at 45 degree intervals that extended in front of the beam (Fig. 3.6). A 4 inch long wedge shaped collector blade was mounted on the end of six of the arms, and a 18 inch long collector blade was mounted between the top and bottom arms of the reference collector mechanism. The collector blade was designed to hold a 0.2 inch wide \times 1.5 to 2 inch long rectangular blotter strip in place while minimizing the disturbance to the flow in the proximity of the collector blade. This reference collector was designed to obtain the local LWC for the airfoils and the engine inlet tested, replacing the two separate reference collectors that were used in the 1985 tests.

The reference collector was positioned so that the blotter strips on the collector blades were at the same position with respect to the test section as the blotter strips that were mounted on the test models. The reference collector was then exposed to a spray cloud under the same test conditions as the models. This test was repeated for all test conditions and all angles of attack tested.

Corrections to the measured LWC were made based on computer predicted blade collection efficiencies. Even though the reference collector was designed to maximize collection efficiency, the impingement efficiency of the collector blades was not 100%. If the blade collection efficiency were 100% then the LWC at the blade would be a direct measure of the LWC in the tunnel. The predicted collector efficiency values for the spray clouds with MVD's of 16 and 20 microns were 86% and 89% respectively. The LWC can be defined as the amount of dye per unit time of collector exposure divided by the theoretical collector impingement efficiency and the concentration of the dye solution:

$$LWC = \frac{\text{Mass of dye per unit time on collector blotter strip}/\bar{\beta} \text{ collector for a given MVD}}{\text{Concentration of dye solution}} \quad (3 - 2)$$

3.6 Mass Flow Measurements

The flow field about an engine inlet is largely dependent on the mass flow through the inlet. To obtain a broad water droplet impingement data base, it was necessary to test the engine inlet at different mass flow rates as well as different angles of attack.

To provide the variations in mass flow, the suction system of the IRT was utilized. The system consisted of a large vacuum chamber and associated vacuum pumps outside the tunnel that were connected to the tunnel test section by a 24 inch diameter pipe. The suction was regulated by a valve that could be opened or closed by an electrical switch that was located inside the control room of the IRT. The tunnel test section vacuum system was connected to an elbow arrangement that extended through the ceiling of the IRT test

section. The elbow was connected to the engine inlet model mount by means of a flexible rubber hose, which allowed for variations in angle of attack.

The mass flow through the system was measured with a KURZ velocity and temperature probe that was inserted in the 24 inch diameter pipe. The KURZ velocity probe was calibrated by the NASA Lewis Icing Research tunnel personnel prior to any engine inlet testing.

The mass flows chosen for the Boeing 737-300 inlet tests were 23 lbm/s and 17.2 lbm/s. These mass flows correspond to capture ratios of 1 and 0.75 respectively which are representative of flight conditions for this inlet.

3.7 Droplet Impingement Data Acquisition

To obtain the water droplet impingement data for a given model the following steps were executed during each impingement test.

1. The pressure for the air and dyed water solution of the spray system were set to the required levels. These pressures were typically set to 106 psig for the dyed water at the supply tank (corresponding to 100 psig at the nozzle) and 65 or 80 psig for air. An air pressure of 65 psig produced a cloud with an MVD of $16 \mu m$ while the 80 psig air pressure produced a cloud with an MVD of $20 \mu m$.
2. The timer that controlled the duration of the spray was set to 2.6 seconds for spray clouds having an MVD of $20 \mu m$ and to 4.5 seconds for spray clouds with MVD of $16 \mu m$. These time durations produced optimum dye impingement on the blotter strips for the concentration (0.0002 by weight) of the dyed water solution used in the 1989 tests.
3. The blotter strips were attached at the required locations on the forward part of the test model. The blotter strips were typically 1.5 inches wide and of various shapes and lengths, depending on the model geometry and angle of attack. The strips were attached to the models with aluminum tape, which was pressed down smoothly to the model to minimize disturbances to flow in the locality of the blotter strips. The blotter paper used in the tests had a smooth and a rough side which yielded different optical properties. The smooth side was placed facing the flow. Each blotter strip was marked on its rough side to identify test run number, test model and strip location on the model. In addition, for the inlet tested the blotter strips were marked to indicate which part of the strip was attached to the outer surface and which part of the strip was attached to the inner surface of the inlet. Fig. 3.7 shows typical of blotter strip installation on airfoils and inlet tested.
4. The following test conditions were set prior to each impingement test:
 - spray system air and water pressures
 - spray duration

- angle of attack
 - temperature and humidity (approximately)
 - true air speed
 - mass flow (inlet only) was adjusted to the required level by opening or closing the regulating valve of the suction system. A precalibrated voltmeter was used to monitor inlet mass flow.
5. The following test variables were recorded for each impingement test (see Appendix B):
- dyed water concentration (constant for all tests)
 - test run and geometry tested
 - freestream static and total pressures (psia)
 - freestream average total temperature in °F measured at three different tunnel locations upstream of the spray bar system
 - true air speed
 - spray system water and air pressures (psig)
 - water pressure (psig) at the nozzles using electric transducers
 - spray time duration (seconds)
 - inlet mass flow in volts (converted to lbm/s using mass flow calibration curve)
6. The spray system was activated and a dye deposit was obtained on the blotter strips. The tunnel air speed was reduced to idle speed (about 10 mph) and the blotter strips were carefully removed from the model and placed in the control room and allowed to dry. The blotter strips were then placed in envelopes that were labeled for future reference.
7. The model was wiped clean and new blotter strips were placed on the model for the next test.
8. Steps 1 to 7 were repeated for all test runs performed. For each test condition five repeated runs were performed to obtain a statistical average.

Test time between runs varied from 10 to 25 minutes depending on model and number of strips used. The tunnel was shut down completely between model changes.

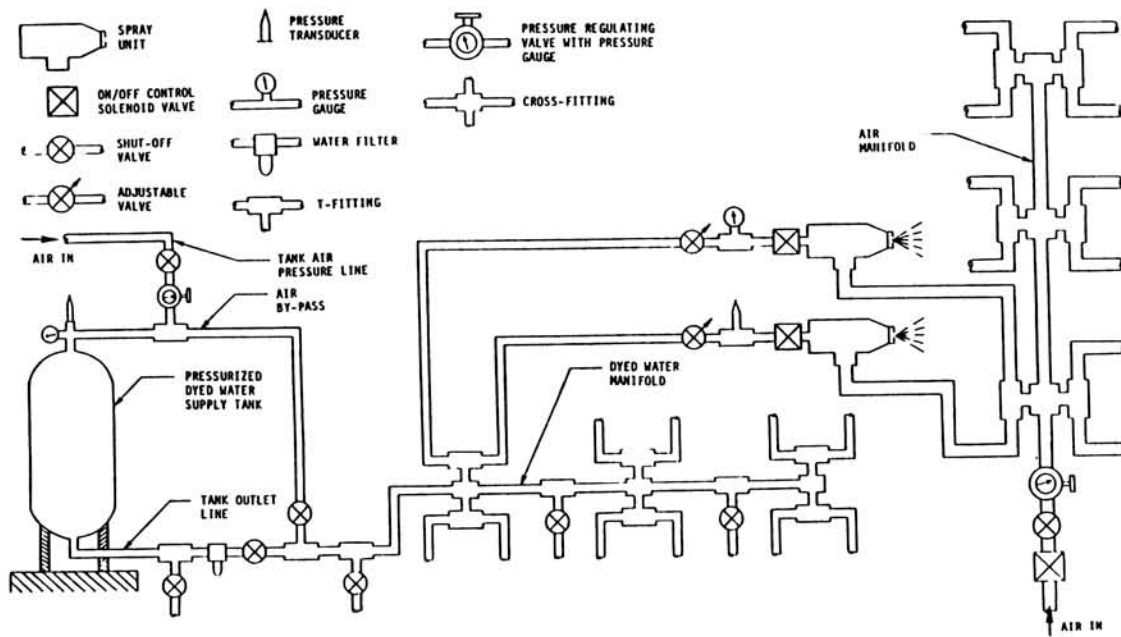


FIGURE 3.1
SCHEMATIC DIAGRAM OF SPRAY SYSTEM

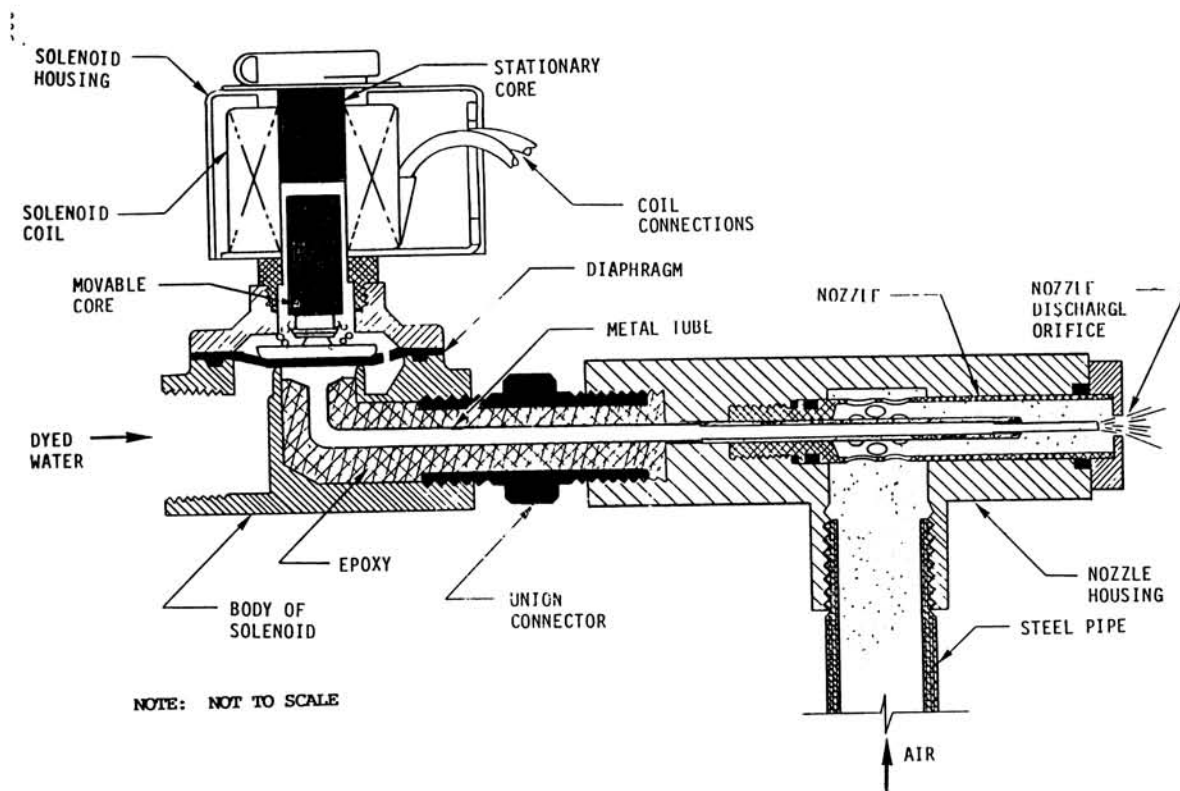


FIGURE 3.2
NOZZLE ASSEMBLY DETAILS

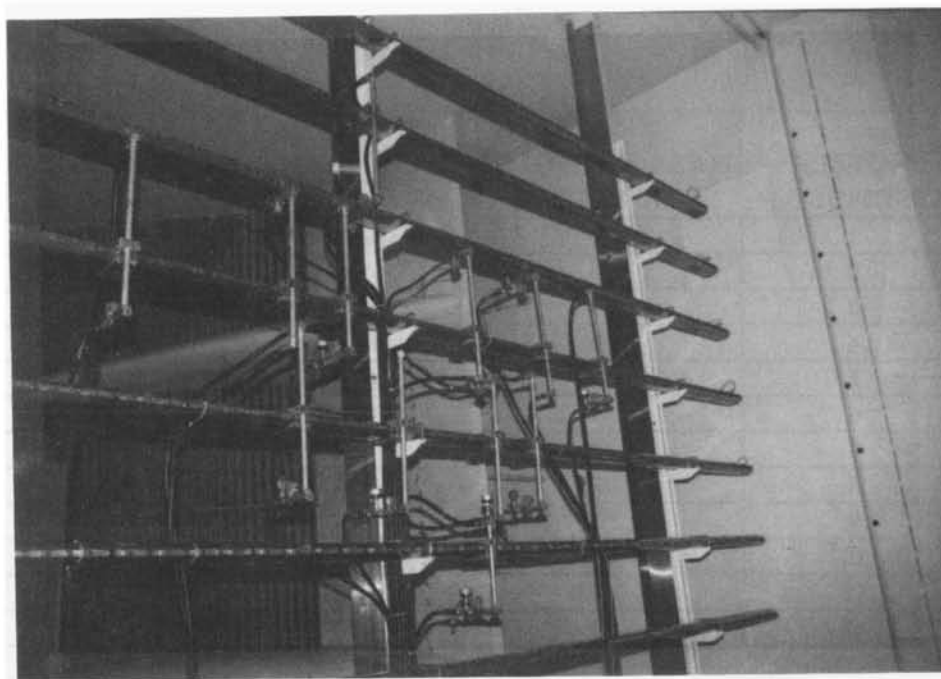
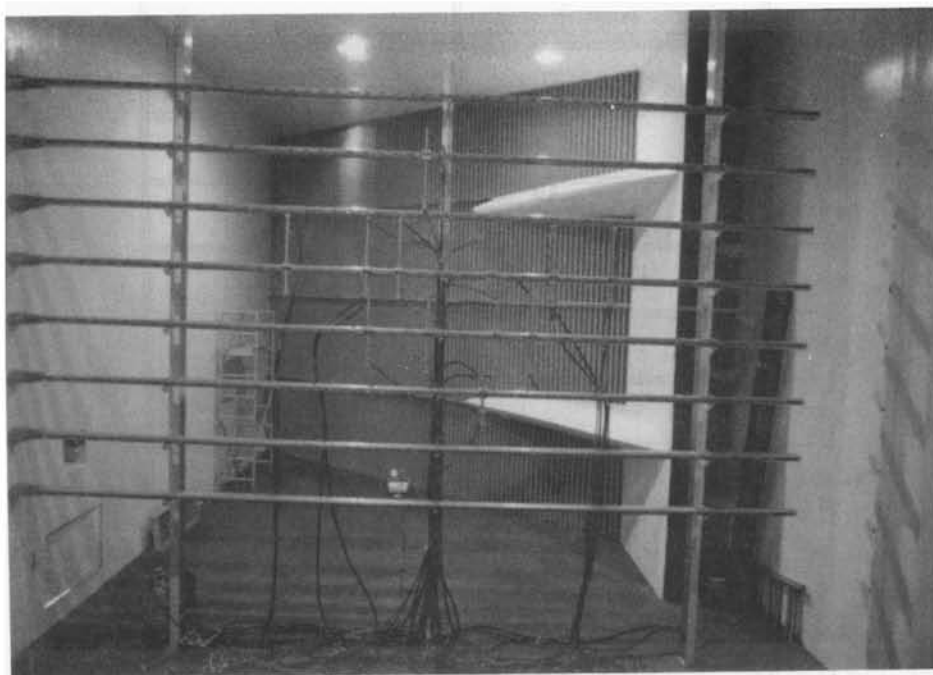
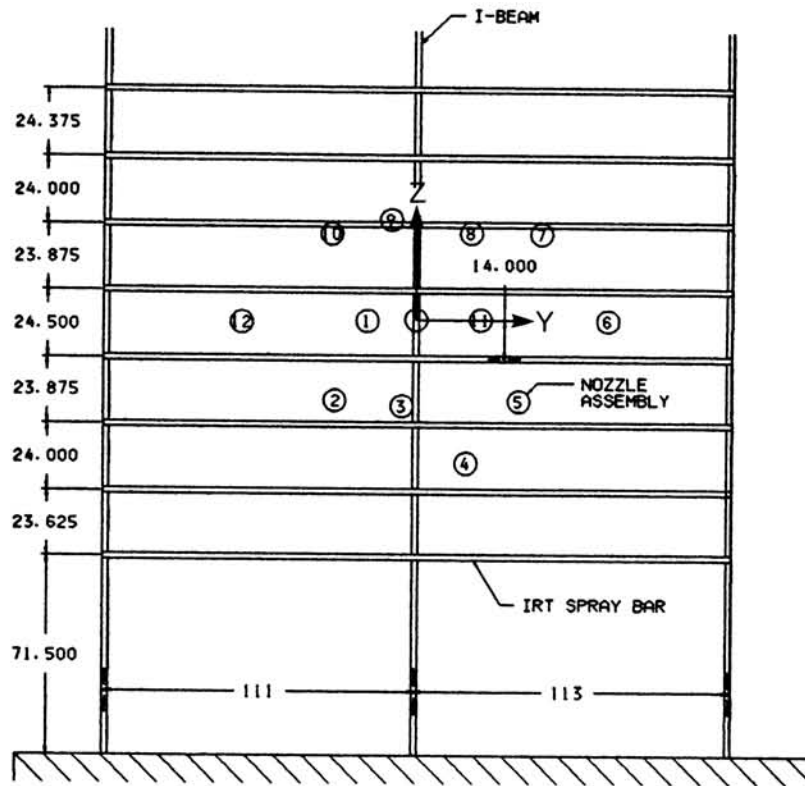


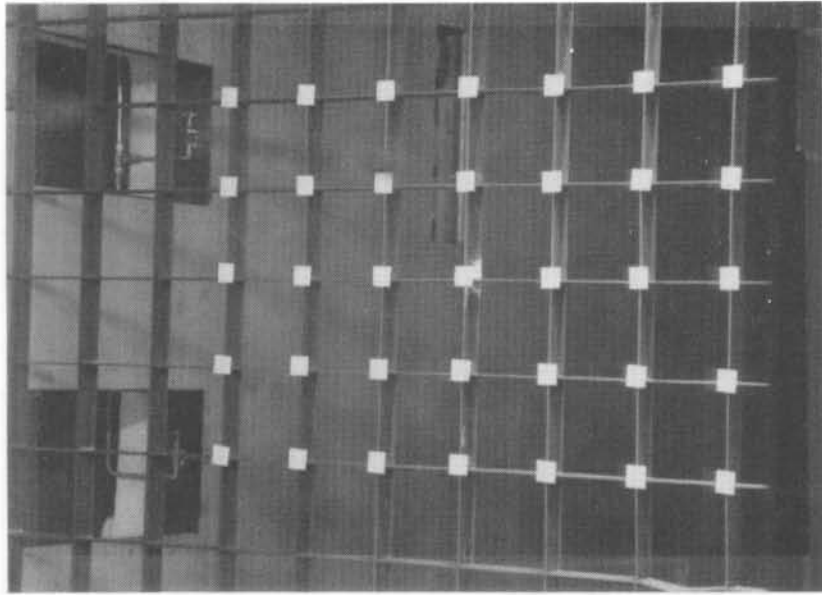
FIGURE 3.3
SPRAY SYSTEM INSTALLED IN IRT PLENUM CHAMBER



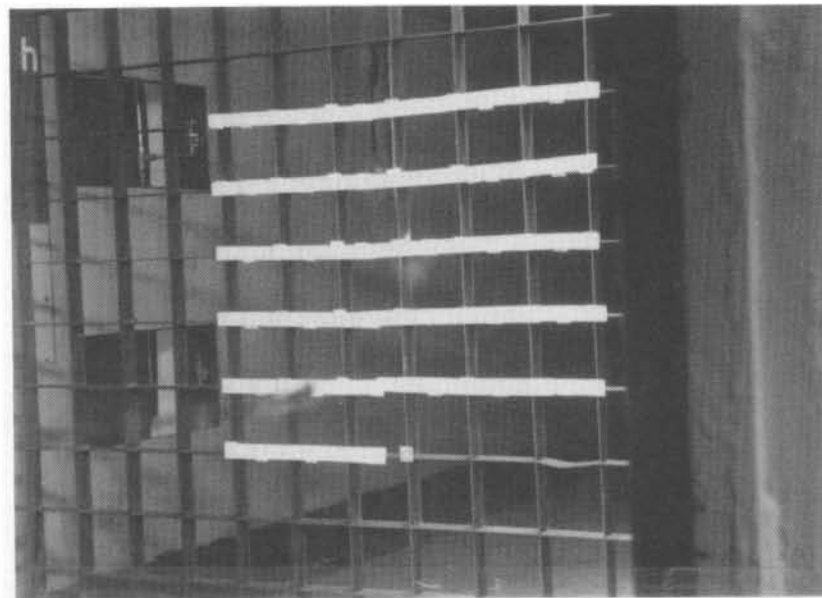
ALL DIMENSIONS IN INCHES

| NOZZLE ASSEMBLY # | NASA STANDARD NOZZLE # | NOZZLE LOCATION COORDINATES IN INCHES | |
|-------------------|------------------------|---------------------------------------|---------|
| | | Y | Z |
| 1 | 40 | -17.5 | -0.5 |
| 2 | 86 | -29.25 | -29.25 |
| 3 | 27 | -5.0 | -31.25 |
| 4 | 109 | 18.125 | -51.75 |
| 5 | 43 | 37.25 | -29.375 |
| 6 | 50 | 69.25 | -.25 |
| 7 | 48 | 45.25 | -31.0 |
| 8 | 107 | 19.75 | 31.25 |
| 9 | 112 | -9.0 | 36.0 |
| 10 | 111 | -30.5 | 31.0 |
| 11 | 104 | 23.25 | 0.0 |
| 12 | 13 | -62.75 | -1.0 |

FIGURE 3.4
NOZZLE LOCATIONS WITH RESPECT TO IRT SPRAY BARS



(A) 1.25in \times 1.25in BLOTTER SQUARES



(B) 1.25in Wide \times 3ft Long BLOTTER STRIPS

FIGURE 3.5
UNIFORMITY GRID WITH BLOTTER STRIPS ATTACHED

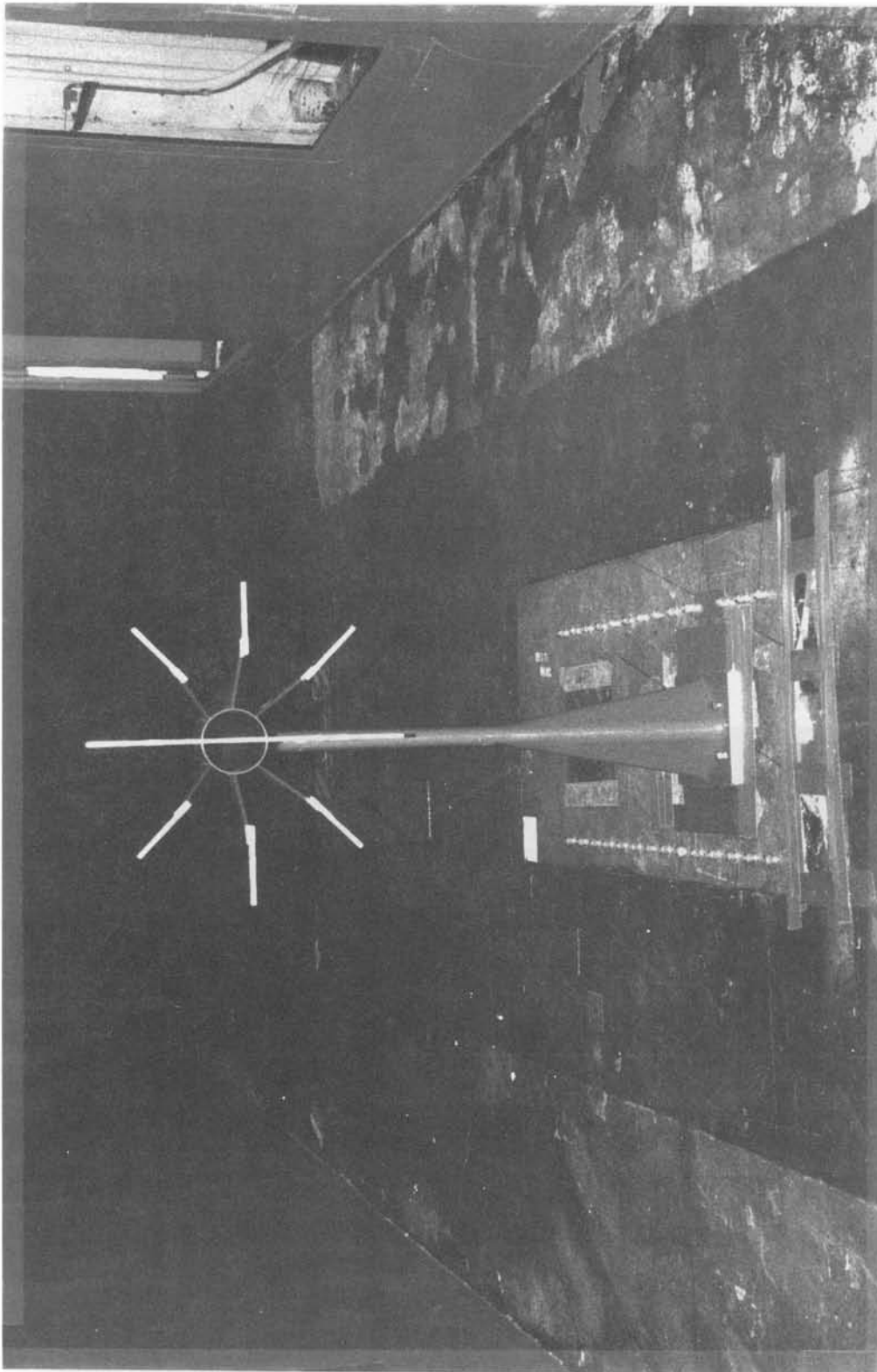
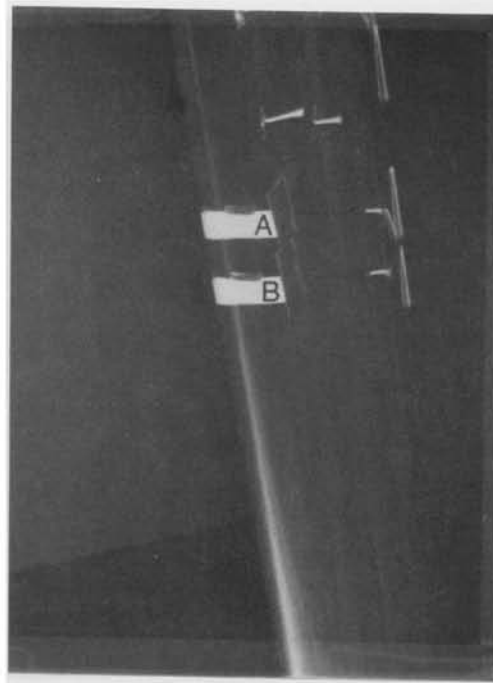
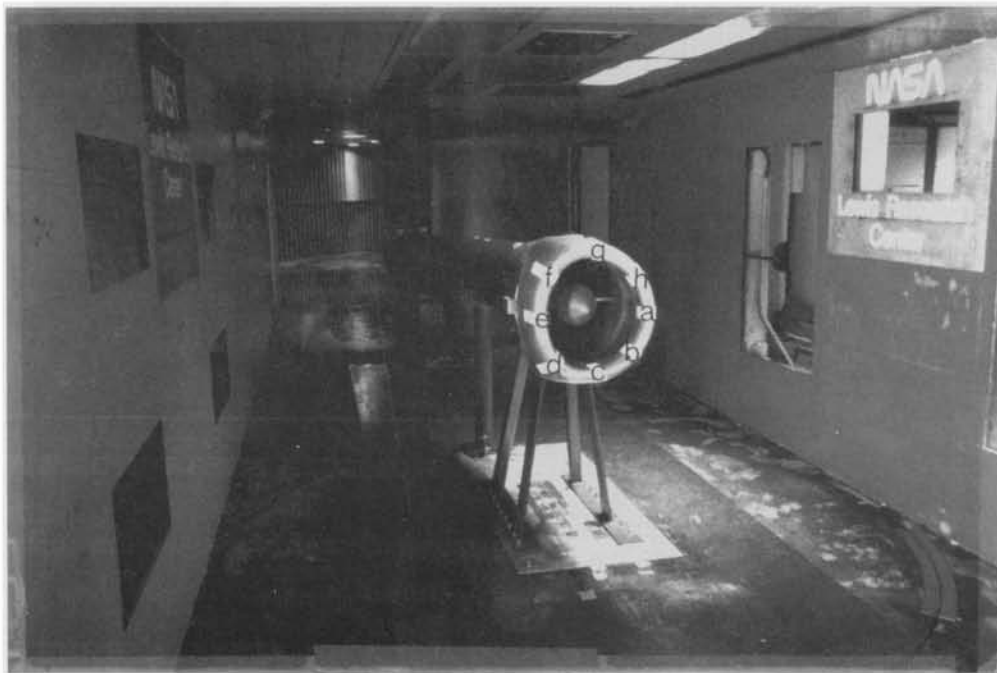


FIGURE 3.6
REFERENCE COLLECTOR MECHANISM USED IN ALL 1989 TESTS

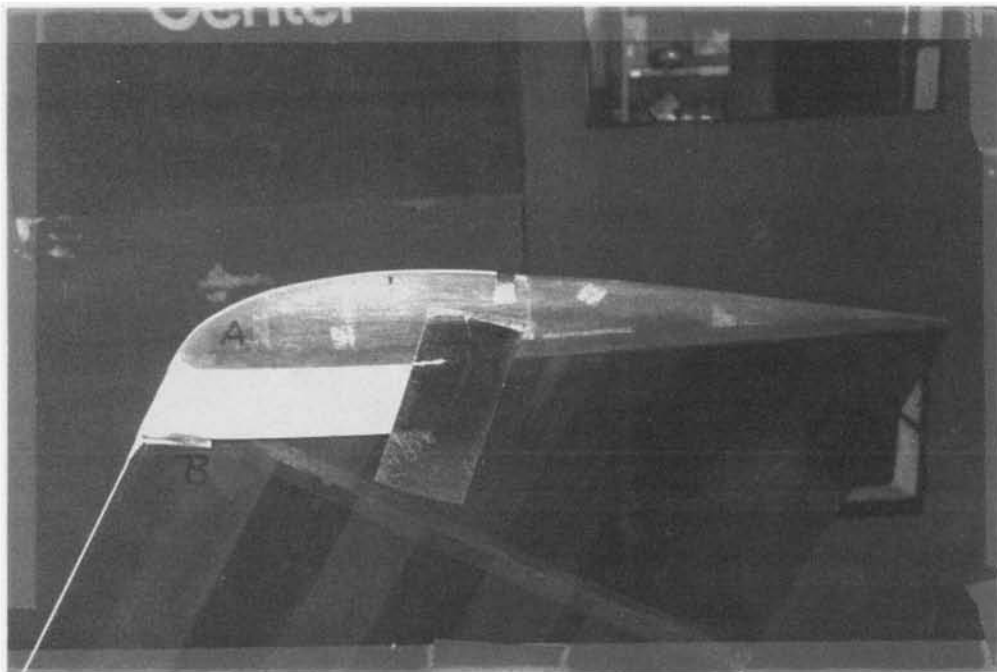


(A) *MS(1) - 0317* SWEPT AIRFOIL



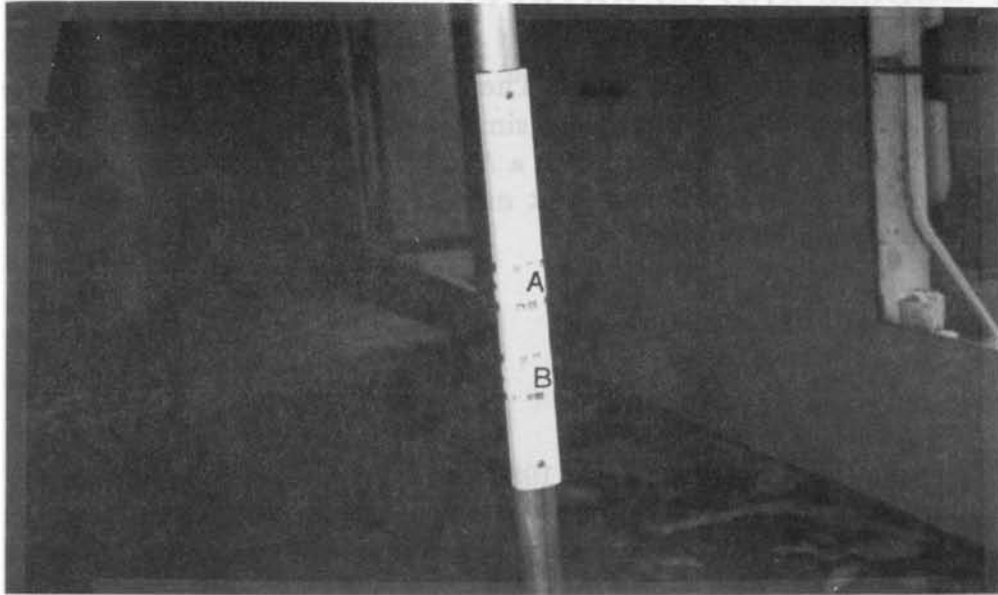
(B) 737 - 300 ENGINE INLET

FIGURE 3.7
BLOTTER STRIP LOCATIONS ON TEST MODELS
(PAGE 1 OF 3)

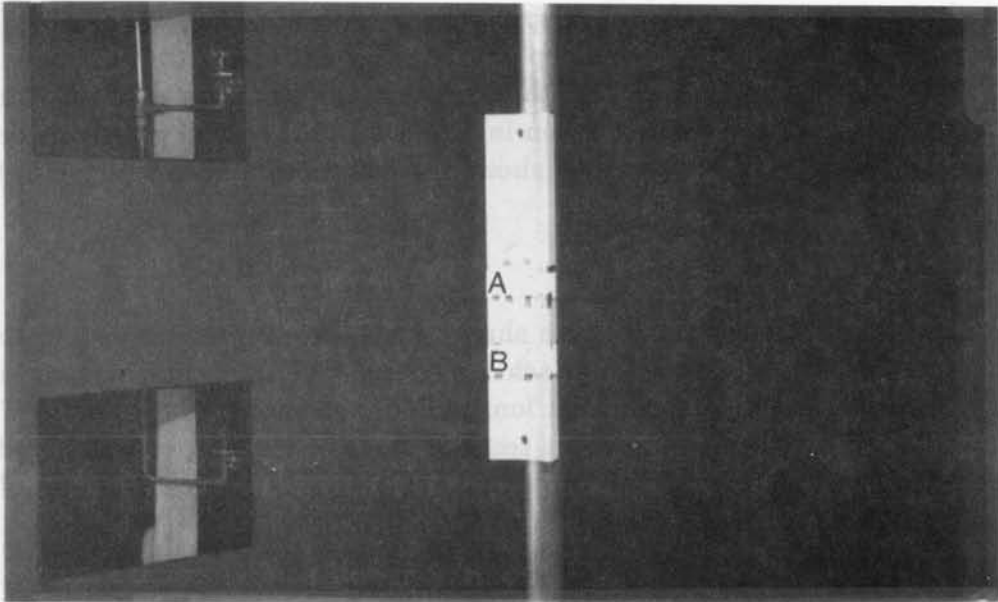


(C) SWEEP WING TIP

FIGURE 3.8
BLOTTER STRIP LOCATIONS ON TEST MODELS
(PAGE 2 OF 3)



(D) SMALL GLAZE ICE SHAPE



(E) LARGE GLAZE ICE SHAPE

FIGURE 3.8
BLOTTER STRIP LOCATIONS ON TEST MODELS
(PAGE 3 OF 3)

4.0 TEST MODELS AND CONDITIONS

There were a total of six models tested. These included a Natural-Laminar-Flow airfoil *NLF(1) – 0414*, a large and a small glaze simulated ice shapes, a swept medium speed *MS(1) – 0317* airfoil, a swept wing tip with a *NACA0012* airfoil section, and a 737 – 300 engine inlet model. Descriptions of the test models and test conditions are given in this section and are summarized in Table 4.1.

4.1 Two-Dimensional Flow Models

4.1.1 *NLF(1) – 0414* Airfoil Section

This airfoil was designed in the early 1980's and is representative of modern natural laminar flow airfoils. The *NLF(1) – 0414* was designed for 70% chord laminar flow on both surfaces, a lift coefficient of 0.4, a Reynolds number of 10^7 and a Mach number of 0.4 (Ref. 13).

The airfoil tested was made of mahogany with a fiberglass trailing edge, had a chord of 36 inches and spanned the height (6 ft) of the tunnel test section. Impingement data for this airfoil were obtained for two angles of attack 0 and 8 degrees and for two cloud MVD's 16 and 20 microns. Two blotter strips A and B were attached to the airfoil during each test run. Strip A was located at midspan, 36 inches above the tunnel floor. Strip B was located 32 inches along the span from the tunnel floor. A summary of test conditions and number of repeats per condition is given in Table 4.1. The airfoil geometry definition is given in Figs. 4.1a and 4.1b. Figure 4.2a shows the installation of this airfoil in the IRT test section.

4.1.2 Simulated Ice Shapes

The large and small glaze simulated ice shapes tested are representative of the types often encountered on aircraft surfaces. Each ice shape was 18 inches in span and was mounted on a two inch in diameter and 6 ft long cylinder as shown in Fig. 4.2b. The only test parameter varied for the impingement tests of the two ice shapes was cloud MVD. Test conditions for these geometries are presented in Table 4.1. The coordinates of the ice shapes are given in Figs. 4.1c and 4.1d.

4.2 Three-Dimensional Flow Models

Models with three-dimensional geometry and/or three-dimensional flow fields tested in 1989 included an infinite swept wing, a low aspect ratio swept wing and an engine inlet. All geometries tested are representative of modern aircraft surfaces.

4.2.1 *MS(1) – 0317 Swept Airfoil*

The *MS(1) – 0317* wing section is representative of medium speed airfoils. It was designed in the mid 1970s for general aviation aircraft (Ref. 14). The airfoil was designed for a lift coefficient of 0.3 a Reynolds number of 1.4×10^7 and a Mach number of 0.68.

The model tested was 6 ft span 30 degree swept wing made of mahogany with a 36 inch chord in the streamwise direction. The coordinates of the *MS(1) – 0317* section are given in Fig. 4.3a. Model installation in the tunnel test section is shown in Fig. 4.4a.

Impingement data for this geometry were obtained for two angles of attack, 0 and 8 degrees, and two MVD's 16 and 20 μm . Blotter strips were attached to the airfoil surface at locations A and B, 36 and 32 inches above the tunnel floor respectively. Each test condition was repeated five times.

A 36 inch chord unswept *MS(1) – 0317* airfoil with 6 ft span was tested in 1985. The swept model used in the 1989 tests was chosen to investigate how sweep angle affects impingement characteristics.

4.2.2 Swept Wing Tip

This was a wooden finite wing model with 30° leading edge sweep. The model had a NACA 0012 wing section normal to the leading edge with a chord length of 15 inches. The wing span was 15 inches and the aspect ratio of the wing was 1.4. This model was selected to study how droplet impingement is affected by the wing tip vortex.

Impingement tests for this model were conducted at two angles of attack, 0 and 8 degrees, and for two MVD sizes, 16 and 20 μm . Blotter strips were attached to this model at three locations. Location A was at the tip of the wing, location B was 42 inches above the tunnel floor and location C was 32 inches above the tunnel floor. All strips were attached to the leading edge of the wing and were shaped to follow the wing surface along the streamwise direction. Blotter strips B and C were V-shaped to fit the wing leading edge. Installation of the wing tip model with blotter strips attached in the IRT test section is shown in Fig. 4.4b.

4.2.3 Boeing 737-300 Engine Inlet Model

This 0.2547 scale inlet model (Boeing Model 5718-1-1) was made out of solid aluminum and was provided by the Boeing Company. Details of this geometry are available on magnetic tape from NASA Lewis Research Center. A brief geometry definition for this inlet is given in Fig. 4.3. Inlet areas of interest are: fan face area 149.77 in^2 , throat area 143.01 in^2 and highlight area 185.58 in^2 .

The 737-300 inlet was tested at inlet mass flows of 17 and 23 lbm/sec (corresponding to capture area ratios of 0.75 and 1 respectively), angles of attack of 0 and 15 degrees, and MVD's of 16 and 20 μm , for a total of four test conditions (see Table 4.1). Each test condition was repeated several times. Blotter strips were attached to the inlet at intervals of 45 degrees giving a total of eight strips. The maximum angle of attack was limited to 15 degrees to keep the inlet model within the uniform cloud region. The inlet was mounted in the tunnel section so that the lower engine lip was parallel to the tunnel

left wall looking downstream. Variations in angle of attack were obtained by rotating the inlet about an axis perpendicular to the tunnel turn table. The inlet installation with mass flow connection and inlet support is shown in Fig. 4.4b. Blotter strips attached to the inlet surface are also shown in this figure.

Impingement data for the 737-300 inlet were also obtained in 1985. The inlet was retested in 1989 in order to resolve discrepancies, between the 1985 experimental and analysis data, observed at $\alpha = 15^\circ$ near the inlet upper lip. These discrepancies were attributed to cloud non-uniformity.

4.3 Reference Collector Mechanism

The reference collector was tested at two tunnel locations corresponding to the location of the engine inlet at 0 and 15 degrees angle of attack. Two droplet MVD's, 16 and 20 μm were used in the collector impingement tests. Each collector test condition was repeated at least five times. Nine blotter strips were attached to the collector as shown in Fig. 4.4d. The long center blade of the collector was used to provide LWC information for all wings and ice shapes. This blade was used in all collector tests with the collector at the $\alpha = 0^\circ$ location. The eight shorter blades were used to determine LWC for the engine inlet.

TABLE 4.1
TEST CONDITION MATRIX

| MODEL DESCRIPTION | TAS mph | α (deg) | MVD μm | Mass Flow lbm/s | Blotter Strips Per Run | Test Runs (See App. B) |
|---|------------|-------------------|----------------|--------------------|---------------------------|---------------------------|
| Simulated Iced Shapes | 165 | - | 20 | - | 2 | 116 - 126 |
| NLF(1)-0414F Airfoil, 36 inch Chord | 165 | 0, 8 | 16, 20 | - | 2 | 215 - 236 |
| 30° Swept MS(1)-0317 Airfoil, 36 inch Chord | 165 | 0, 8 | 16, 20 | - | 2 | 148 - 167 |
| 30° Swept NACA 0012 Wing Tip, 15 inch Chord | 165 | 0, 8 | 16, 20 | - | 3 | 127 - 147 |
| Boeing 737-300 Inlet Model | 171 | 0, 15 | 16 | 17 | 8 | 168 - 173, 179 - 180 |
| Boeing 737-300 Inlet Model | 173 | 0 | 20 | 23 | 8 | 174 - 176, 177 - 178 |
| Boeing 737-300 Inlet Model | 171 | 15 | 20 | 23 | 8 | 174 - 176, 177 - 178 |
| Reference Collector Mechanism | 165 | 0, 15 | 16, 20 | - | 8 - 9 | 95 - 115 |

| X/C | Y/C | X/C | Y/C | X/C | Y/C |
|---------|---------|---------|---------|----------|----------|
| .000000 | .000000 | .245187 | .074349 | .735392 | .047492 |
| .000085 | .001585 | .261054 | .075830 | .750058 | .042542 |
| .000299 | .003274 | .277233 | .077161 | .764925 | .037208 |
| .001231 | .007144 | .293699 | .078380 | .779951 | .031694 |
| .002695 | .010618 | .310424 | .079454 | .795034 | .026178 |
| .004989 | .014163 | .327391 | .080369 | .810124 | .020750 |
| .008005 | .017552 | .344571 | .081151 | .825179 | .015483 |
| .011774 | .020769 | .361925 | .081781 | .840076 | .010464 |
| .016268 | .023816 | .379421 | .082240 | .854693 | .005783 |
| .021468 | .026795 | .397052 | .082536 | .868960 | .001467 |
| .027356 | .029735 | .414812 | .082677 | .882768 | -.002475 |
| .033891 | .032633 | .432667 | .082633 | .896006 | -.006044 |
| .041042 | .035480 | .450558 | .082429 | .908644 | -.009267 |
| .048811 | .038317 | .468450 | .082047 | .920659 | -.012161 |
| .057201 | .041092 | .486327 | .081507 | .931980 | -.014739 |
| .066189 | .043825 | .504159 | .080794 | .942511 | -.017008 |
| .075767 | .046482 | .521931 | .079893 | .952200 | -.018994 |
| .085915 | .049070 | .539641 | .078779 | .961042 | -.020722 |
| .096610 | .051588 | .557254 | .077489 | .969034 | -.022206 |
| .107826 | .054033 | .574742 | .075988 | .976155 | -.023456 |
| .119545 | .056398 | .592064 | .074285 | .982370 | -.024492 |
| .131756 | .058692 | .609177 | .072377 | .987660 | -.025333 |
| .144443 | .060917 | .626040 | .070245 | .992021 | -.026006 |
| .157592 | .063092 | .642629 | .067900 | .995456 | -.026519 |
| .171193 | .065206 | .658928 | .065348 | .997952 | -.026872 |
| .185212 | .067240 | .674926 | .062510 | .999480 | -.027067 |
| .199628 | .069172 | .690586 | .059376 | 1.000000 | -.027122 |
| .214447 | .071009 | .705860 | .055889 | | |
| .229647 | .072735 | .720751 | .055194 | | |

(A) *NLF(1)* – 0414 AIRFOIL (UPPER SURFACE)

FIGURE 4.1
DEFINITION OF TWO-DIMENSIONAL TEST GEOMETRIES
(PAGE 1 OF 4)

| X/C | Y/C | X/C | Y/C | X/C | Y/C |
|---------|----------|---------|----------|----------|----------|
| .000000 | .000000 | .235525 | -.048542 | .726433 | -.046065 |
| .000085 | -.001535 | .252387 | -.049901 | .743743 | -.042296 |
| .000164 | -.002120 | .269586 | -.051189 | .761642 | -.038850 |
| .000740 | -.004536 | .287087 | -.052411 | .779550 | -.035991 |
| .002095 | -.006984 | .304866 | -.053561 | .797188 | -.033529 |
| .004175 | -.009008 | .322901 | -.054635 | .814513 | -.031444 |
| .007129 | -.010993 | .341156 | -.055635 | .831368 | -.029735 |
| .010874 | -.012933 | .359611 | -.056539 | .847719 | -.028310 |
| .015540 | -.014882 | .378260 | -.057344 | .863493 | -.027230 |
| .021096 | -.016854 | .397074 | -.058052 | .878523 | -.026450 |
| .027380 | -.018787 | .416017 | -.058658 | .892802 | -.025925 |
| .034569 | -.020742 | .435049 | -.059142 | .906336 | -.025641 |
| .042393 | -.022654 | .454127 | -.059517 | .919043 | -.025539 |
| .050985 | -.024572 | .473222 | -.059785 | .930841 | -.025569 |
| .060274 | -.026487 | .492319 | -.059950 | .941715 | -.025689 |
| .070243 | -.028383 | .511402 | -.060012 | .951668 | -.025861 |
| .080881 | -.030259 | .530430 | -.059979 | .960696 | -.026061 |
| .092159 | -.032116 | .549361 | -.059792 | .968804 | -.026275 |
| .104058 | -.033945 | .568160 | -.059456 | .975996 | -.026483 |
| .116557 | -.035741 | .586782 | -.058982 | .982266 | -.026675 |
| .129635 | -.037497 | .605204 | -.058340 | .987613 | -.026858 |
| .143277 | -.039212 | .623397 | -.057533 | .992033 | -.027036 |
| .157457 | -.040888 | .641303 | -.056524 | .995503 | -.027211 |
| .172148 | -.042421 | .658920 | -.055246 | .997994 | -.027367 |
| .187328 | -.044107 | .676262 | -.053698 | .999497 | -.027475 |
| .202969 | -.045646 | .693229 | -.051845 | 1.000000 | -.027514 |
| .219043 | -.047125 | .709795 | -.049388 | | |

(B) *NLF*(1) – 0414 AIRFOIL (LOWER SURFACE)

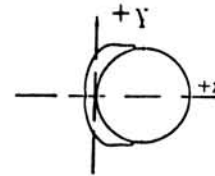
FIGURE 4.1

DEFINITION OF TWO-DIMENSIONAL TEST GEOMETRIES
(PAGE 2 OF 4)

COORDINATES FOR 2 MINUTE GLAZE ICE ACCRETION
(NOTE: DATA FROM NASA - LEWIS)

$C = .0508 \text{ m} = 2.0''$

X/C



| | | | | | |
|------------|------------|------------|------------|------------|------------|
| 1.0000000 | 0.9980649 | 0.9922500 | 0.9825492 | 0.9688901 | 0.9516240 |
| 0.9310589 | 0.9071791 | 0.8801693 | 0.8502499 | 0.8188995 | 0.7850649 |
| 0.7489684 | 0.7108700 | 0.6710334 | 0.6297538 | 0.5873248 | 0.5440689 |
| 0.4999999 | 0.4759901 | 0.4524940 | 0.4290000 | 0.4054999 | 0.3820097 |
| 0.3584803 | 0.3355491 | 0.3122243 | 0.2890708 | 0.2673995 | 0.2446043 |
| 0.2220708 | 0.1991948 | 0.1762047 | 0.1531397 | 0.1303445 | 0.1108405 |
| 0.0909448 | 0.0724606 | 0.0558996 | 0.0394547 | 0.0247559 | 0.0099842 |
| -0.0042106 | -0.0170197 | -0.0281004 | -0.0373091 | -0.0450689 | -0.0515197 |
| -0.0580197 | -0.0644389 | -0.0698149 | -0.0747105 | -0.0804842 | -0.0849507 |
| -0.0852500 | -0.0850000 | -0.0850000 | -0.0854055 | -0.0842637 | -0.0799999 |
| -0.0839192 | -0.0852854 | -0.0850196 | -0.0853640 | -0.0842637 | -0.0813838 |
| -0.0760491 | -0.0694646 | -0.0637953 | -0.0585098 | -0.0538406 | -0.0481850 |
| -0.0410039 | -0.0333346 | -0.0256988 | -0.0163307 | -0.0048189 | 0.0073898 |
| 0.0204154 | 0.0348799 | 0.0477657 | 0.0610098 | 0.0794842 | 0.0791141 |
| 0.1165746 | 0.1383858 | 0.1608444 | 0.1835490 | 0.2056909 | 0.2272854 |
| 0.2490747 | 0.2716141 | 0.2944901 | 0.3174704 | 0.3403739 | 0.3624055 |
| 0.3854153 | 0.4083858 | 0.4313503 | 0.4542657 | 0.4771495 | 0.4999999 |
| 0.5395039 | 0.5788838 | 0.6178936 | 0.6562834 | 0.6938090 | 0.7302244 |
| 0.7645295 | 0.7971752 | 0.8279586 | 0.8566948 | 0.8823385 | 0.9058799 |
| 0.9271240 | 0.9459153 | 0.9620984 | 0.9755492 | 0.9861495 | 0.9938051 |
| 0.9984390 | 1.0000000 | 0.0000000 | 0.0000000 | 0.0000000 | 0.0000000 |

Y/C

| | | | | | |
|------------|------------|------------|------------|------------|------------|
| 0.0000000 | -0.0439291 | -0.0876947 | -0.1309448 | -0.1733444 | -0.2145551 |
| -0.2533504 | -0.2901789 | -0.3247655 | -0.3568247 | -0.3851002 | -0.4107795 |
| -0.4336042 | -0.4533602 | -0.4698345 | -0.4828699 | -0.4923149 | -0.4980550 |
| -0.4999999 | -0.4999999 | -0.4999999 | -0.4999999 | -0.4999999 | -0.4999999 |
| -0.5004880 | -0.4961358 | -0.4949743 | -0.4965157 | -0.5057697 | -0.5114841 |
| -0.5181849 | -0.5234605 | -0.5227931 | -0.5178602 | -0.5121495 | -0.4995293 |
| -0.4870098 | -0.4728503 | -0.4561396 | -0.4393857 | -0.4210649 | -0.4027755 |
| -0.3840905 | -0.3643640 | -0.3437046 | -0.3220746 | -0.2999350 | -0.2773307 |
| -0.2547400 | -0.2321455 | -0.2092795 | -0.1862951 | -0.1634546 | -0.1404801 |
| -0.1170353 | -0.0935157 | -0.0700197 | -0.0465000 | -0.0231201 | 0.0000000 |
| 0.0231909 | 0.0460394 | 0.0690197 | 0.0919939 | 0.1148994 | 0.1376947 |
| 0.1599605 | 0.1819841 | 0.2042341 | 0.2265805 | 0.2490747 | 0.2712952 |
| 0.2931043 | 0.3147538 | 0.3364448 | 0.3573306 | 0.3772105 | 0.3966594 |
| 0.4155649 | 0.4334054 | 0.4524644 | 0.4709704 | 0.4846043 | 0.4993896 |
| 0.5114388 | 0.5179999 | 0.5230097 | 0.5255294 | 0.5205452 | 0.5124488 |
| 0.5052302 | 0.5008640 | 0.4998089 | 0.4999999 | 0.5000687 | 0.5055137 |
| 0.5050589 | 0.5053602 | 0.5052793 | 0.5042439 | 0.5024742 | 0.4999999 |
| 0.4984389 | 0.4937401 | 0.4859053 | 0.4749507 | 0.4609094 | 0.4438444 |
| 0.4242952 | 0.4021042 | 0.3774153 | 0.3503856 | 0.3222046 | 0.2919939 |
| 0.2599290 | 0.2261790 | 0.1909507 | 0.1544388 | 0.1168700 | 0.0784606 |
| 0.0394449 | 0.0000000 | 0.0000000 | 0.0000000 | 0.0000000 | 0.0000000 |

(C) SMALL GLAZE ICE SHAPE

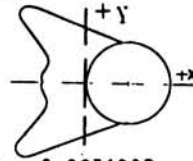
FIGURE 4.1
DEFINITION OF TWO-DIMENSIONAL TEST GEOMETRIES
(PAGE 3 OF 4)

COORDINATES FOR 15 MINUTE GLAZE ICE ACCRETION
(NOTE: DATA FROM NASA - LEWIS)

C = .0508 m = 2.0"

X/C

| | | | | | |
|------------|------------|------------|------------|------------|------------|
| 1.0000000 | 0.9955845 | 0.9822499 | 0.9605452 | 0.9307696 | 0.8934802 |
| 0.8493739 | 0.8019350 | 0.7490787 | 0.6915748 | 0.6303247 | 0.5662991 |
| 0.4999999 | 0.4750000 | 0.4499999 | 0.4250000 | 0.3999999 | 0.3749999 |
| 0.3515000 | 0.3279999 | 0.3044999 | 0.2810000 | 0.2574999 | 0.2339998 |
| 0.2104999 | 0.1869999 | 0.1635000 | 0.1399999 | 0.1164998 | 0.0929999 |
| 0.0695000 | 0.0460000 | 0.0225000 | -0.0010000 | -0.0245000 | -0.0480000 |
| -0.0714999 | -0.0949998 | -0.1184999 | -0.1420000 | -0.1654999 | -0.1890000 |
| -0.2124999 | -0.2359999 | -0.2595000 | -0.2829999 | -0.3064999 | -0.3299999 |
| -0.3534999 | -0.3769999 | -0.4004999 | -0.4239998 | -0.4474999 | -0.4710000 |
| -0.4944999 | -0.5179999 | -0.5415000 | -0.5649999 | -0.6299999 | -0.6599998 |
| -0.6899999 | -0.7200000 | -0.7549999 | -0.7749999 | -0.7749999 | -0.7649999 |
| -0.7499999 | -0.7249998 | -0.6899999 | -0.6599998 | -0.6299999 | -0.5899999 |
| -0.5500000 | -0.5249999 | -0.5049999 | -0.4800000 | -0.4650000 | -0.4499999 |
| -0.4399999 | -0.4250000 | -0.4199999 | -0.4250000 | -0.4349999 | -0.4599999 |
| -0.4800000 | -0.4899999 | -0.4899999 | -0.4899999 | -0.4750000 | -0.4899999 |
| -0.4899999 | -0.4899999 | -0.4800000 | -0.4599999 | -0.4349999 | -0.4250000 |
| -0.4199999 | -0.4250000 | -0.4399999 | -0.4499999 | -0.4650000 | -0.4800000 |
| -0.5049999 | -0.5249999 | -0.5500000 | -0.5899999 | -0.6299999 | -0.6599998 |
| -0.6899999 | -0.7249998 | -0.7499999 | -0.7649999 | -0.7749999 | -0.7749999 |
| -0.7549999 | -0.7200000 | -0.6899999 | -0.6599998 | -0.6299999 | -0.5899999 |
| -0.5415000 | -0.5179999 | -0.4944999 | -0.4710000 | -0.4474999 | -0.4239998 |
| -0.4004999 | -0.3769999 | -0.3534999 | -0.3299999 | -0.3064999 | -0.2829999 |
| -0.2595000 | -0.2359999 | -0.2124999 | -0.1890000 | -0.1654999 | -0.1420000 |
| -0.1184999 | -0.0949998 | -0.0714999 | -0.0480000 | -0.0245000 | -0.0010000 |
| 0.0225000 | 0.0460000 | 0.0695000 | 0.0929999 | 0.1164998 | 0.1399999 |
| 0.1635000 | 0.1869999 | 0.2104999 | 0.2339998 | 0.2574999 | 0.2810000 |
| 0.3044999 | 0.3279999 | 0.3515000 | 0.3749999 | 0.3999999 | 0.4250000 |
| 0.4499999 | 0.4750000 | 0.4999999 | 0.0000000 | 0.0000000 | 0.0000000 |
| 0.5662991 | 0.6303247 | 0.6915748 | 0.0000000 | 0.0000000 | 0.0000000 |
| 0.7490787 | 0.8019350 | 0.8493739 | 0.8934783 | 0.9307696 | 0.9605452 |
| 0.9822499 | 0.9955845 | 1.0000000 | 0.0000000 | 0.0000000 | 0.0000000 |

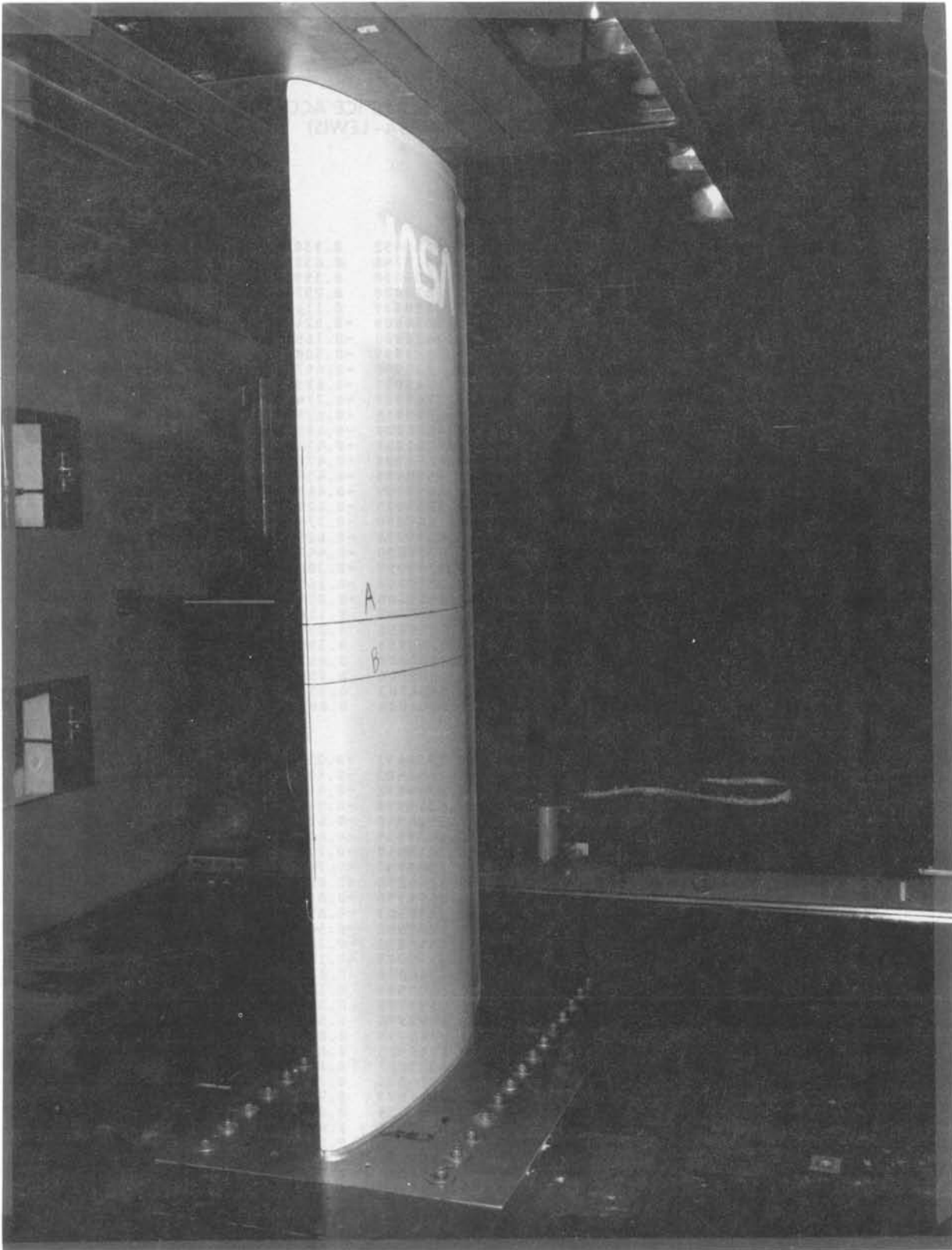


Y/C

| | | | | | |
|------------|------------|------------|------------|------------|------------|
| 0.0000000 | -0.0663148 | -0.1320450 | -0.1946691 | -0.2538443 | -0.3085057 |
| -0.3576849 | -0.3985392 | -0.4335451 | -0.4618403 | -0.4827144 | -0.4955844 |
| -0.4999998 | -0.4999998 | -0.4999998 | -0.4999998 | -0.4999998 | -0.4999998 |
| -0.5092498 | -0.5184999 | -0.5277499 | -0.5369998 | -0.5462497 | -0.5554978 |
| -0.5647499 | -0.5739939 | -0.5832439 | -0.5924940 | -0.6017439 | -0.6109939 |
| -0.6202439 | -0.6294938 | -0.6387440 | -0.6479939 | -0.6572440 | -0.6664939 |
| -0.6757439 | -0.6849939 | -0.6942438 | -0.7034940 | -0.7127439 | -0.7219899 |
| -0.7312400 | -0.7404900 | -0.7497399 | -0.7589900 | -0.7682401 | -0.7774881 |
| -0.7867399 | -0.7959899 | -0.8052400 | -0.8144898 | -0.8237396 | -0.8329887 |
| -0.8422393 | -0.8514891 | -0.8607381 | -0.8699996 | -0.8799985 | -0.8899985 |
| -0.9099994 | -0.8999985 | -0.8799990 | -0.8399983 | -0.8149990 | -0.7749998 |
| -0.7449998 | -0.6999997 | -0.6649999 | -0.6249998 | -0.5899998 | -0.5449998 |
| -0.4949998 | -0.4649999 | -0.4349998 | -0.3949998 | -0.3649998 | -0.3399998 |
| -0.3099998 | -0.2799997 | -0.2449998 | -0.2149999 | -0.1849998 | -0.1499999 |
| -0.1149998 | -0.0899997 | -0.0600000 | -0.0300000 | 0.0000000 | 0.0300000 |
| 0.0600000 | 0.0899997 | 0.1149998 | 0.1499999 | 0.1849998 | 0.2149999 |
| 0.2449998 | 0.2799997 | 0.3099998 | 0.3399999 | 0.3649998 | 0.3949998 |
| 0.4349998 | 0.4649999 | 0.4949998 | 0.5449998 | 0.5899998 | 0.6249998 |
| 0.6649999 | 0.6999997 | 0.7449998 | 0.7749998 | 0.8149990 | 0.8399983 |
| 0.8799990 | 0.8999985 | 0.9099994 | 0.8999985 | 0.8999985 | 0.8699996 |
| 0.8607381 | 0.8514891 | 0.8422393 | 0.8329887 | 0.8237396 | 0.8144898 |
| 0.8052400 | 0.7959899 | 0.7867399 | 0.7774881 | 0.7682401 | 0.7589900 |
| 0.7497399 | 0.7404900 | 0.7312400 | 0.7219899 | 0.7127439 | 0.7034940 |
| 0.6942438 | 0.6849939 | 0.6757439 | 0.6664939 | 0.6572440 | 0.6479939 |
| 0.6387440 | 0.6294938 | 0.6202439 | 0.6109939 | 0.6017439 | 0.5924940 |
| 0.5832439 | 0.5739939 | 0.5647499 | 0.5554978 | 0.5462497 | 0.5369998 |
| 0.5277499 | 0.5184999 | 0.5092498 | 0.4999998 | 0.4999998 | 0.4999998 |
| 0.4999998 | 0.4999998 | 0.4999998 | 0.0000000 | 0.0000000 | 0.0000000 |
| 0.4955844 | 0.4827144 | 0.4618403 | 0.0000000 | 0.0000000 | 0.0000000 |
| 0.4335451 | 0.3985392 | 0.3576849 | 0.3085057 | 0.2538443 | 0.1946691 |
| 0.1320450 | 0.0663148 | 0.0000000 | 0.0000000 | 0.0000000 | 0.0000000 |

(D) LARGE GLAZE ICE SHAPE

FIGURE 4.1
DEFINITION OF TWO-DIMENSIONAL TEST GEOMETRIES
(PAGE 4 OF 4)



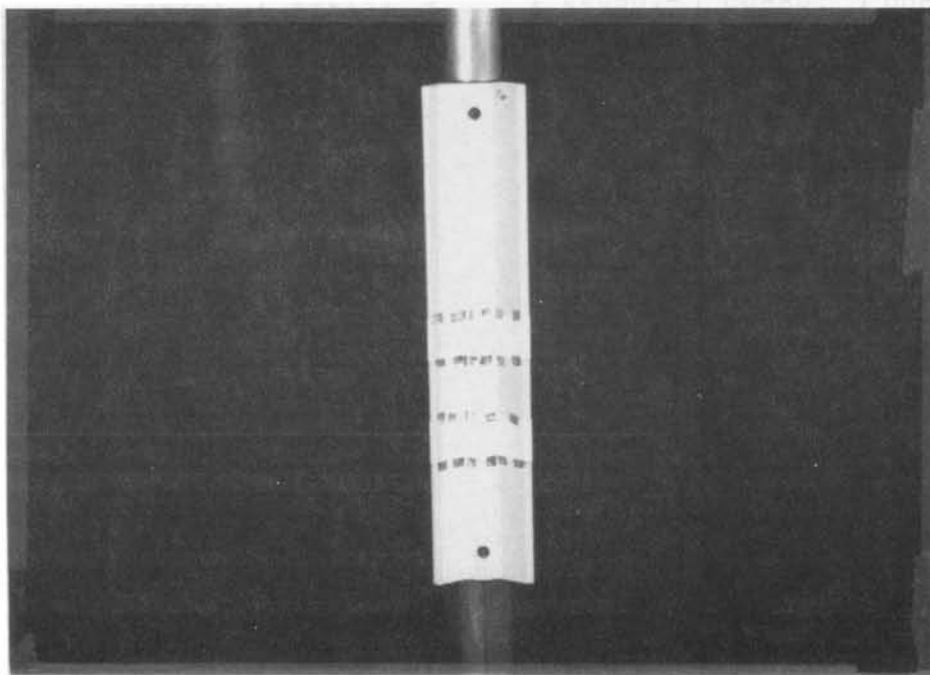
(A) *NLF(1) - 0414* AIRFOIL

FIGURE 4.2

INSTALLATION OF TWO-DIMENSIONAL MODELS IN IRT TEST SECTION
(PAGE 1 OF 2)



(B) SMALL GLAZE ICE SHAPE



(C) LARGE GLAZE ICE SHAPE

FIGURE 4.2
INSTALLATION OF TWO-DIMENSIONAL MODELS IN IRT TEST SECTION
(PAGE 2 OF 2)

| X/C | Y/C UPPER | Y/C LOWER |
|--------|--------------|--------------|
| .00000 | .00099 | .00099 |
| .00200 | .01248 | -.00857 |
| .00500 | .01950 | -.01366 |
| .01250 | .03099 | -.02105 |
| .02500 | .04322 | -.02866 |
| .03750 | .05210 | -.03423 |
| .05000 | .05893 | -.03865 |
| .07500 | .06840 | -.04541 |
| .10000 | .07511 | -.05058 |
| .12500 | .08033 | -.05477 |
| .15000 | .08454 | -.05817 |
| .17500 | .08805 | -.06099 |
| .20000 | .09096 | -.06330 |
| .22500 | .09339 | -.06527 |
| .25000 | .09536 | -.06685 |
| .27500 | .09694 | -.06812 |
| .30000 | .09815 | -.06909 |
| .32500 | .09901 | -.06978 |
| .35000 | .09952 | -.07021 |
| .37500 | .09972 | -.07036 |
| .40000 | .09956 | -.07019 |
| .42500 | .09909 | -.06967 |
| .45000 | .09826 | -.06880 |
| .47500 | .09700 | -.06755 |

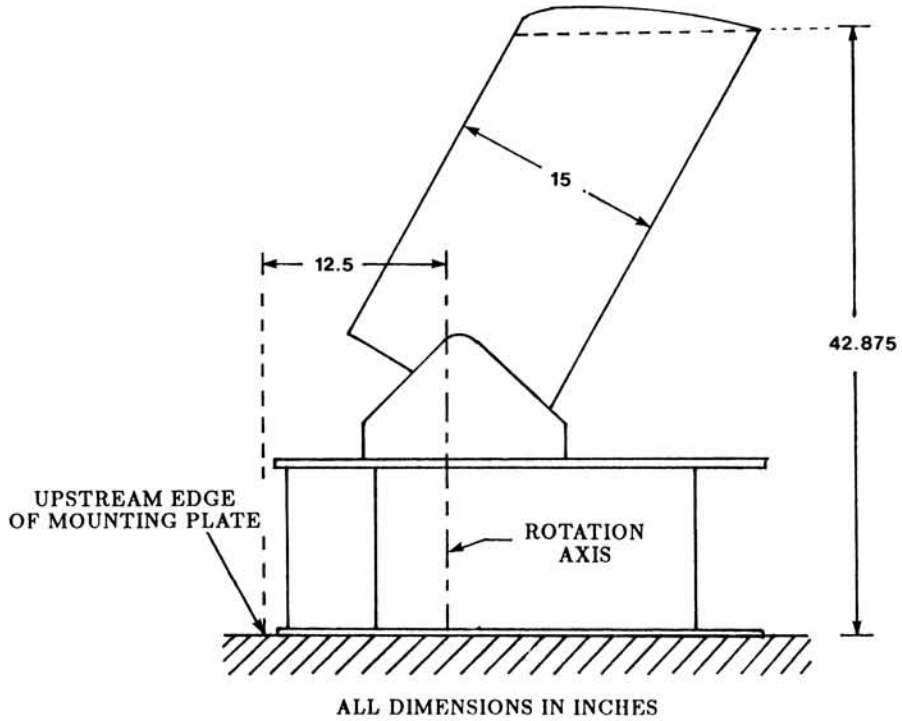
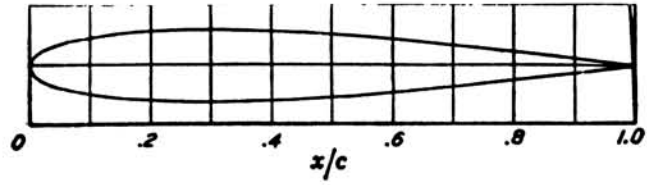
| X/C | Y/C UPPER | Y/C LOWER |
|---------|--------------|--------------|
| .50000 | .09535 | -.06591 |
| .52500 | .09323 | -.06389 |
| .55000 | .09073 | -.06138 |
| .57500 | .08777 | -.05845 |
| .60000 | .08448 | -.05501 |
| .62500 | .08079 | -.05106 |
| .65000 | .07672 | -.04674 |
| .67500 | .07232 | -.04214 |
| .70000 | .06763 | -.03735 |
| .72500 | .06269 | -.03255 |
| .75000 | .05755 | -.02780 |
| .77500 | .05225 | -.02309 |
| .80000 | .04687 | -.01857 |
| .82500 | .04132 | -.01433 |
| .85000 | .03576 | -.01049 |
| .87500 | .03013 | -.00719 |
| .90000 | .02444 | -.00460 |
| .92500 | .01873 | -.00289 |
| .95000 | .01302 | -.00232 |
| .97500 | .00720 | -.00324 |
| 1.00000 | .00125 | -.00597 |
| | | |
| | | |
| | | |

(A) MS(1) – 0317 30° SWEEP AIRFOIL

FIGURE 4.3

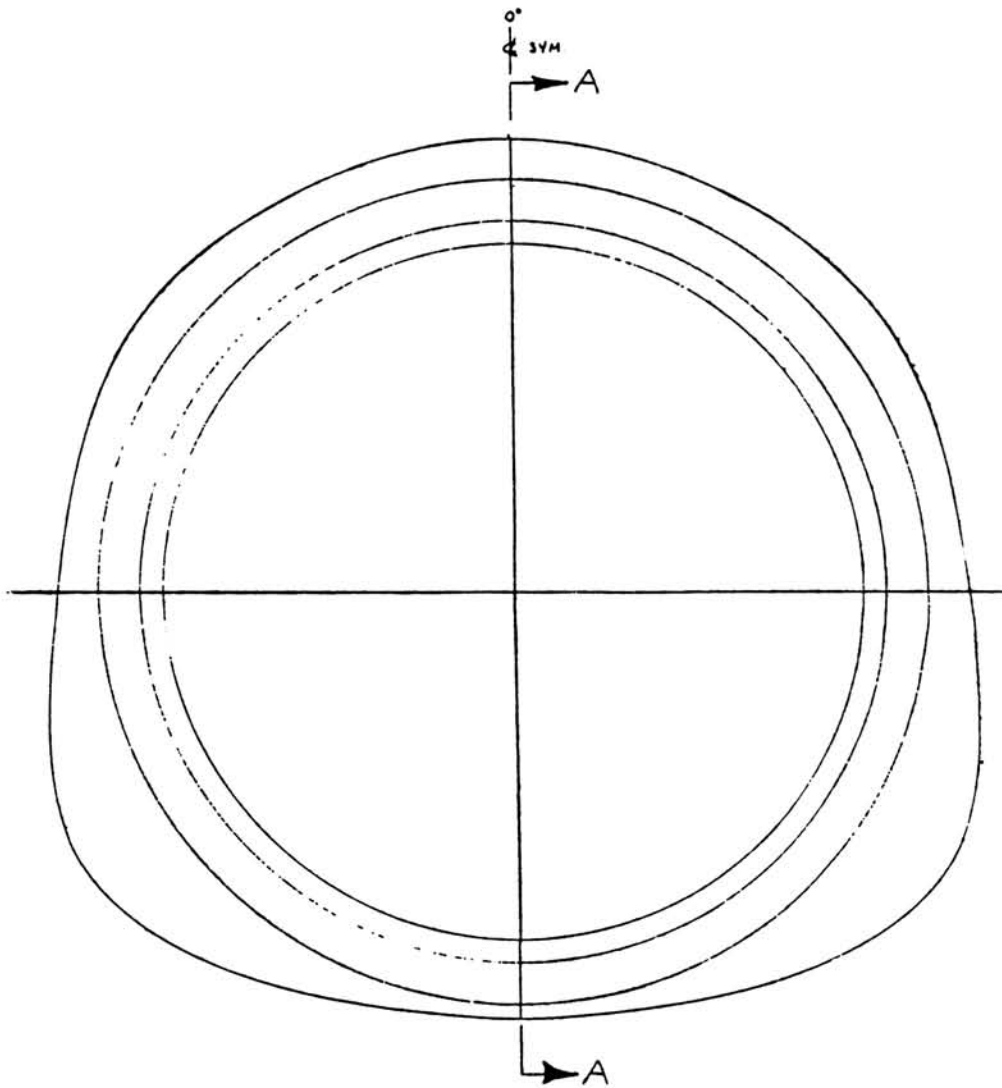
DEFINITION OF THREE-DIMENSIONAL TEST GEOMETRIES
(PAGE 1 OF 5)

| x (per cent c) | y (per cent c) |
|------------------------|------------------------|
| 0 | 0 |
| 0.5 | |
| 1.25 | 1.894 |
| 2.5 | 2.615 |
| 5.0 | 3.555 |
| 7.5 | 4.200 |
| 10 | 4.683 |
| 15 | 5.345 |
| 20 | 5.737 |
| 25 | 5.941 |
| 30 | 6.002 |
| 40 | 5.803 |
| 50 | 5.294 |
| 60 | 4.563 |
| 70 | 3.664 |
| 80 | 2.623 |
| 90 | 1.448 |
| 95 | 0.807 |
| 100 | 0.126 |



(B) NACA 0012 30° SWEEP WING TIP

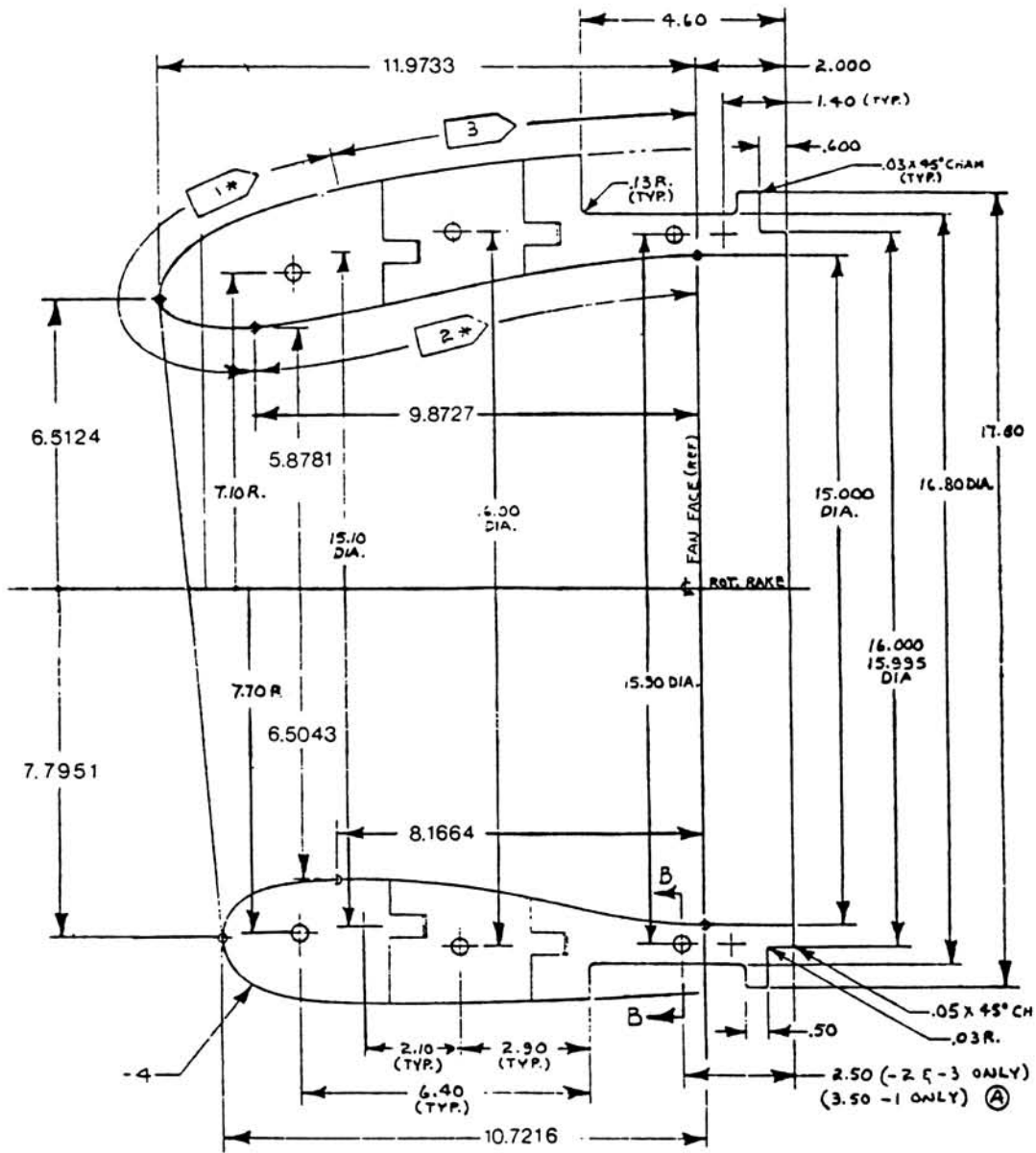
FIGURE 4.3
DEFINITION OF THREE-DIMENSIONAL TEST GEOMETRIES
(PAGE 2 OF 5)



(C) 737-300 BOEING ENGINE INLET - FRONT VIEW

FIGURE 4.3

DEFINITION OF THREE-DIMENSIONAL TEST GEOMETRIES
(PAGE 3 OF 5)



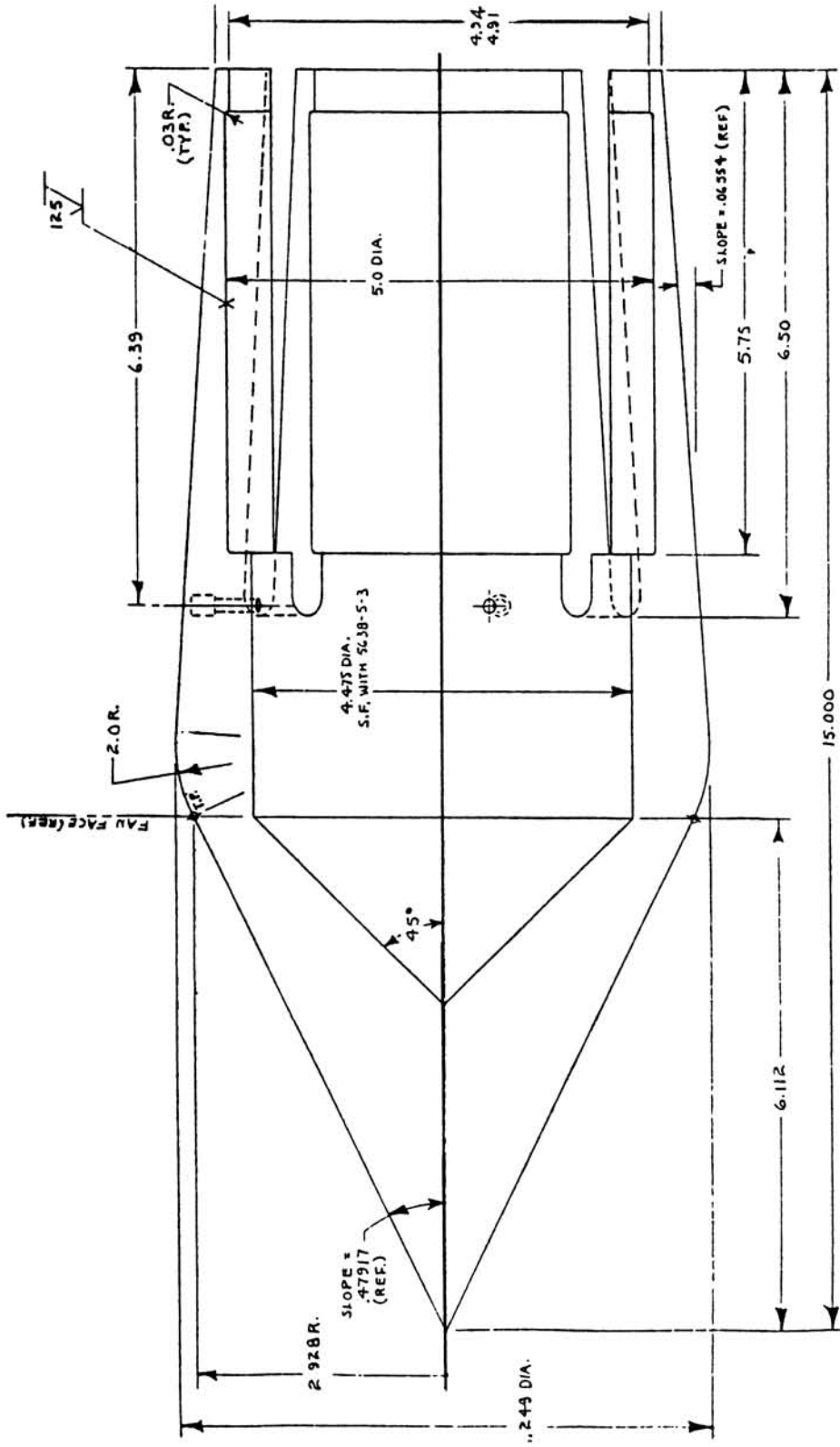
SEC A-A

All dimensions in inches

(D) 737-300 BOEING ENGINE INLET - CROSS SECTION

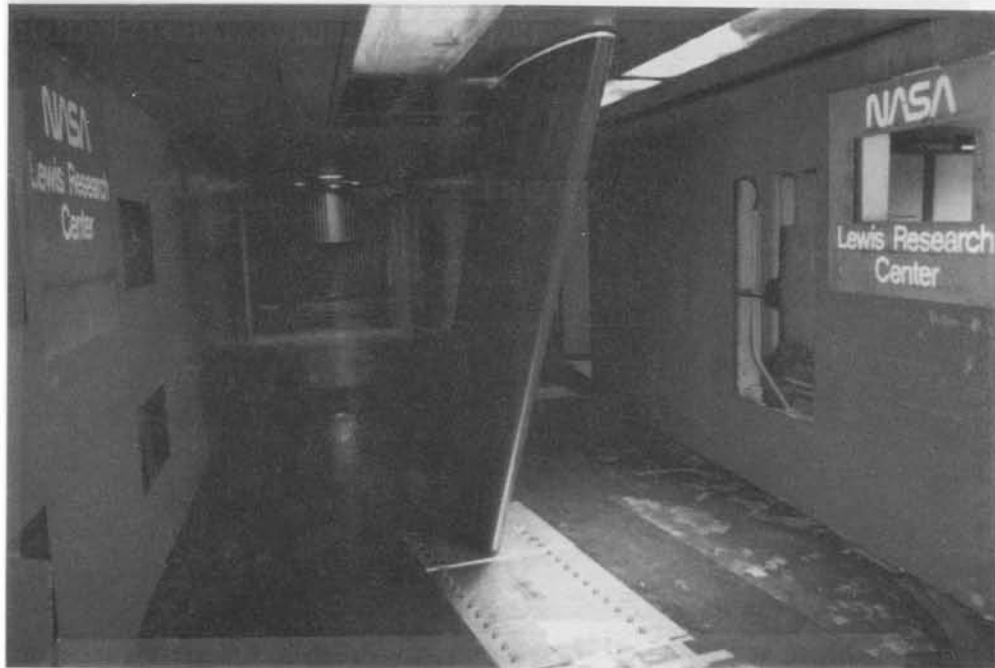
FIGURE 4.3

DEFINITION OF THREE-DIMENSIONAL TEST GEOMETRIES
(PAGE 4 OF 5)

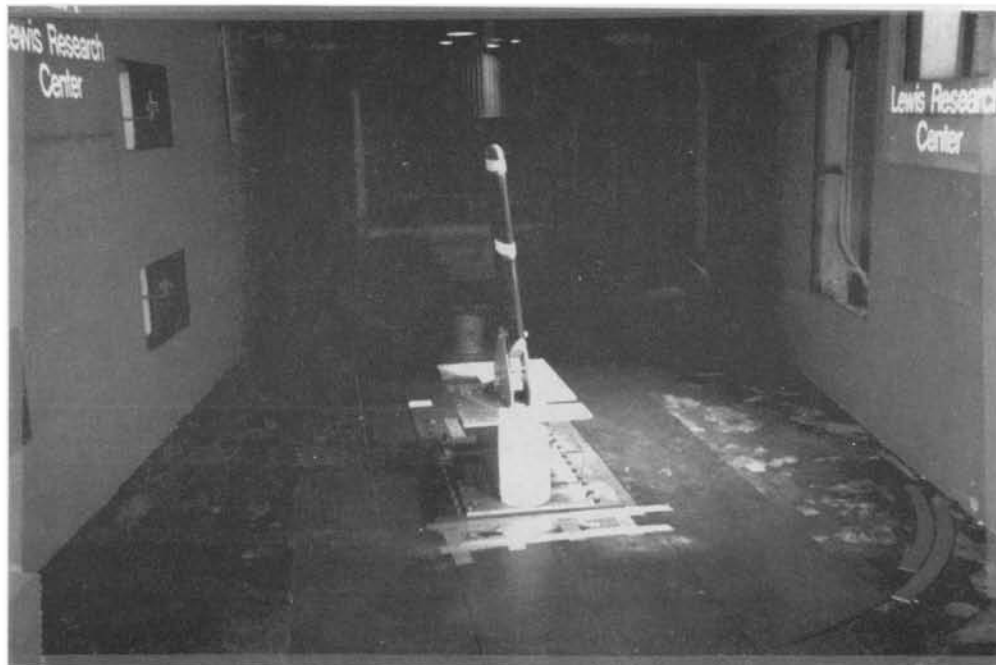


(E) 737-300 BOEING ENGINE INLET - CENTER BODY

FIGURE 4.3
DEFINITION OF THREE-DIMENSIONAL TEST GEOMETRIES
(PAGE 5 OF 5)



(A) *MS(1)* – 0317 30° SWEPT AIRFOIL

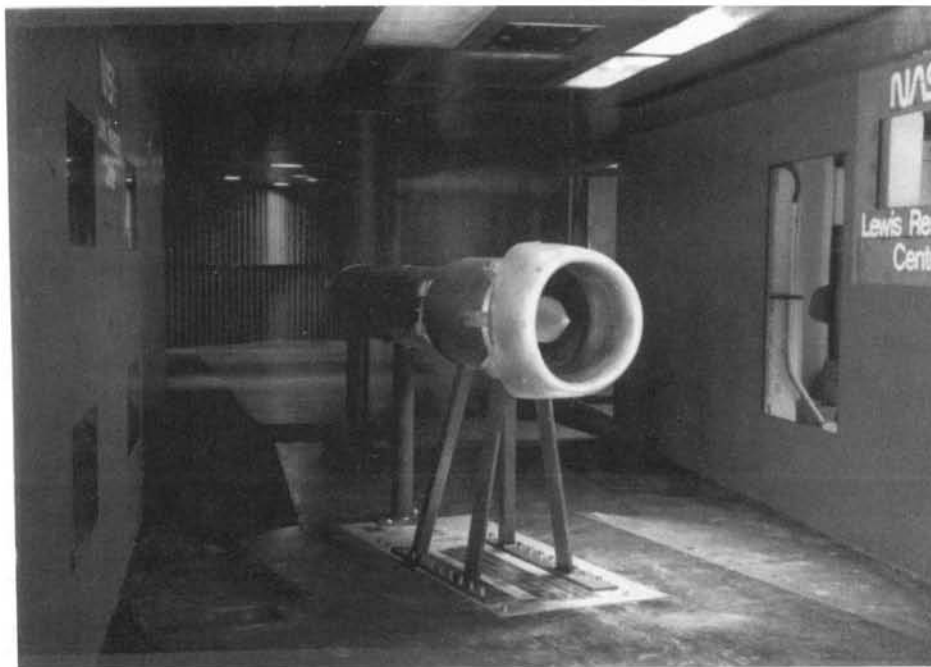
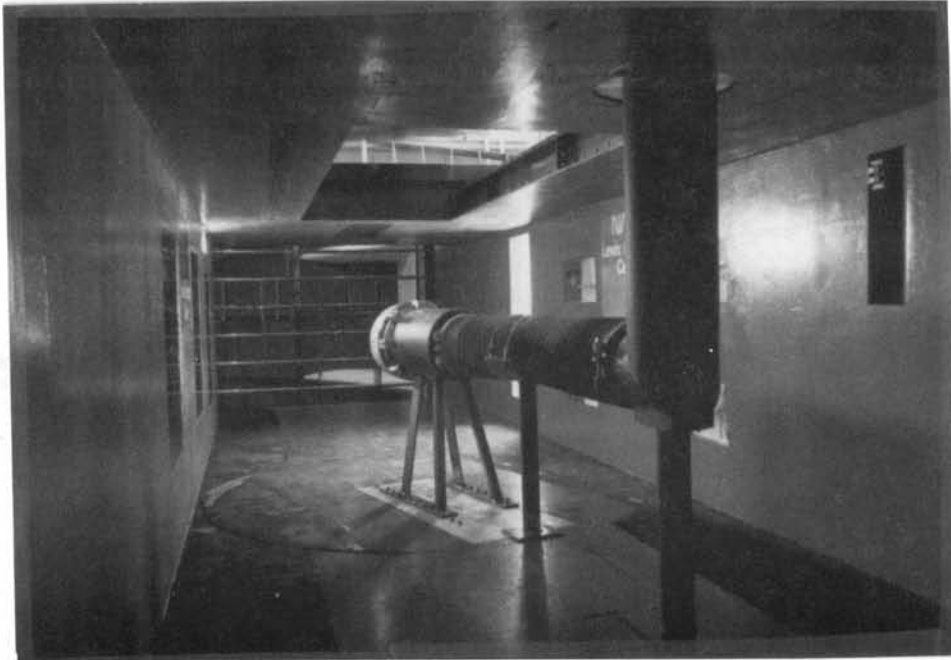


(B) NACA 0012 30° SWEPT WING TIP

FIGURE 4.4

INSTALLATION OF THREE-DIMENSIONAL TEST MODELS
IN IRT TEST SECTION

(PAGE 1 OF 2)



(C) 737-300 BOEING ENGINE INLET

FIGURE 4.4
INSTALLATION OF THREE-DIMENSIONAL TEST MODELS
IN IRT TEST SECTION
(PAGE 2 OF 2)

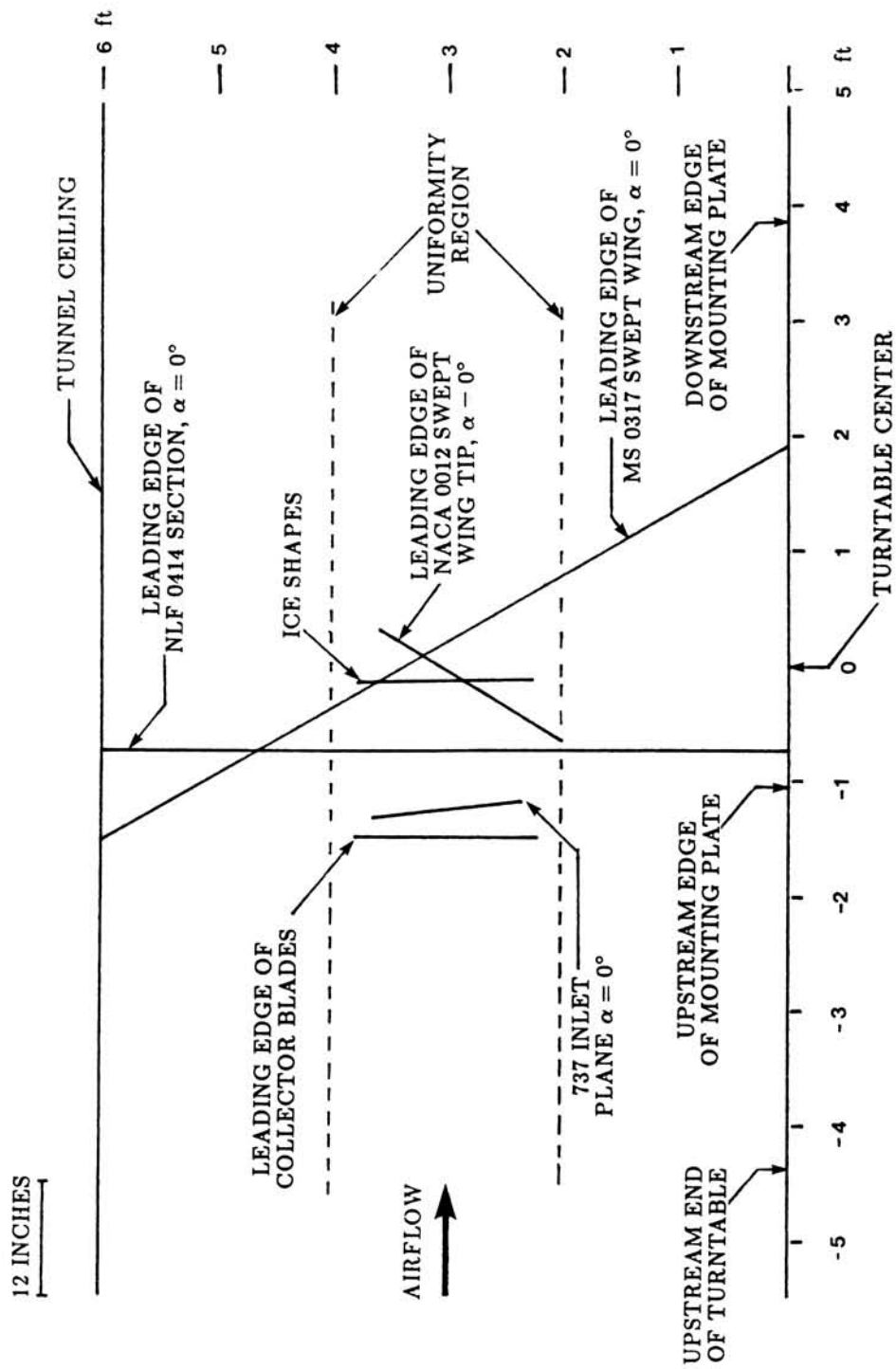


FIGURE 4.5
AXIAL LOCATIONS OF TEST MODELS IN IRT TEST SECTION

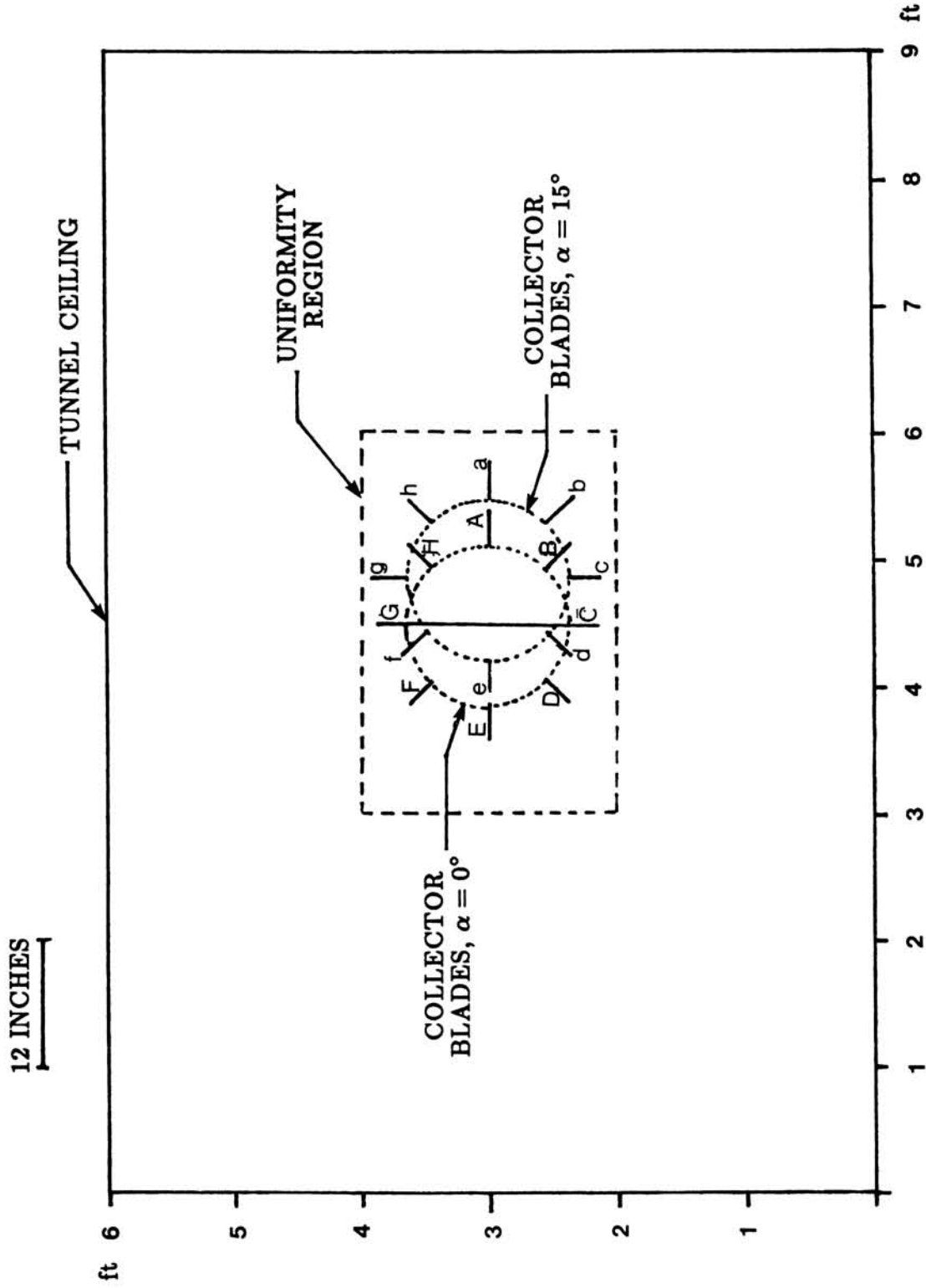


FIGURE 4.6
 LOCATION OF REFERENCE COLLECTOR IN IRT TEST SECTION
 (LOOKING DOWNSTREAM)

5.0 DATA REDUCTION METHOD

The laser reflectance method used to reduce the 1989 impingement data is detailed in Ref. 10. In summary, the reflectance method is based on the assumption that the reflectance of the dyed paper is a measure of the dye mass per unit area of the paper. Dyed regions on the blotter strip corresponding to high impingement rates are darker in color and reflect less light than those corresponding to low impingement rates. Regions with no dye accumulation are white and reflect the maximum amount of laser light. The relation between dye concentration and laser reflectance is not linear and is determined from calibration tests. To maximize the sensitivity of the reflectance method, the dye used in the tests must have a strong absorption at the wavelength of the laser radiation. This is accomplished by using a blue dye whose maximum absorption occurs at 629.5 nm, which is very close to the wavelength (632.8 nm) of the red He-Ne laser employed in the data reduction system.

5.1 Reflectance Calibration Curve

The laser reflectance calibration curve relates laser reflectance to dye mass on the blotter strip. The curve is a standard against which the reflectance of each blotter strip is compared during the data reduction process. If the type of dye, the blotter paper and the laser instrumentation remain constant the curve does not change.

Due to minor changes made to the laser reflectometer system a new calibration curve was produced for the analysis of all 1989 test data. To produce the new laser reflectance calibration curve a series of tests were performed in the IRT during the 1989 test period. In each of these tests a large square of blotter paper was placed on the uniformity grid and was exposed to the spray cloud for a short period of time. By varying the time exposure to the spray cloud blotter squares with various color intensities were obtained. Blotter samples were cut from each large blotter square. The reflectance and dye mass for each of the samples was measured using the laser and absorption spectroscopy methods respectively. The dye mass from each blotter sample was then divided by the area of the sample and the reflectance of each sample was normalized by the reflectance of the white blotter paper. A total of 19 dyed blotter samples of various areas were used to define the 1989 laser calibration curve. Raw and normalized calibration data are given in table 5.1. The 1989 and 1985 laser calibration curves are shown in Fig. 5.1. Both calibration curves show similar trends.

5.2 Automated Data Reduction System

The laser reflectometer and data acquisition system used for the analysis of the 1985 impingement data were also utilized for the current tests. A block diagram of the complete data reduction system is presented in Fig. 5.2. Details of the design aspects of the system are given in Ref. 10. A brief description of the data reduction system is provided below.

The main components of the reflectometer are (a) a red He-Ne laser used to scan the blotter strips, (b) a rotating drum for mounting the blotter strips, (c) a convergent lens

for collecting the reflected light, and (d) a photodetector which converts the reflected light collected by the lens into a voltage (V_1) which is stored for further analysis. A splitter glass plate and another photodetector are also shown and are used to monitor fluctuations in laser output. The voltage (V_2) from the second photodetector is also stored and is used in the data analysis.

The digital data acquisition system controls the operation of the reflectometer and is used to analyze and plot the data. The main components of this system are a desk top computer with two disk drives, a plotter and a printer, and two voltmeters for monitoring the voltages from the photodetectors.

5.3 Data Reduction Process

The reduction of the impingement data was performed in two main steps. During the first step reflectivity values were extracted from the dyed blotter strip and were stored in the form of voltages on disk. During the second step the reflectivity values were transformed into plots of impingement efficiency versus surface distance measured with respect to some reference point on the model.

To extract the impingement data from a single blotter strip, the strip was mounted on the drum of the laser reflectometer and one to three horizontal scans were obtained depending on blotter strip geometry. Straight strips were scanned at three different horizontal locations. Curved strips were scanned at one horizontal location. Curved strips were required for the swept MS-0317 airfoil and the swept wing tip in order to fit these geometries along constant streamwise sections. Because the whole strip could not be mounted on the drum these strips had to be scanned in small sections and hence were much more difficult to analyze. The data from each section of each curved strip were stored in different files which had to be combined into a single file for final analysis (see Appendix A).

For each scan the voltages V_1 and V_2 from the two photodetectors were recorded and stored on disk. The reflectometer takes 47 reflectivity readings per inch of each horizontal scan at equal space intervals.

To transform reflectivity into a plot of impingement efficiency versus surface distance, the following steps were used:

1. The raw reflectivity values were divided by the reflectivity of the bare blotter paper to obtain normalized reflectivity data. The following equation was used for each data point of the dyed blotter paper

$$R_{norm} = \frac{(V_1/V_2)_{DyedBlotterPaper}}{(V_1/V_2)_{BareBlotterPaper}} \quad (5 - 1)$$

Note that $(V_1/V_2)_{BareBlotterPaper}$ is the average of 1000 data points measured on a reference blotter strip.

2. The normalized reflectivity data were converted into dye mass per unit area using the laser calibration curve.

3. The impingement efficiency value for each data point recorded was obtained from the following equation.

$$\bar{\beta} = \frac{\text{Dye mass per unit area corresponding to a given data point}}{\text{Average mass per unit area of reference collector}} \times \bar{\beta}_{\text{Collector}} \quad (5 - 2)$$

This equation is valid if the collector and the model have been exposed to sprays of identical duration, as is the case here.

All collector strips were analyzed prior to the analysis of the test model strips. Each collector strip was scanned and an average mass per unit area was calculated for the strip. This value was used as the denominator in eq. (5-2). The value of $\bar{\beta}_{\text{Collector}}$ depends on the MVD of the spray cloud and on cloud droplet distribution. The MVD's of the spray clouds used in the current tests were $16\mu\text{m}$ and $20\mu\text{m}$. The corresponding theoretical collector efficiency values were 0.86 and 0.89.

5.4 Laser Reflectance Method Error Analysis

The repeatability and accuracy of the laser reflectance method depends on the accuracy of the laser reflectance calibration curve, the stability of the laser output power, the uniformity of blotter paper composition, the degree of dye penetration into the blotter paper, and the dye concentration range over which data are collected. These factors are discussed below.

The dye concentration values for the data points used in defining the laser reflectance calibration curve were obtained by absorption spectroscopy. The accuracy of this method was verified by analyzing several samples of dye solution of known concentrations. These concentrations were in the range of 200 to 500 milligrams of dye per liter of water. Absorption spectroscopy reproduced the concentrations of the sample solutions accurate to within .6 milligram/liter (i.e., $\pm 0.3\%$).

To further validate the calibration method, groups of dyed blotter samples with nearly identical reflectance values were produced and analyzed by absorption spectroscopy. Results from this test are shown in Table 5.1.

The relation between normalized reflectance and dye mass is monotonic; dye mass per unit area increases as reflectance is decreased. The results of Table 5.1 can be used to determine an estimate for the uncertainty in the calibration curve. Upon close examination of the data it is seen that in some cases blotter samples with identical reflectivity values differ in dye mass by less than 2% from the average mass. Also, samples for which absorption spectroscopy produced identical dye concentrations differ in reflectivity by less than 2% from the average reflectivity. It is reasonable to conclude that the uncertainty in the calibration curve is of the order of 2%.

During the early stages of the development of the laser reduction method, it was found that the output light intensity of the laser beam varied significantly over long periods of time. Since the light reflected from the blotter paper is a direct function of the incident light, the laser fluctuations must be monitored and taken into account during the data

reduction. First, the He-Ne laser used in the preliminary studies was replaced with a polarized He-Ne laser. Experience indicates that polarized lasers give a more stable output. Second, optical feedback was incorporated to monitor any remaining fluctuations in laser power. During the data reduction, the effect of laser power fluctuations is essentially eliminated by using the ratio of the collected signal to the feedback signal as explained in section III. The optical feedback design was tested by scanning a reference bare blotter strip a number of times over a period of several months. Each time 400 reflectance measurements were obtained and the average of the 400 data points was evaluated. The standard deviation of these averaged reflectance values was found to be $\pm 0.3\%$.

The uniformity of the reflectivity of an unsprayed (bare) piece of blotter paper was measured by scanning 200 points at five horizontal locations. The variation in reflectance was $\pm 1.3\%$ from the average value based on 1000 (5×200) reflectance measurements. This variation in reflectance is due to the roughness of the paper itself and due to variation in the composition of the blotter paper.

Penetration of dye into the blotter paper should be avoided because the data reduction is based on surface reflectance measurements. This was accomplished by keeping the spray time short. A series of tests were performed to establish the optimum spray time for each droplet size used in the actual impingement experiments. During these tests blotter strips were exposed to sprays of various time durations. After each test the penetration of dye into the paper was examined using a microscope. Spray times of the order of 3 to 5 seconds produced penetrations of the order of 10% of the blotter thickness. This level of penetration was acceptable and did not affect the quality of the data.

The discussion above indicates that the error in measuring reflectance is of the order of 2%. The corresponding error in extracting the dye mass per unit area of blotter paper needs to be determined. Let the absolute error in reflectance be dR . The absolute error in dye mass per unit area dC is a function of R and dR where R is the normalized reflectance. For R values close to 1 a given dR has a small dC associated with it. Near the low end of the reflectivity axis (e.g. for R values near 0.3) the same value of dR produces a large dC . In both cases the percent error in dye mass per unit area (dC/C) is large. In the first case dC is small, but C is also very small, so the ratio dC/C is large. In the second case dC is large, while C has some finite size, so the ratio dC/C remains large. Between these extremes there is a region where dC/C is reduced to a minimum. This region of low values in dC/C corresponds to a certain range of absolute normalized reflectivity. This range of reflectivity is determined by differentiating R with respect to C and plotting dC/C as a function of R . The calibration curve is first approximated with cubic splines and the differentiation is performed numerically. Plots of dC/C versus R for $dR = 0.01, 0.02$ and 0.03 are given in Fig. 5.3. To maintain, for example, the percent error in the measurement of dye mass per unit area to less than 10%, assuming 1% error in normalized reflectance (i.e., $dR = 0.01$), the normalized reflectance of the dyed blotter paper must be in the range of 0.57 to 0.90. We also note that to obtain reflectance values within the required range the concentration of the dye solution and the duration of the spray must be chosen carefully.

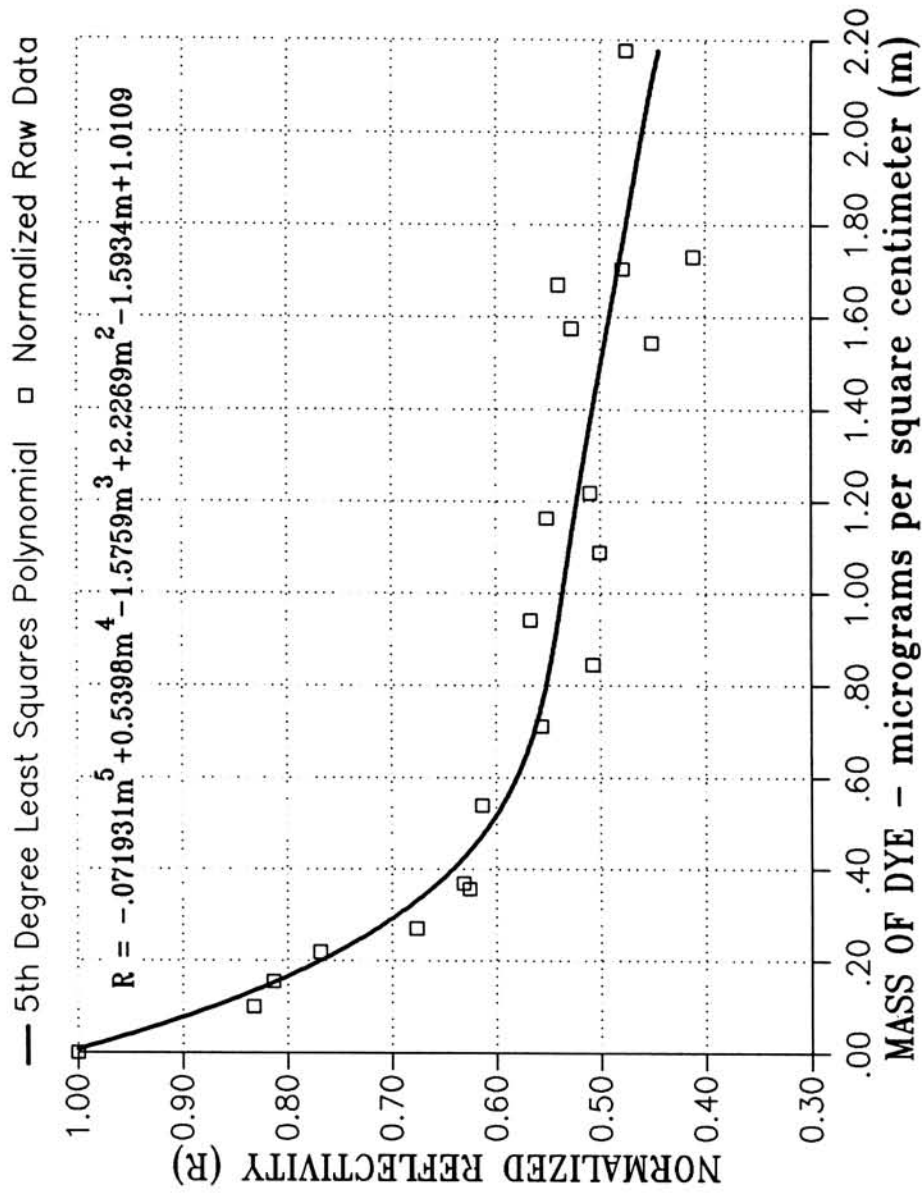


FIGURE 5.1
STANDARD LASER CALIBRATION CURVE

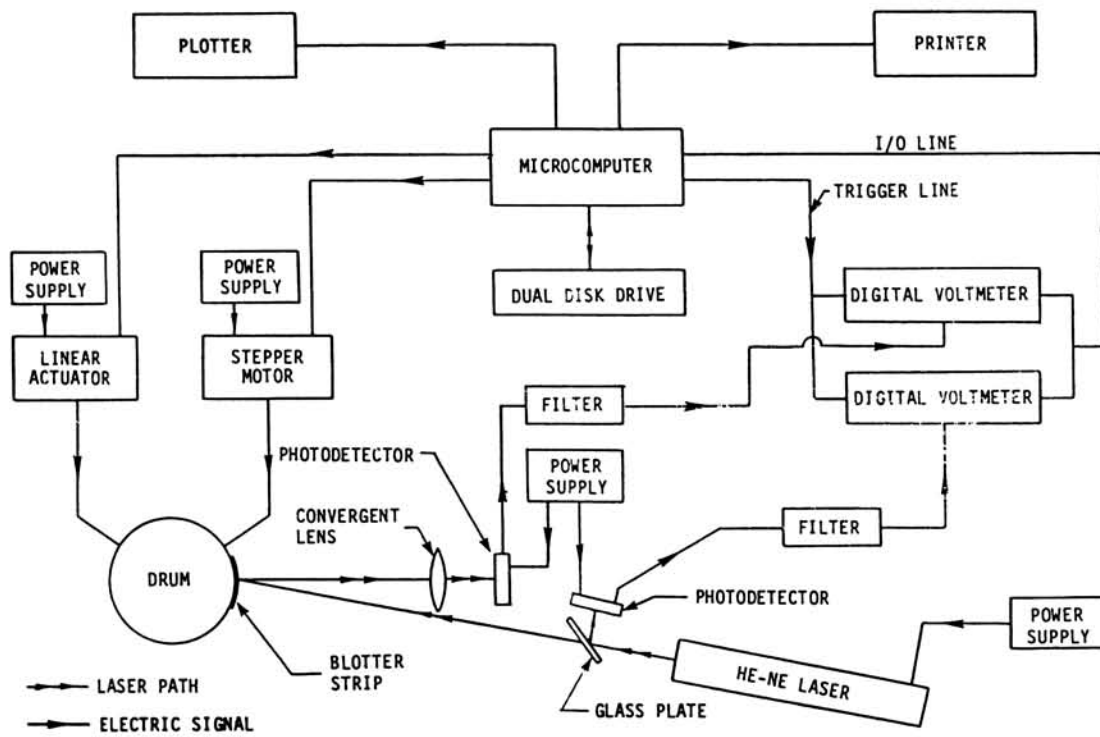


FIGURE 5.2

BLOCK DIAGRAM OF DATA REDUCTION SYSTEM

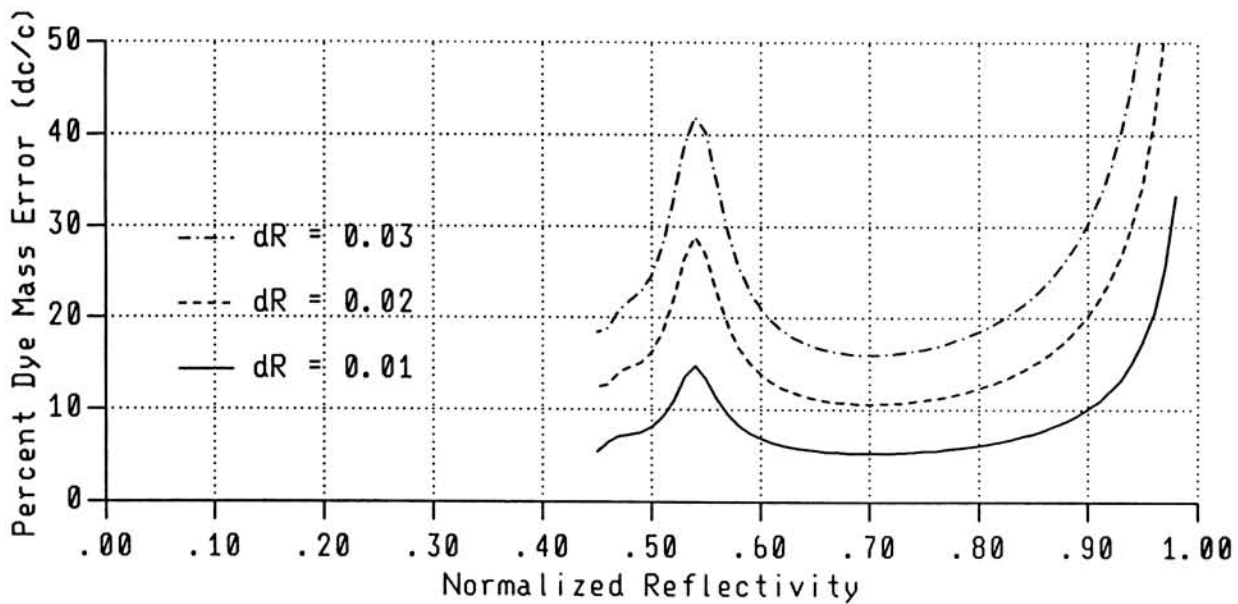


FIGURE 5.3

PLOT OF dC/C AS A FUNCTION OF NORMALIZED REFLECTIVITY

6.0 ANALYSIS METHODS

Computer codes to predict the local impingement efficiency of two-dimensional geometries have been available since the 1940s. More recently, three-dimensional codes have been developed to predict the local impingement efficiency distribution of complex geometries. These codes are currently used in the design of de-icing and anti-icing systems of modern aircraft.

Analysis data presented in this report have been obtained by two- and three-dimensional trajectory computer codes. In these codes the calculation of water impingement involves the following main steps:

- Body surface definition
- Calculation of the flow field
- Droplet trajectory calculation
- Calculation of local impingement efficiency as a function of surface distance.

Brief descriptions of the computer codes used to produce the analysis impingement data presented in Section 7 are given below.

6.1 Two-Dimensional Analysis Code

A trajectory computer code from Boeing Military Airplanes (Ref. 15) were used to produce analysis data for the NLF-0414 airfoil. In this code the surface geometry definition is a cubic spline fit between user specified points. The flow field is generated using a finite difference formulation of the compressible streamfunction equation. Droplet trajectories are calculated by solving equation (2 – 1) by a modified Euler scheme, for each droplet size of the discrete distribution given in Fig. 2.1. Local impingement efficiency is calculated using the a two-dimensional version of the method described in Section 6.2 below.

6.2 Three-Dimensional Analysis Code

Analysis impingement data for the Boeing 737-300 inlet were obtained using a Boeing trajectory computer code. The three-dimensional analysis follows the same basic steps as the two-dimensional analysis code described in Section 6.1.1. The aircraft surface is defined by bi-cubic splines that provide a smooth and well defined surface (Ref. 16). The flow field is obtained by a full potential code (Ref. 17). The potential flow velocity is calculated at both mesh intersections and mesh-surface intersections.

Individual water droplets, whose size is determined from the distributions measured experimentally (see Fig. 2.1), are traced to their point of impingement on the body surface. Droplet trajectories are calculated by solving equation (2 – 1) by a variable step 4th order Adams predictor corrector method (Refs. 1,18). At each computed trajectory position, the potential flow computational mesh cell is located and the flow velocity at that position

is linearly interpolated from the cell corner velocities. This is true for all flow field cells. For cells intersecting the body surface a least squares technique is used to determine local velocities.

The impingement efficiency $\bar{\beta}$ is evaluated numerically as the ratio of impinging surface particle flux to the freestream flux. The local value of $\bar{\beta}$ for each point on the body surface is simply the ratio of that infinitesimal area at freestream to the corresponding impingement area at the surface as shown in Fig. 2.2.

7.0 RESULTS AND DISCUSSION

Experimental water droplet impingement data for all geometries tested are presented in this section. Analysis impingement data are also presented for the NLF(1)-0414 airfoil and the Boeing 737-300 engine inlet. All data are in the form of local impingement efficiency plotted versus surface distance (β - curve). Surface distance is measured with respect to a reference point termed the highlight. For all test models except ice shapes, the highlight point is the most forward (upstream) point on the geometry at an angle of attack of zero degrees. This point is also used as the reference point for all other angles of attack. For airfoil and wing geometries the surface distance is negative along the upper surface and positive along the lower surface. For the engine inlet, positive surface distance is along the inlet inner surface while negative surface distance corresponds to the inlet outer surface. The highlight locations and surface distance conventions for airfoils, ice shapes and inlet are summarized in Figs. 7.1 and 7.2. The main features of each β - curve are:

1. Curve overall shape
2. Magnitude and location of peak efficiency
3. Extent of impingement limits

All experimental curves presented were obtained by averaging data from several blotter strips. In some cases experimental data from as many as ten blotter strips were used to produce a single averaged impingement curve. Consider for example the large glaze ice shape. Five test runs were performed for this geometry at identical test conditions. During each run two blotter strips were attached to the surface of the ice shape giving a total of ten blotter strips per test condition. For most geometries five test runs at identical test conditions were performed (see Table 4.1). By repeating each test several times and averaging the results, small fluctuations in tunnel conditions and spray system performance are averaged out.

The blotter strips used to produce each averaged impingement curve are given at the top of each curve. The notation used to identify each strip is as follows:

RUN G E AA BS

where,

1. RUN indicates the run number
2. G indicates the type of geometry. Possible values for G are: N for NLF(1) – 0414, I for Ice shapes, M for MS(1)-0317, W for Wing Tip and 3 for 737-300 inlet.
3. E indicates the collector efficiency. A value of 6 corresponds to a collector efficiency of 0.86 and an MVD of $16 \mu m$. A value of 9 corresponds to a collector efficiency of 0.89 and an MVD of $20 \mu m$.

4. AA is the Angle of Attack with possible values of 0, 8 and 15 degrees.
5. BS indicates the blotter strips used in the averaging process. For each geometry tested blotter strips were attached to the geometry at several locations identified by capital letters. Blotter strips used and corresponding locations for all geometries tested are given below.
 - a . *NLF*(1) – 0414 - Blotter strips A and B corresponding to locations along the airfoil span at 36 and 32 inches above the tunnel floor respectively.
 - b . ICE SHAPES - Blotter strips A and B corresponding to locations along the span of each ice shape at 36 and 32 inches above the tunnel floor respectively.
 - c . *MS*(1) – 0317 - Blotter strips A and B corresponding to locations along the wing span at 36 and 32 inches above the tunnel floor respectively.
 - d . WING TIP - Blotter strip A at the wing tip and blotter strips B and C corresponding to locations along the wing span at 42 and 32 inches above the tunnel floor respectively.
 - e . 737-300 engine inlet - Blotter strips A, B, C, D, E, F, G and H at 45 degrees intervals from the inlet upper lip. Strip A corresponds to $\theta = 0^\circ$ and strip H corresponds to $\theta = 315^\circ$ (see Fig. 3.7B).

Consider for example Figure 7.29A2. The strip identification numbers shown at the top of this figure are 1773900BH and 1783900BH. These IDs indicate that four strips were used to produce the average impingement curve, the B and H strips of runs 177 and 178 of the 737-300 inlet tested at an angle of attack of 0 degrees and an MVD of $20 \mu m$.

All experimental data have been smoothed using a three point moving average algorithm. The smoothing technique was applied to each individual $\bar{\beta}$ - curve prior to averaging.

For airfoil, ice shapes and wing geometries the impingement limits on the upper surface and lower surfaces are given by $S_{U_{max}}$ and $S_{L_{max}}$ respectively. For engine inlets the impingement limit on the inner is given by $S_{I_{max}}$ while that on the outer surface is given by $S_{O_{max}}$. Values for the impingement limits are provided with each averaged impingement curve. These values were obtained by comparing the results from the laser reflectance method with measurements of the extent of dye on each blotter strip based on visual inspection. The reader is cautioned, however, that the numerical values of the impingement limits are approximate because the extent of water impingement cannot be determined precisely from the experimental results. The uncertainty in locating the limits of impingement is partly due to experimental conditions which varied somewhat between repeated runs as discussed above and partly due to the data reduction process. The reflectance measurements obtained from the laser reflectometer were normalized by the reflectance

value of the bare blotter paper before they were converted into dye mass using the method described in section 5.3. Although, the bare blotter paper has nearly uniform reflectance properties, small variations do exist. These variations make the prediction of the exact locations of the impingement limits difficult. To verify the impingement limits given by the laser reflectance method all blotter strips were also inspected visually. The impingement limits were obtained by measuring the distance from the highlight to the point where no significant amount of dye could be detected by the naked eye.

The modified inertia parameter, $K_{0_{mvd}}$, given in the figures was calculated from the following formula:

$$K_{0_{mvd}} = K \frac{\lambda}{\lambda_s}$$

where the inertia parameter, K , was defined in equation (2 – 1) and λ/λ_s is a function of Reynolds number based on MVD and is the ratio of the true range of droplet as projectile injected into still air to the range of droplet as projectile following Stoke's law. The values of λ/λ_s were obtained from the following fourth degree polynomial which is a close fit of the curve given in Fig. 6 of Ref. 7.

$$\frac{\lambda}{\lambda_s} = -0.022466X^4 + 0.20109X^3 - 0.59067X^2 + 0.36072X + 0.74544$$

$$X = \log_{10} Re_{mvd}, \quad 6 \leq Re_{mvd} \leq 1000$$

In calculating the inertia parameter, K , the following reference lengths were used:

1. NLF(1)-0414 airfoil, $L = 36$ inches
2. Small and Large Glaze Ice Shapes, $L = 2$ inches (cylinder diameter)
3. MS(1)-0317 airfoil, $L = 36$ inches
4. NACA 0012 Wing Tip, $L = 15/\cos(30) = 17.32$ inches
5. Boeing 737-300 Inlet , $L = 15$ inches (diameter at compressor face)

All analysis data presented in this section have been obtained using the experimental droplet distributions given in Tables 2.1 and 2.2. Analysis calculations were performed with the codes discussed in section 6.

7.1 Test Repeatability Results

Test repeatability for all models tested is demonstrated in Figs. 7.3 through 7.10. These figures indicate that in most cases the largest variation in $\bar{\beta}$ takes place at the point of maximum impingement efficiency. The curves presented in Figs. 7.3-7.10 can be used to establish error bounds for the experimental data.

The formula below provides a conservative estimate of test repeatability based on the variation in $\bar{\beta}_{max}$ for repeated tests.

$$Test\ Repeatability\ \% = \pm \frac{0.5(\bar{\beta}_{max\ maximum\ of\ all\ runs} - \bar{\beta}_{max\ minimum\ of\ all\ runs})}{\bar{\beta}_{max\ average\ of\ all\ runs}}$$

A percentage of less than 20 % will be regarded as low, and will be considered to be indicative of good test repeatability.

It must be noted that the above equation establishes an upper error bound for the experimental data based on a single point on each impingement curve, the point of maximum impingement efficiency. In general, all other points on each impingement curve vary to a lesser degree from the corresponding points on the average impingement curve. Thus, the equation above provides a conservative estimate of test repeatability.

For the NLF(1)-0414 airfoil test repeatability was approximately $\pm 25\%$ from the average impingement curve (Figs. 7.3 and 7.4). The repeatability for the case of $\alpha = 8^\circ$, $MVD = 16\ \mu m$ was $\pm 41\%$ from the average, and indicates that there is a problem with the experimental data in this case.

Test repeatability for the large and small glaze ice shapes was $\pm 31\%$ and $\pm 24\%$ respectively (see Figs. 7.5 and 7.6).

Typical repeatability results for the MS(1)-0317 swept airfoil are provided in Fig. 7.7 and indicate that the individual impingement curves vary by $\pm 17\%$ from the average.

For the NACA 0012 swept wing tip test repeatability was in the range of $\pm 6\%$ to $\pm 13\%$ depending on spanwise location as shown in Fig. 7.8.

Figures 7.9 and 7.10 present typical test repeatability for the Boeing 737-300 inlet. For this geometry test repeatability ranged from $\pm 7\%$ to $\pm 19\%$ depending on MVD and circumferential location.

Impingement limits (“Curve tails”) show good repeatability for all test configurations.

7.2 Two-Dimensional Impingement Data

Experimental and analysis water droplet impingement results for the NLF(1)-0414, and experimental impingement data for the large and small glaze ice shapes are discussed here. The analytical impingement curves for the NLF(1)-0414 airfoil were obtained with the computer code discussed in section 6.1.

7.2.1 NLF(1) – 0414 Airfoil Section

The designation NLF(1)-0414 indicates a natural laminar flow (first) airfoil with a design lift coefficient of 0.4 (04) and a thickness of 14 percent chord (Ref. 13). The airfoil tested had a 36 inch chord and spanned the height (6 ft) of the tunnel test section. The main test variables were angle of attack and spray mean volumetric diameter (MVD). Blotter strips were positioned at two spanwise locations (A and B) for each run. Location A was 36 inches (midspan) and location B was 32 inches above the tunnel floor. Averaged water droplet impingement data for the NLF(1)-0414 at 0 and 8 degrees angle of attack and MVDs of 16 and 20 μm are summarized in Fig. 7.11. The impingement curves for each configuration tested are presented in Figs. 7.12-7.15.

Referring to Fig. 7.11 the following general trends are observed. For a given angle of attack the maximum impingement efficiency, the extent of impingement and the overall collection efficiency (area of impingement curve) decrease as MVD is decreased from 20 μm to 16 μm . As the angle of attack is increased, the point of maximum impingement moves toward the lower surface and the impingement limits on the lower surface move toward the trailing edge.

The overall agreement between experiment and analysis is good for both MVDs and angles of attack. The analytical peak efficiencies, however, are higher at $\alpha = 0^\circ$, and lower at $\alpha = 8^\circ$ than the corresponding experimental values. The main difference between the experimental and analytical data is that in the experimental data the maximum impingement efficiency for a given MVD increases with angle of attack. The increase in $\bar{\beta}_{max}$ with angle of attack for certain airfoil sections has been observed by other investigators (see Ref. 7 pp. 36 and 37). The analytical data for this airfoil, however, show the opposite trend. The reason for this discrepancy between test and analysis data is not clear at this point.

7.2.2 Small and Large Glaze Ice Shapes

Averaged water droplet impingement data for the large and small glaze ice shapes are presented in Figs. 7.16 and 7.17 respectively. Both simulated ice shapes had a symmetric cross-section and were at zero incidence (i.e., symmetric flow conditions). Thus, symmetric $\bar{\beta}$ distributions are expected. The asymmetries observed near the centers of the impingement curves for the large and small glaze ice shapes are mainly due to the blotter paper. It was very difficult to form the paper to follow precisely the shape of the simulated ice. Furthermore, small wrinkles were formed on the blotter strips during their installation on the surface of the ice shapes, which modified the reflectance properties of the blotter paper.

The maximum values of impingement efficiency for the large glaze ice shape occur near the "horn" regions as shown in Fig. 7.16. These values should be approximately equal due to flow symmetry. However, the impingement efficiency at the lower "horn" (see Fig. 4.2 B, left side looking downstream) has a maximum value of 0.54 while the corresponding value on the upper horn is 0.26. Possible reasons for this discrepancy include problems with the installation of the blotter strips around the horn regions and flow angularity.

7.3 Three-Dimensional Impingement Data

Experimental water droplet impingement data for the swept MS(1)-0317 airfoil, the NACA 0012 swept wing tip and the Boeing 737-300 inlet are presented below. Analytical impingement data for the Boeing inlet are also presented and are compared with the experimental results. The analysis results for the inlet have been obtained using the method described in section 6.2.

7.3.1 Swept MS(1) – 317 Airfoil

This wing had a medium speed (MS) 17% thick airfoil section with a design lift coefficient of 0.3. The wing chord was 36 inches in the streamwise direction and the wing span was 6 ft. The wing leading edge sweep angle was 30 degrees. This model was chosen to investigate the effect of sweep angle on collection efficiency. The model was built full span to simulate an infinite swept airfoil. The sweep angle produced a spanwise flow thus, the flow was three-dimensional.

Impingement data were obtained at $\alpha = 0$ and 8 degrees and for spray clouds with MVDs of 16 and 20 μm . Blotter strips were positioned at two spanwise locations A and B, 36 and 32 inches above the tunnel floor respectively. The blotter strips were in the chordwise (streamwise) direction. A summary of all experimental water droplet impingement data for this swept airfoil is presented in Fig. 7.18. The impingement curves for each test case are presented in Figs. 7.19-7.22.

The experimental results show that the impingement efficiency curves are practically the same at the two spanwise locations A and B for all conditions tested. This indicates that there was a constant spanwise flow and hence the desired infinite airfoil effect was achieved.

At $\alpha = 0$ degrees the maximum impingement efficiency is approximately 56% for strip A and 59% for strip B for an MVD of 20 μm . The $\bar{\beta}_{max}$ values for the 16 μm MVD case are 30% for strip A and 39 % for strip B. In all cases the location of $\bar{\beta}_{max}$ is on the lower surface of the airfoil, near the leading edge. Total water impingement, extent of impingement limits and $\bar{\beta}_{max}$ are less for the smaller MVD size as expected.

Similar trends are observed at $\alpha = 8$ degrees with respect to MVD size and strip location. For this angle of attack the location of $\bar{\beta}_{max}$ moves further aft along the lower surface and the limits of impingement are significantly greater than for the $\alpha = 0$ degrees case. An interesting feature of the experimental results is that for a given MVD $\bar{\beta}_{max}$ increases with angle of attack (see Fig. 7.18). This trend is similar to that observed with the NLF(1)-0414 airfoil.

7.3.2 NACA 0012 Swept Wing Tip

Water droplet impingement data for this model are summarized in Fig. 7.23. Detailed impingement data are presented in Figs. 7.24-7.27. This was a finite wing with a 30° leading edge sweep angle and an aspect ratio of 1.4. The NACA 0012 wing section was perpendicular to the leading edge with a chord length of 15 inches. The flow around this geometry was highly three-dimensional due to the sweep angle and low aspect ratio of this wing. This geometry was tested to investigate the effect of the wing tip vortex on water droplet impingement characteristics.

Tests at $\alpha = 0$ and 8 degrees were performed for spray clouds with MVDs of 16 and $20 \mu m$. Blotter strips were positioned at the wing tip, location A, and at two spanwise locations, B and C, 42 and 32 inches above the tunnel floor respectively (see Figs. 3.8C and 4.4 B). Strip A on the wing tip ran from station B, at the wing leading edge, to about 50% tip chord (see Fig. 3.8C) The highlight for strip A was located at the leading edge of the wing at spanwise location B. There is no upper or lower surface for strip A. Positive surface distance for this strip is measured from the leading edge to the trailing edge of the wing tip.

At $\alpha = 0^\circ$ the impingement efficiency curves at spanwise locations B and C are symmetric with respect to the highlight due to symmetric flow conditions. The maximum impingement efficiency at these two locations is not significantly affected by MVD or location and it varies from 0.75 to 0.8. The total impingement and the extent of impingement, however, is greater for the larger MVD size as expected. The maximum impingement efficiency for strip A is practically the same as that of strips B and C and is not significantly affected by MVD. The total collection efficiency for this strip is also greater for the larger MVD. The experimental results show that water impingement at the wing tip was limited to the forward 20% of the tip.

At $\alpha = 8^\circ$ the point of maximum impingement and the impingement limits at locations B and C shift slightly toward the lower surface. The maximum impingement efficiency, total water droplet impingement and extent of impingement limits are greater for the larger MVD. Similar trends with MVD are observed for strip A. The extent of impingement for strip A is considerably reduced at the higher angle of attack due to the presence of the tip vortex. As angle of attack is increased the vortex strength and vortex core diameter are increased. The larger vortex causes a larger disturbance to the flow locally and a reduction in water droplet impingement.

Referring to Fig. 7.23 (summary of results) certain trends in the experimental data require further discussion. For the $20\mu m$ MVD case, the maximum impingement efficiency at locations B and C are very similar for both angles of attack. This is not the case for strip A for which impingement efficiency is higher at $\alpha = 8^\circ$. It is not clear why $\bar{\beta}_{max}$ for strip A should increase with \angle of attack. For MVD = $16 \mu m$, the results show that $\bar{\beta}_{max}$ for $\alpha = 8^\circ$ at all spanwise locations is lower than the corresponding $\bar{\beta}_{max}$ values at $\alpha = 0^\circ$. Furthermore, $\bar{\beta}_{max}$ in this case is a function of location, being maximum at location A and minimum at location C. The reasons for the observed differences in $\bar{\beta}_{max}$ for the two MVD sizes are not clear. It is possible that these differences in trends are

due to experimental error in achieving the desired experimental conditions. However, test repeatability for this test geometry at $\alpha = 8^\circ$ was very good.

A few comments regarding the impingement limits are also in order. The experimental impingement curves for $\alpha = 0^\circ$, indicate that the extent of impingement is not significantly affected by MVD. At $\alpha = 8^\circ$ several of the impingement curves fall off abruptly. These discrepancies are attributed to the reflectance properties of the blotter paper which were modified by the adhesive tape used to mount the strips on the wing. The correct values for the impingement limits are the numerical values given below each curve. These values were obtained by careful examination of the raw laser reflectance data and by visual inspection of the blotter strips.

7.3.3 Boeing 737-300 Engine Inlet

This inlet had a non-axisymmetric three-dimensional geometry which, when placed at a high angle of attack, produced a complex flow pattern. The flowfield was complicated further by variations in mass flow through the inlet used to simulate different inlet capture area ratios. The resulting flow configuration was a challenging test case for the experimental and analytical methods.

For this geometry, the test variables included α , MVD and inlet mass flow. The high mass flow (23 lbm/sec) corresponds to an inlet capture area ratio of 1. The low mass flow (17 lbm/sec) corresponds to a capture area ratio of 0.75.

A total of 8 blotter strips were positioned around the inlet for each test. The strips were set at 45 degree intervals corresponding to $\theta = 0, 45, 90, 135, 180, 225, 270$ and 325 degrees (see Fig. 3.7B). Two to five runs were made for each combination of α , MVD and mass flow setting. Results from several of these runs were averaged to produce the impingement curves shown in Figs. 7.28-7.30. Analytical data are also presented in these figures. Figure 7.28 provides a summary of all experimental results obtained for the Boeing 737-300. Detailed results for the $\alpha = 0^\circ$ and $\alpha = 15^\circ$ test cases are presented in Fig. 7.29 and Fig. 7.30 respectively.

The engine inlet model was mounted in the tunnel with the top ($\theta = 0^\circ$) and bottom ($\theta = 180^\circ$) of the inlet in a horizontal plane. Due to the symmetry of the flow with respect to a horizontal plane through locations A ($\theta = 0^\circ$) and E ($\theta = 180^\circ$) the impingement curves for strips B and H should be the same. This is also true for strips C and G and strips D and F. Thus, all B and H strips for a given test condition were combined into a single averaged impingement curve. The same was done with all C and G and all D and F strips.

Water droplet impingement data for this inlet were presented in Reference 10. These data were obtained in the September 1985 tests. Discrepancies between the analytical and the 1985 test results for the case of $\alpha = 15$ degrees were observed and these differences (particularly for $\theta = 0$ degrees) were attributed to non-uniform dye distribution in the droplet cloud. To clarify some of these discrepancies some of the test points were repeated during the current tests. Extra attention was paid to the cloud uniformity in the current

tests. The result being that the new experimental data are in much better agreement with the analytical data.

At $\alpha = 0$ degrees the following trends are observed from the experimental data presented in Fig. 7.29:

- a . Reducing the inlet mass flow from 23 to 17 lbm/s causes the location of $\bar{\beta}_{max}$ to shift toward the inner cowl (positive s).
- b . For the same mass flow and cloud MVD, the location of $\bar{\beta}_{max}$ moves progressively toward the inner cowl as θ varies from 0 to 180 degrees. The maximum impingement limits are observed at $\theta = 135^\circ$ and $\theta = 180^\circ$.
- c . For the low mass flow and cloud MVD the area under the impingement curves is reduced indicating lower total water impingement.
- d . The analytical impingement curves are wider than the experimental curves. The correlation between experiment and theory is good in most cases. The analysis data indicate that the maximum value of $\bar{\beta}_{max}$ occurs at $\theta = 90^\circ$ in all cases presented and that the maximum impingement limits are at $\theta = 135^\circ$.

Referring to Fig. 7.30 the following trends are observed for the case $\alpha = 15$ degrees.

- a . For a given circumferential location (constant θ) reducing the inlet mass flow from 23 to 17 lbm/s causes the location of $\bar{\beta}_{max}$ to shift toward the inner cowl (positive s)
- b . For the same mass flow and cloud MVD, the location of $\bar{\beta}_{max}$ moves progressively from the inner cowl at $\theta = 0^\circ$ to the outer cowl at $\theta = 180^\circ$. The maximum impingement limits are observed at $\theta = 135^\circ$.
- c . For the low mass flow and cloud MVD the area under the impingement curves is reduced indicating lower total water impingement.
- d . The analytical impingement curves are in all cases wider than the experimental curves. The correlation between experiment and theory is good in most cases. The experimental values of $\bar{\beta}_{max}$ are in general higher than the corresponding analytical values. The analysis results indicate that the extent of the impingement limits is maximum at $\theta = 135^\circ$ and the maximum $\bar{\beta}_{max}$ occurs $\theta = 90^\circ$.

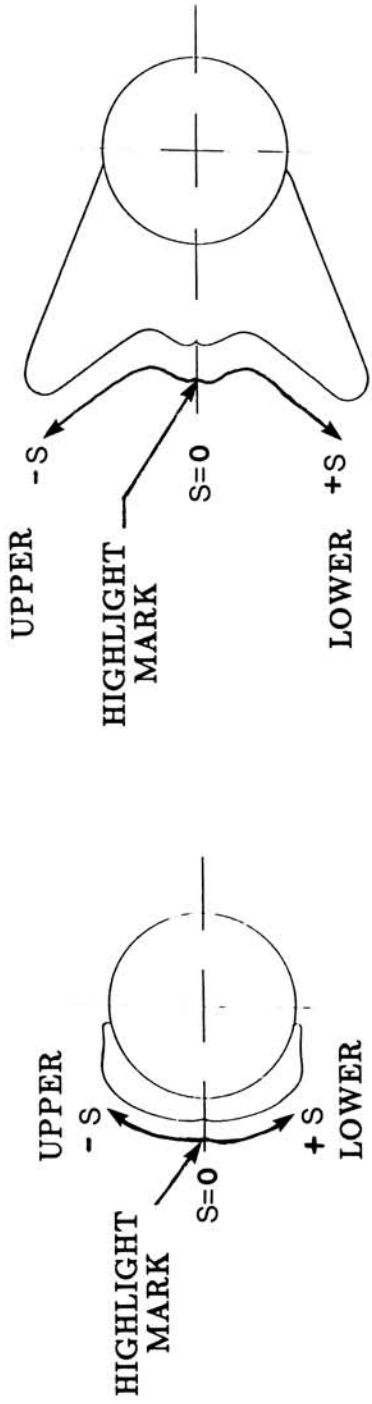
More details regarding impingement trends for the Boeing 737-300 inlet can be found in Ref. 10.

TABLE 7.1
REFERENCE COLLECTOR DYE MASS FOR AIRFOILS,
ICE SHAPES AND WING TIP

| Test Condition | Collector Dye Mass in $\mu g/cm^2$ |
|--|------------------------------------|
| $\alpha = 0, 8^\circ$, MVD = $20 \mu m$, Locations A and B | 2.223 |
| $\alpha = 0, 8^\circ$, MVD = $16 \mu m$, Locations A and B | 2.608 |

TABLE 7.2
REFERENCE COLLECTOR DYE MASS FOR ENGINE INLET

| Test Condition | Collector Dye Mass in $\mu g/cm^2$ | | | | | | | |
|---------------------------------------|------------------------------------|--------------------------------|--------------------------------|---------------------------------|---------------------------------|---------------------------------|---------------------------------|---------------------------------|
| | $\theta = 0^\circ$ Strip A | $\theta = 45^\circ$ Strip B | $\theta = 90^\circ$ Strip C | $\theta = 135^\circ$ Strip D | $\theta = 180^\circ$ Strip E | $\theta = 225^\circ$ Strip F | $\theta = 270^\circ$ Strip G | $\theta = 315^\circ$ Strip H |
| $\alpha = 0^\circ$, MVD= $20 \mu m$ | 2.1738 | 2.0456 | 2.0968 | 2.3740 | 2.5218 | 2.3638 | 2.2723 | 1.8466 |
| $\alpha = 0^\circ$, MVD= $16 \mu m$ | 2.4418 | 2.2987 | 2.4401 | 2.5842 | 2.6127 | 2.4975 | 2.5977 | 2.1527 |
| $\alpha = 15^\circ$, MVD= $20 \mu m$ | 1.5618 | 1.5514 | 1.8894 | 2.0640 | 2.2003 | 2.0755 | 1.7509 | 1.6261 |
| $\alpha = 15^\circ$, MVD= $16 \mu m$ | 2.2866 | 2.3565 | 2.5111 | 2.6744 | 2.6926 | 2.5766 | 2.6116 | 2.3594 |



SMALL GLAZE ICE

LARGE GLAZE ICE

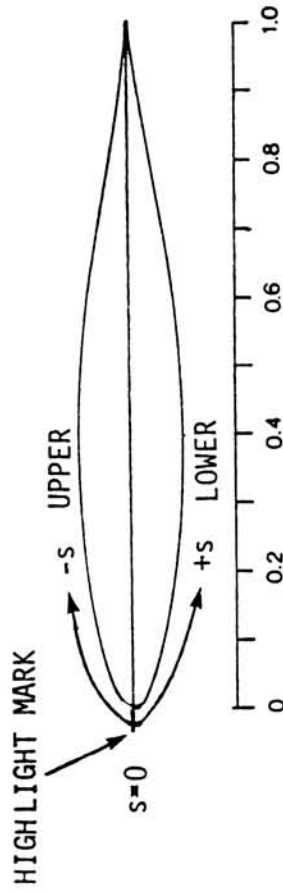


FIGURE 7.1
HIGHLIGHT MARKS AND SURFACE DISTANCE CONVENTION
FOR WINGS AND ICE SHAPES

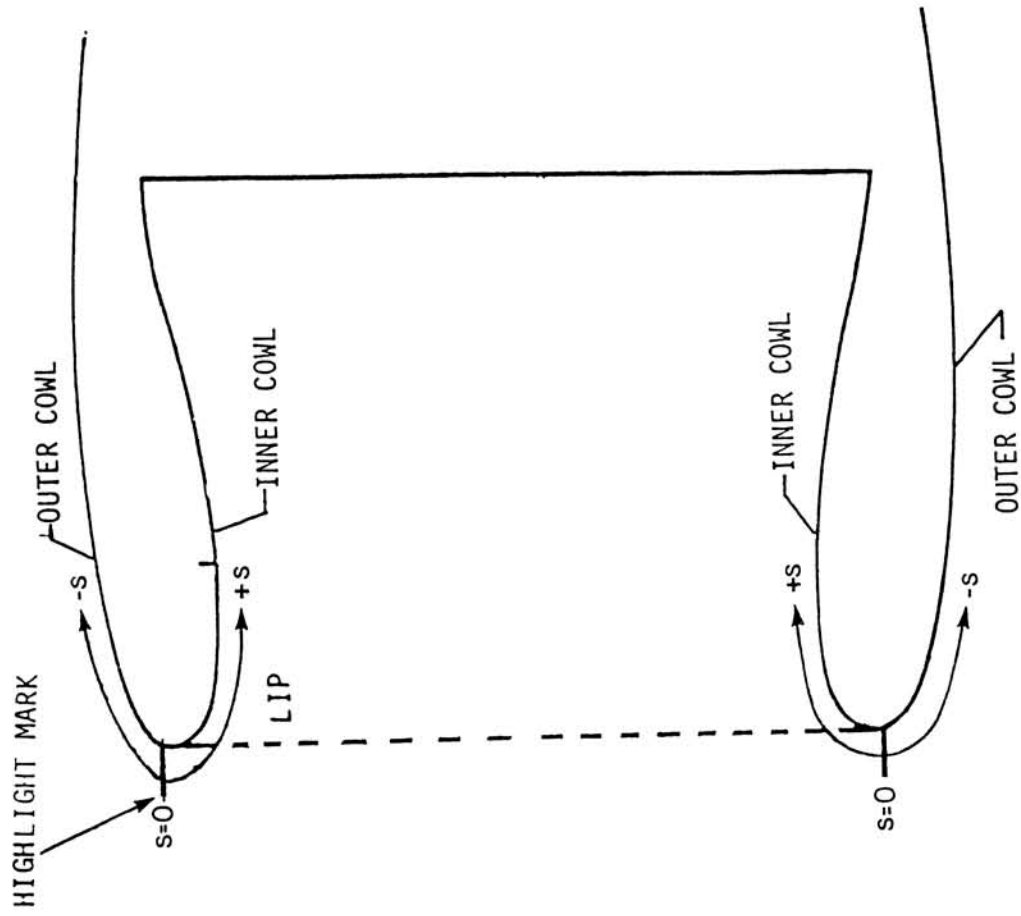
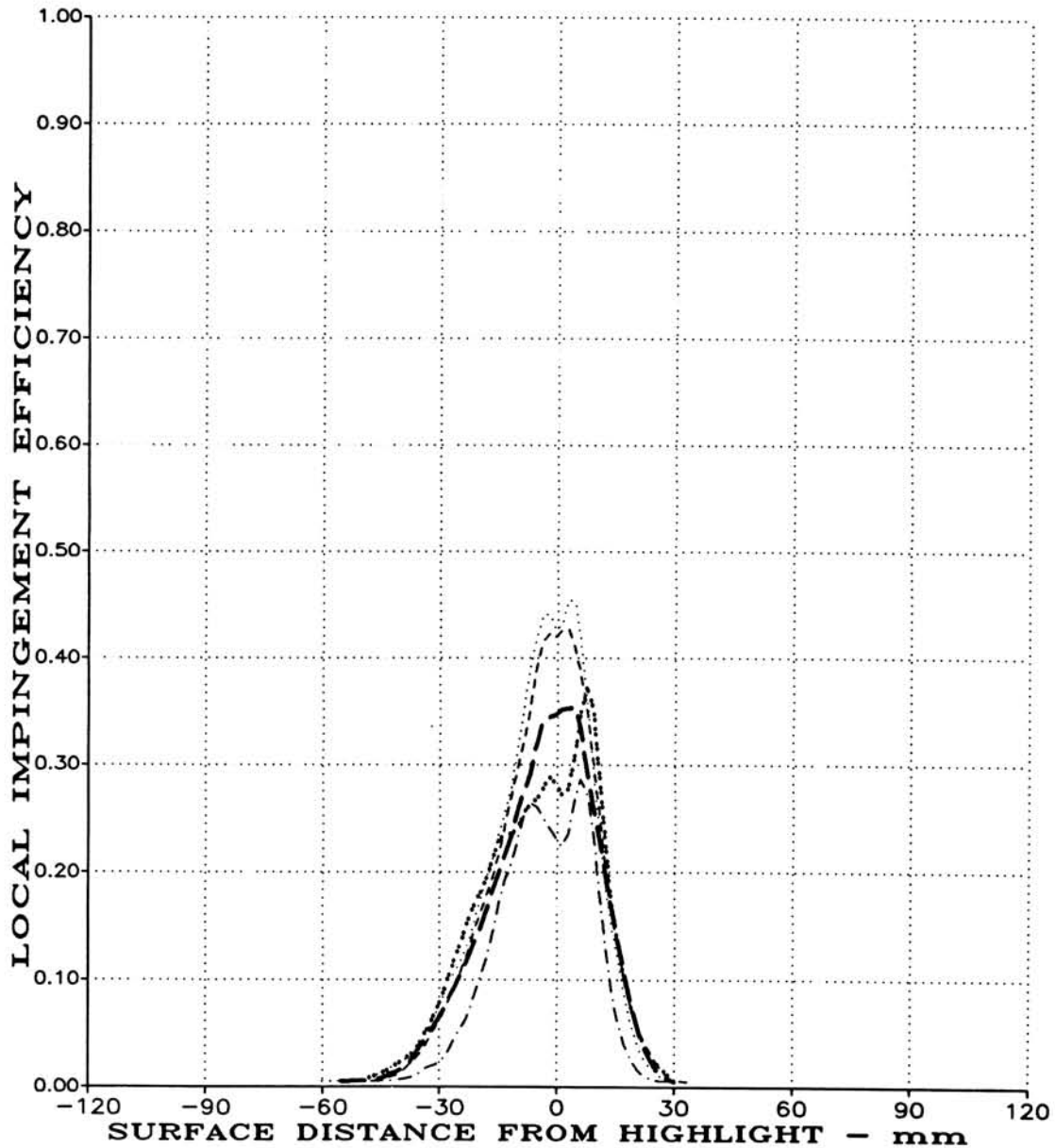


FIGURE 7.2
HIGHLIGHT MARKS AND SURFACE DISTANCE CONVENTION
FOR ENGINE INLETS

TEST RUN ID: 220N900A, 221N900A, 222N900A,
223N900A, 224N900A, 225N900A



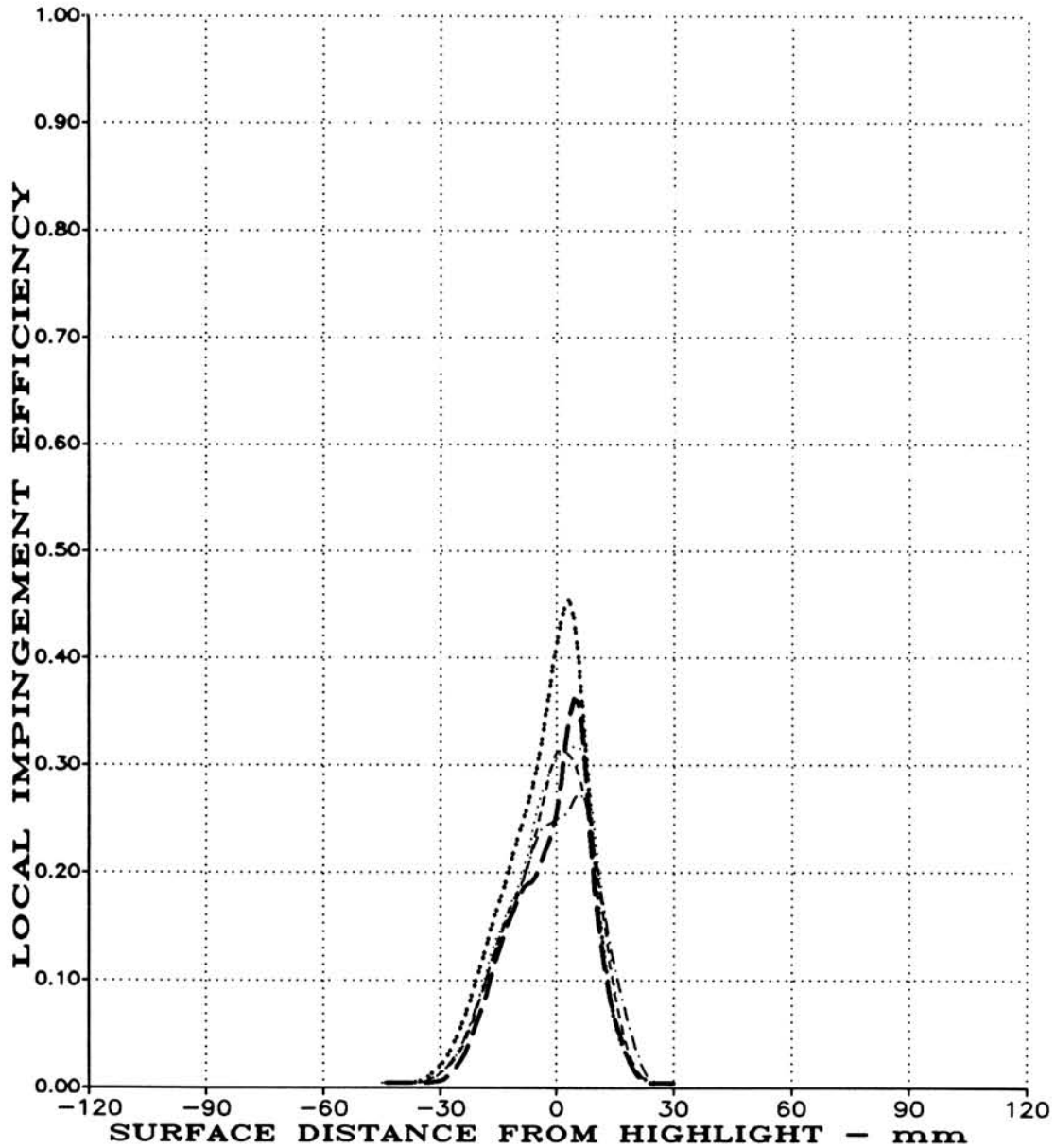
(Positive Surface Distance, S, on Lower Surface)

(A) MVD = 20 MICRONS, STRIP A

FIGURE 7.3

TEST REPEATABILITY FOR NLF(1)-0414 AIRFOIL AT $\alpha = 0^\circ$
(PAGE 1 OF 2).

TEST RUN ID: 226N600A, 227N600A, 228N600A,
229N600A, 230N600A



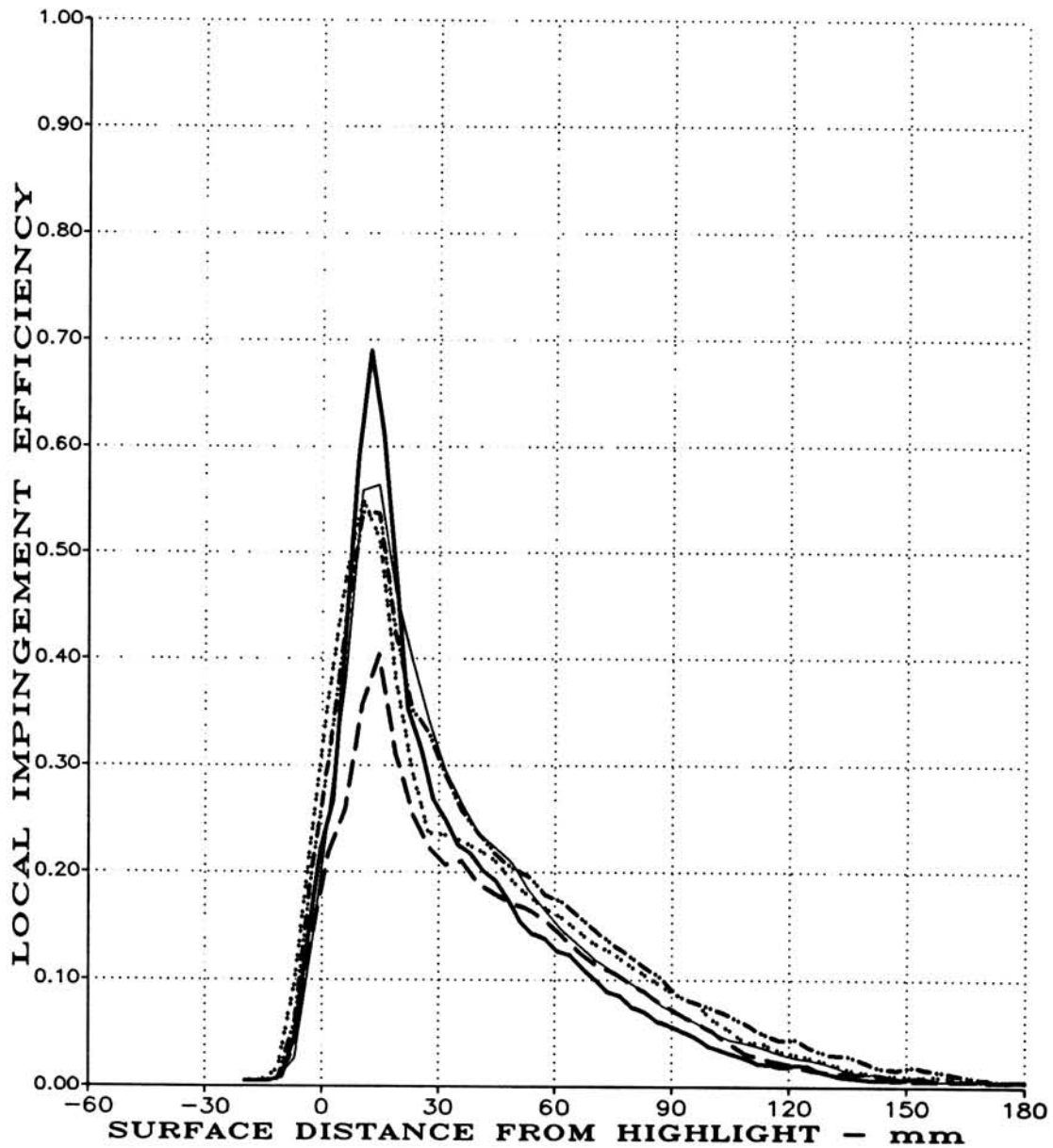
(Positive Surface Distance, S, on Lower Surface)

(B) MVD = 16 MICRONS, STRIP A

FIGURE 7.3

TEST REPEATABILITY FOR NLF(1)-0414 AIRFOIL AT $\alpha = 0^\circ$
(PAGE 2 OF 2).

TEST RUN ID: 215N908A, 216N908A, 217N908A,
218N908A, 219N908A



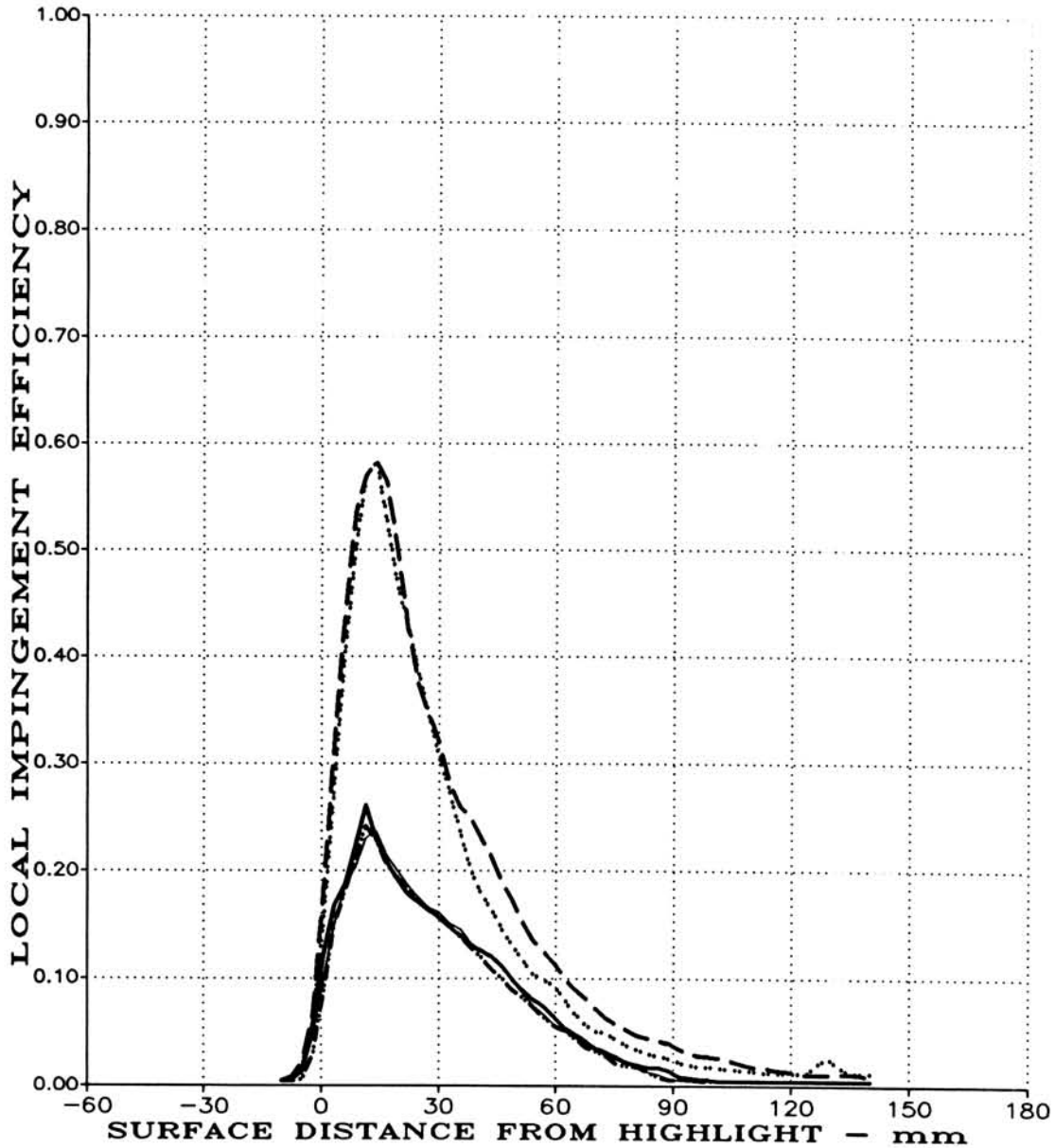
(Positive Surface Distance, S, on Lower Surface)

(A) MVD = 20 MICRONS, STRIP A

FIGURE 7.4

TEST REPEATABILITY FOR NLF(1)-0414 AIRFOIL AT $\alpha = 8^\circ$
(PAGE 1 OF 2).

TEST RUN ID: 232N608A, 233N608A, 234N608A,
235N608A, 236N608A



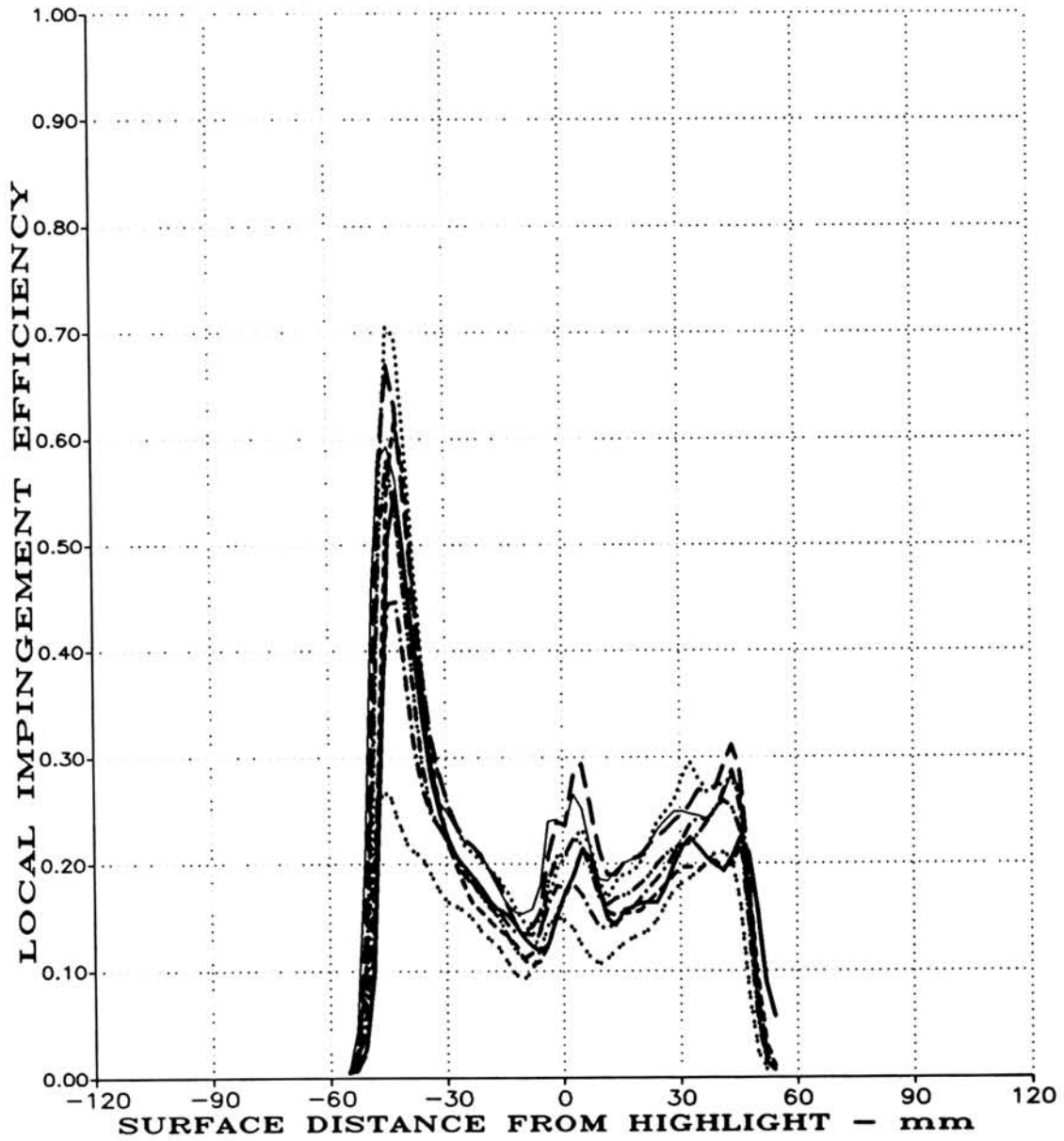
(Positive Surface Distance, S, on Lower Surface)

(B) MVD = 16 MICRONS, STRIP A

FIGURE 7.4

TEST REPEATABILITY FOR NLF(1)-0414 AIRFOIL AT $\alpha = 8^\circ$
(PAGE 2 OF 2).

TEST RUN ID: 116I900A, 117I900A, 118I900A,
119I900A, 120I900A



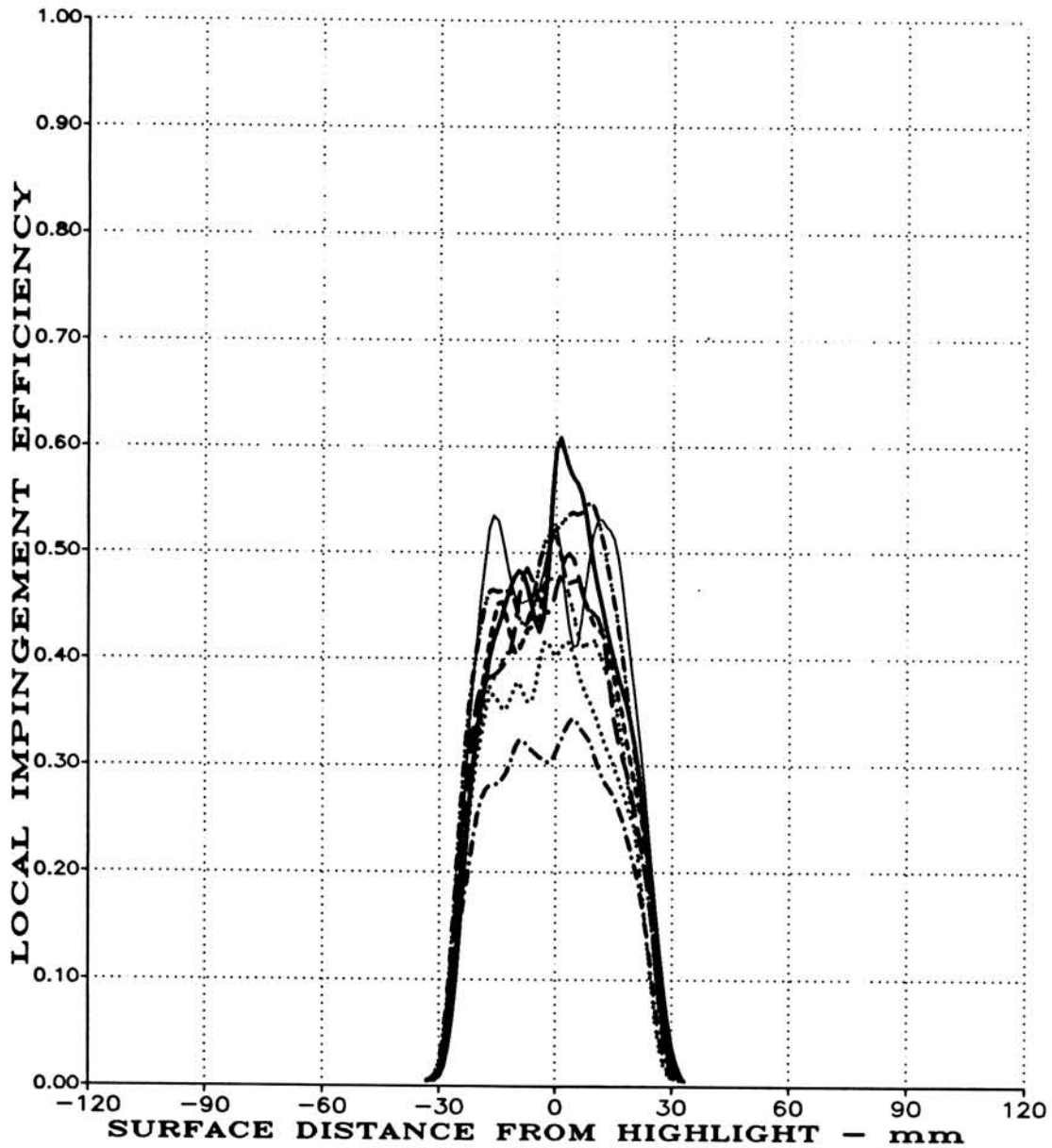
(Positive Surface Distance, S, on Lower Surface)

MVD = 20 MICRONS, STRIP A

FIGURE 7.5

TEST REPEATABILITY FOR LARGE GLAZE ICE SHAPE AT $\alpha = 0^\circ$

TEST RUN ID: 121I900A, 122I900A, 123I900A,
124I900A, 125I900A, 126I900A



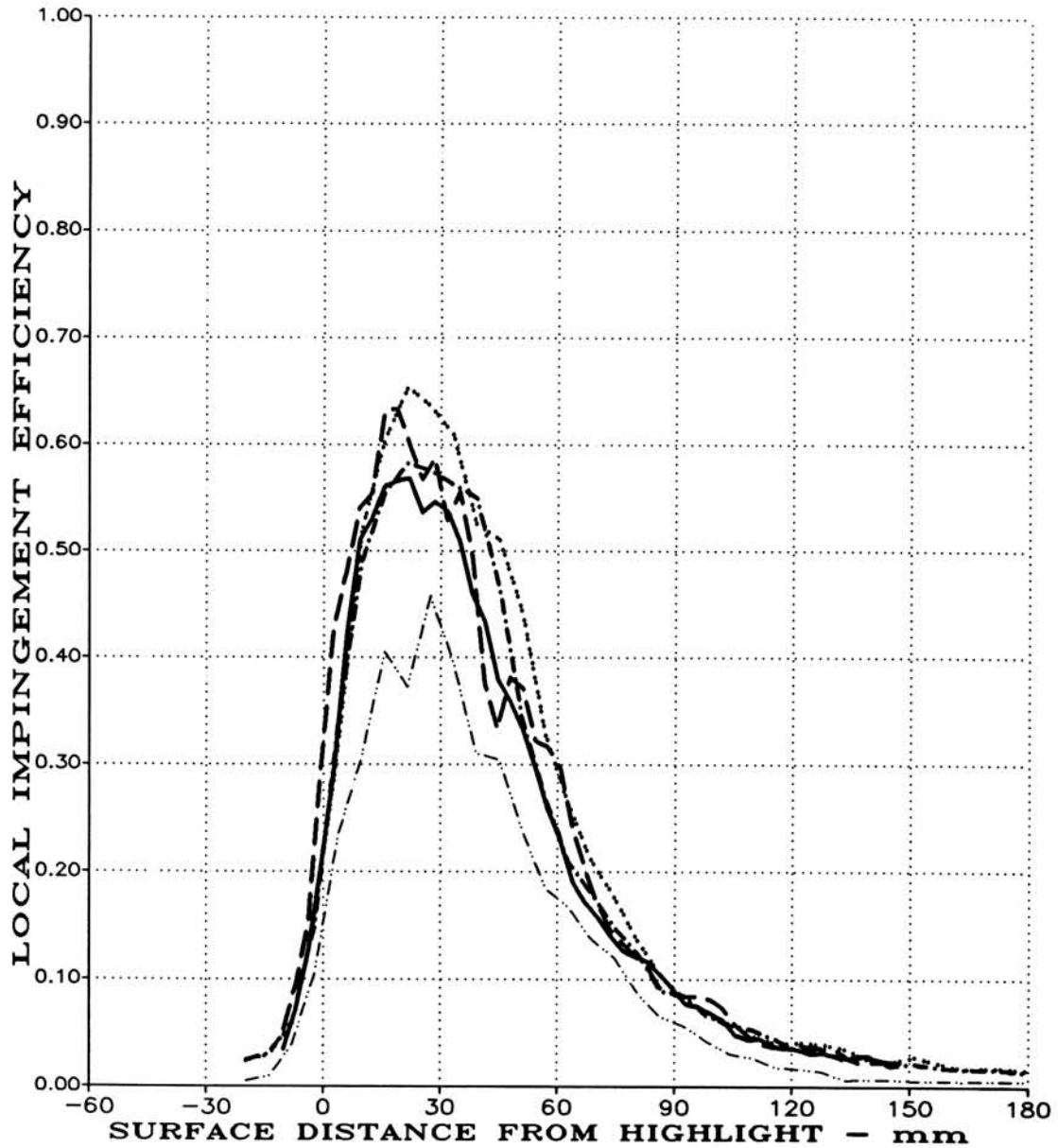
(Positive Surface Distance, S, on Lower Surface)

MVD = 20 MICRONS, STRIP A

FIGURE 7.6

TEST REPEATABILITY FOR SMALL GLAZE ICE SHAPE AT $\alpha = 0^\circ$

TEST RUN ID: 163M908A, 164M908A, 165M908A,
166M908A, 167M908A



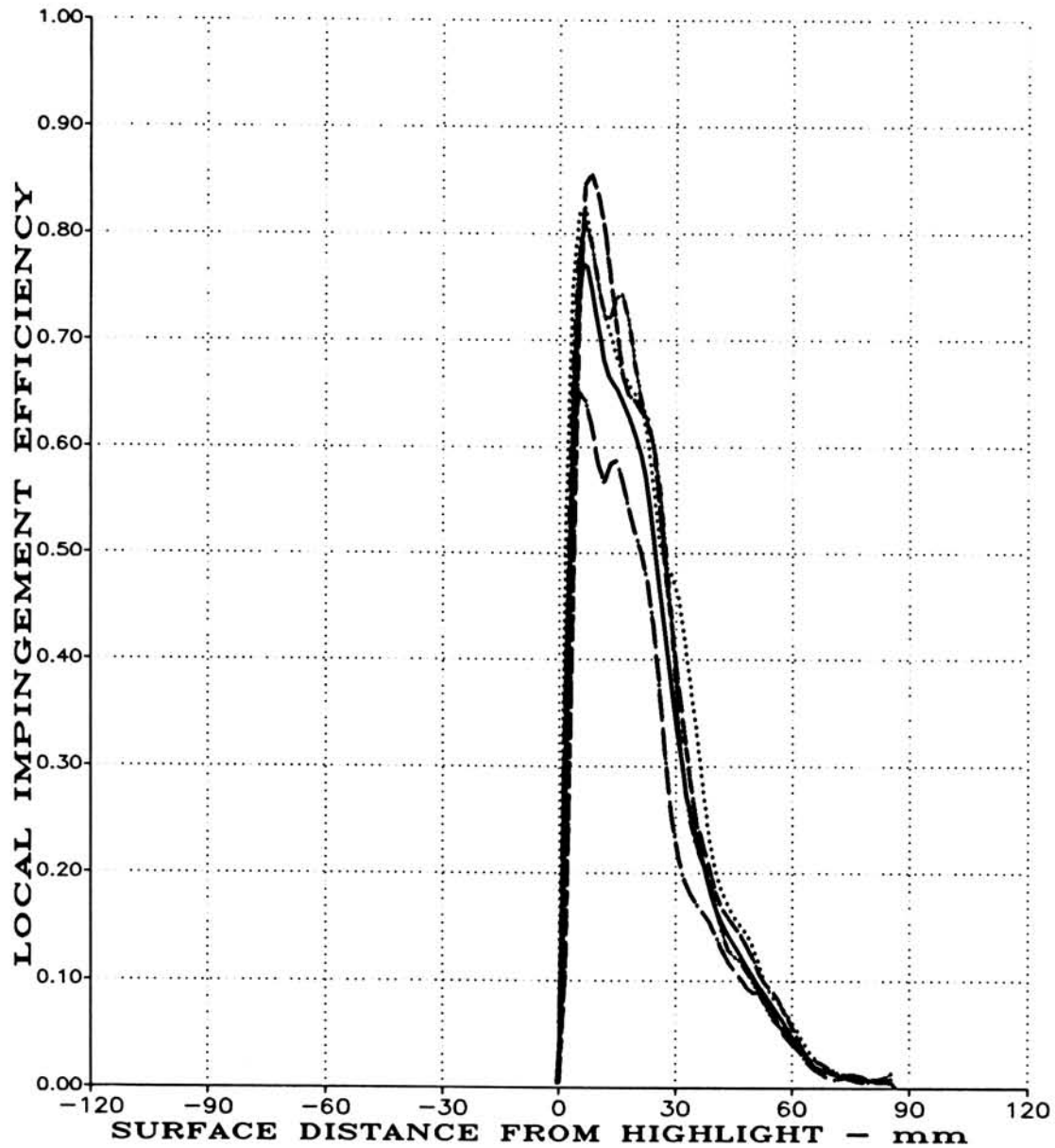
(Positive Surface Distance, S, on Lower Surface)

MVD = 20 MICRONS, STRIP A

FIGURE 7.7

TEST REPEATABILITY FOR MS(1)-0317 AIRFOIL AT $\alpha = 8^\circ$

TEST RUN ID: 127W900A, 128W900A, 129W900A,
130W900A, 131W900A



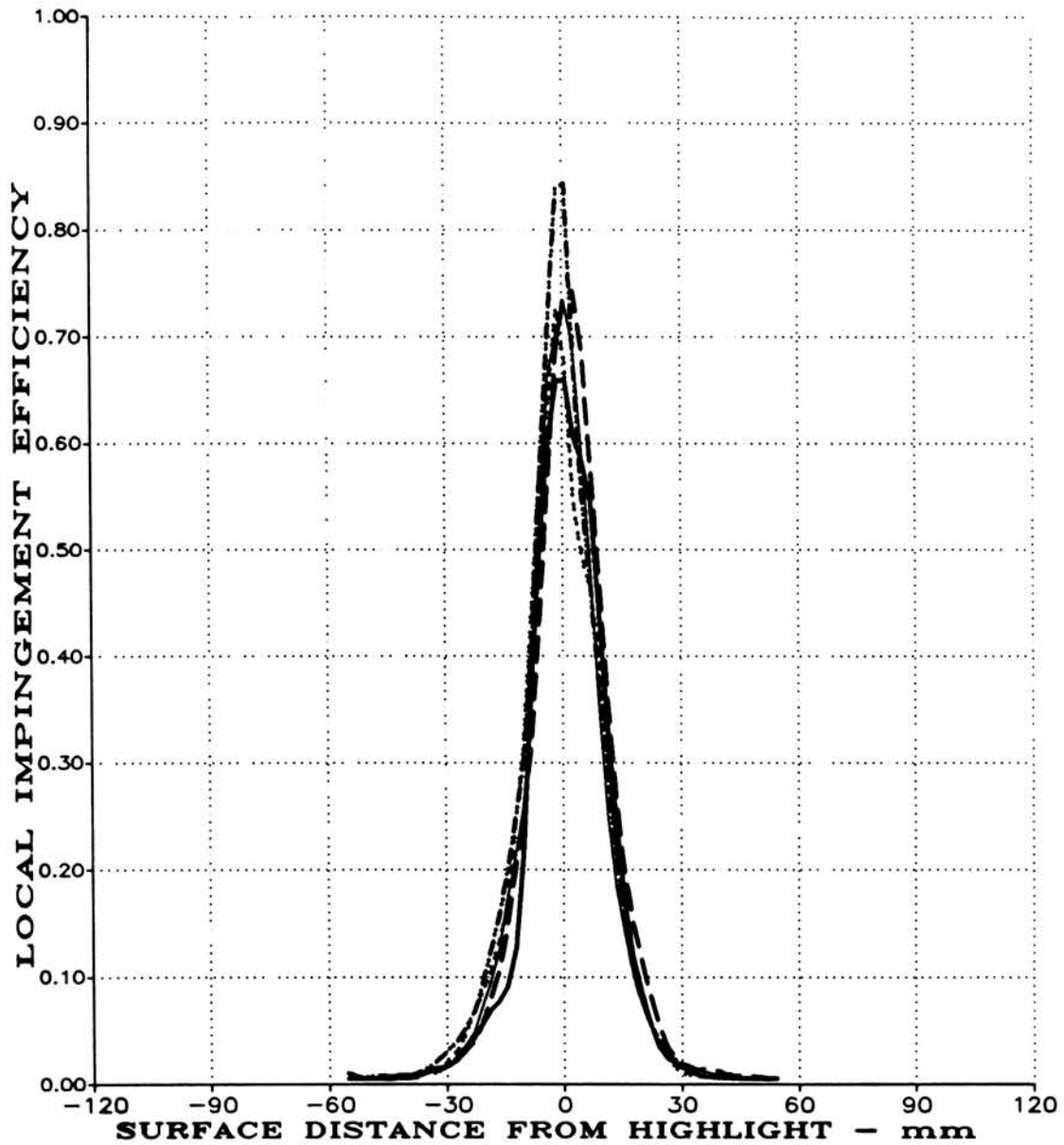
(Positive Surface Distance, S, on Lower Surface)

(A) MVD = 20 MICRONS, STRIP A

FIGURE 7.8

TEST REPEATABILITY FOR NACA 0012 SWEEP WING TIP AT $\alpha = 0^\circ$
(PAGE 1 OF 3).

TEST RUN ID: 127W900B, 128W900B, 129W900B,
130W900B, 131W900B



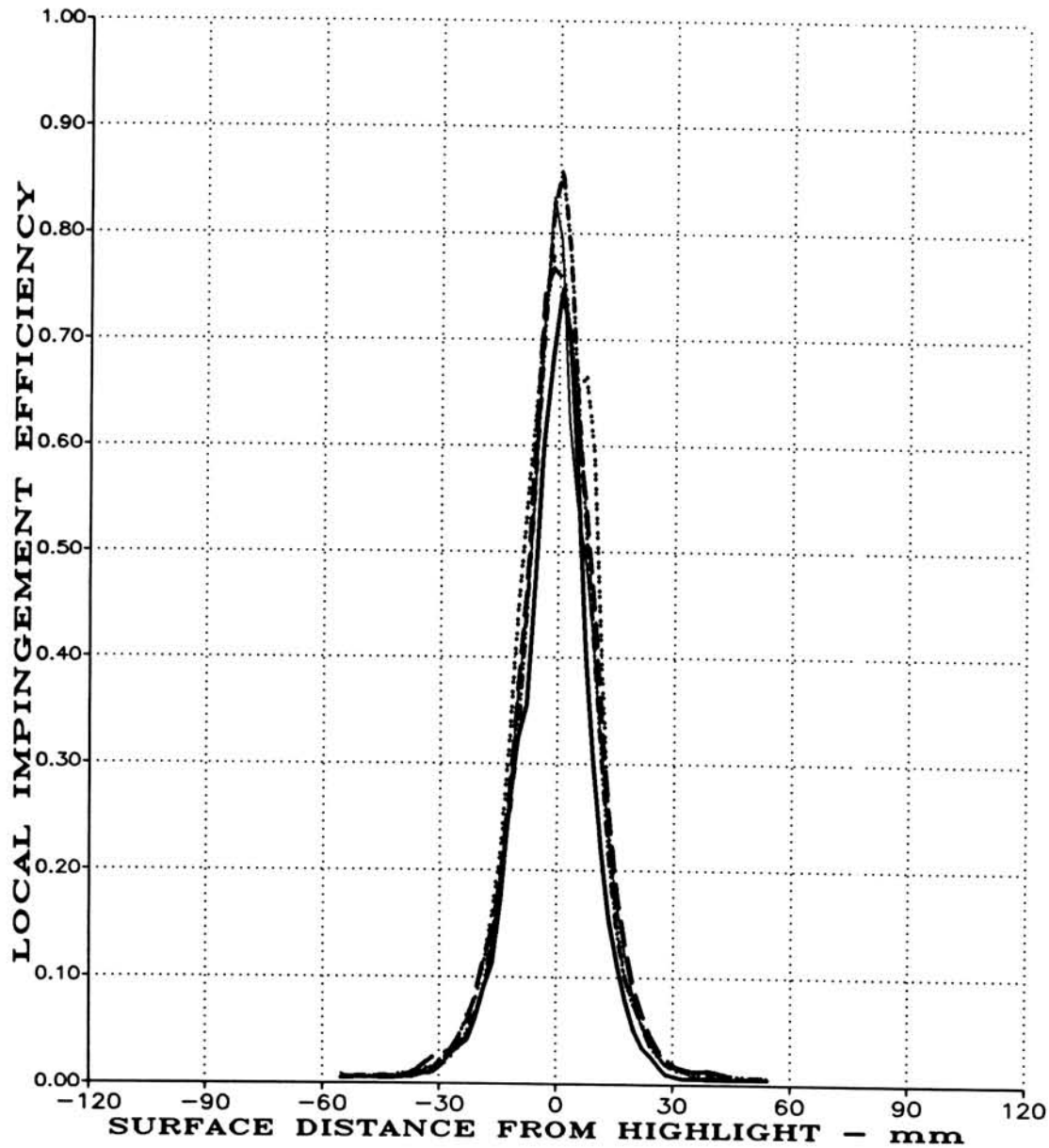
(Positive Surface Distance, S, on Lower Surface)

(B) MVD = 20 MICRONS, STRIP B

FIGURE 7.8

TEST REPEATABILITY FOR NACA 0012 SWEEP WING TIP AT $\alpha = 0^\circ$
(PAGE 2 OF 3).

TEST RUN ID: 127W900C, 128W900C, 129W900C,
130W900C, 131W900C

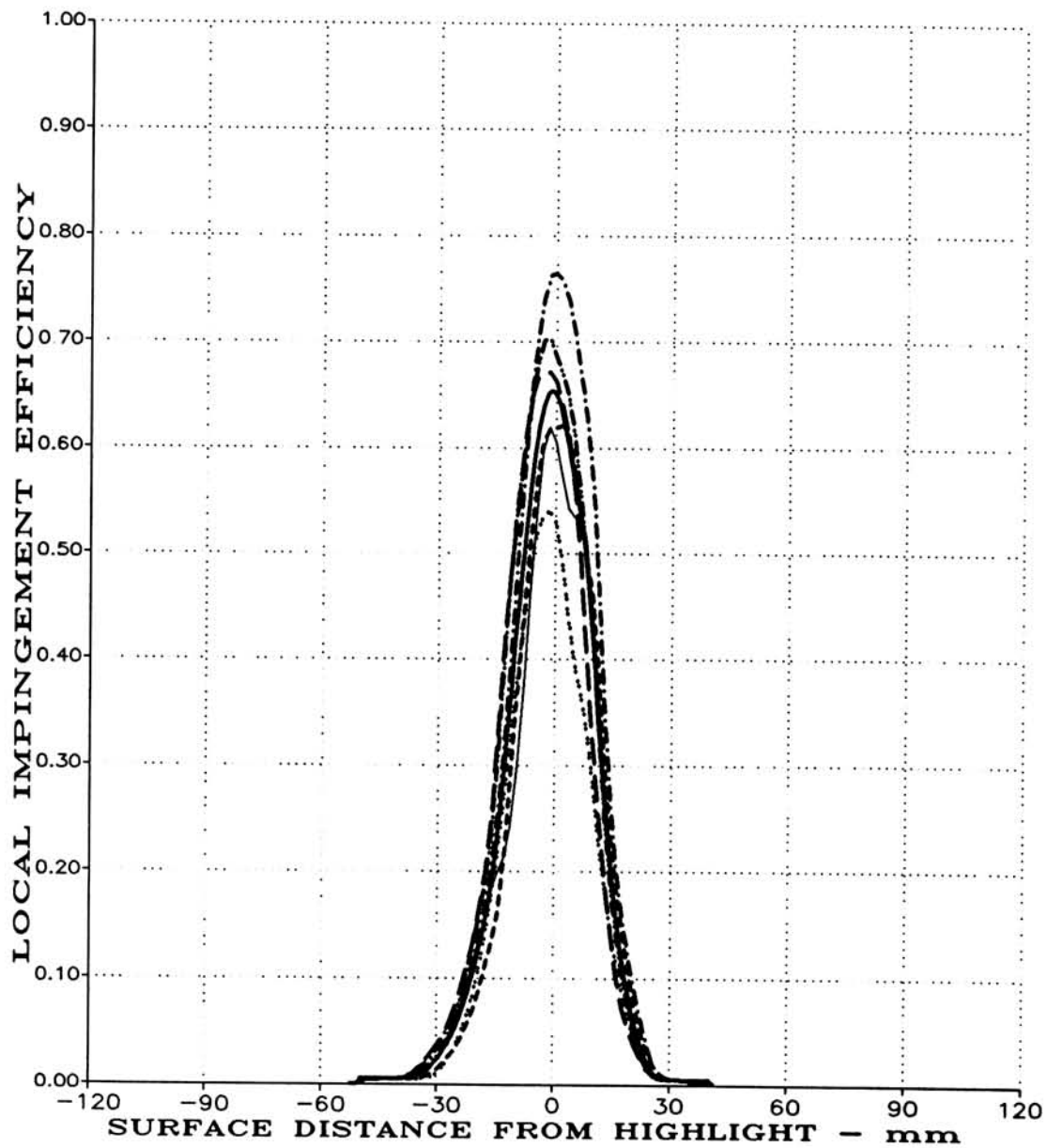


(Positive Surface Distance, S, on Lower Surface)

(C) MVD = 20 MICRONS, STRIP C

FIGURE 7.8

TEST REPEATABILITY FOR NACA 0012 SWEEP WING TIP AT $\alpha = 0^\circ$
(PAGE 3 OF 3).



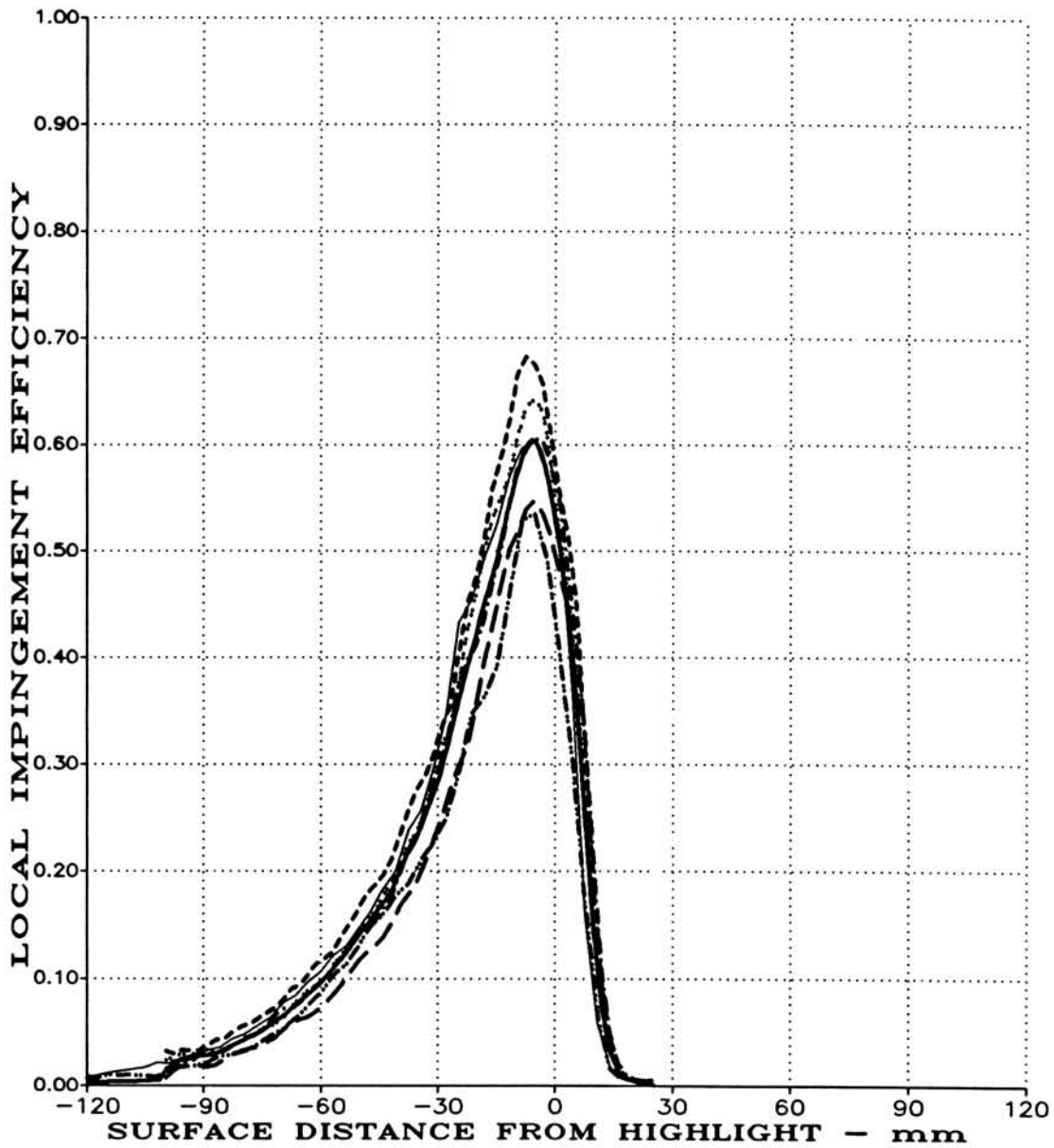
(Positive Surface Distance, S, on Inner Surface)

(A) MVD = 20 MICRONS, MASS FLOW = 22.96 LBM/S, $\theta = 90^\circ, 270^\circ$

FIGURE 7.9

TEST REPEATABILITY FOR BOEING 737-300 INLET AT $\alpha = 15^\circ$
(PAGE 1 OF 3).

TEST RUN ID: 1743915DF, 1753915DF, 1763915DF

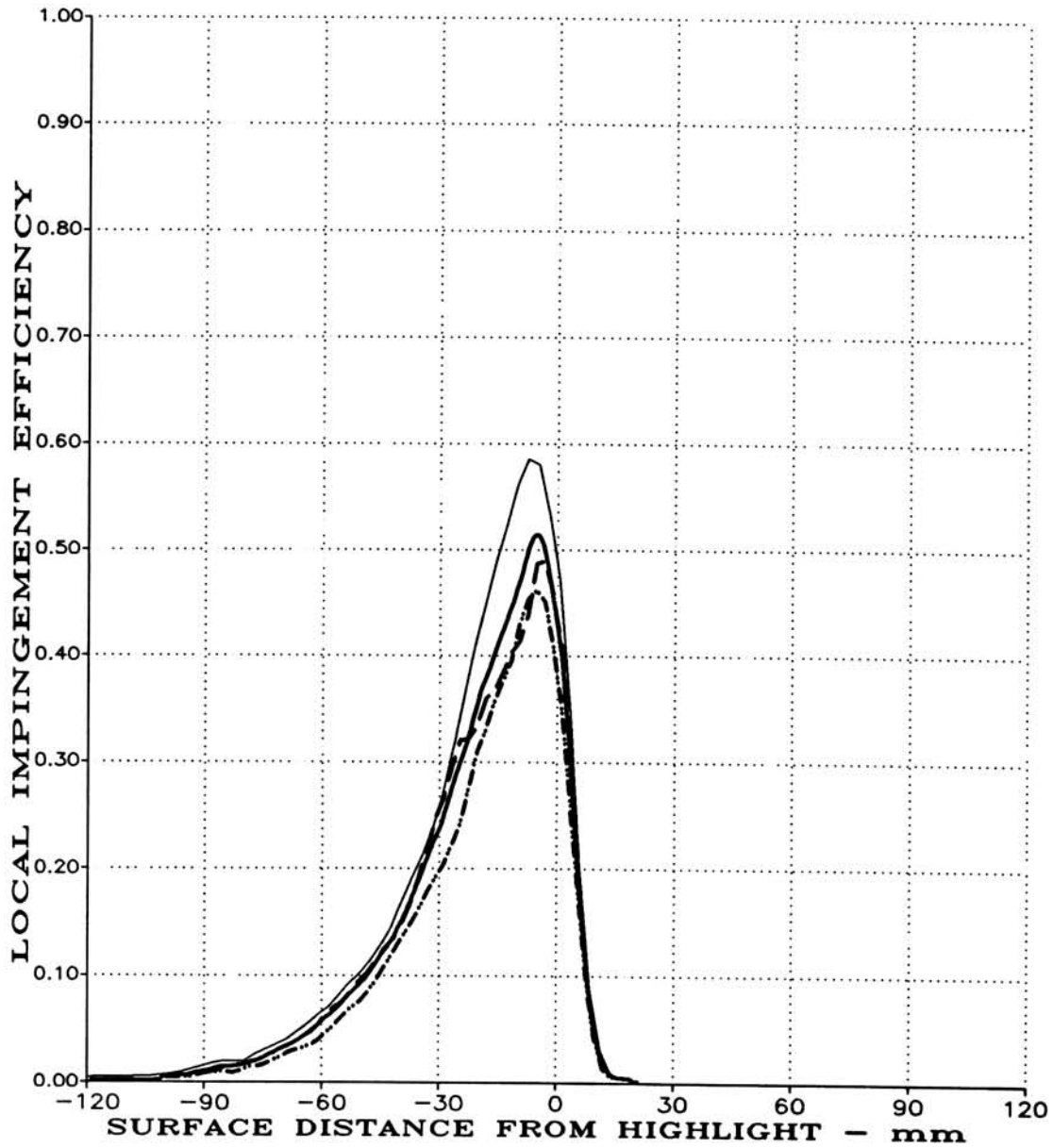


(Positive Surface Distance, S, on Inner Surface)

(B) MVD = 20 MICRONS, MASS FLOW = 22.96 LBM/S, $\theta = 135^\circ, 225^\circ$

FIGURE 7.9

TEST REPEATABILITY FOR BOEING 737-300 AIRFOIL AT $\alpha = 15^\circ$
(PAGE 2 OF 3).



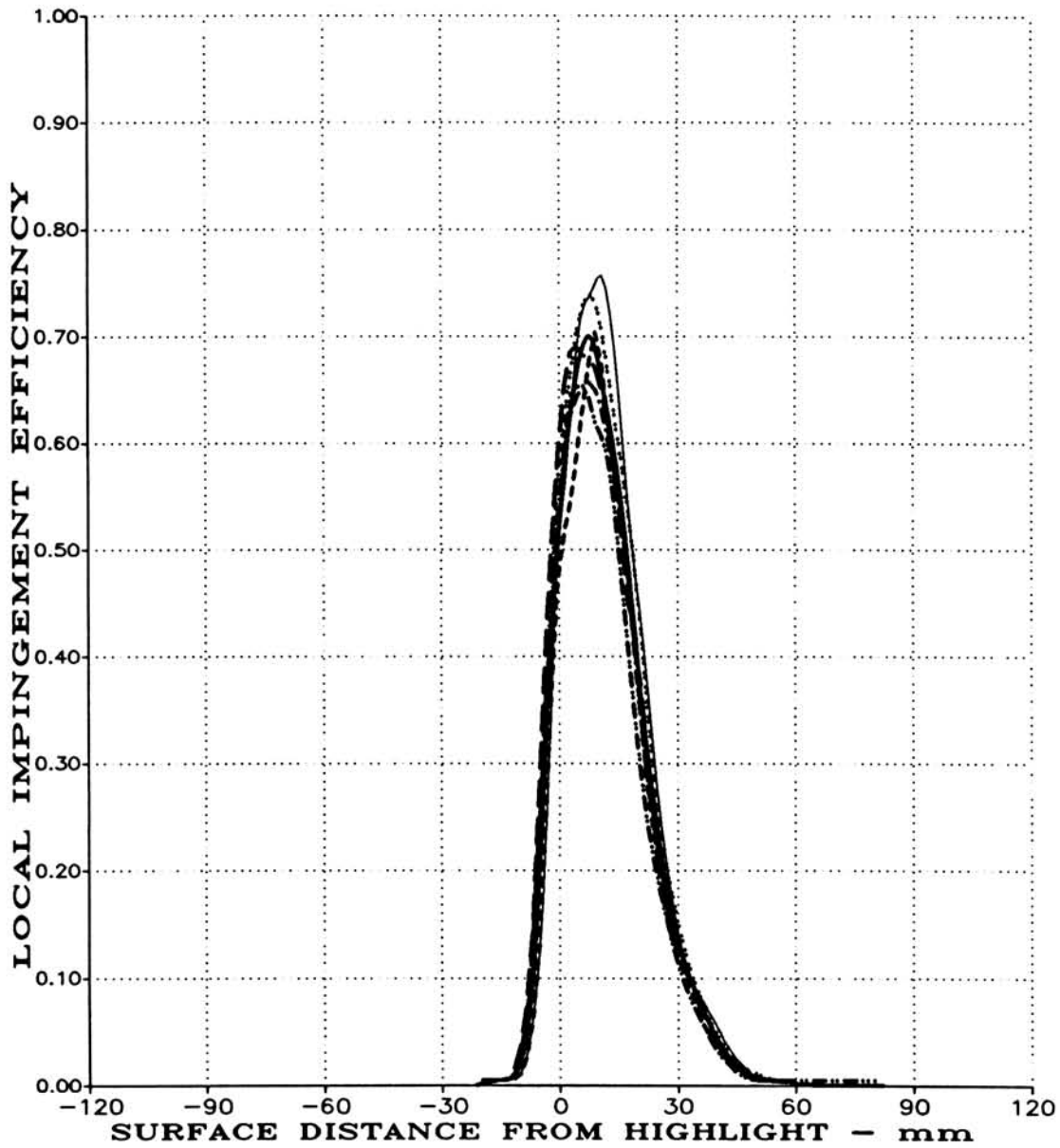
(Positive Surface Distance, S, on Inner Surface)

(C) MVD = 20 MICRONS, MASS FLOW = 22.96 LBM/S, $\theta = 180^\circ$

FIGURE 7.9

TEST REPEATABILITY FOR BOEING 737-300 INLET AT $\alpha = 15^\circ$
(PAGE 3 OF 3).

TEST RUN ID: 1683615A, 1693615A, 1703615A,
1713615A, 1723615A, 1733615A

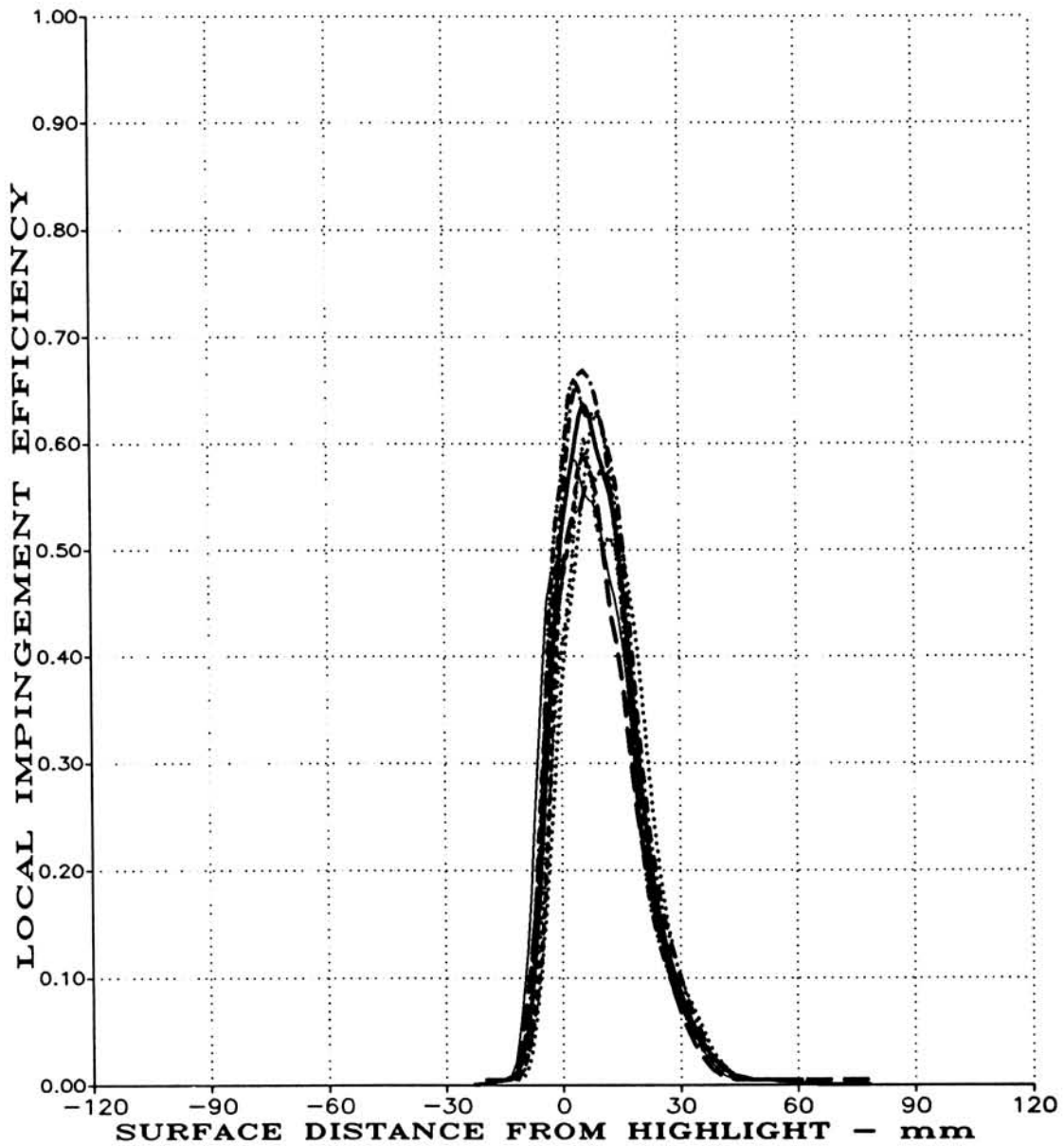


(Positive Surface Distance, S, on Inner Surface)

(A) MVD = 16 MICRONS, MASS FLOW = 17.2 LBM/S, $\theta = 0^\circ$

FIGURE 7.10

TEST REPEATABILITY FOR BOEING 737-300 INLET AT $\alpha = 15^\circ$
(PAGE 1 OF 5).

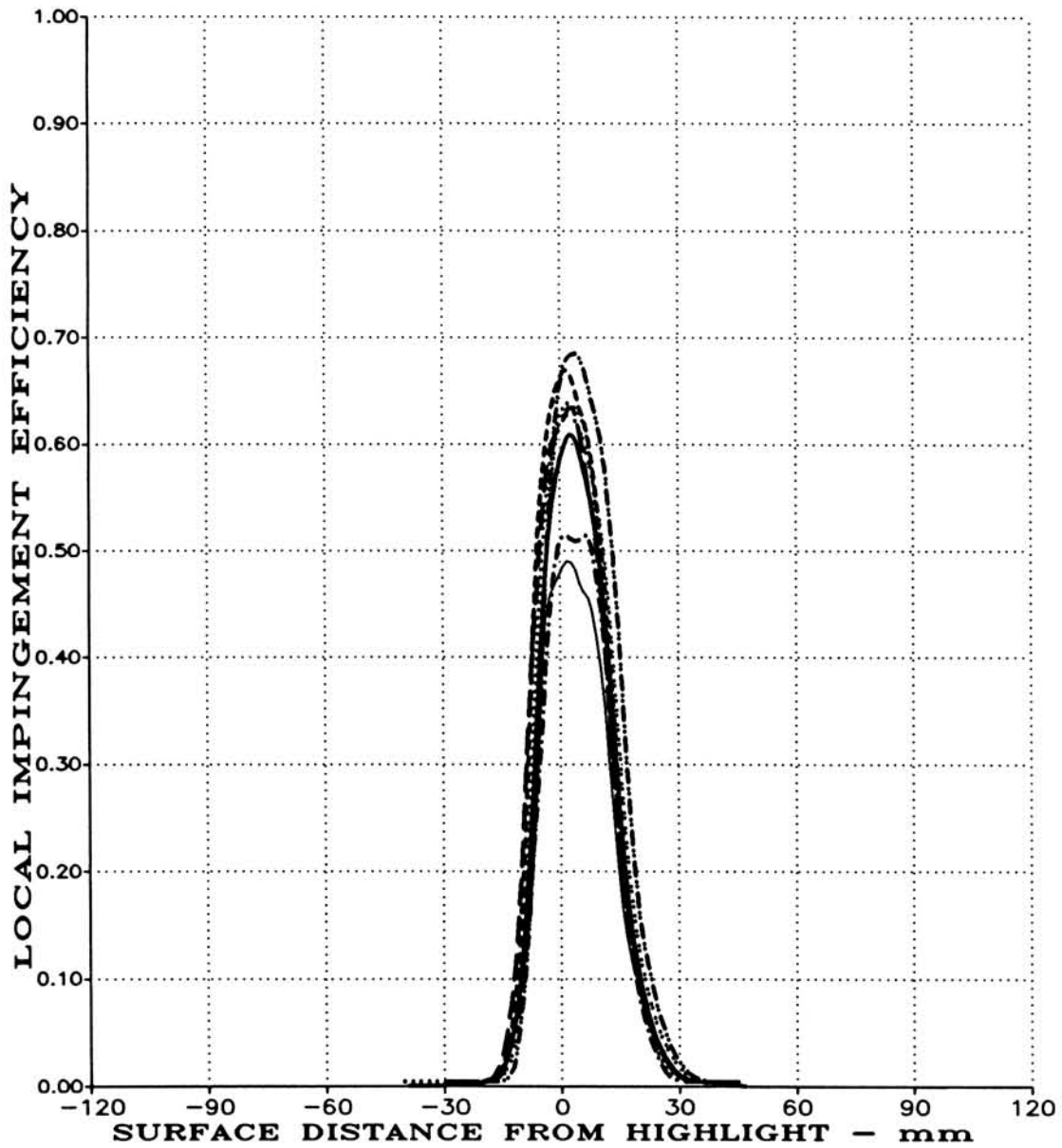


(Positive Surface Distance, S, on Inner Surface)

(B) MVD = 16 MICRONS, MASS FLOW = 17.2 LBM/S, $\theta = 45^\circ, 315^\circ$

FIGURE 7.10

TEST REPEATABILITY FOR BOEING 737-300 INLET AT $\alpha = 15^\circ$
(PAGE 2 OF 5).

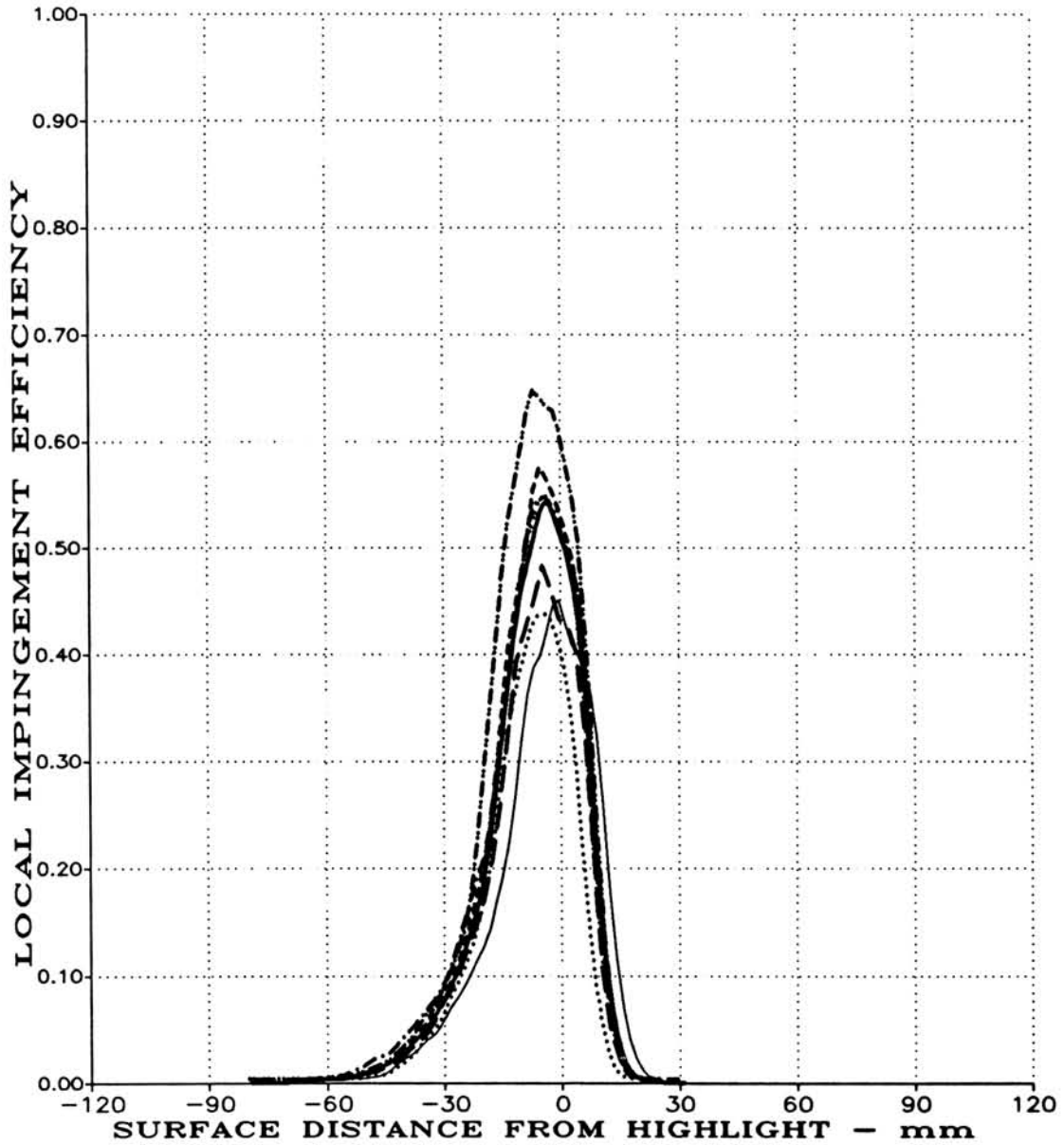


(Positive Surface Distance, S, on Inner Surface)

(C) MVD = 16 MICRONS, MASS FLOW = 17.2 LBM/S, $\theta = 90^\circ, 270^\circ$

FIGURE 7.10

TEST REPEATABILITY FOR BOEING 737-300 INLET AT $\alpha = 15^\circ$
(PAGE 3 OF 5).



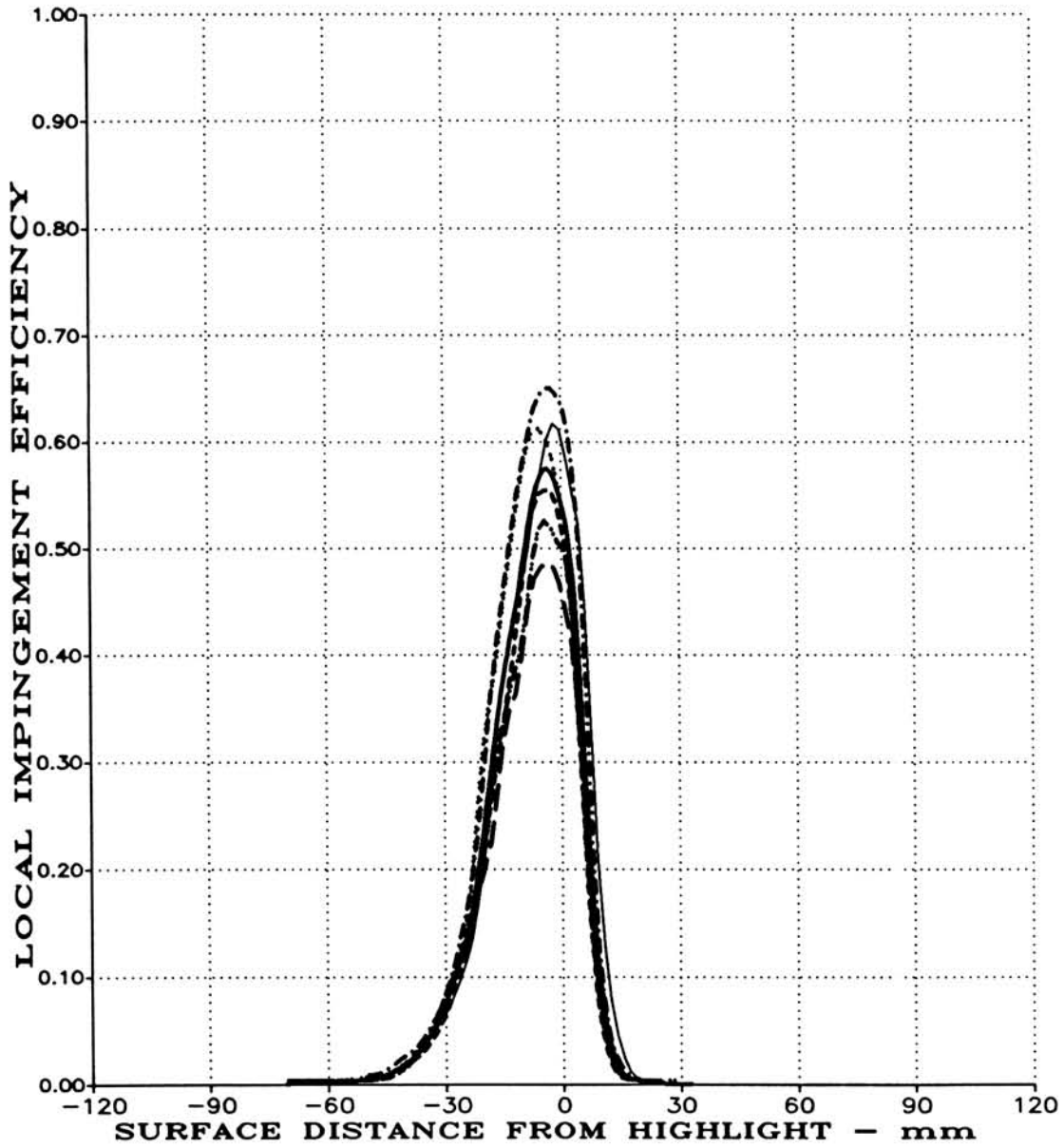
(Positive Surface Distance, S, on Inner Surface)

(D) MVD = 16 MICRONS, MASS FLOW = 17.2 LBM/S, $\theta = 135^\circ, 225^\circ$

FIGURE 7.10

TEST REPEATABILITY FOR BOEING 737-300 INLET AT $\alpha = 15^\circ$
(PAGE 4 OF 5).

TEST RUN ID: 1683615E, 1693615E, 1703615E,
1713615E, 1723615E, 1733615E



(Positive Surface Distance, S, on Inner Surface)

(E) MVD = 16 MICRONS, MASS FLOW = 17.2 LBM/S, $\theta = 180^\circ$

FIGURE 7.10

TEST REPEATABILITY FOR BOEING 737-300 INLET AT $\alpha = 15^\circ$
(PAGE 5 OF 5).

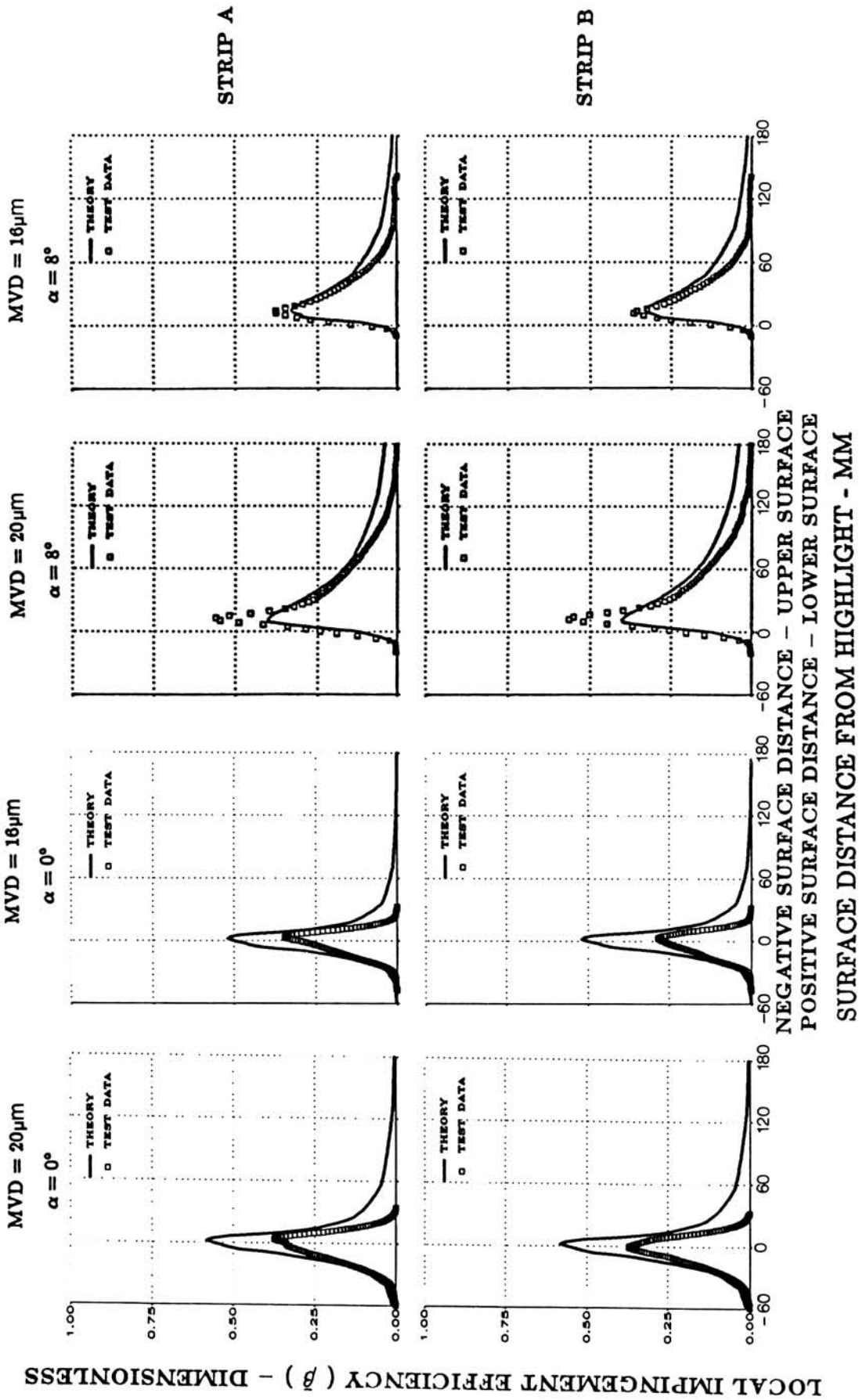
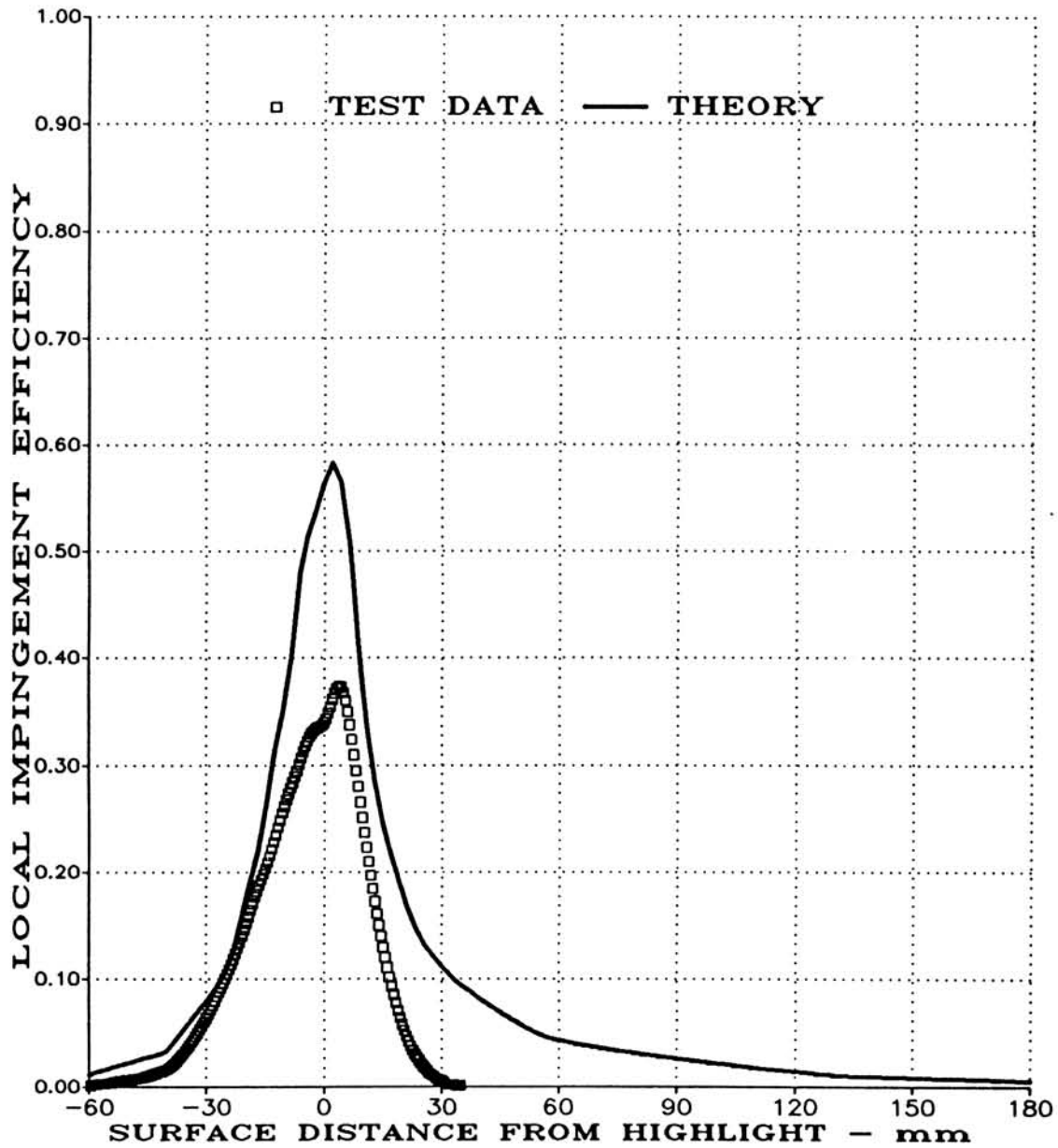


FIGURE 7.11
 AVERAGED LOCAL WATER IMPINGEMENT EFFICIENCY DATA
 FOR NLF(1)-0414 AIRFOIL. SUMMARY OF RESULTS.

TEST RUN ID: 220N900A, 221N900A, 222N900A,
223N900A, 224N900A, 225N900A



(Positive Surface Distance, S, on Lower Surface)

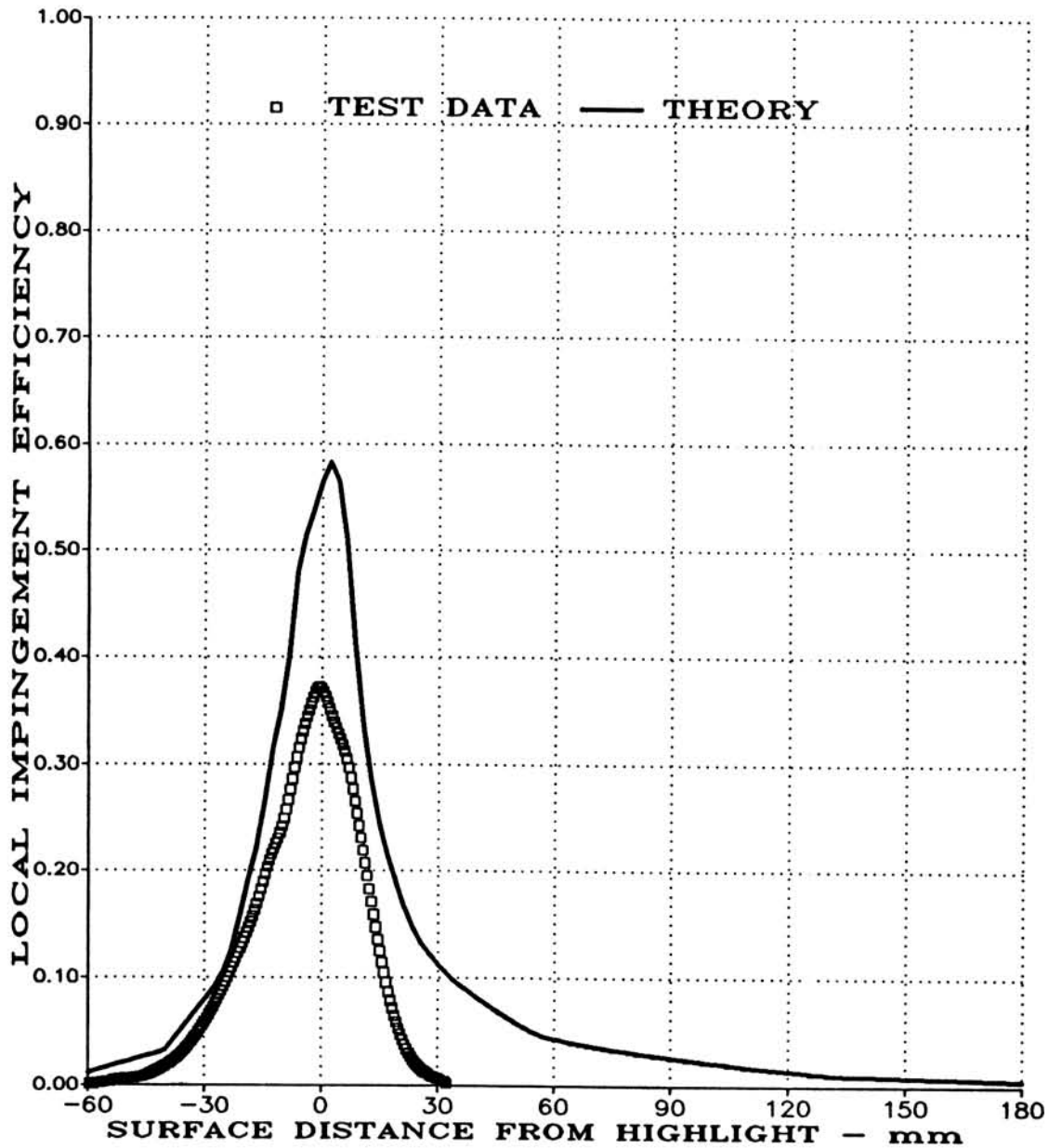
$$\bar{\beta}_{max} = 0.373, S_{U_{max}} = -48mm, S_{L_{max}} = 28mm \text{ (Experiment)}$$

(A) STRIP A, MVD = 20 MICRONS

FIGURE 7.12

AVERAGED LOCAL WATER IMPINGEMENT EFFICIENCY DATA
FOR NLF(1)-0414 AIRFOIL AT $\alpha = 0^\circ$ ($V_\infty = 165$ mph, $K_{0_{mvd}} = 0.036$)
(PAGE 1 OF 2).

TEST RUN ID: 220N900B, 221N900B, 222N900B,
223N900B, 224N900B, 225N900B



(Positive Surface Distance, S, on Lower Surface)

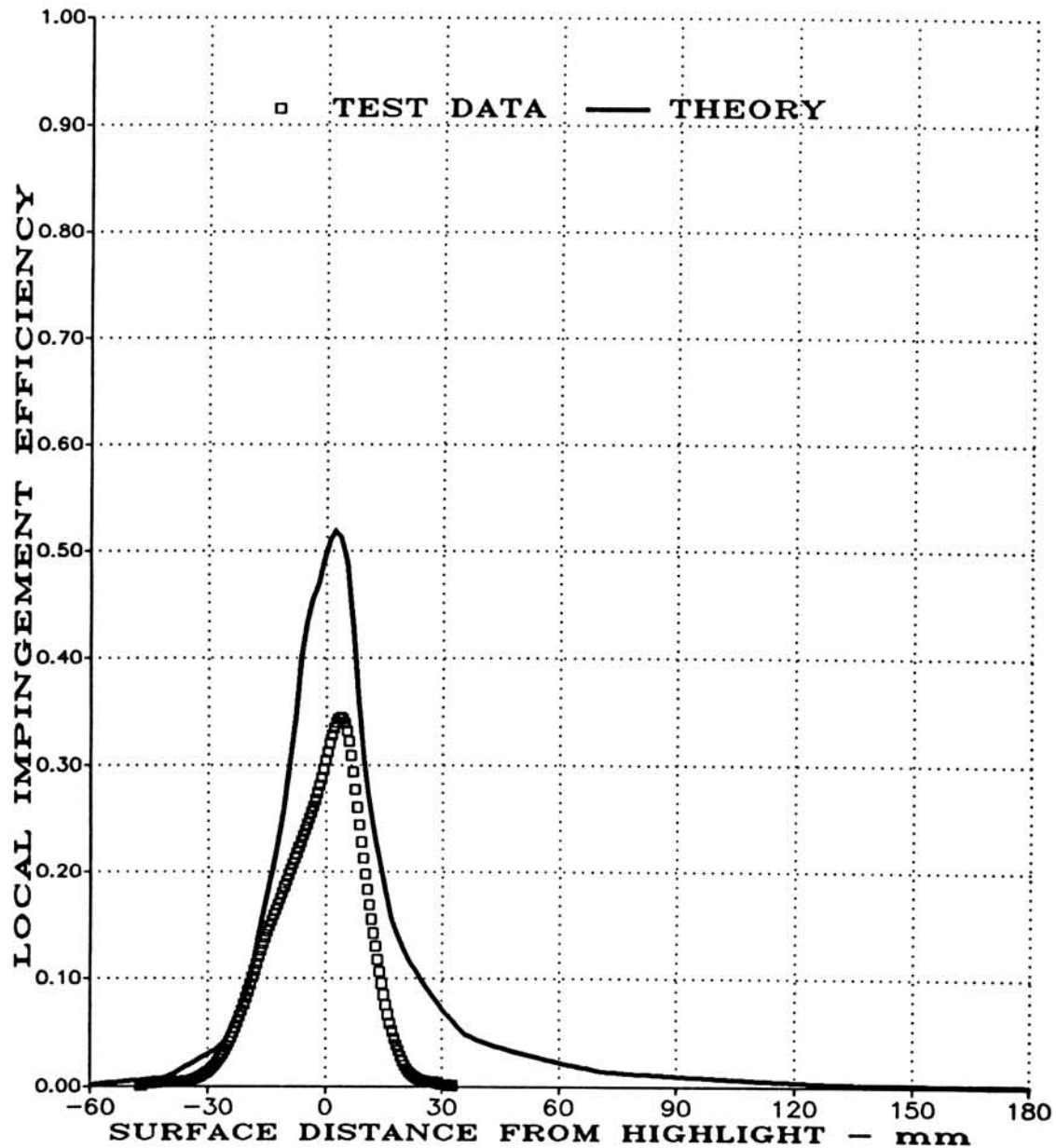
$$\bar{\beta}_{max} = 0.372, S_{U_{max}} = -48mm, S_{L_{max}} = 28mm \text{ (Experiment)}$$

(A) STRIP B, MVD = 20 MICRONS

FIGURE 7.12

AVERAGED LOCAL WATER IMPINGEMENT EFFICIENCY DATA
FOR NLF(1)-0414 AIRFOIL AT $\alpha = 0^\circ$ ($V_\infty = 165$ mph, $K_{0_{mvd}} = 0.036$)
(PAGE 2 OF 2).

TEST RUN ID: 226N600A, 227N600A, 228N600A,
229N600A, 230N600A



(Positive Surface Distance, S, on Lower Surface)

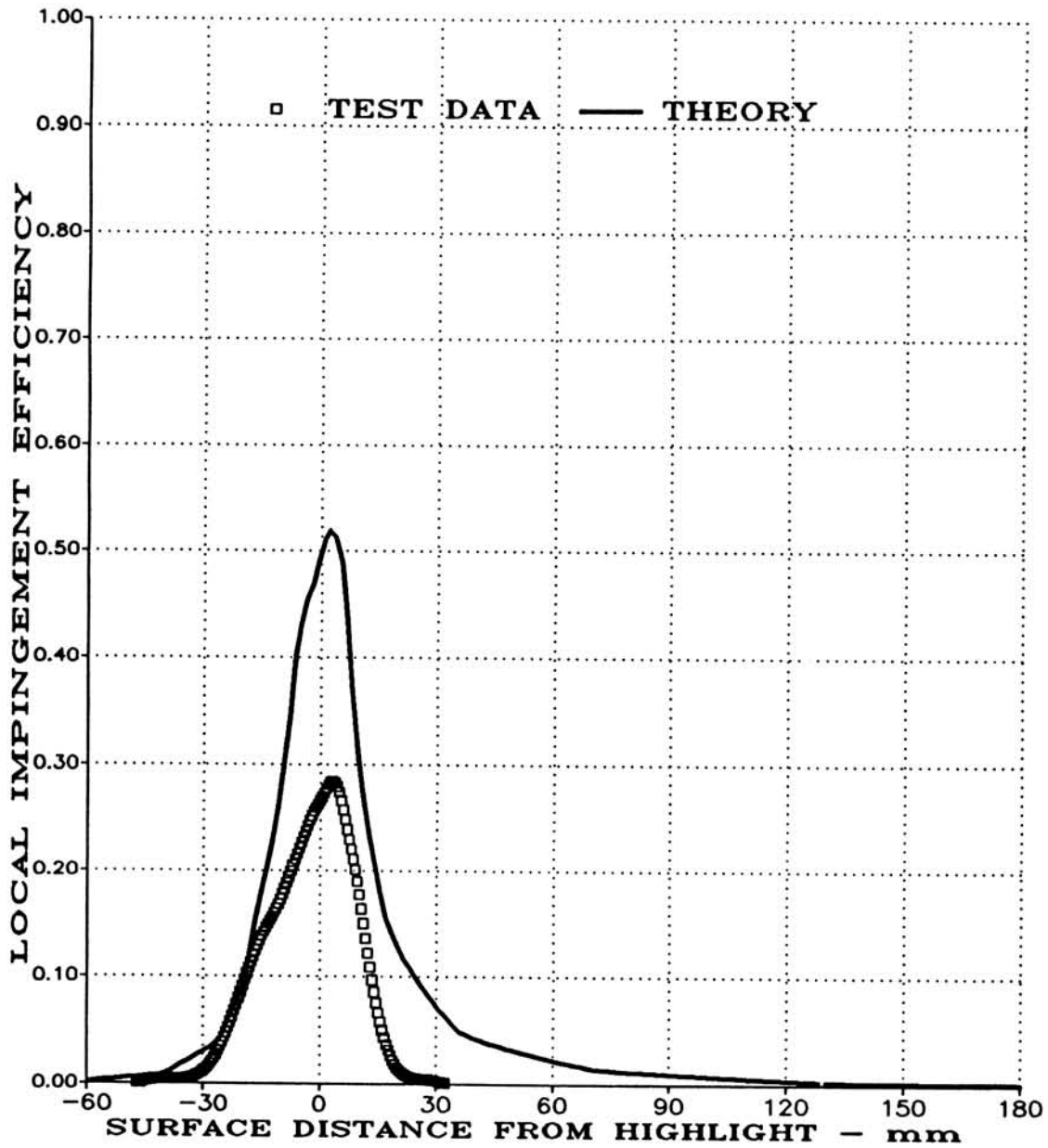
$\bar{\beta}_{max} = 0.344$, $S_{U_{max}} = -37mm$, $S_{L_{max}} = 20mm$ (Experiment)

(A) STRIP A, MVD = 16 MICRONS

FIGURE 7.13

AVERAGED LOCAL WATER IMPINGEMENT EFFICIENCY DATA
FOR NLF(1)-0414 AIRFOIL AT $\alpha = 0^\circ$ ($V_\infty = 165$ mph, $K_{0_{mvd}} = 0.025$)
(PAGE 1 OF 2).

TEST RUN ID: 226N600B, 227N600B, 228N600B,
229N600B, 230N600B



(Positive Surface Distance, S, on Lower Surface)

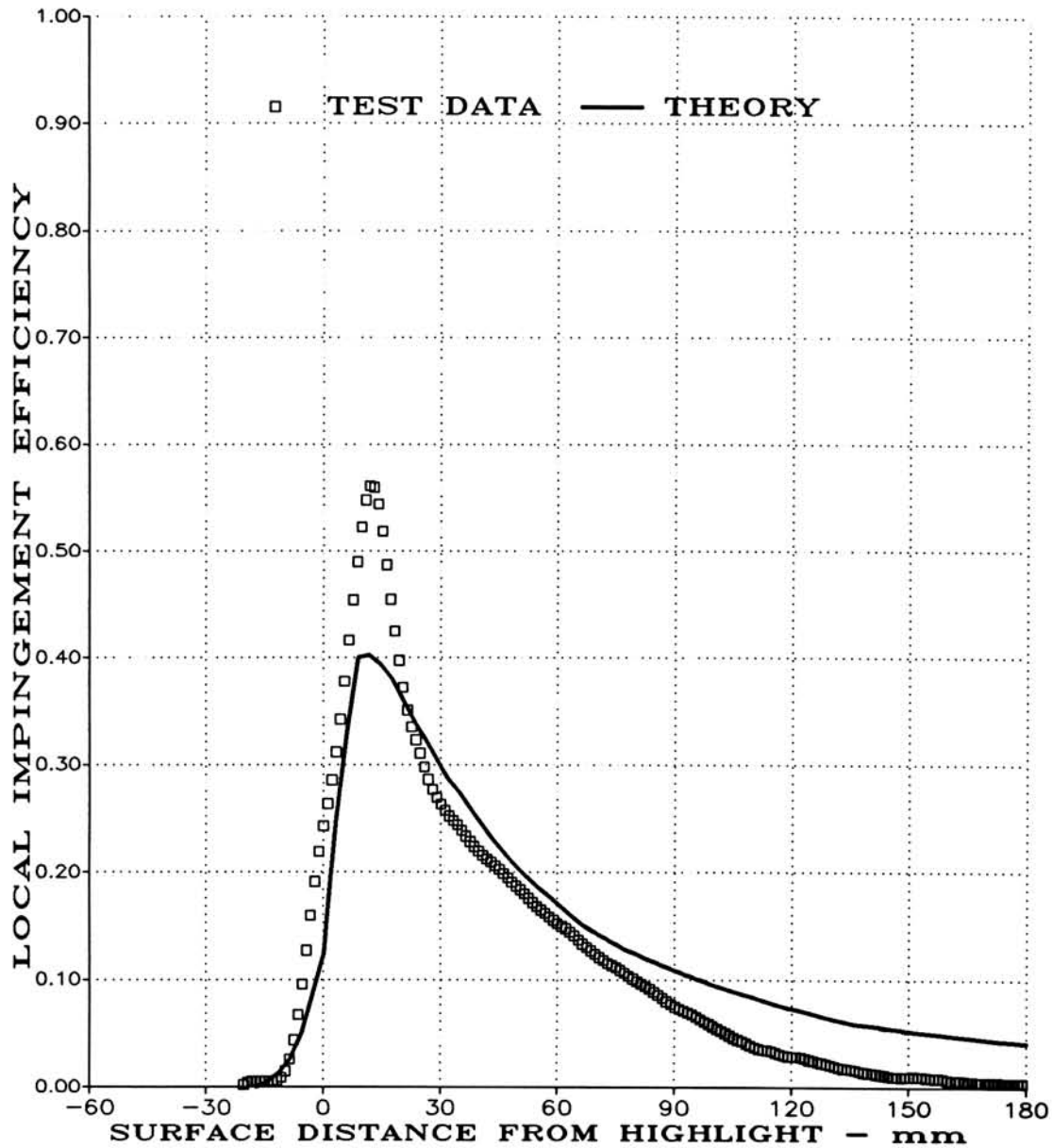
$\bar{\beta}_{max} = 0.285$, $S_{U_{max}} = -37mm$, $S_{L_{max}} = 20mm$ (Experiment)

(A) STRIP B, MVD = 16 MICRONS

FIGURE 7.13

AVERAGED LOCAL WATER IMPINGEMENT EFFICIENCY DATA
FOR NLF(1)-0414 AIRFOIL AT $\alpha = 0^\circ$ ($V_\infty = 165$ mph, $K_{0_{mvd}} = 0.025$)
(PAGE 2 OF 2).

TEST RUN ID: 215N908A, 216N908A, 217N908A,
218N908A, 219N908A



(Positive Surface Distance, S, on Lower Surface)

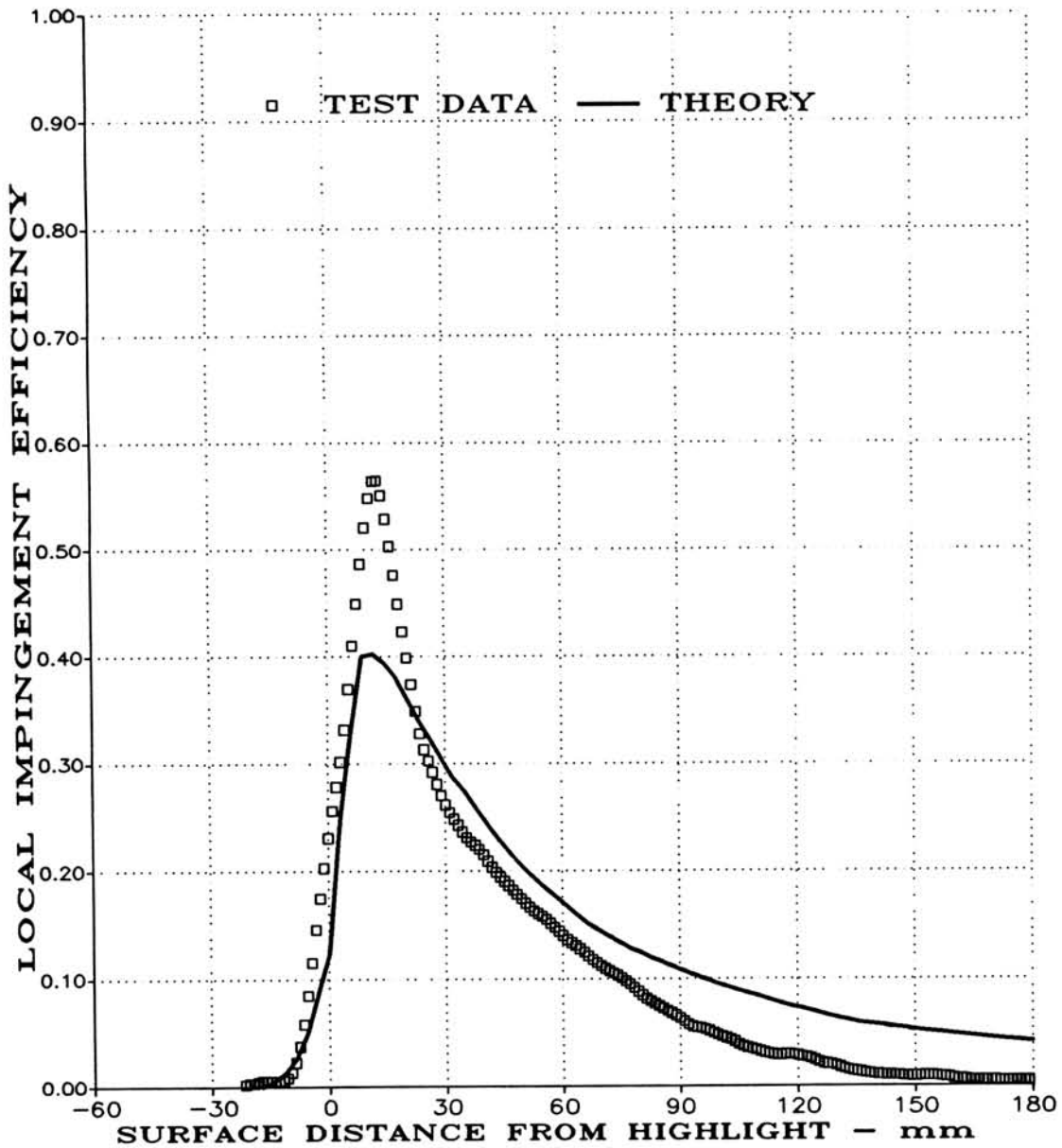
$\bar{\beta}_{max} = 0.562, S_{U_{max}} = -10mm, S_{L_{max}} = 230mm$ (Experiment)

(A) STRIP A, MVD = 20 MICRONS

FIGURE 7.14

AVERAGED LOCAL WATER IMPINGEMENT EFFICIENCY DATA
FOR NLF(1)-0414 AIRFOIL AT $\alpha = 8^\circ$ ($V_\infty = 165$ mph, $K_{0,mvd} = 0.036$)
(PAGE 1 OF 2).

TEST RUN ID: 215N908B, 216N908B, 217N908B,
218N908B, 219N908B



(Positive Surface Distance, S, on Lower Surface)

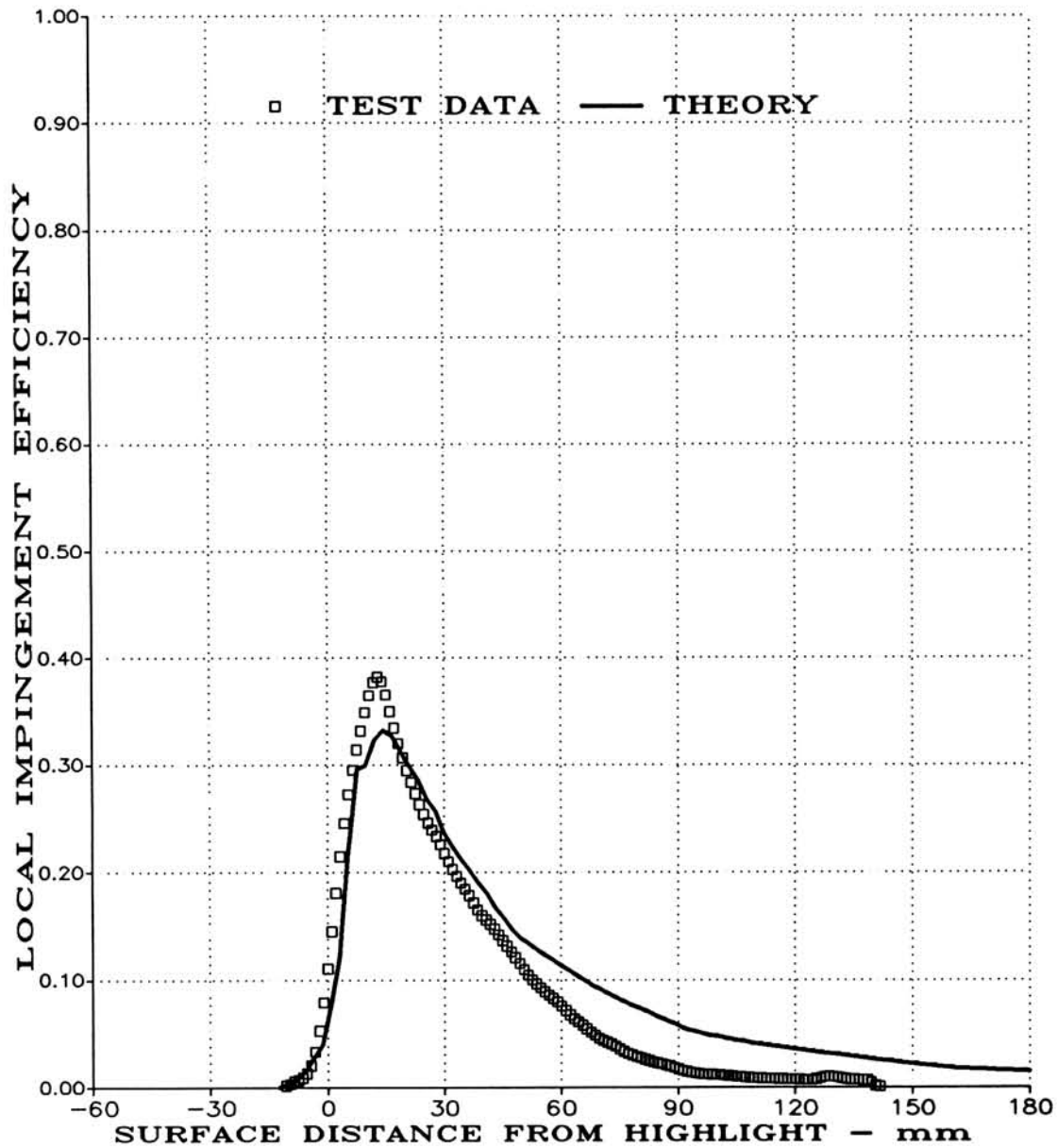
$$\bar{\beta}_{max} = 0.566, S_{U_{max}} = -10mm, S_{L_{max}} = 230mm \text{ (Experiment)}$$

(A) STRIP B, MVD = 20 MICRONS

FIGURE 7.14

AVERAGED LOCAL WATER IMPINGEMENT EFFICIENCY DATA
FOR NLF(1)-0414 AIRFOIL AT $\alpha = 8^\circ$ ($V_\infty = 165$ mph, $K_{0,mvd} = 0.036$)
(PAGE 2 OF 2).

TEST RUN ID: 232N608A, 233N608A, 234N608A,
235N608A, 236N608A



(Positive Surface Distance, S, on Lower Surface)

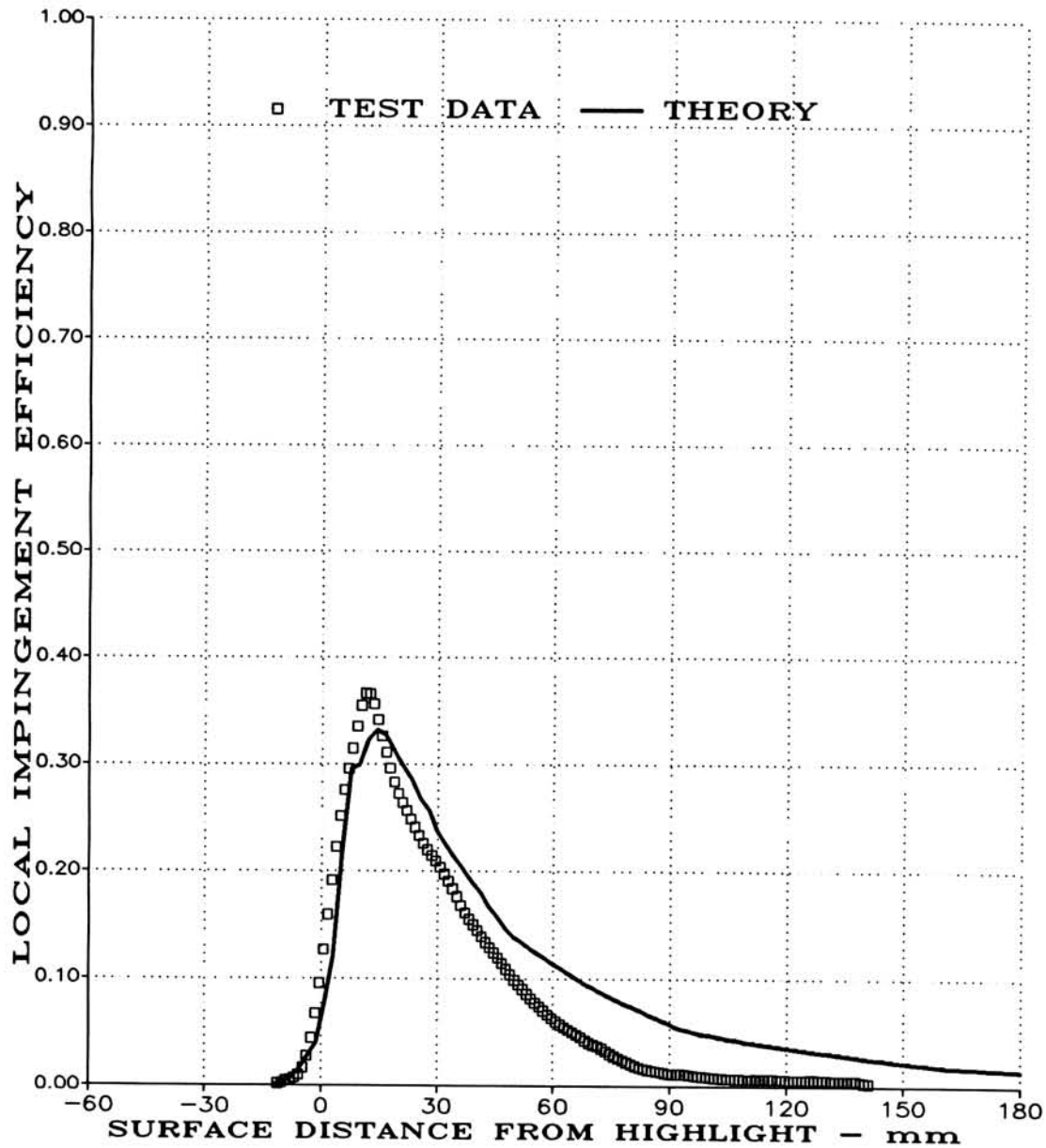
$\bar{\beta}_{max} = 0.382$, $S_{U_{max}} = -5mm$, $S_{L_{max}} = 127mm$ (Experiment)

(A) STRIP A, MVD = 16 MICRONS

FIGURE 7.15

AVERAGED LOCAL WATER IMPINGEMENT EFFICIENCY DATA
FOR NLF(1)-0414 AIRFOIL AT $\alpha = 8^\circ$ ($V_\infty = 165$ mph, $K_{0,mvd} = 0.025$)
(PAGE 1 OF 2).

TEST RUN ID: 232N608B, 233N608B, 234N608B,
235N608B, 236N608B



(Positive Surface Distance, S, on Lower Surface)

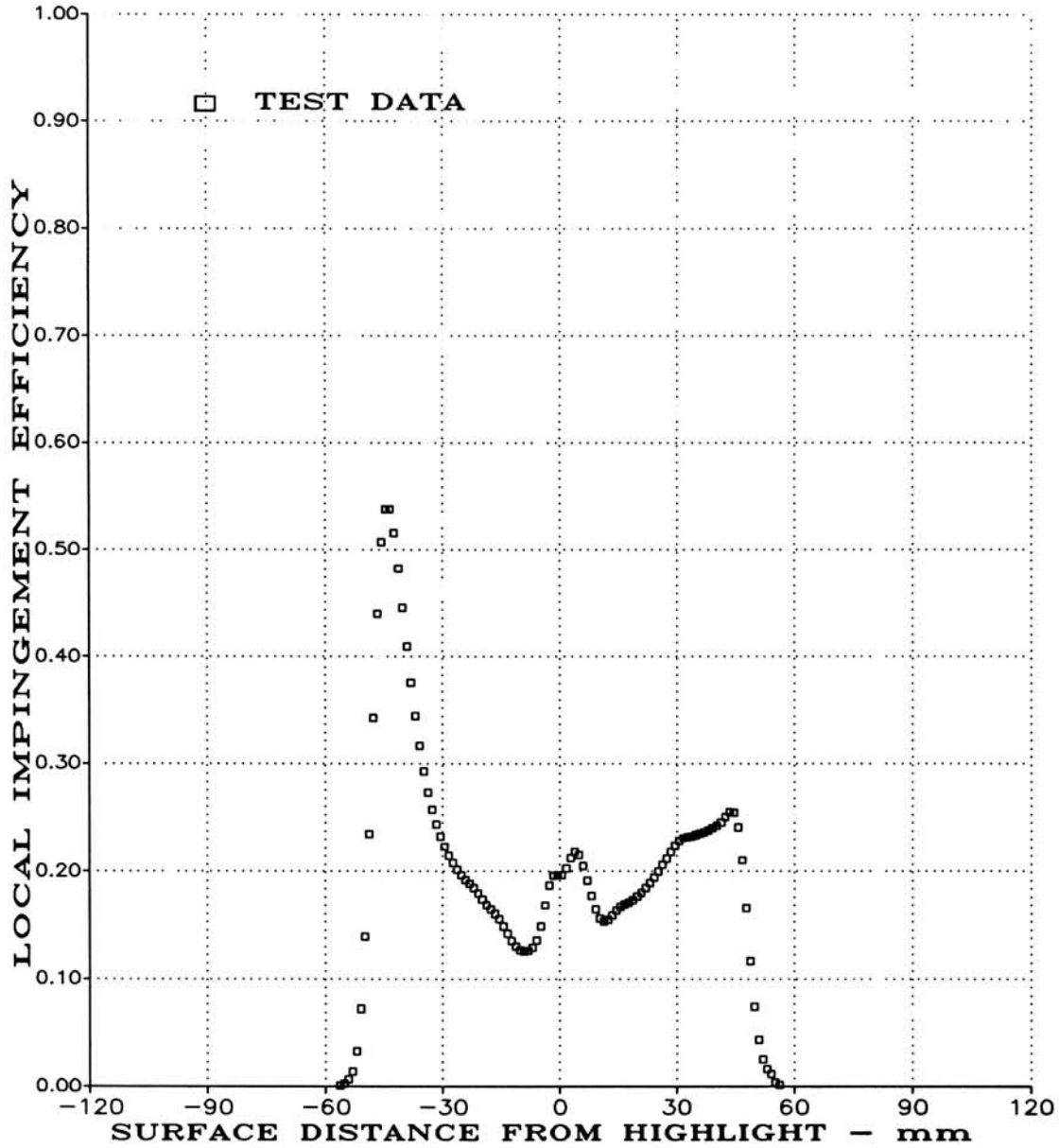
$\bar{\beta}_{max} = 0.368$, $S_{U_{max}} = -5mm$, $S_{L_{max}} = 127mm$ (Experiment)

(A) STRIP B, MVD = 16 MICRONS

FIGURE 7.15

AVERAGED LOCAL WATER IMPINGEMENT EFFICIENCY DATA
FOR NLF(1)-0414 AIRFOIL AT $\alpha = 8^\circ$ ($V_\infty = 165$ mph, $K_{0_{mvd}} = 0.025$)
(PAGE 2 OF 2).

TEST RUN ID: 116I900AB, 117I900AB, 118I900AB,
119I900AB, 120I900AB



(Positive Surface Distance, S, on Lower Surface)

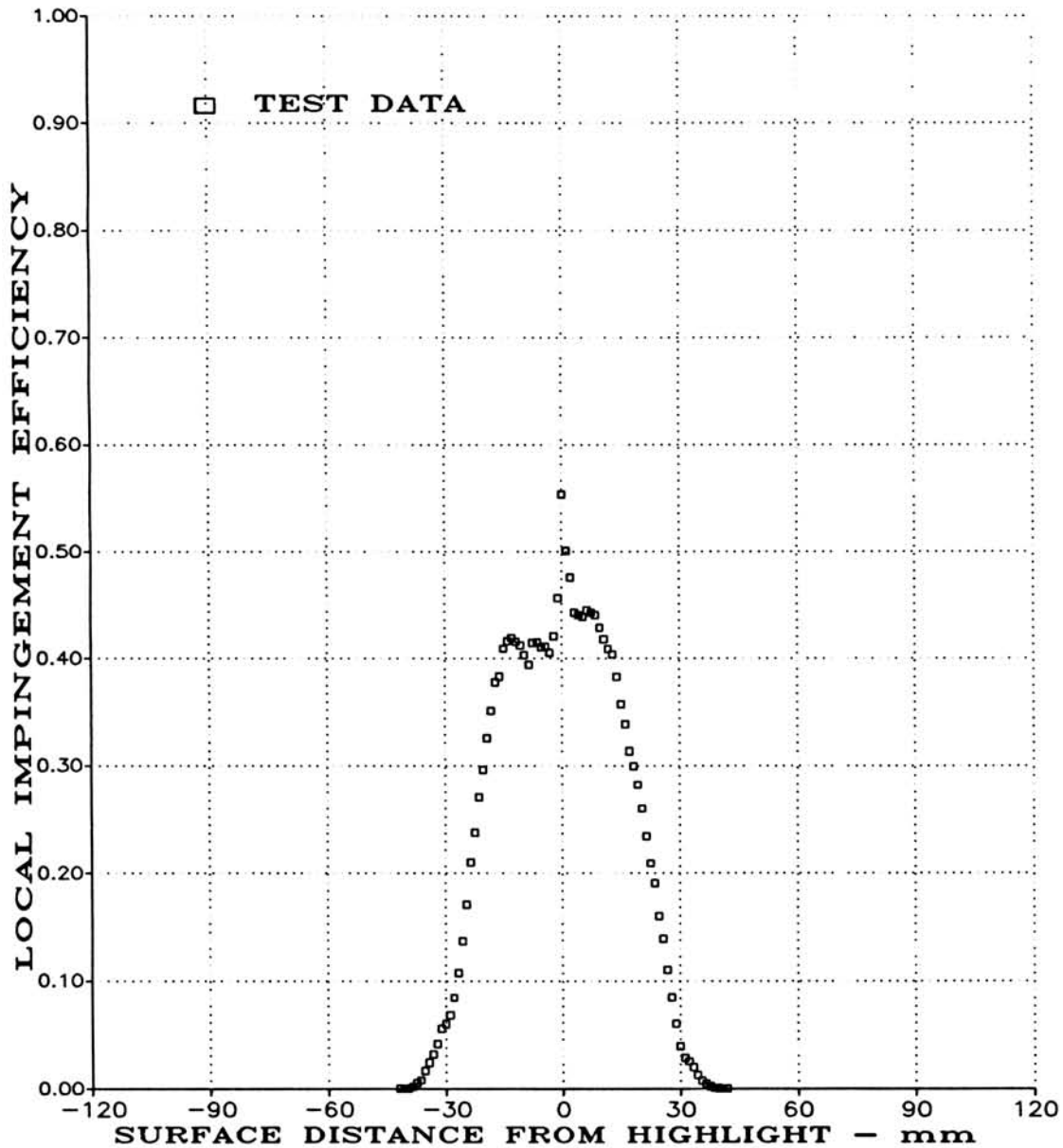
$$\bar{\beta}_{max} = 0.540, S_{U_{max}} = -53mm, S_{L_{max}} = 53mm \text{ (Experiment)}$$

(A) STRIPS A,B, MVD = 20 MICRONS

FIGURE 7.16

AVERAGED LOCAL WATER IMPINGEMENT EFFICIENCY DATA
FOR LARGE GLAZE ICE SHAPE, MOUNTED ON 2 INCH CYLINDER,
AT $\alpha = 0^\circ$ ($V_\infty = 165$ mph, $K_{0_{mvd}} = 0.648$).

TEST RUN ID: 121I900A, 122I900A, 123I900A,
124I900A, 125I900A



(Positive Surface Distance, S, on Lower Surface)

$$\bar{\beta}_{max} = 0.460, S_{U_{max}} = -37mm, S_{L_{max}} = 37mm \text{ (Experiment)}$$

(A) STRIPS A,B, MVD = 20 MICRONS

FIGURE 7.17

AVERAGED LOCAL WATER IMPINGEMENT EFFICIENCY DATA
FOR SMALL GLAZE ICE SHAPE, MOUNTED ON 2 INCH CYLINDER,
AT $\alpha = 0^\circ$ ($V_\infty = 165$ mph, $K_{0_{mvd}} = 0.648$).

LOCAL IMPINGEMENT EFFICIENCY (θ) - DIMENSIONLESS

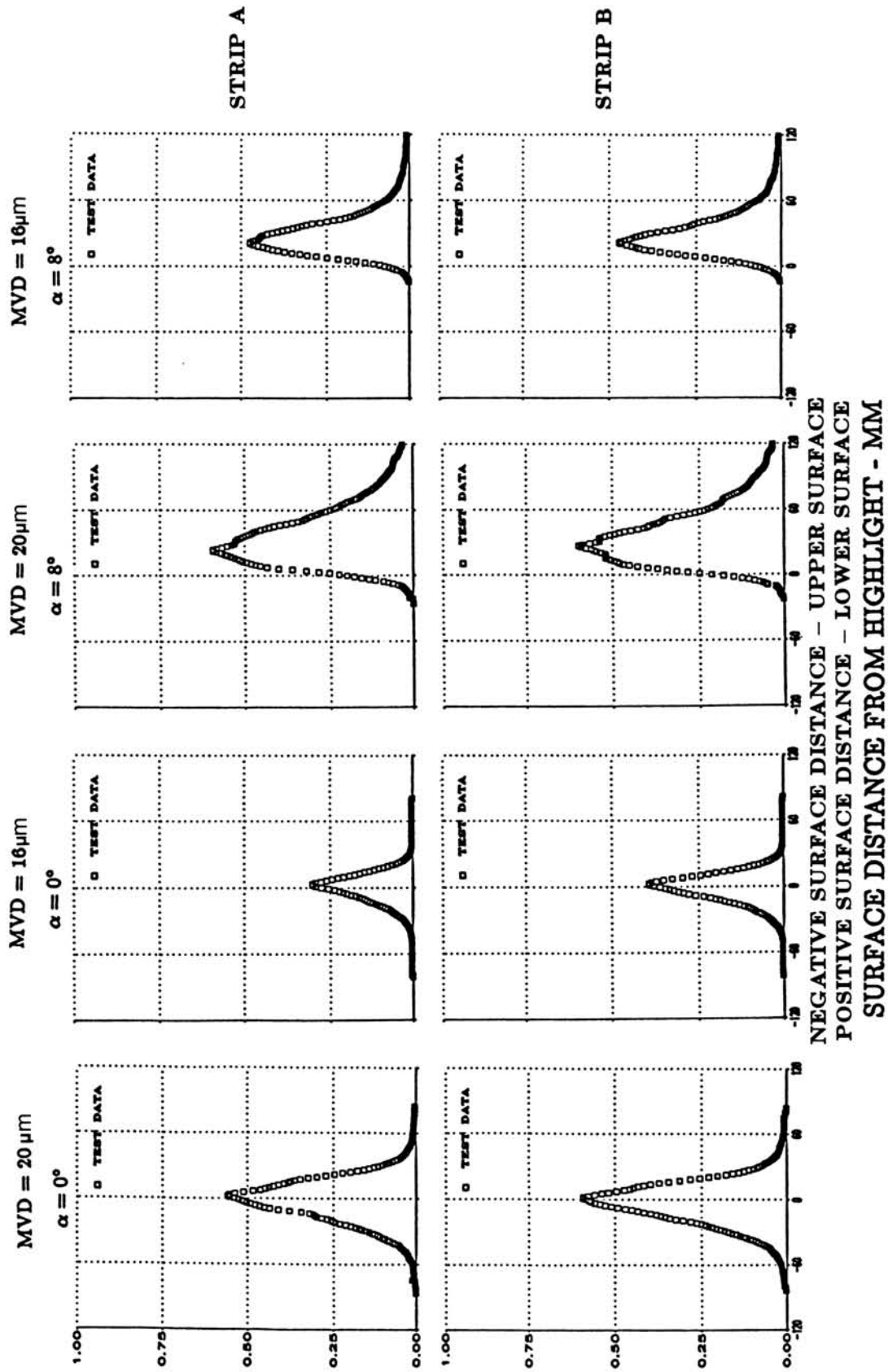
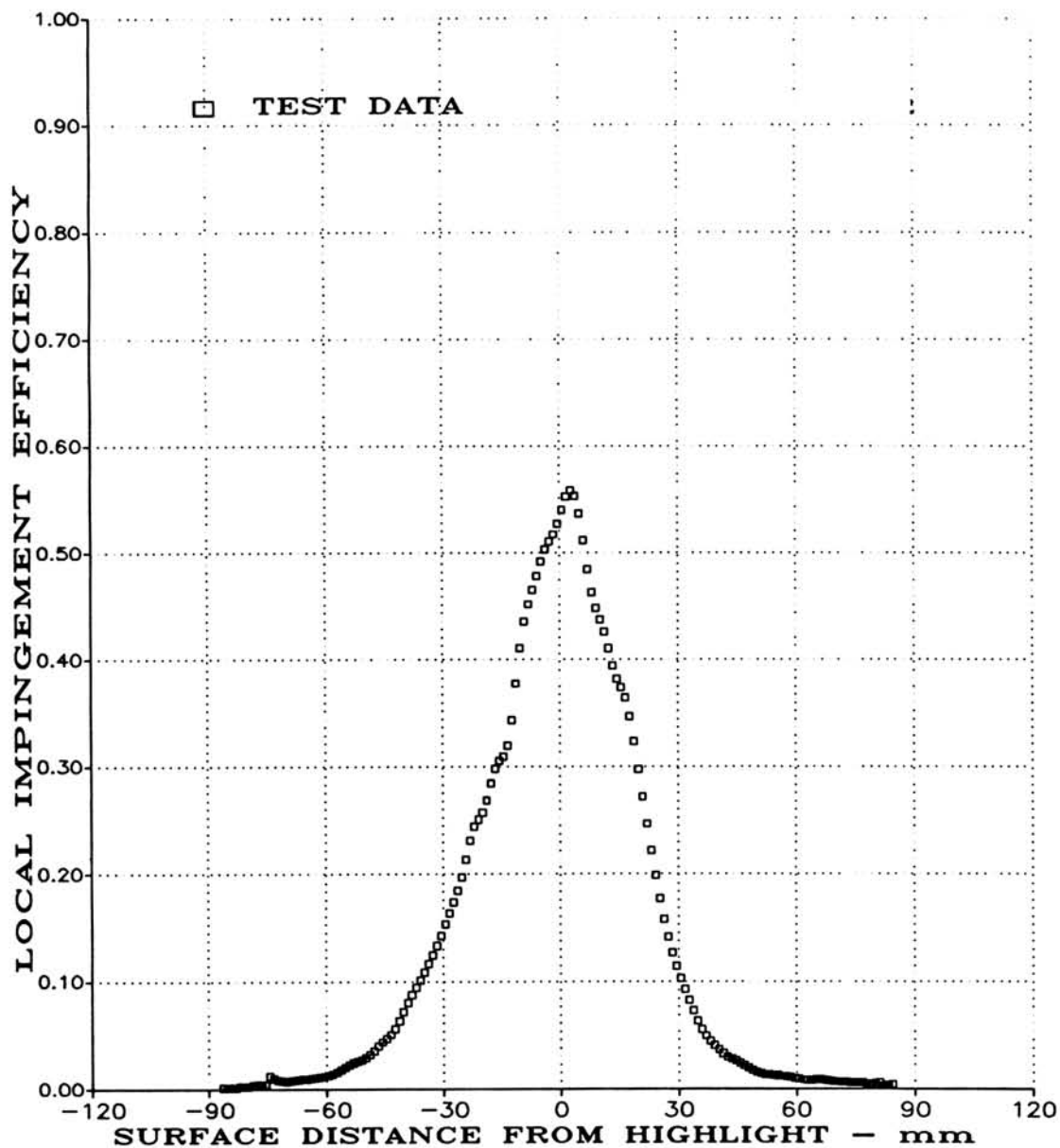


FIGURE 7.18

AVERAGED LOCAL WATER IMPINGEMENT EFFICIENCY DATA FOR MS(1)-0317 AIRFOIL. SUMMARY OF RESULTS.

TEST RUN ID: 149M900A, 150M900A, 151M900A,
152M900A, 153M900A



(Positive Surface Distance, S, on Lower Surface)

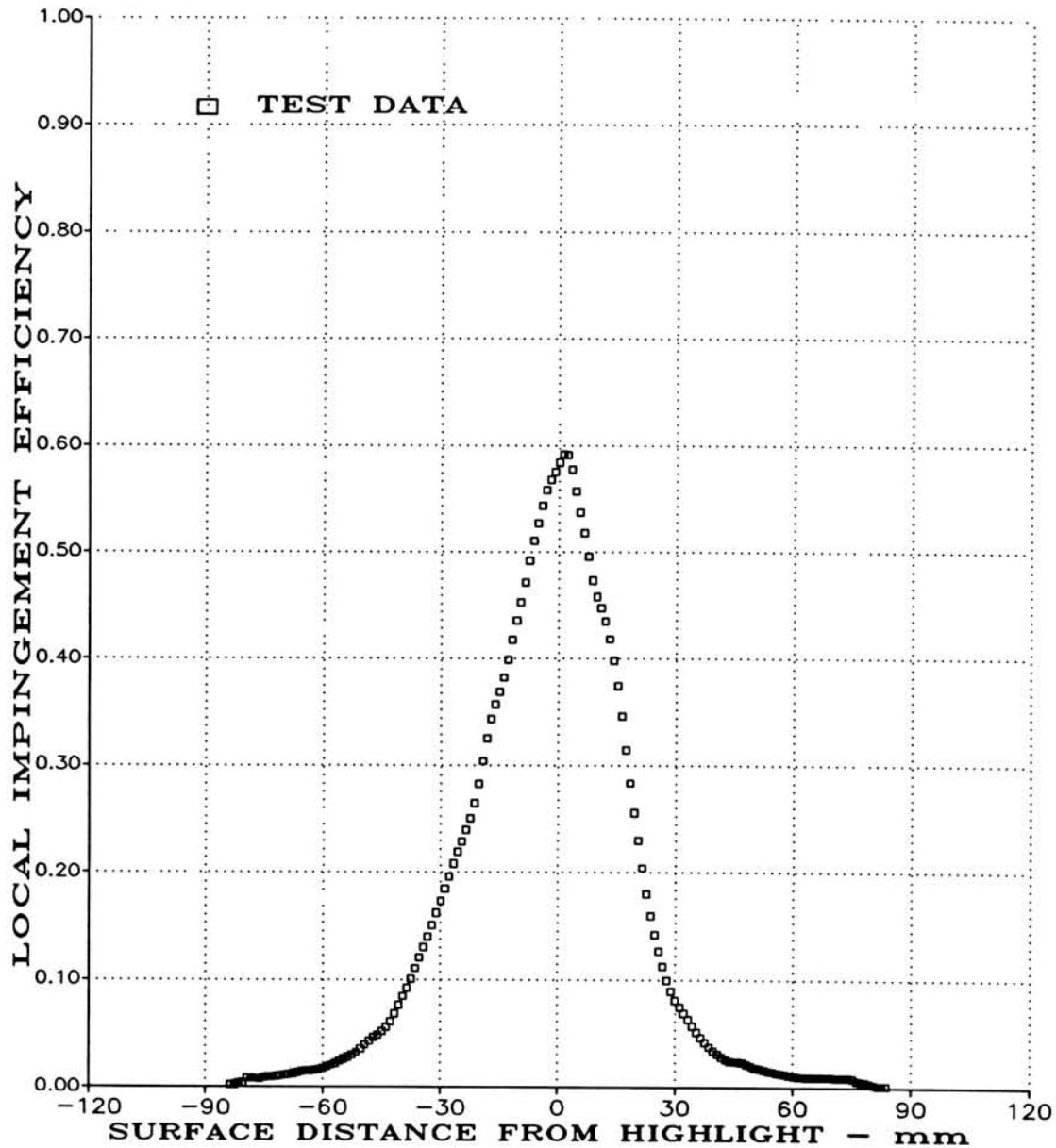
$$\bar{\beta}_{max} = 0.558, S_{U_{max}} = -63mm, S_{L_{max}} = 65mm$$

(A) STRIP A, MVD = 20 MICRONS

FIGURE 7.19

AVERAGED LOCAL WATER IMPINGEMENT EFFICIENCY DATA
FOR MS(1)-0317 AIRFOIL AT $\alpha = 0^\circ$ ($V_\infty = 165$ mph, $K_{0_{mvd}} = 0.036$)
(PAGE 1 OF 2).

TEST RUN ID: 149M900B, 150M900B, 151M900B,
152M900B, 153M900B



(Positive Surface Distance, S, on Lower Surface)

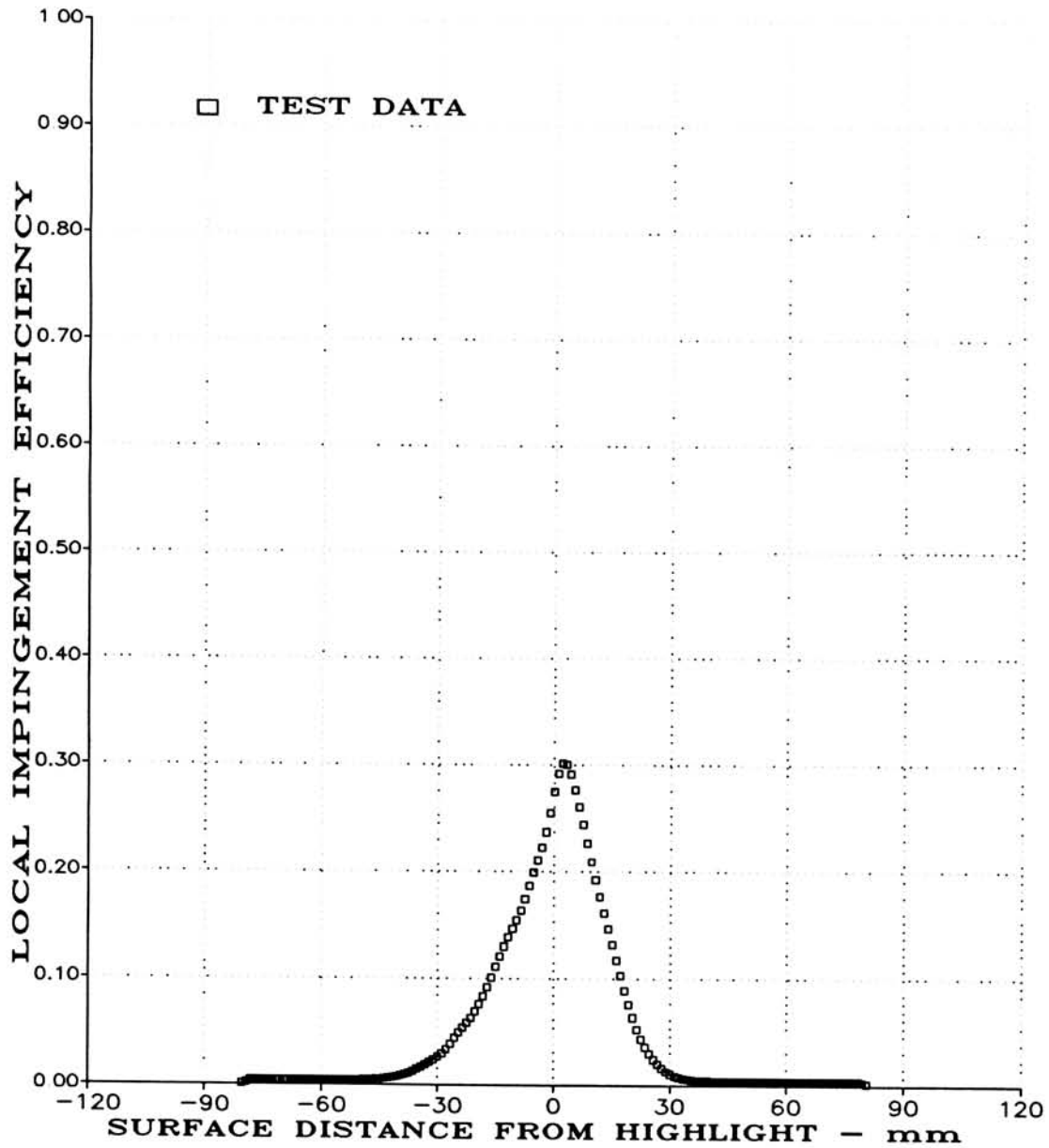
$$\bar{\beta}_{max} = 0.593, S_{U_{max}} = -63mm, S_{L_{max}} = 65mm$$

(B) STRIP B, MVD = 20 MICRONS

FIGURE 7.19

AVERAGED LOCAL WATER IMPINGEMENT EFFICIENCY DATA
FOR MS(1)-0317 AIRFOIL AT $\alpha = 0^\circ$ ($V_\infty = 165$ mph, $K_{0_{mvd}} = 0.036$)
(PAGE 2 OF 2).

TEST RUN ID: 154M600A, 155M600A, 156M600A,
157M600A



(Positive Surface Distance, S, on Lower Surface)

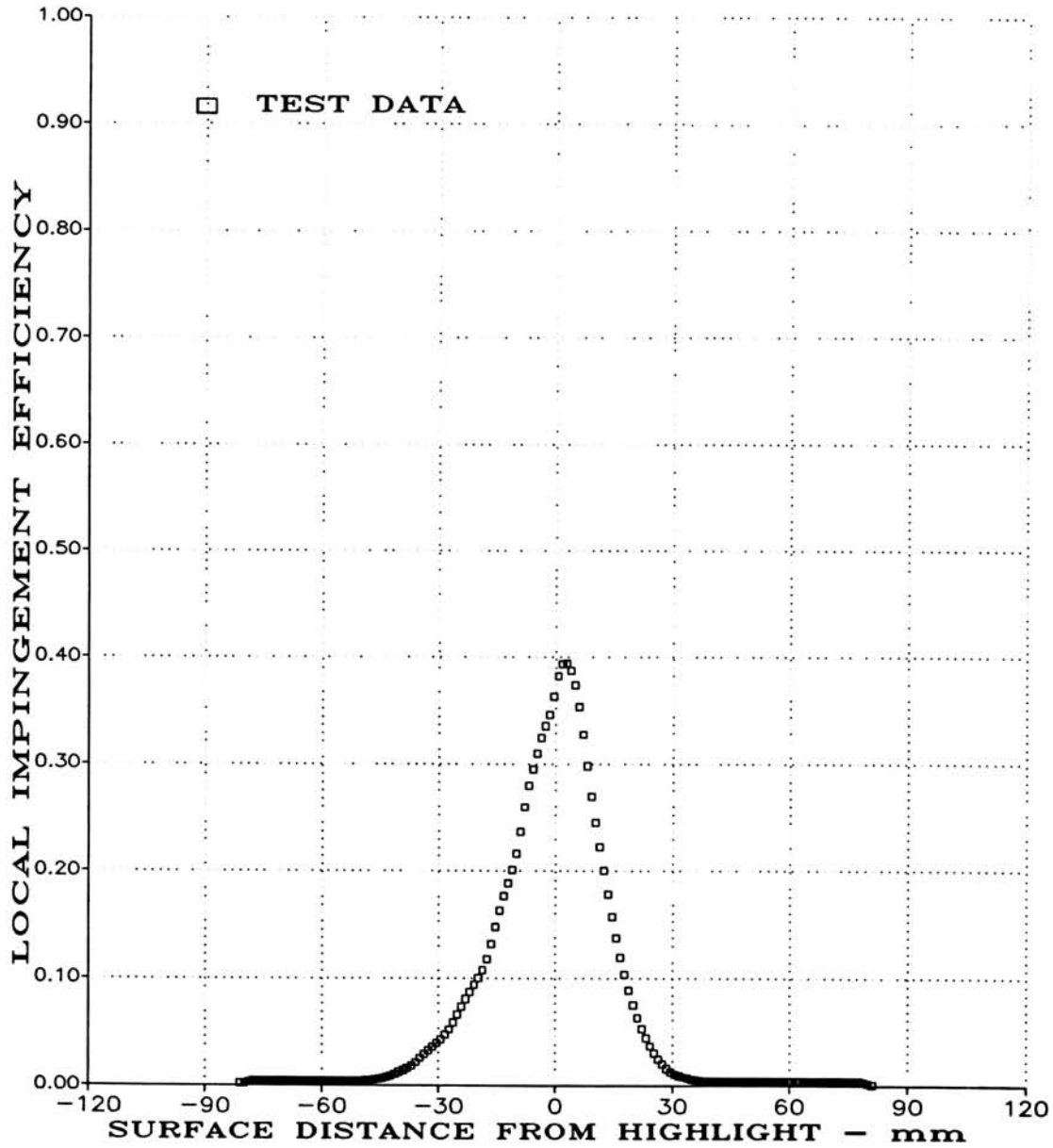
$$\bar{\beta}_{maz} = 0.302, S_{U_{maz}} = -40mm, S_{L_{maz}} = 30mm$$

(A) STRIP A, MVD = 16 MICRONS

FIGURE 7.20

AVERAGED LOCAL WATER IMPINGEMENT EFFICIENCY DATA
FOR MS(1)-0317 AIRFOIL AT $\alpha = 0^\circ$ ($V_\infty = 165$ mph, $K_{0_{mvd}} = 0.025$)
(PAGE 1 OF 2).

TEST RUN ID: 154M600B, 155M600B, 156M600B,
157M600B



(Positive Surface Distance, S, on Lower Surface)

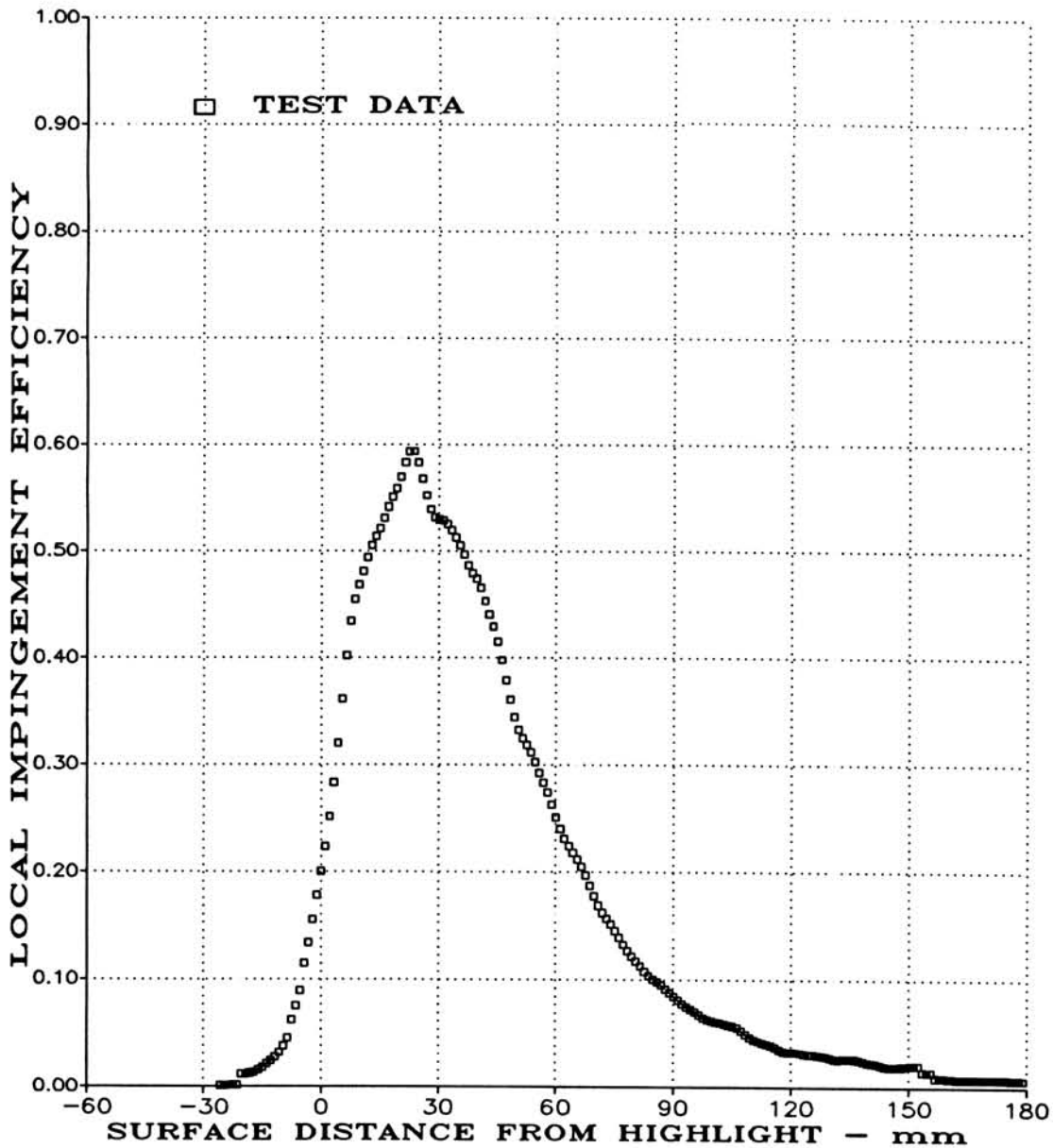
$$\bar{\beta}_{max} = 0.395, S_{U_{max}} = -40mm, S_{L_{max}} = 29mm$$

(B) STRIP B, MVD = 16 MICRONS

FIGURE 7.20

AVERAGED LOCAL WATER IMPINGEMENT EFFICIENCY DATA
FOR MS(1)-0317 AIRFOIL AT $\alpha = 0^\circ$ ($V_\infty = 165$ mph, $K_{0_{mvd}} = 0.025$)
(PAGE 2 OF 2).

TEST RUN ID: 163M908A, 164M908A, 165M908A,
166M908A, 167M908A



(Positive Surface Distance, S, on Lower Surface)

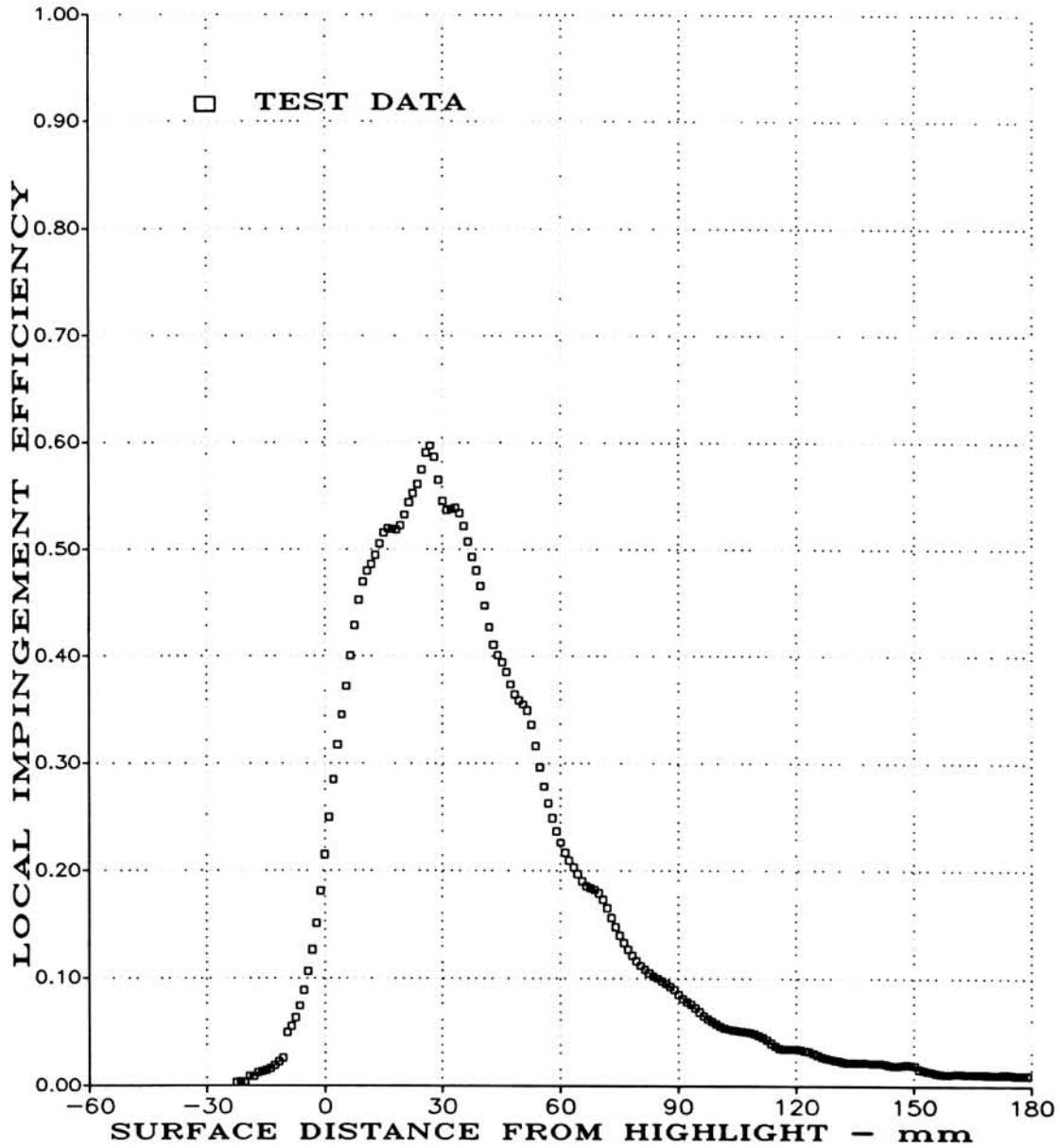
$$\bar{\beta}_{max} = 0.595, S_{U_{max}} = -12mm, S_{L_{max}} = 155mm$$

(A) STRIP A, MVD = 20 MICRONS

FIGURE 7.21

AVERAGED LOCAL WATER IMPINGEMENT EFFICIENCY DATA
FOR MS(1)-0317 AIRFOIL AT $\alpha = 8^\circ$ ($V_\infty = 165$ mph, $K_{0_{mvd}} = 0.036$)
(PAGE 1 OF 2).

TEST RUN ID: 163M908B, 164M908B, 165M908B,
166M908B, 167M908B



(Positive Surface Distance, S, on Lower Surface)

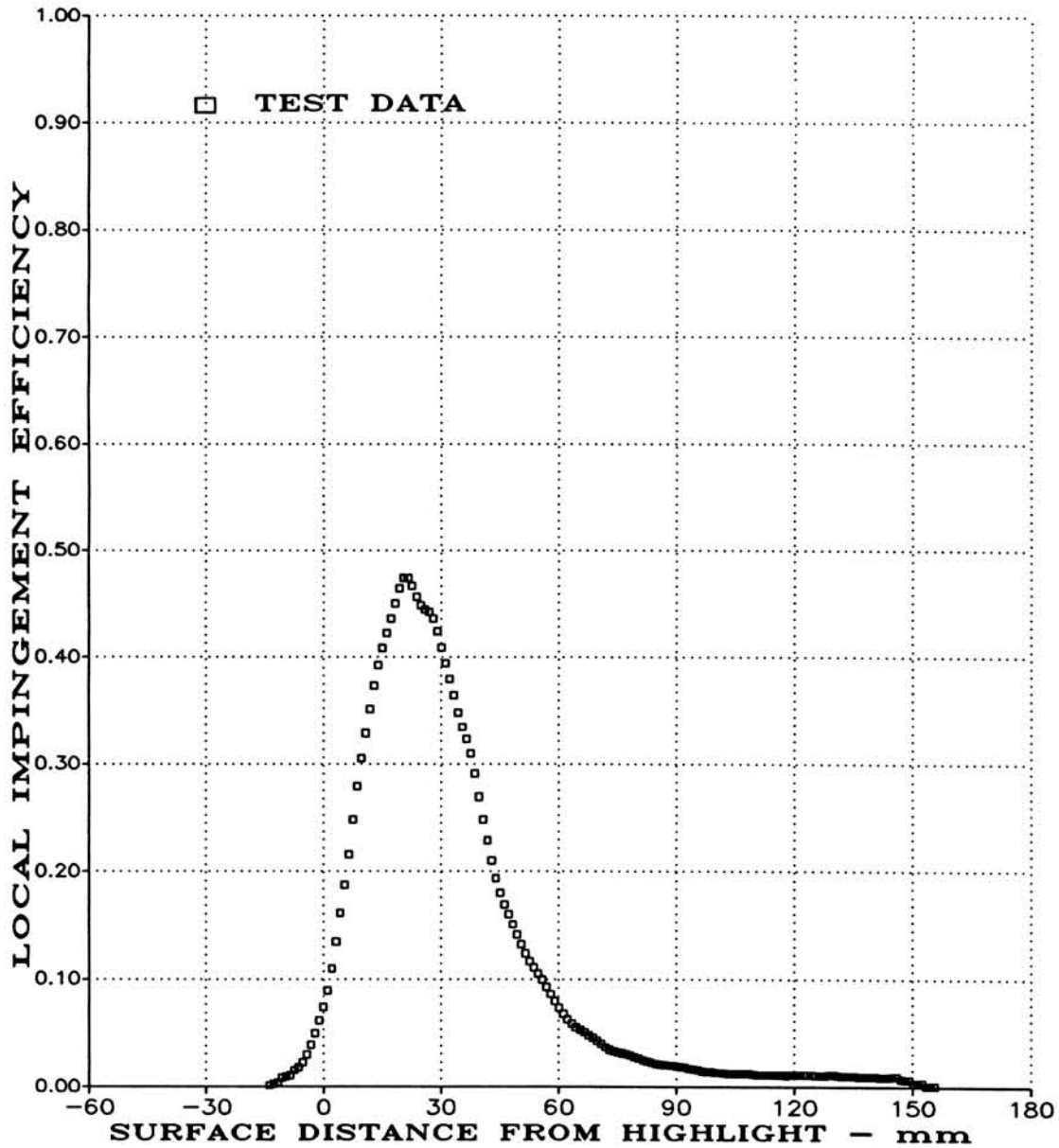
$$\bar{\beta}_{max} = 0.597, S_{U_{max}} = -10mm, S_{L_{max}} = 155mm$$

(B) STRIP B, MVD = 20 MICRONS

FIGURE 7.21

AVERAGED LOCAL WATER IMPINGEMENT EFFICIENCY DATA
FOR MS(1)-0317 AIRFOIL AT $\alpha = 8^\circ$ ($V_\infty = 165$ mph, $K_{0_{mvd}} = 0.036$)
(PAGE 2 OF 2).

TEST RUN ID: 158M608A, 159M608A, 160M608A,
161M608A, 162M608A



(Positive Surface Distance, S, on Lower Surface)

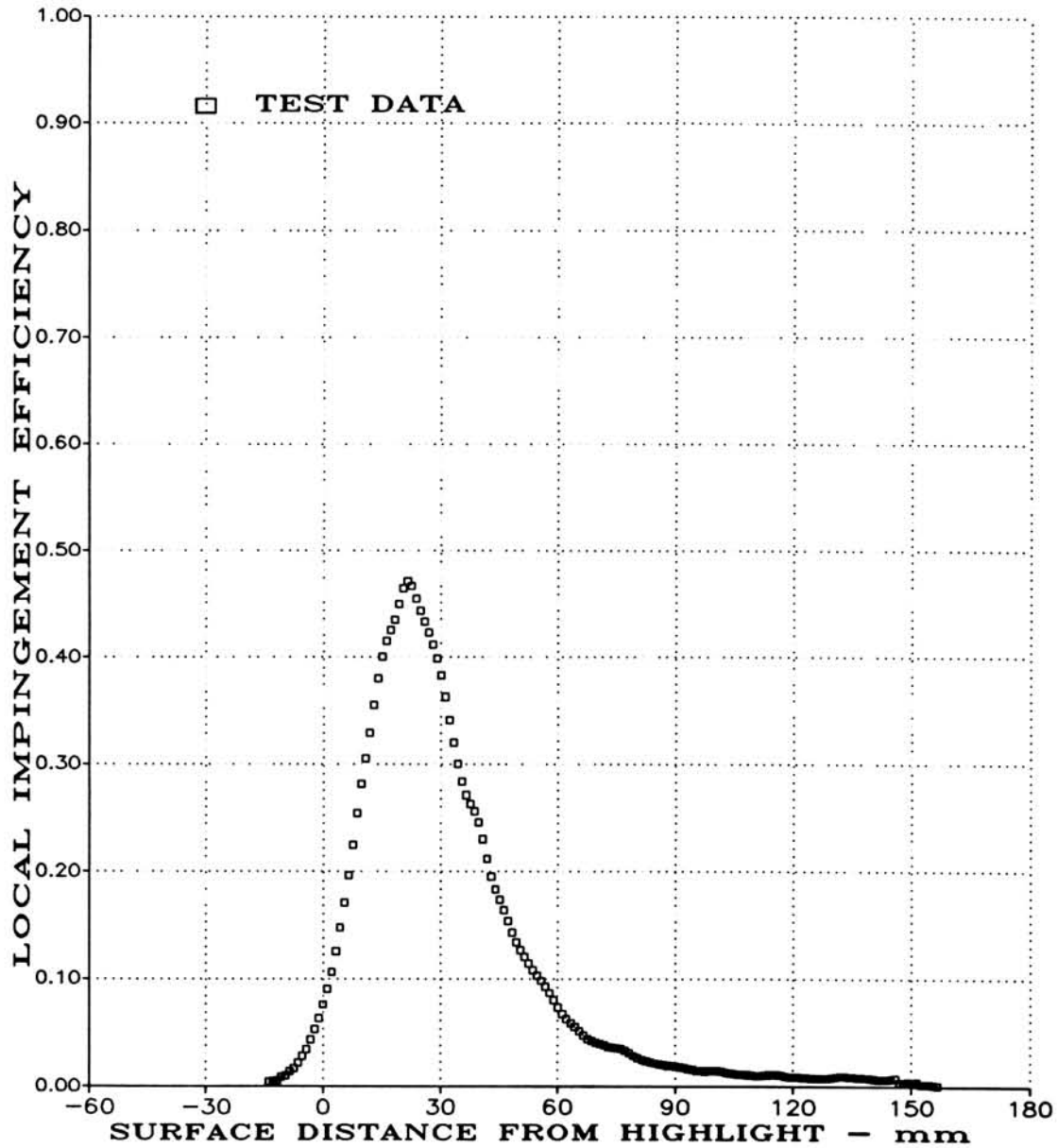
$$\bar{\beta}_{max} = 0.475, S_{U_{max}} = -4mm, S_{L_{max}} = 106mm$$

(A) STRIP A, MVD = 16 MICRONS

FIGURE 7.22

AVERAGED LOCAL WATER IMPINGEMENT EFFICIENCY DATA
FOR MS(1)-0317 AIRFOIL AT $\alpha = 8^\circ$ ($V_\infty = 165$ mph, $K_{0_{mvd}} = 0.025$)
(PAGE 1 OF 2).

TEST RUN ID: 158M608B, 159M608B, 160M608B,
161M608B, 162M608B



(Positive Surface Distance, S , on Lower Surface)

$$\bar{\beta}_{max} = 0.472, S_{U_{max}} = -4mm, S_{L_{max}} = 110mm$$

(B) STRIP B, MVD = 16 MICRONS

FIGURE 7.22

AVERAGED LOCAL WATER IMPINGEMENT EFFICIENCY DATA
FOR MS(1)-0317 AIRFOIL AT $\alpha = 8^\circ$ ($V_\infty = 165$ mph, $K_{0_{mvd}} = 0.025$)
(PAGE 2 OF 2).

LOCAL IMPINGEMENT EFFICIENCY (β) - DIMENSIONLESS

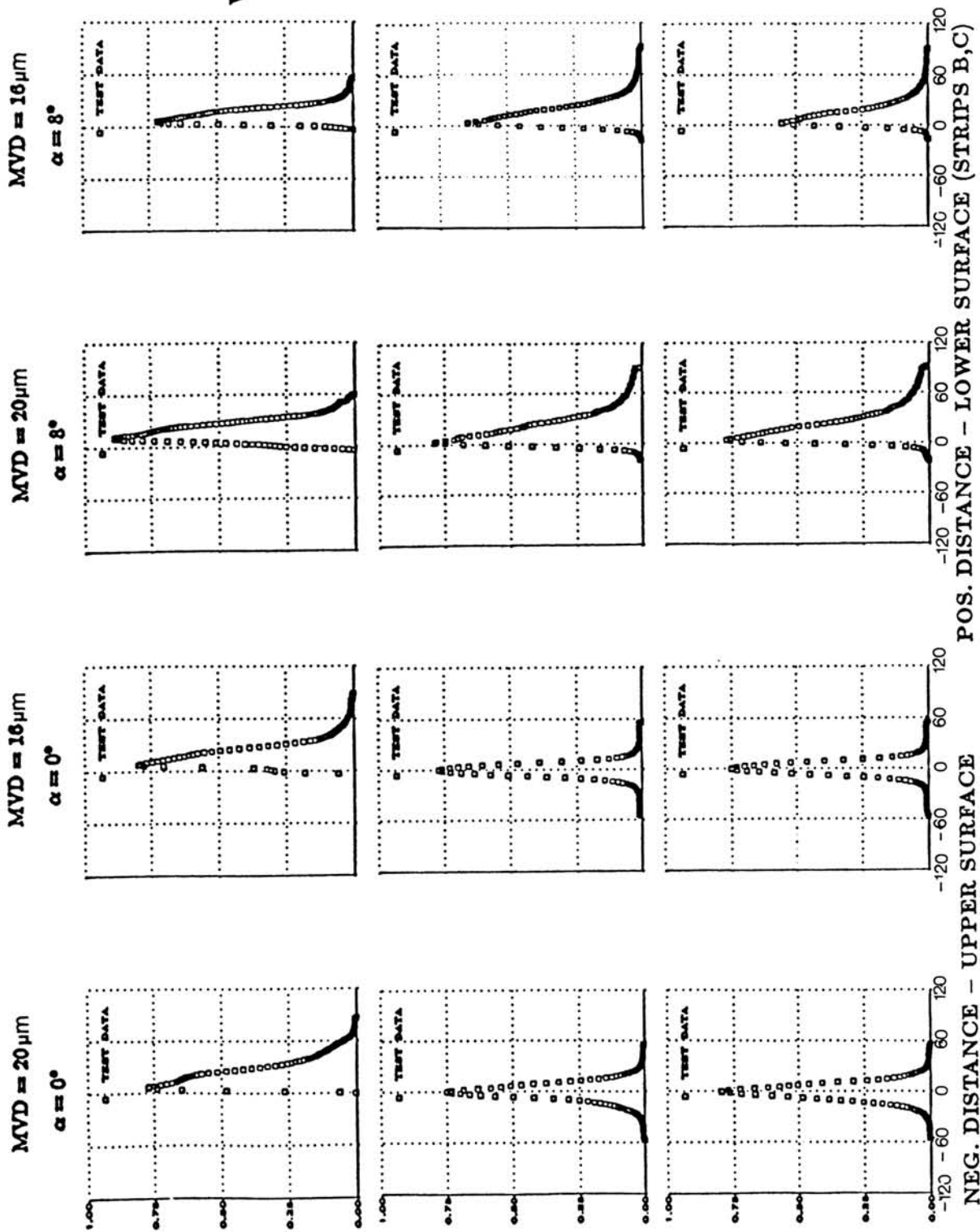
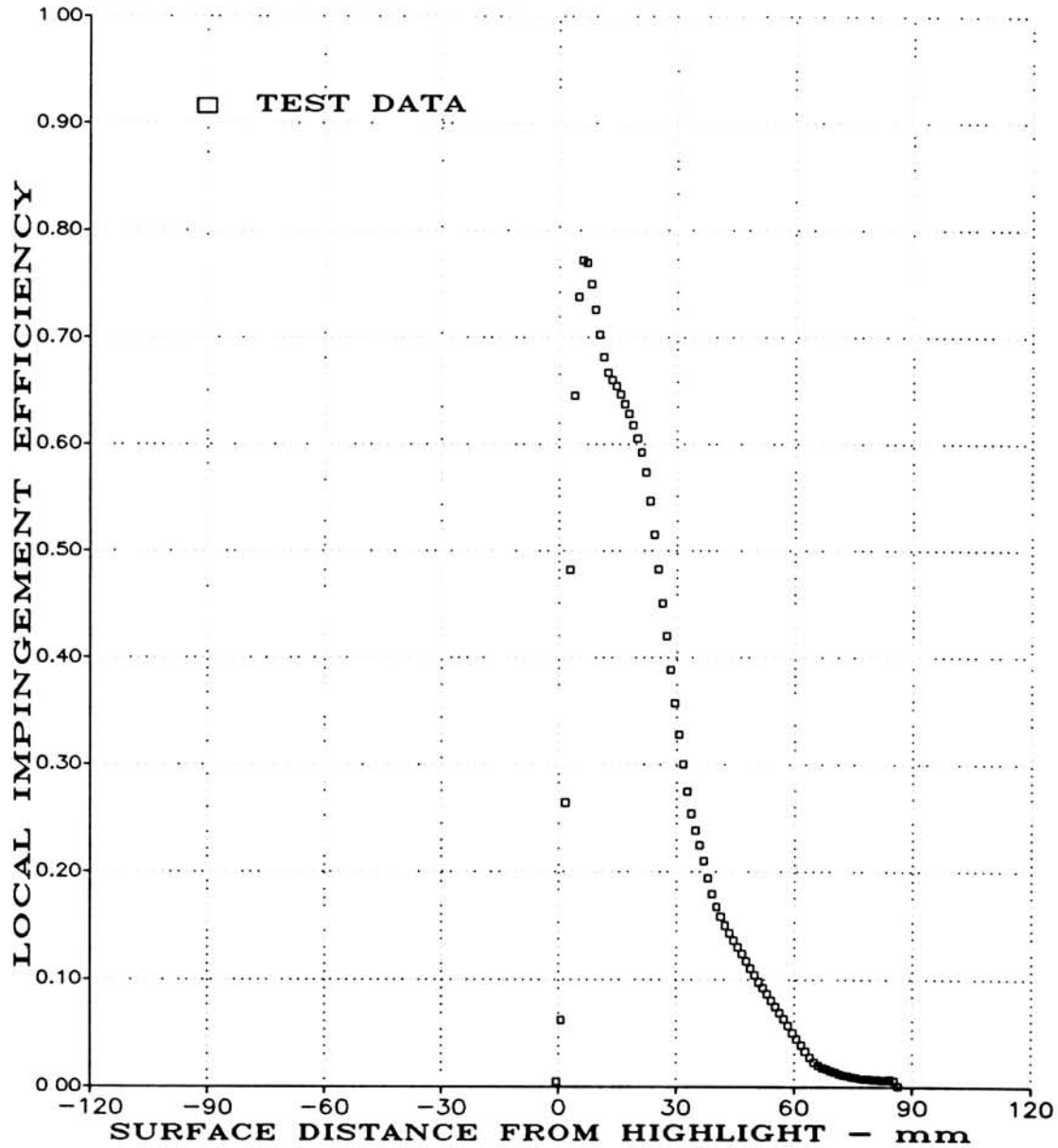


FIGURE 7.23
AVERAGED LOCAL WATER IMPINGEMENT EFFICIENCY DATA FOR
NACA 0012 SWEEP WING TIP. SUMMARY OF RESULTS.

TEST RUN ID: 127W900A, 128W900A, 129W900A,
130W900A, 131W900A



(Positive Surface Distance, S, on Lower Surface)

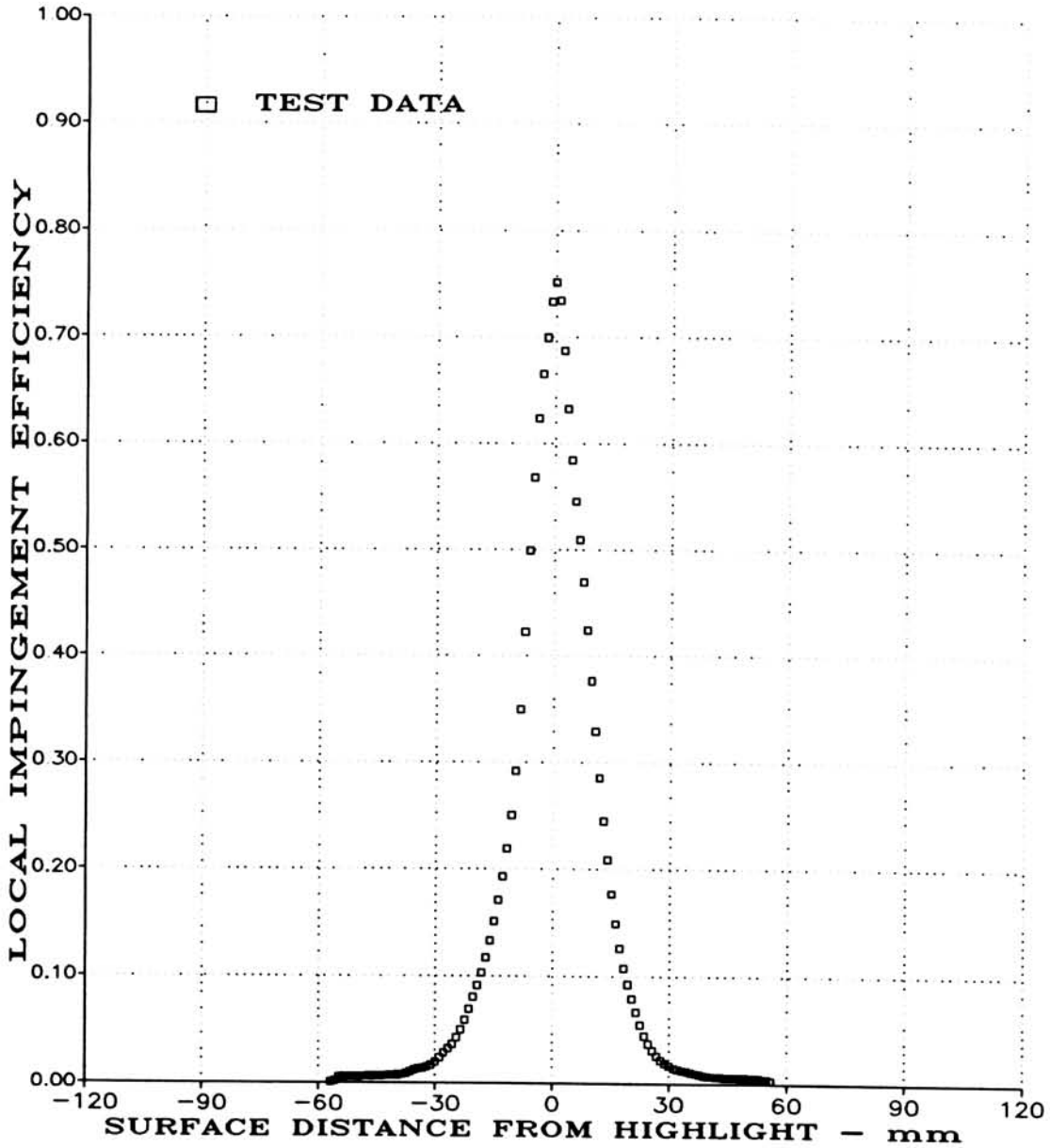
$$\bar{\beta}_{max} = 0.774, S_{total} = 76mm$$

(A) STRIP A, MVD = 20 MICRONS

FIGURE 7.24

AVERAGED LOCAL WATER IMPINGEMENT EFFICIENCY DATA
FOR NACA 0012 SWEEP WING TIP AT $\alpha = 0^\circ$ ($V_\infty = 165$ mph, $K_{0mvd} = 0.075$)
(PAGE 1 OF 3).

TEST RUN ID: 127W900B, 128W900B, 129W900B,
130W900B, 131W900B



(Positive Surface Distance, S, on Lower Surface)

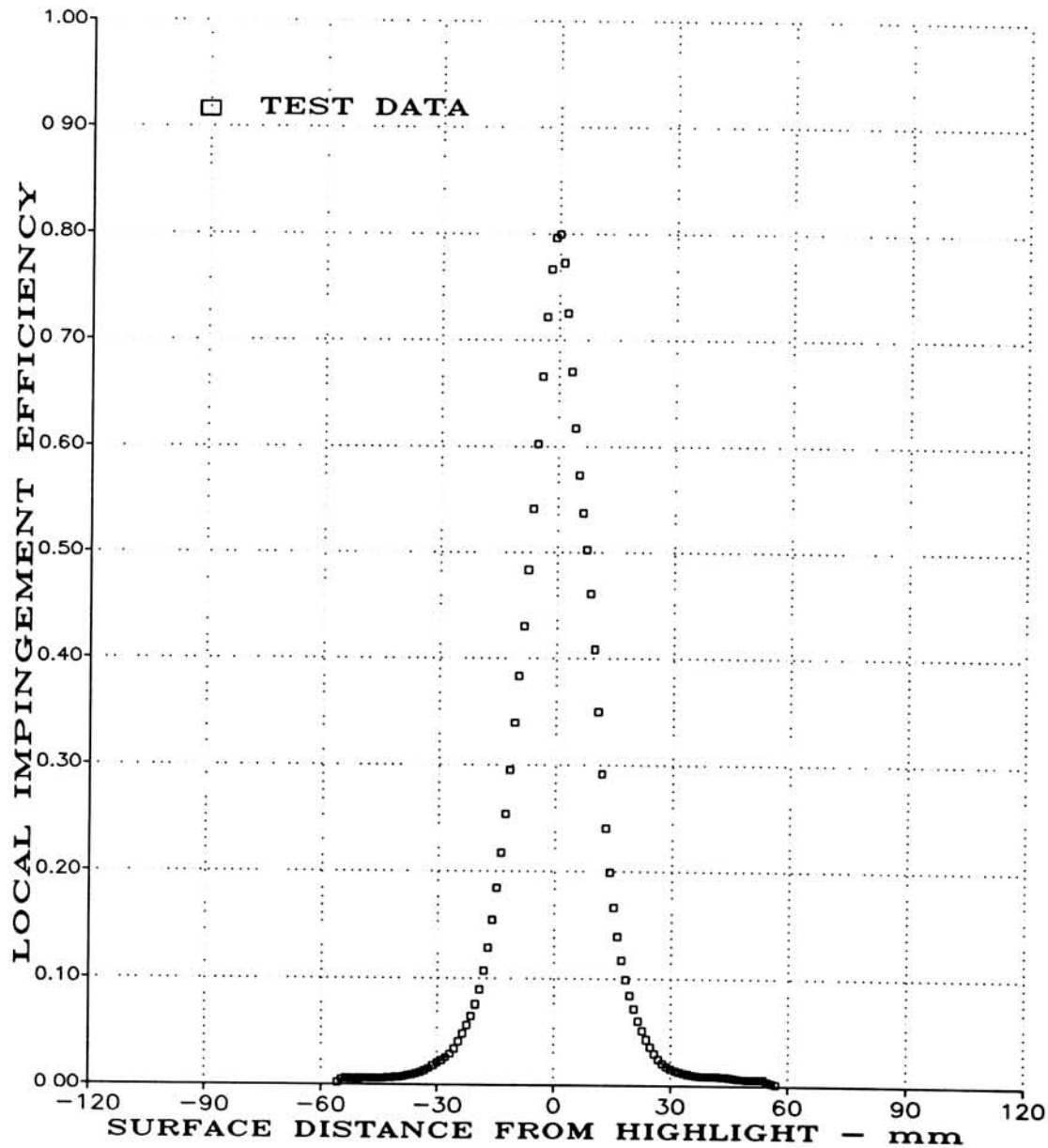
$$\bar{\beta}_{max} = 0.750, S_{U_{max}} = -40mm, S_{L_{max}} = 40mm$$

(B) STRIP B, MVD = 20 MICRONS

FIGURE 7.24

AVERAGED LOCAL WATER IMPINGEMENT EFFICIENCY DATA
FOR NACA 0012 SWEEP WING TIP AT $\alpha = 0^\circ$ ($V_\infty = 165$ mph, $K_{0_{mvd}} = 0.075$)
(PAGE 2 OF 3).

TEST RUN ID: 127W900C, 128W900C, 129W900C,
130W900C, 131W900C



(Positive Surface Distance, S, on Lower Surface)

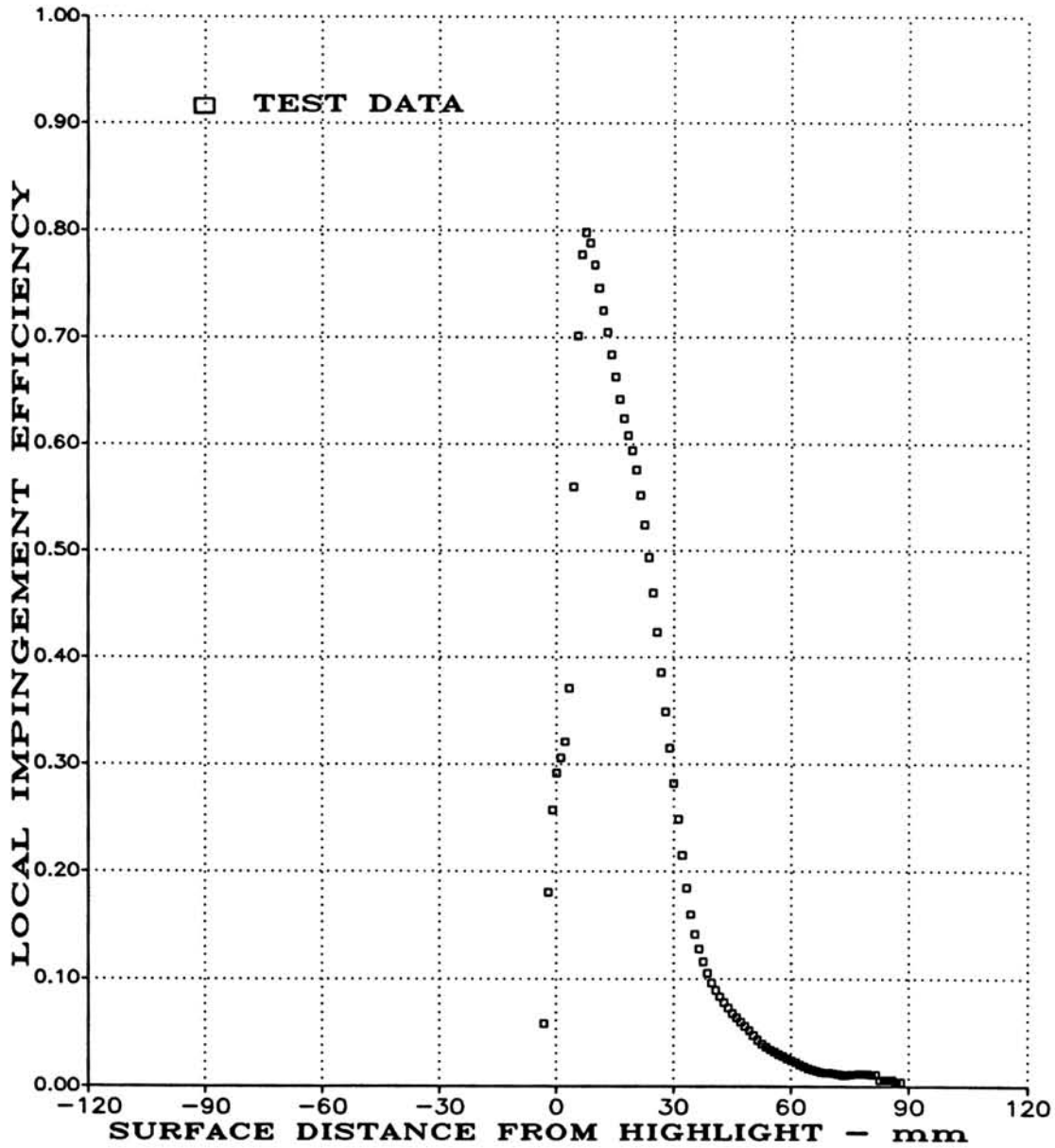
$$\bar{\beta}_{max} = 0.802, S_{U_{max}} = -40mm, S_{L_{max}} = 40mm$$

(C) STRIP C, MVD = 20 MICRONS

FIGURE 7.24

AVERAGED LOCAL WATER IMPINGEMENT EFFICIENCY DATA
FOR NACA 0012 SWEEP WING TIP AT $\alpha = 0^\circ$ ($V_\infty = 165$ mph, $K_{0_{mvd}} = 0.075$)
(PAGE 3 OF 3).

TEST RUN ID: 132W600A, 133W600A, 134W600A,
135W600A, 136W600A



(Positive Surface Distance, S, on Lower Surface)

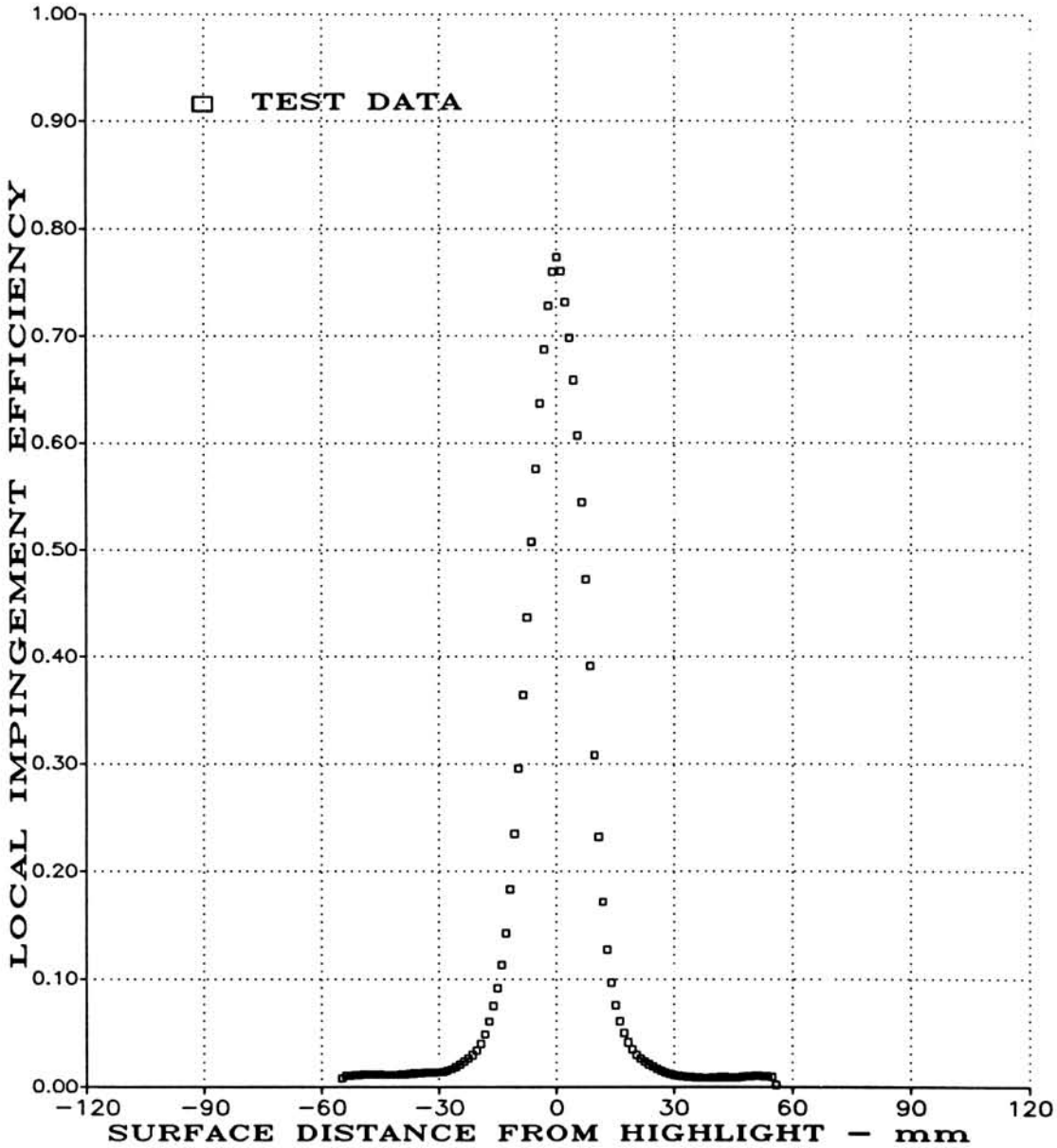
$$\bar{\beta}_{max} = 0.798, S_{total} = 64mm$$

(A) STRIP A, MVD = 16 MICRONS

FIGURE 7.25

AVERAGED LOCAL WATER IMPINGEMENT EFFICIENCY DATA
FOR NACA 0012 SWEEP WING TIP AT $\alpha = 0^\circ$ ($V_\infty = 165$ mph, $K_{0_{mvd}} = 0.052$)
(PAGE 1 OF 3).

TEST RUN ID: 132W600B, 133W600B, 134W600B,
135W600B, 136W600B



(Positive Surface Distance, S, on Lower Surface)

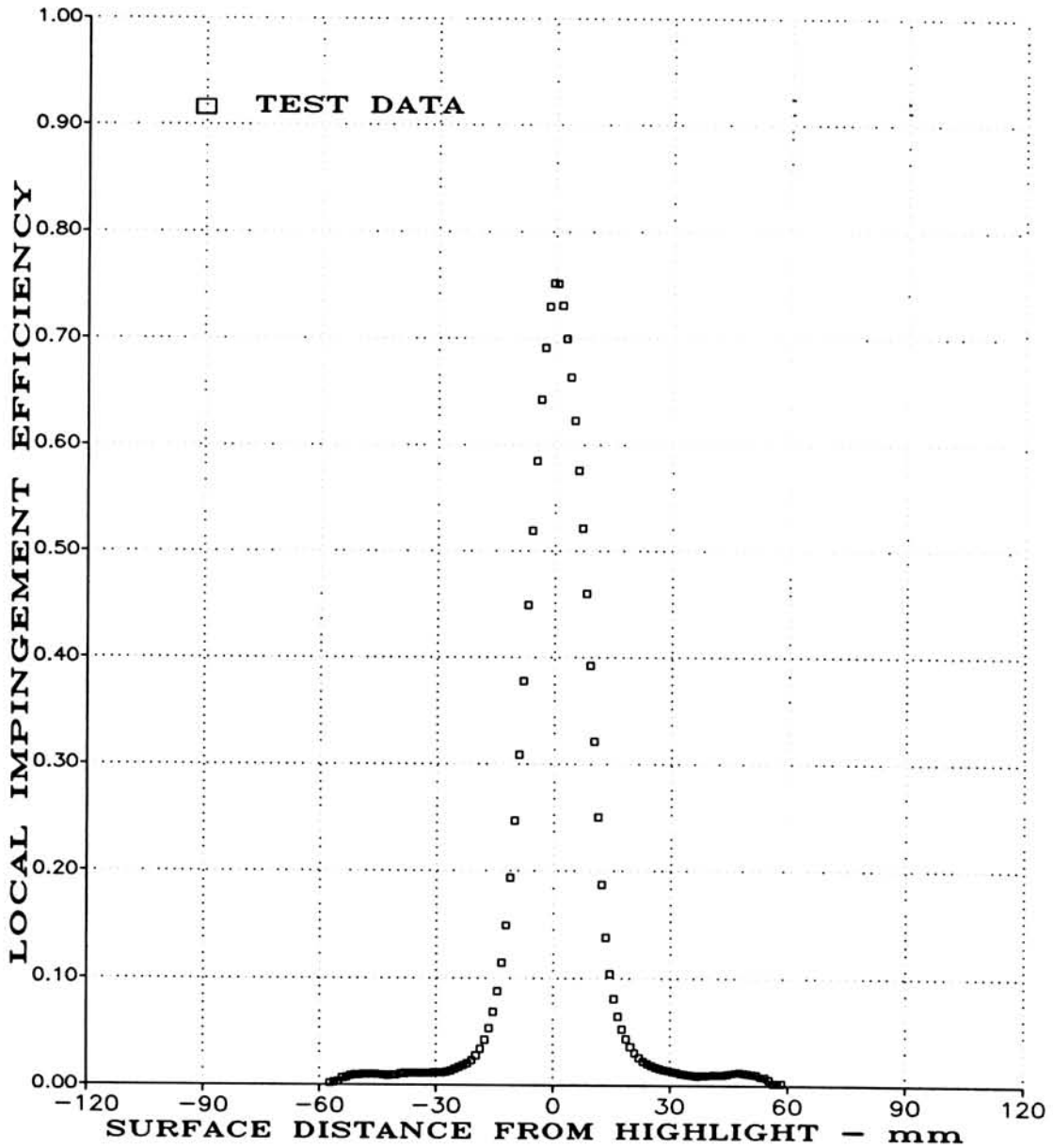
$$\bar{\beta}_{max} = 0.773, S_{U_{max}} = -30mm, S_{L_{max}} = 30mm$$

(B) STRIP B, MVD = 16 MICRONS

FIGURE 7.25

AVERAGED LOCAL WATER IMPINGEMENT EFFICIENCY DATA
FOR NACA 0012 SWEEP WING TIP AT $\alpha = 0^\circ$ ($V_\infty = 165$ mph, $K_{0,mvd} = 0.052$)
(PAGE 2 OF 3).

TEST RUN ID: 132W600C, 133W600C, 134W600C,
135W600C, 136W600C



(Positive Surface Distance, S, on Lower Surface)

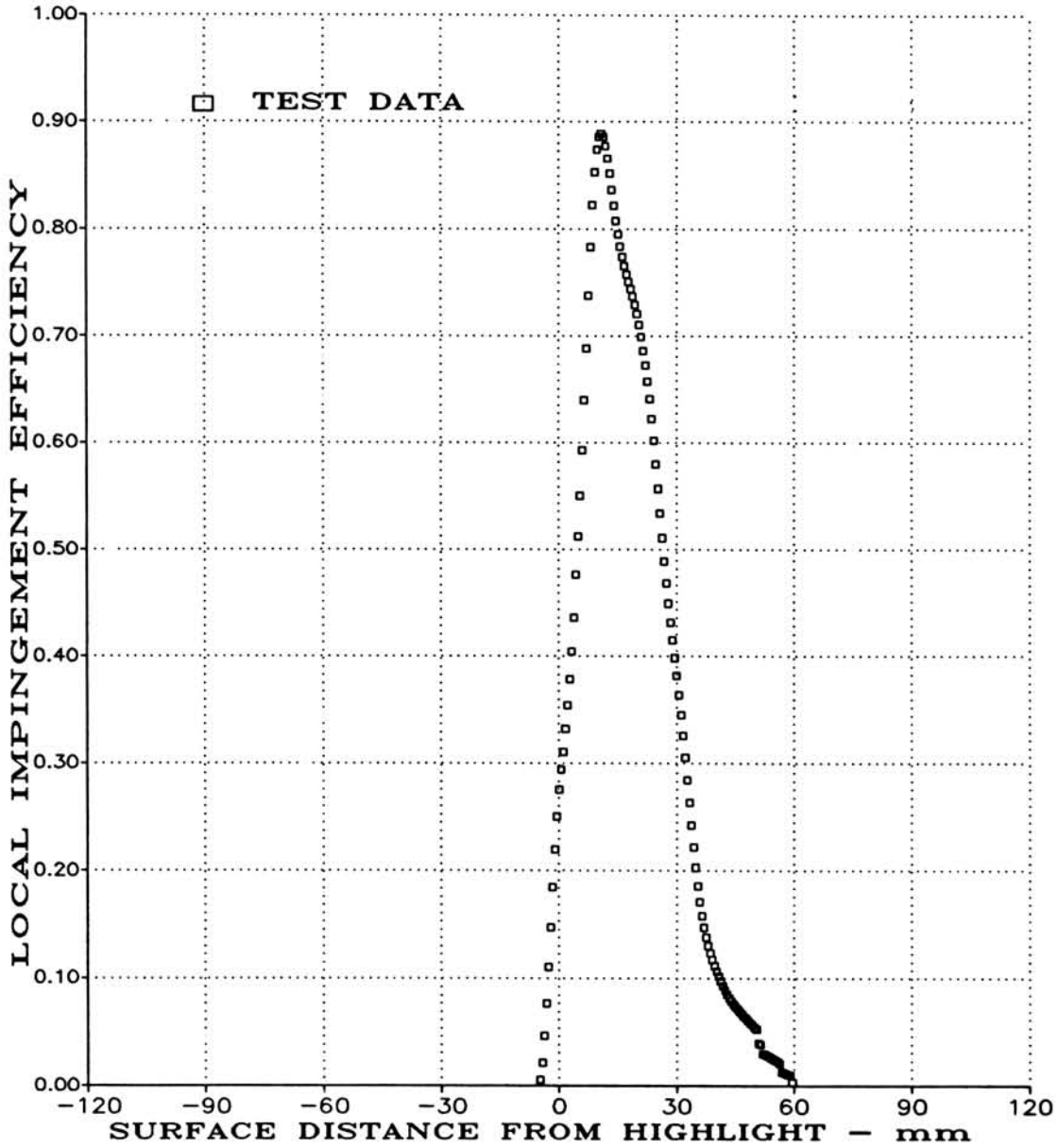
$$\bar{\beta}_{max} = 0.755, S_{U_{max}} = -30mm, S_{L_{max}} = 30mm$$

(C) STRIP C, MVD = 16 MICRONS

FIGURE 7.25

AVERAGED LOCAL WATER IMPINGEMENT EFFICIENCY DATA
FOR NACA 0012 SWEEP WING TIP AT $\alpha = 0^\circ$ ($V_\infty = 165$ mph, $K_{0_{mvd}} = 0.052$)
(PAGE 3 OF 3).

TEST RUN ID: 143W908A, 144W908A, 145W908A,
146W908A, 147W908A



(Positive Surface Distance, S, on Lower Surface)

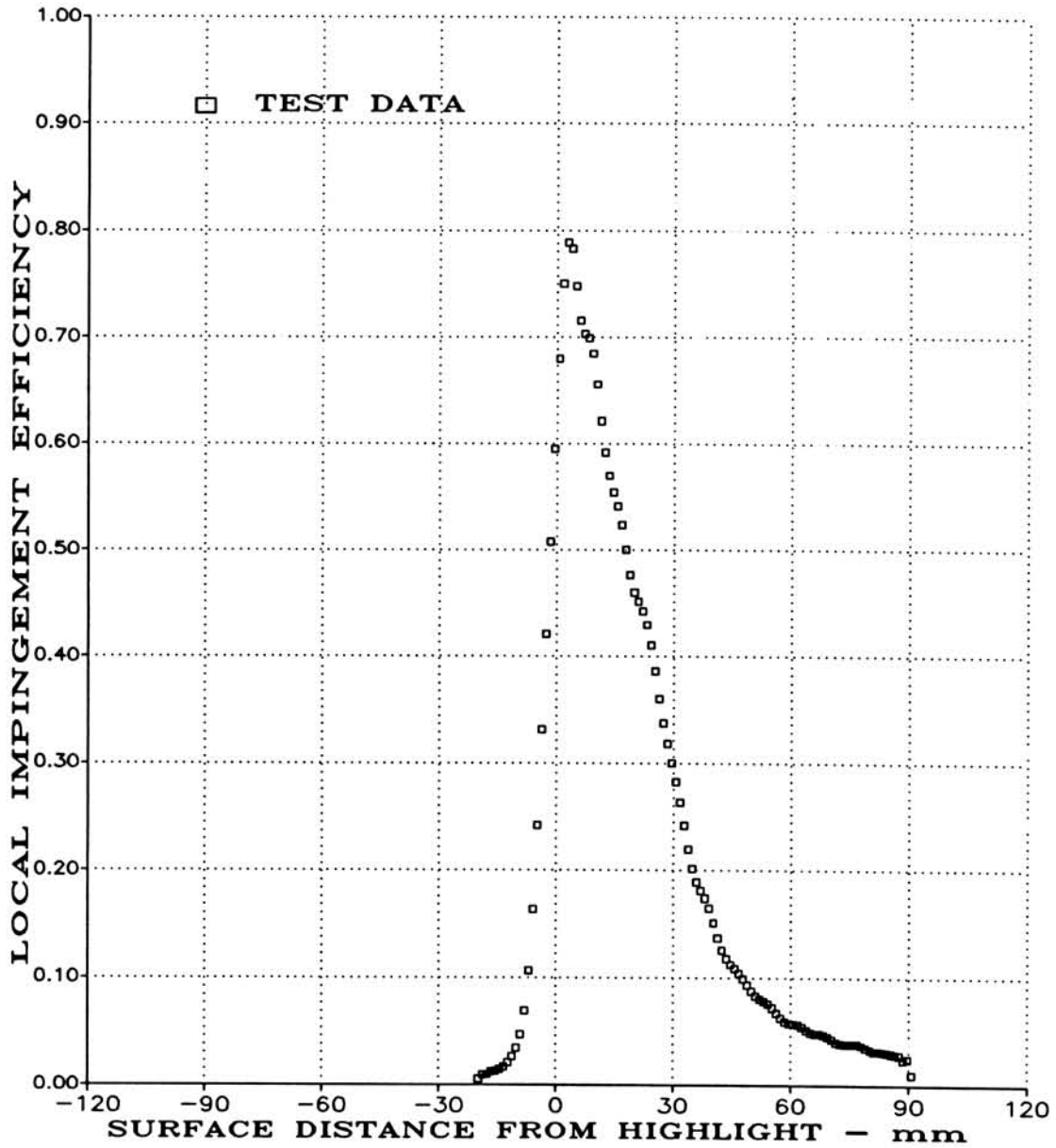
$$\bar{\beta}_{max} = 0.889, S_{total} = 56mm$$

(A) STRIP A, MVD = 20 MICRONS

FIGURE 7.26

AVERAGED LOCAL WATER IMPINGEMENT EFFICIENCY DATA
FOR NACA 0012 SWEEP WING TIP AT $\alpha = 8^\circ$ ($V_\infty = 165$ mph, $K_{0_{mvd}} = 0.075$)
(PAGE 1 OF 3).

TEST RUN ID: 143W908B, 144W908B, 145W908B,
146W908B, 147W908B



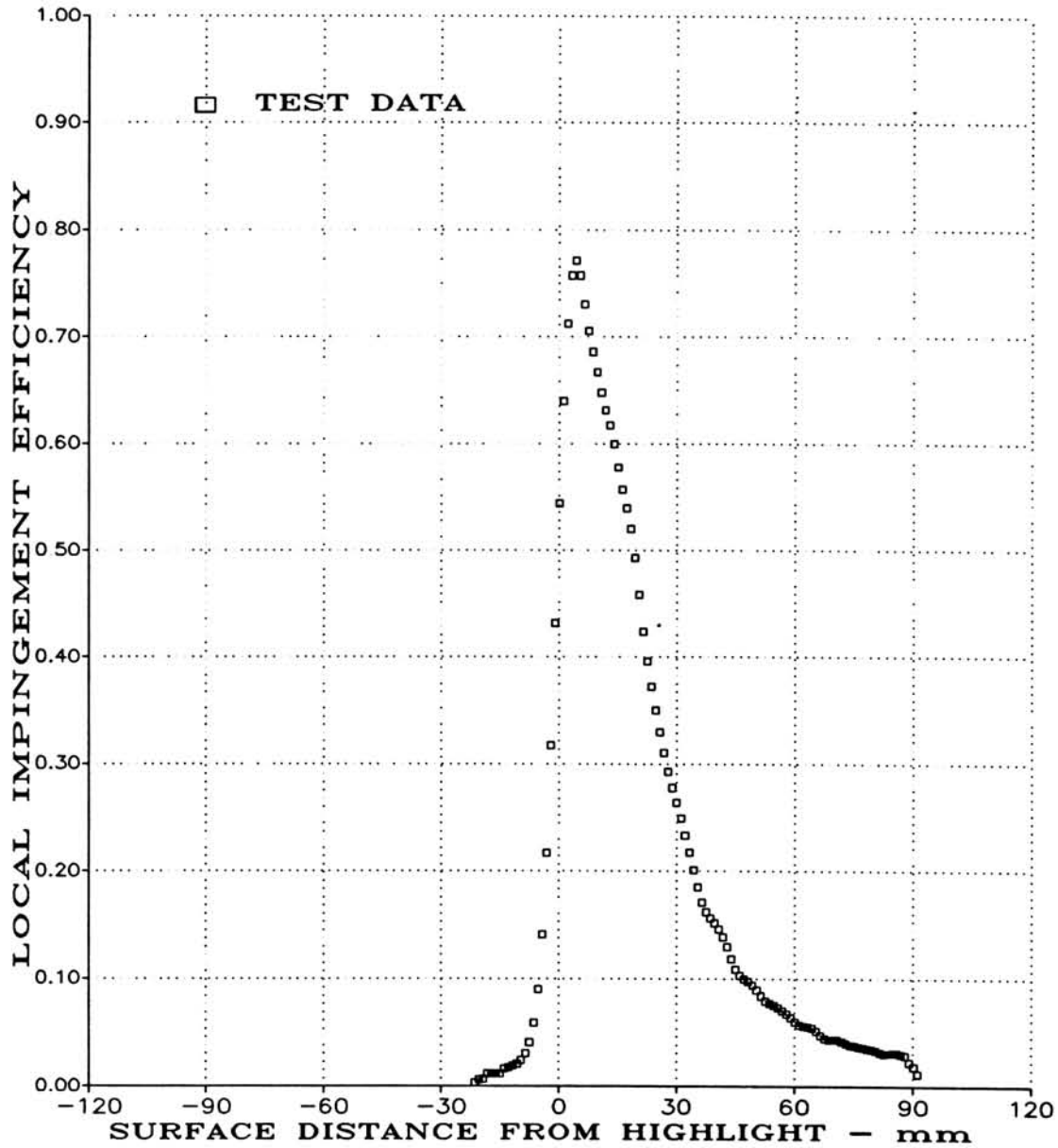
(Positive Surface Distance, S, on Lower Surface)
 $\bar{\beta}_{max} = 0.790$, $S_{U_{max}} = -12mm$, $S_{L_{max}} = 100mm$

(B) STRIP B, MVD = 20 MICRONS

FIGURE 7.26

AVERAGED LOCAL WATER IMPINGEMENT EFFICIENCY DATA
FOR NACA 0012 SWEEP WING TIP AT $\alpha = 8^\circ$ ($V_\infty = 165$ mph, $K_{0_{mvd}} = 0.075$)
(PAGE 2 OF 3).

TEST RUN ID: 143W908C, 144W908C, 145W908C,
146W908C, 147W908C



(Positive Surface Distance, S, on Lower Surface)

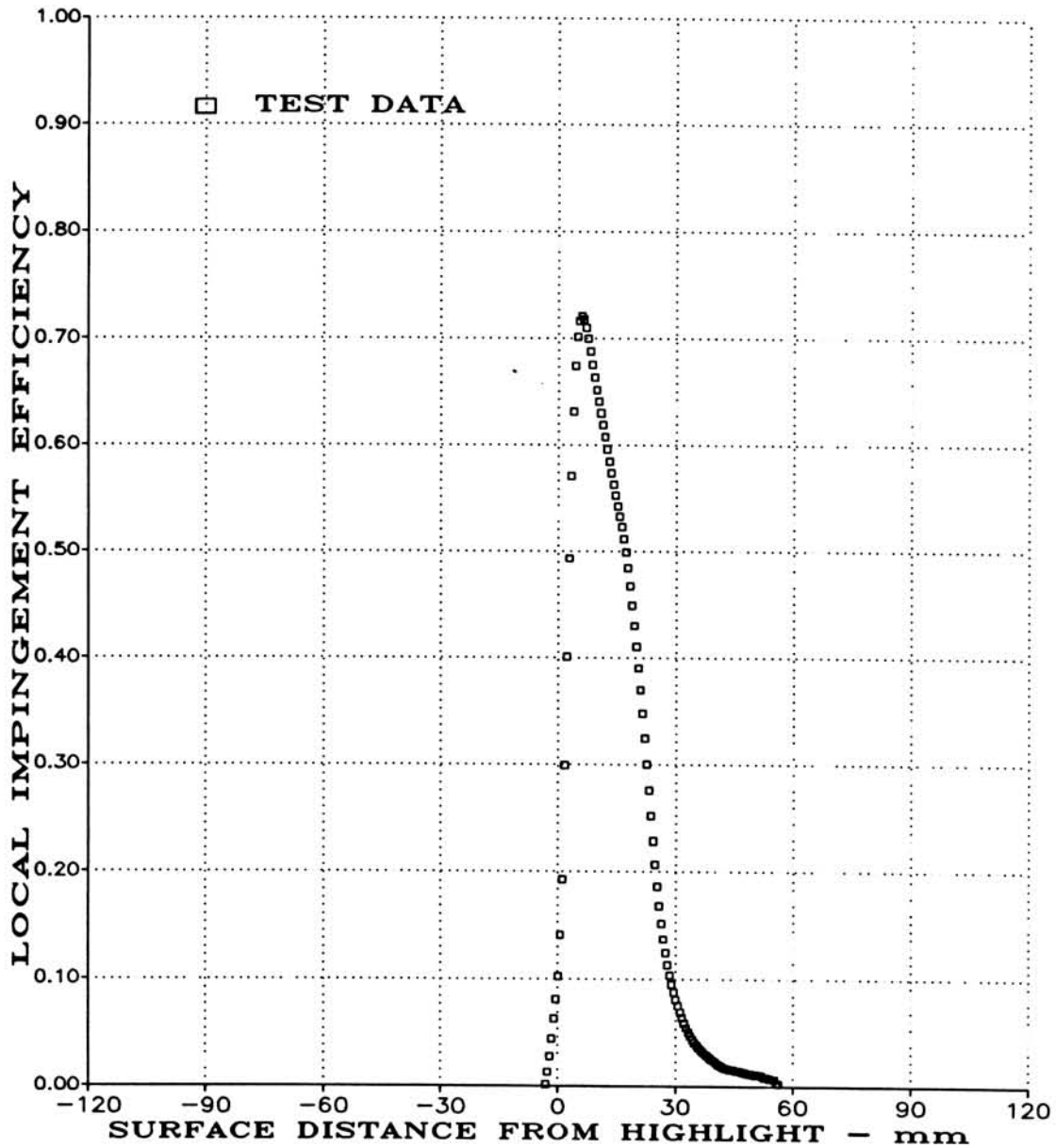
$$\bar{\beta}_{max} = 0.770, S_{U_{max}} = -13mm, S_{L_{max}} = 101mm$$

(C) STRIP C, MVD = 20 MICRONS

FIGURE 7.26

AVERAGED LOCAL WATER IMPINGEMENT EFFICIENCY DATA
FOR NACA 0012 SWEEP WING TIP AT $\alpha = 8^\circ$ ($V_\infty = 165$ mph, $K_{0_{mvd}} = 0.075$)
(PAGE 3 OF 3).

TEST RUN ID: 137W608A, 138W608A, 139W608A,
140W608A, 141W608A



(Positive Surface Distance, S , on Lower Surface)

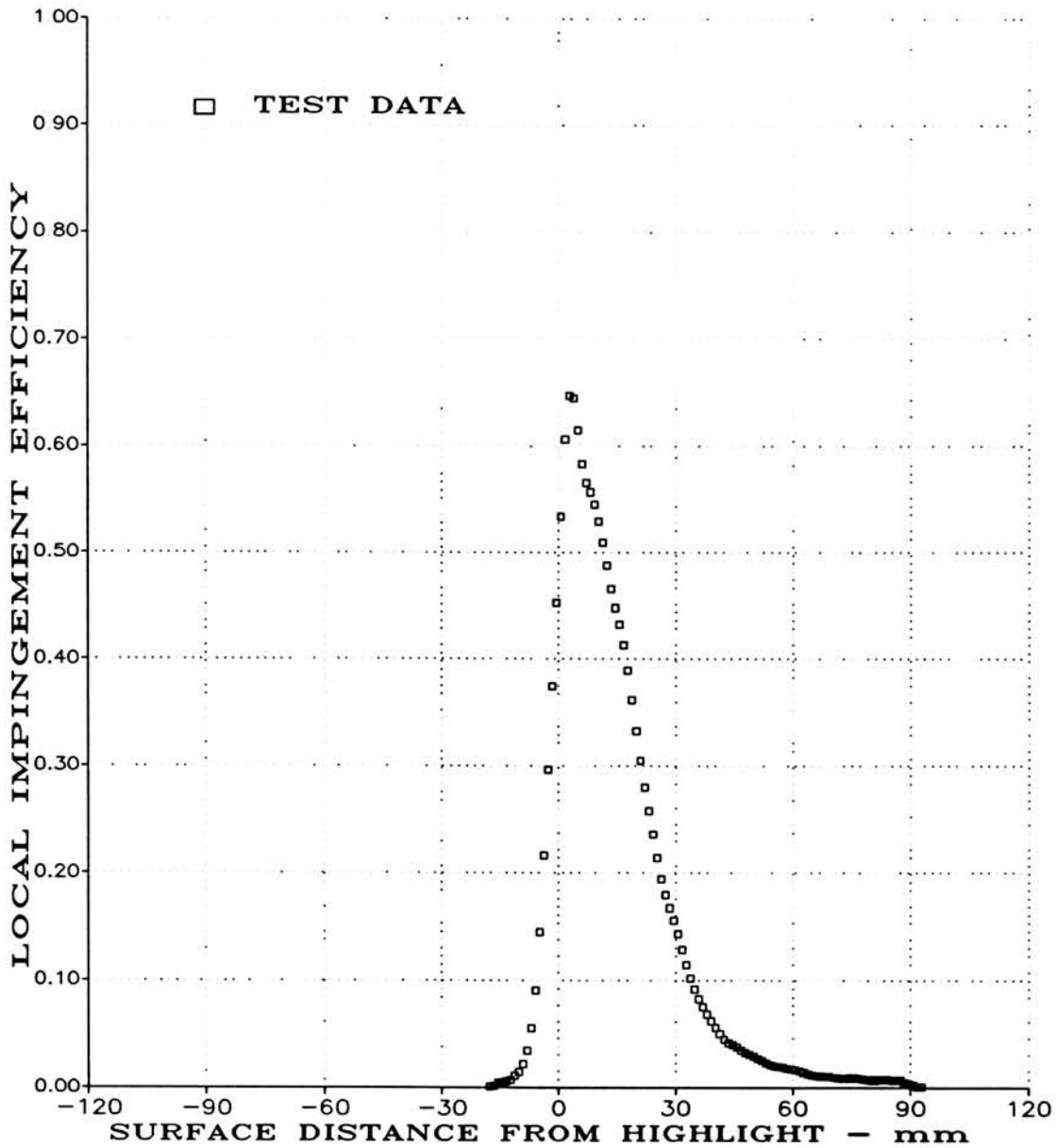
$$\bar{\beta}_{max} = 0.721, S_{total} = 49mm$$

(A) STRIP A, MVD = 16 MICRONS

FIGURE 7.27

AVERAGED LOCAL WATER IMPINGEMENT EFFICIENCY DATA
FOR NACA 0012 SWEEP WING TIP AT $\alpha = 8^\circ$ ($V_\infty = 165$ mph, $K_{0_{mvd}} = 0.052$)
(PAGE 1 OF 3).

TEST RUN ID: 137W608B, 138W608B, 139W608B,
140W608B, 141W608B



(Positive Surface Distance, S , on Lower Surface)

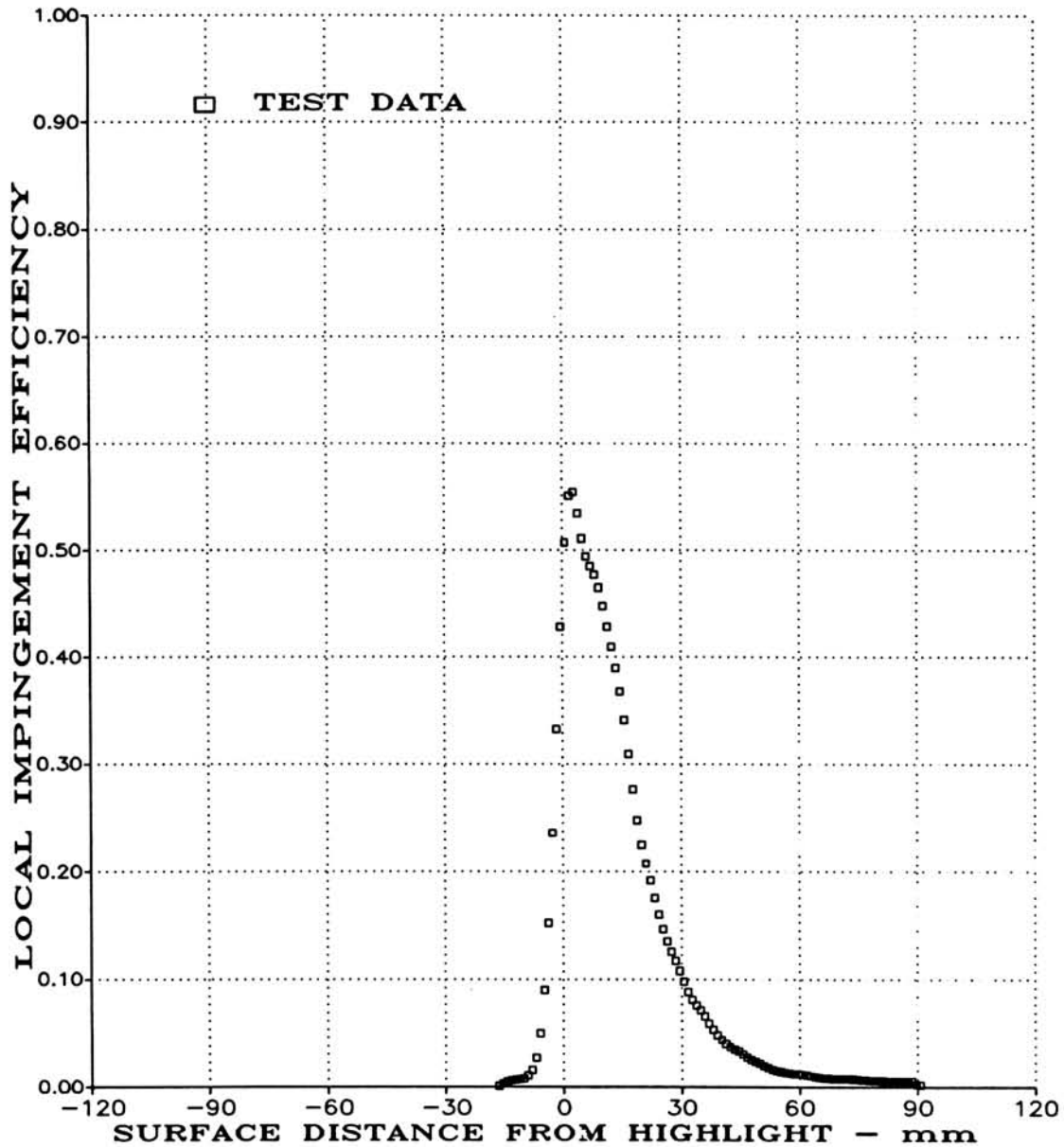
$$\bar{\beta}_{max} = 0.650, S_{U_{max}} = -9mm, S_{L_{max}} = 67mm$$

(B) STRIP B, MVD = 16 MICRONS

FIGURE 7.27

AVERAGED LOCAL WATER IMPINGEMENT EFFICIENCY DATA
FOR NACA 0012 SWEEP WING TIP AT $\alpha = 8^\circ$ ($V_\infty = 165$ mph, $K_{0_{mvd}} = 0.052$)
(PAGE 2 OF 3).

TEST RUN ID: 137W608C, 138W608C, 139W608C,
140W608C, 141W608C



(Positive Surface Distance, S, on Lower Surface)

$$\bar{\beta}_{max} = 0.557, S_{U_{max}} = -9mm, S_{L_{max}} = 67mm$$

(C) STRIP C, MVD = 16 MICRONS

FIGURE 7.27

AVERAGED LOCAL WATER IMPINGEMENT EFFICIENCY DATA
FOR NACA 0012 SWEEP WING TIP AT $\alpha = 8^\circ$ ($V_\infty = 165$ mph, $K_{0_{mvd}} = 0.052$)
(PAGE 3 OF 3).

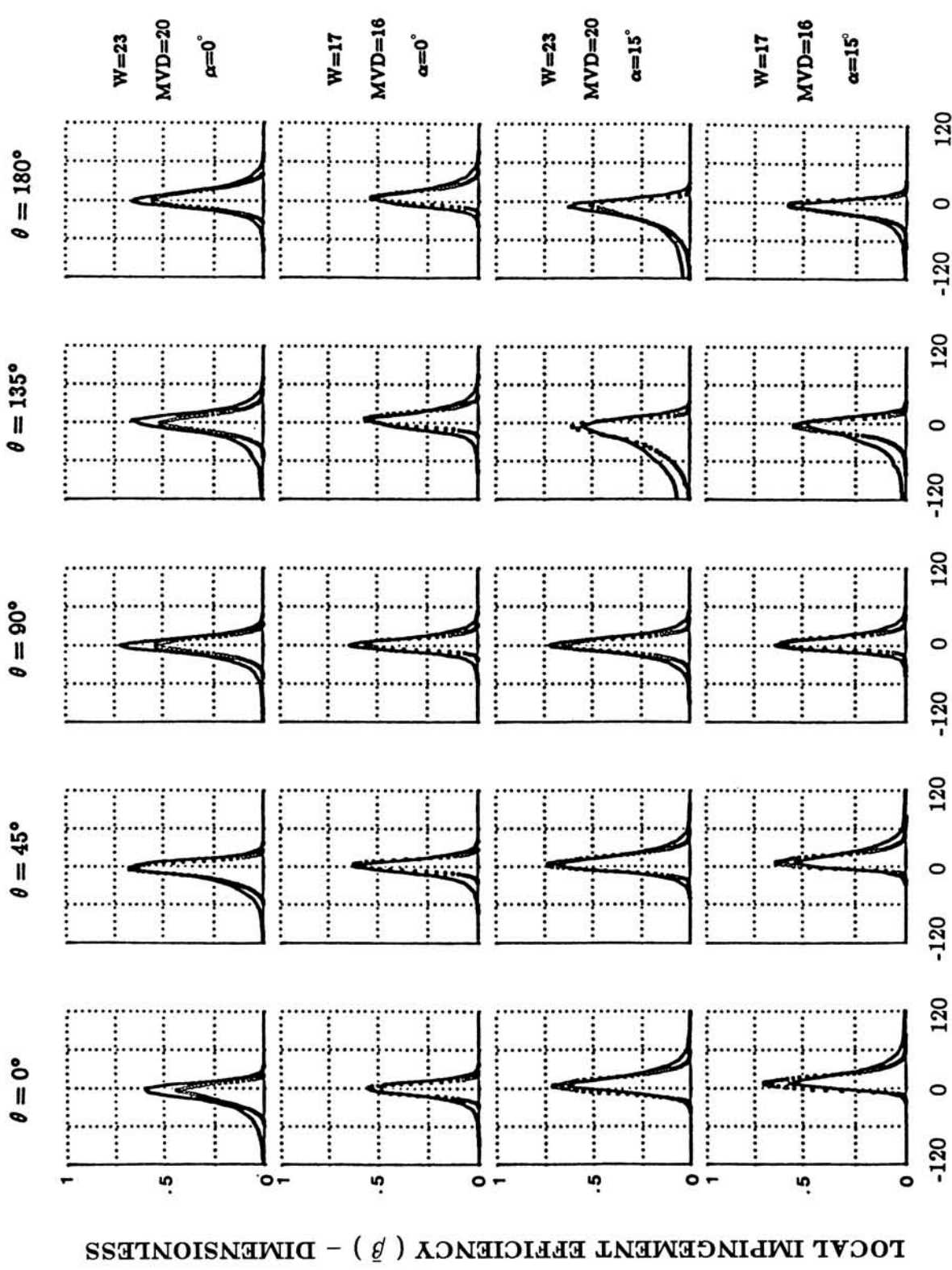
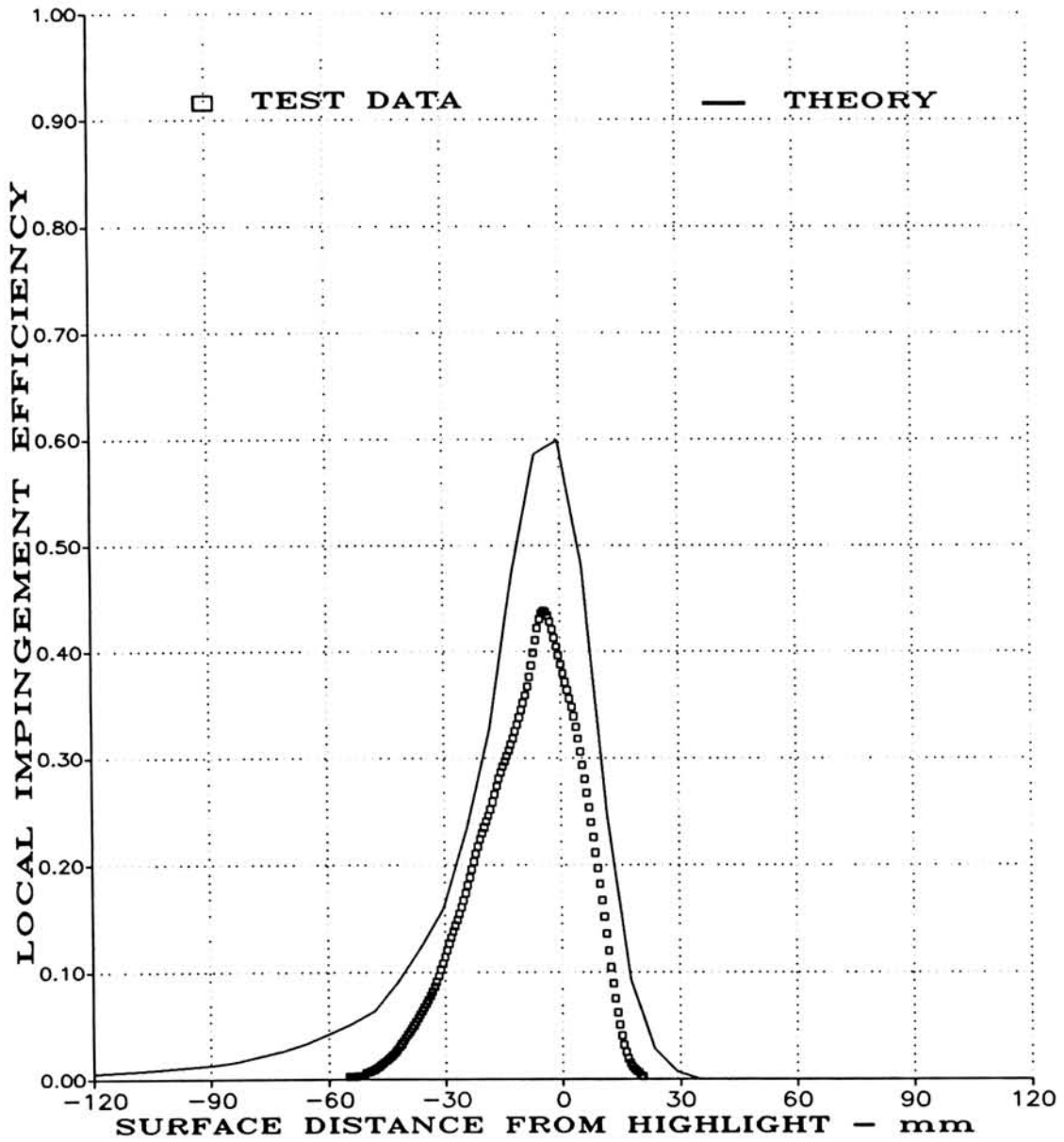


FIGURE 7.28

AVERAGED LOCAL WATER IMPINGEMENT EFFICIENCY DATA FOR BOEING 737-300 INLET. SUMMARY OF RESULTS.



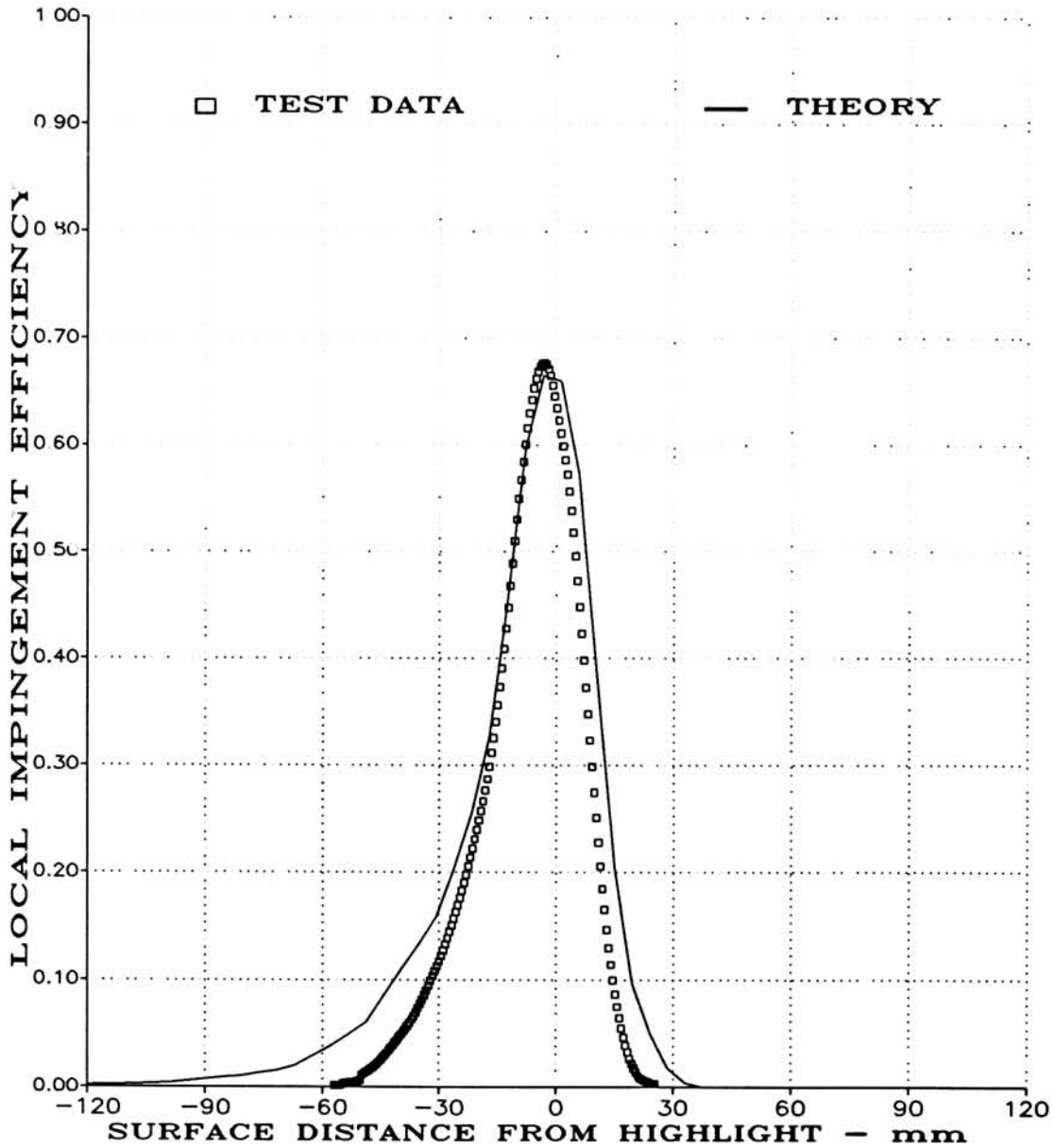
(Positive Surface Distance, S, on Inner Surface)

$$\bar{\beta}_{max} = 0.440, S_{O_{max}} = -60mm, S_{I_{max}} = 20mm \text{ (Experiment)}$$

(A1) STRIP A, $\theta = 0^\circ$, MVD = 20 MICRONS, MASS FLOW = 23 LBM/SEC

FIGURE 7.29

AVERAGED LOCAL WATER IMPINGEMENT EFFICIENCY DATA
 FOR BOEING 737-300 INLET AT $\alpha = 0^\circ$ ($V_\infty = 173$ mph, $K_{0_{mvd}} = 0.089$)
 (PAGE 1 OF 10).



(Positive Surface Distance, S, on Inner Surface)

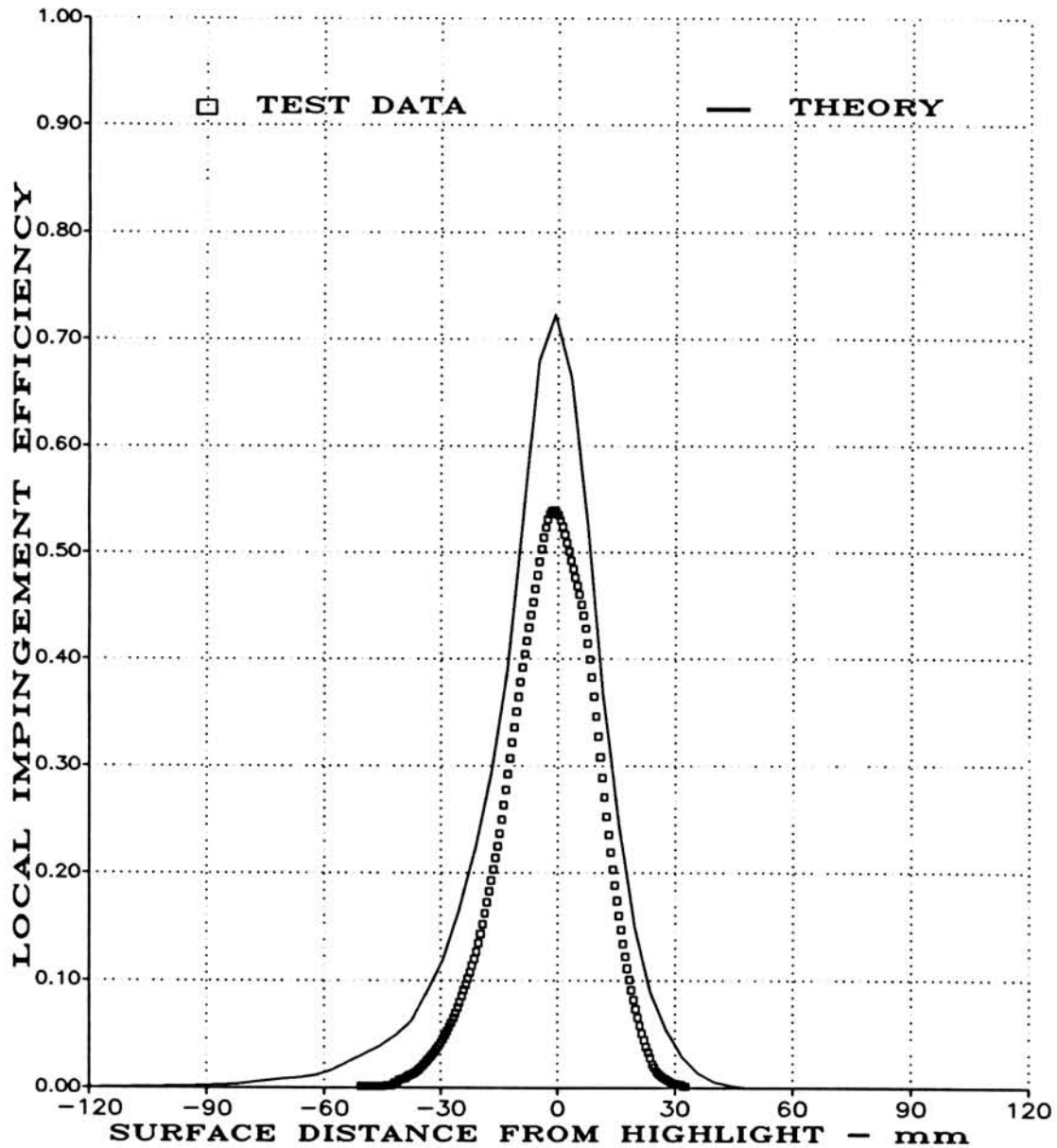
$$\bar{\beta}_{max} = 0.680, S_{O_{max}} = -55mm, S_{I_{max}} = 23mm \text{ (Experiment)}$$

(A2) STRIPS B,H, $\theta = 45^\circ$, MVD = 20 MICRONS, MASS FLOW = 23 LBM/SEC

FIGURE 7.29

AVERAGED LOCAL WATER IMPINGEMENT EFFICIENCY DATA
 FOR BOEING 737-300 INLET AT $\alpha = 0^\circ$ ($V_\infty = 173$ mph, $K_{0_{mvd}} = 0.089$)
 (PAGE 2 OF 10).

TEST RUN ID: 1773900CG, 1783900CG



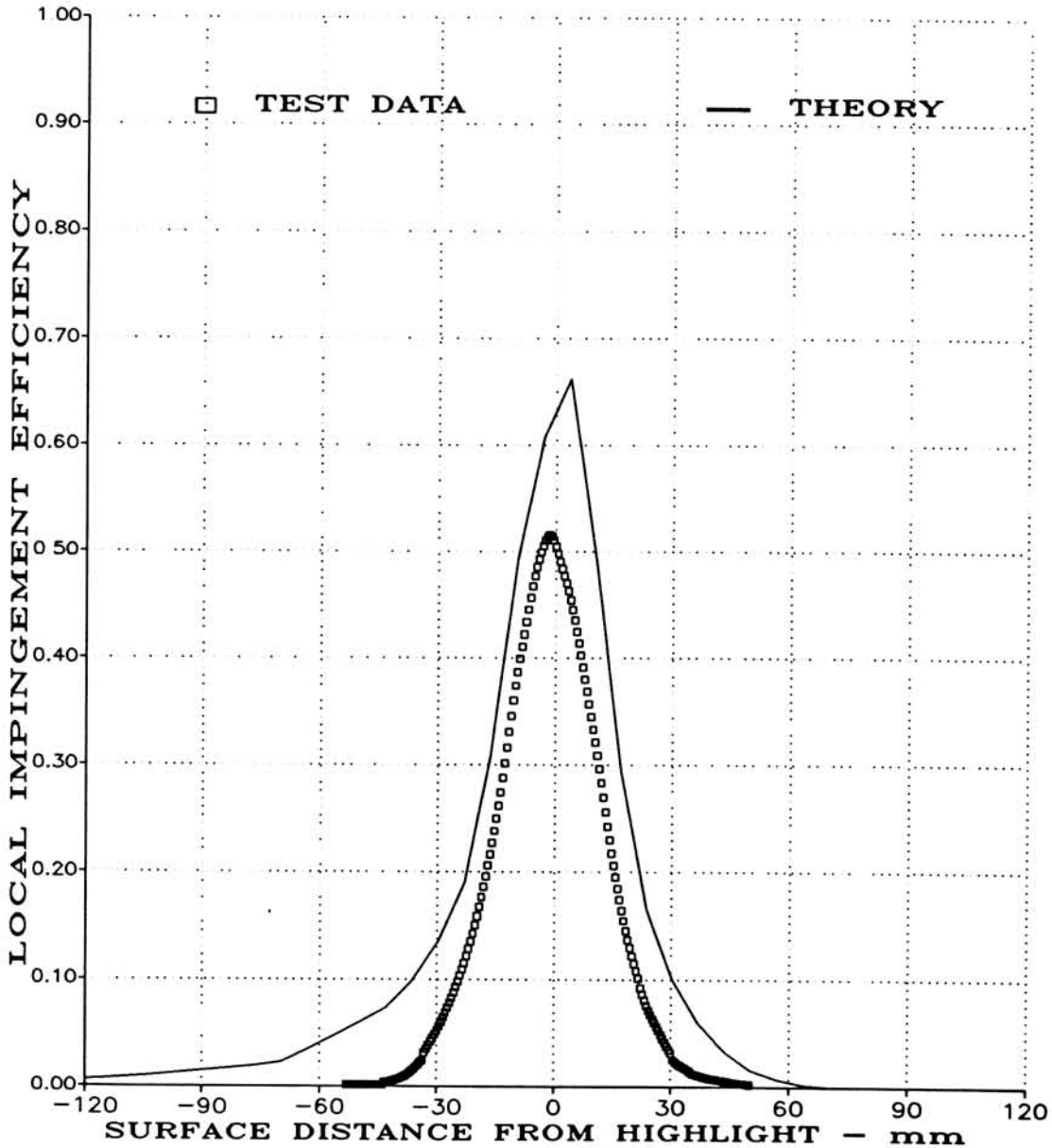
(Positive Surface Distance, S, on Inner Surface)

$$\bar{\beta}_{max} = 0.540, S_{O_{max}} = -43mm, S_{I_{max}} = 28mm \text{ (Experiment)}$$

(A3) STRIPS C,G, $\theta = 90^\circ$, MVD = 20 MICRONS, MASS FLOW = 23 LBM/SEC

FIGURE 7.29

AVERAGED LOCAL WATER IMPINGEMENT EFFICIENCY DATA
FOR BOEING 737-300 INLET AT $\alpha = 0^\circ$ ($V_\infty = 173$ mph, $K_{0_{mvd}} = 0.089$)
(PAGE 3 OF 10).



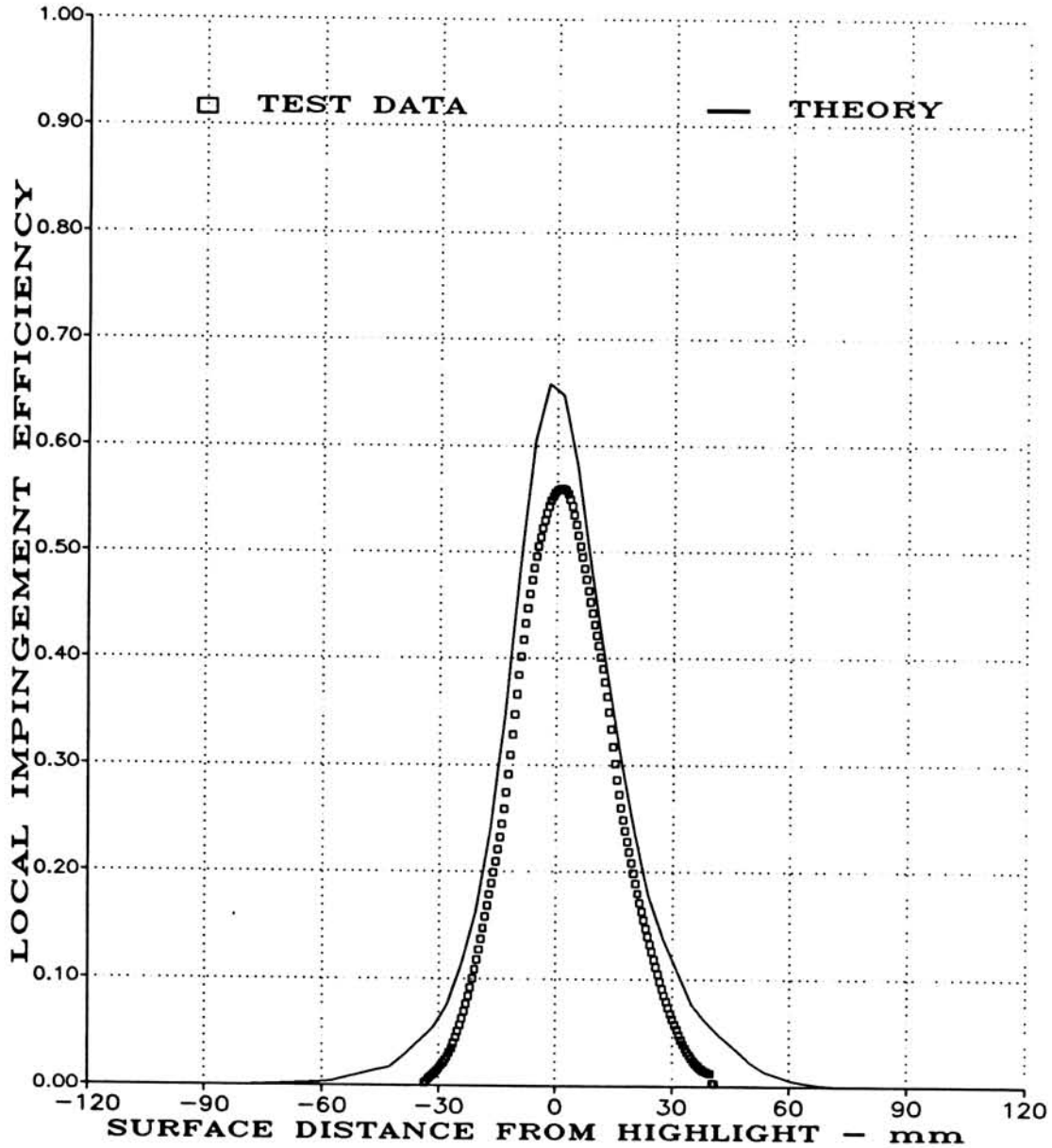
(Positive Surface Distance, S, on Inner Surface)

$$\bar{\beta}_{max} = 0.520, S_{O_{max}} = -46mm, S_{I_{max}} = 34mm \text{ (Experiment)}$$

(A4) STRIPS D,F, $\theta = 135^\circ$, MVD = 20 MICRONS, MASS FLOW = 23 LBM/SEC

FIGURE 7.29

AVERAGED LOCAL WATER IMPINGEMENT EFFICIENCY DATA
 FOR BOEING 737-300 INLET AT $\alpha = 0^\circ$ ($V_\infty = 173$ mph, $K_{O_{mvd}} = 0.089$)
 (PAGE 4 OF 10).



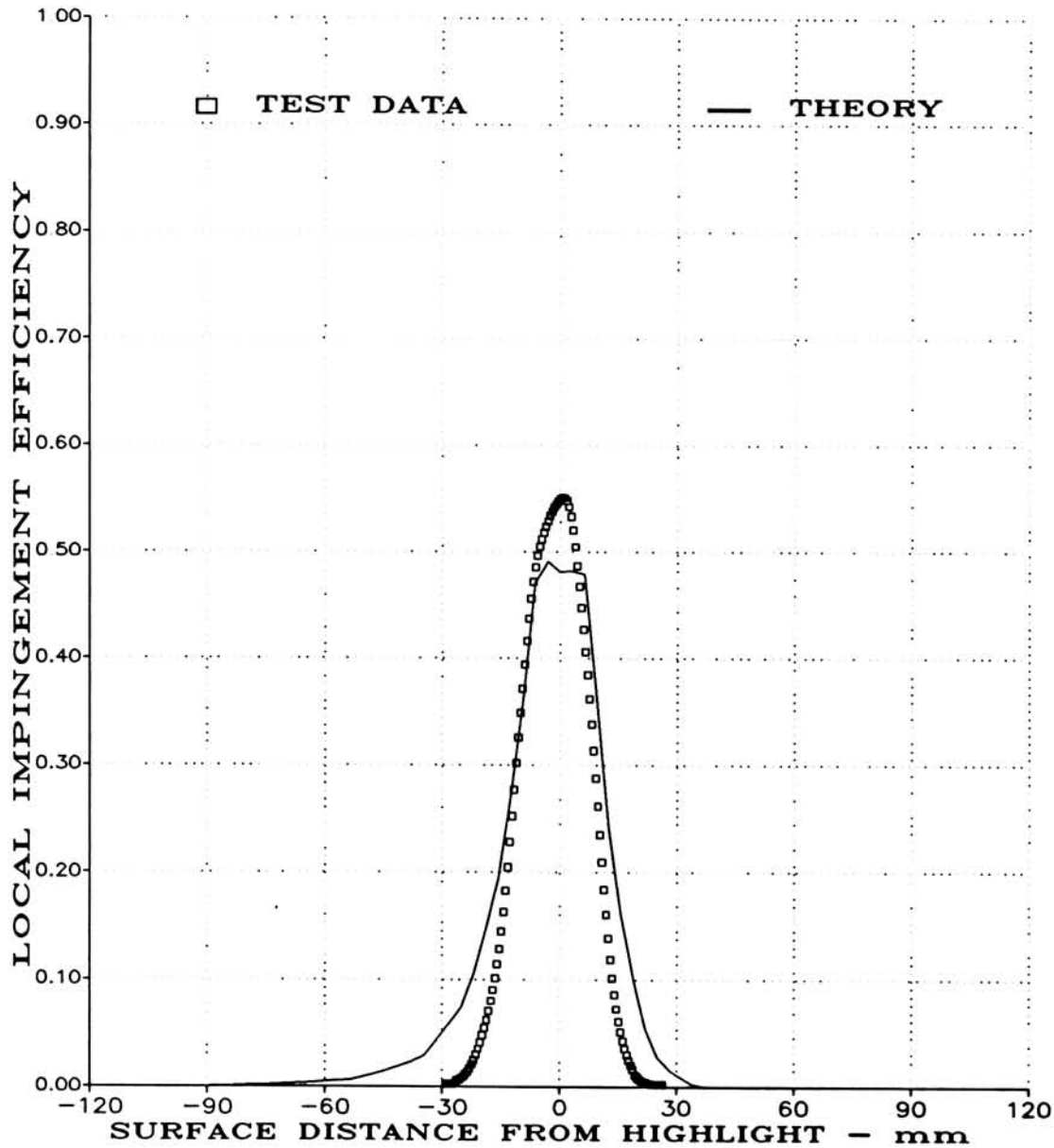
(Positive Surface Distance, S, on Inner Surface)

$$\bar{\beta}_{max} = 0.560, S_{O_{max}} = -38mm, S_{I_{max}} = 40mm \text{ (Experiment)}$$

(A5) STRIP E, $\theta = 180^\circ$, MVD = 20 MICRONS, MASS FLOW = 23 LBM/SEC

FIGURE 7.29

AVERAGED LOCAL WATER IMPINGEMENT EFFICIENCY DATA
 FOR BOEING 737-300 INLET AT $\alpha = 0^\circ$ ($V_\infty = 173$ mph, $K_{0_{mvd}} = 0.089$)
 (PAGE 5 OF 10).



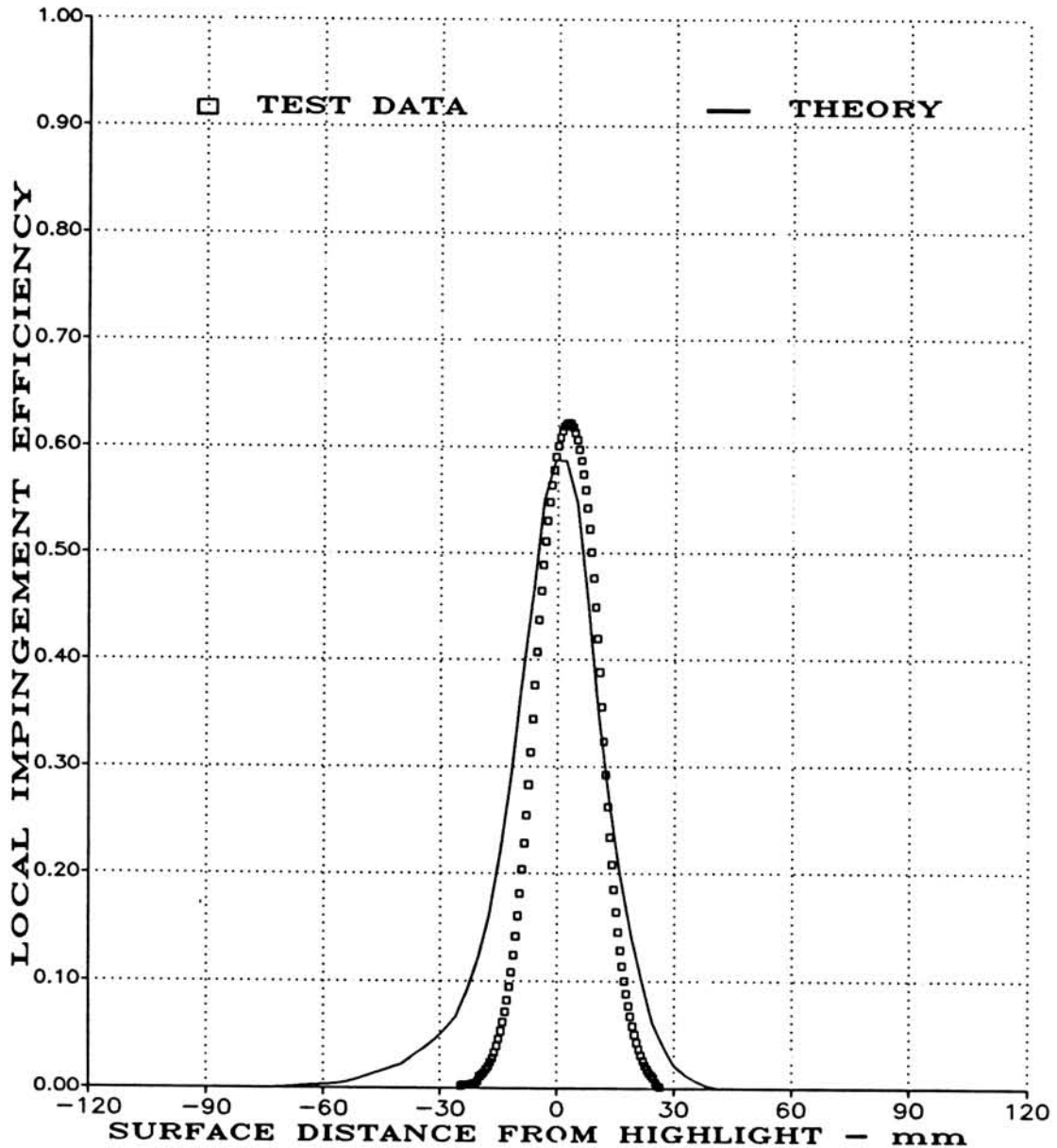
(Positive Surface Distance, S, on Inner Surface)

$$\bar{\beta}_{max} = 0.550, S_{O_{max}} = -28mm, S_{I_{max}} = 23mm \text{ (Experiment)}$$

(B1) STRIP A, $\theta = 0^\circ$, MVD = 16 MICRONS, MASS FLOW = 17 LBM/SEC

FIGURE 7.29

AVERAGED LOCAL WATER IMPINGEMENT EFFICIENCY DATA
 FOR BOEING 737-300 INLET AT $\alpha = 0^\circ$ ($V_\infty = 173$ mph, $K_{O_{mvd}} = 0.062$)
 (PAGE 6 OF 10).



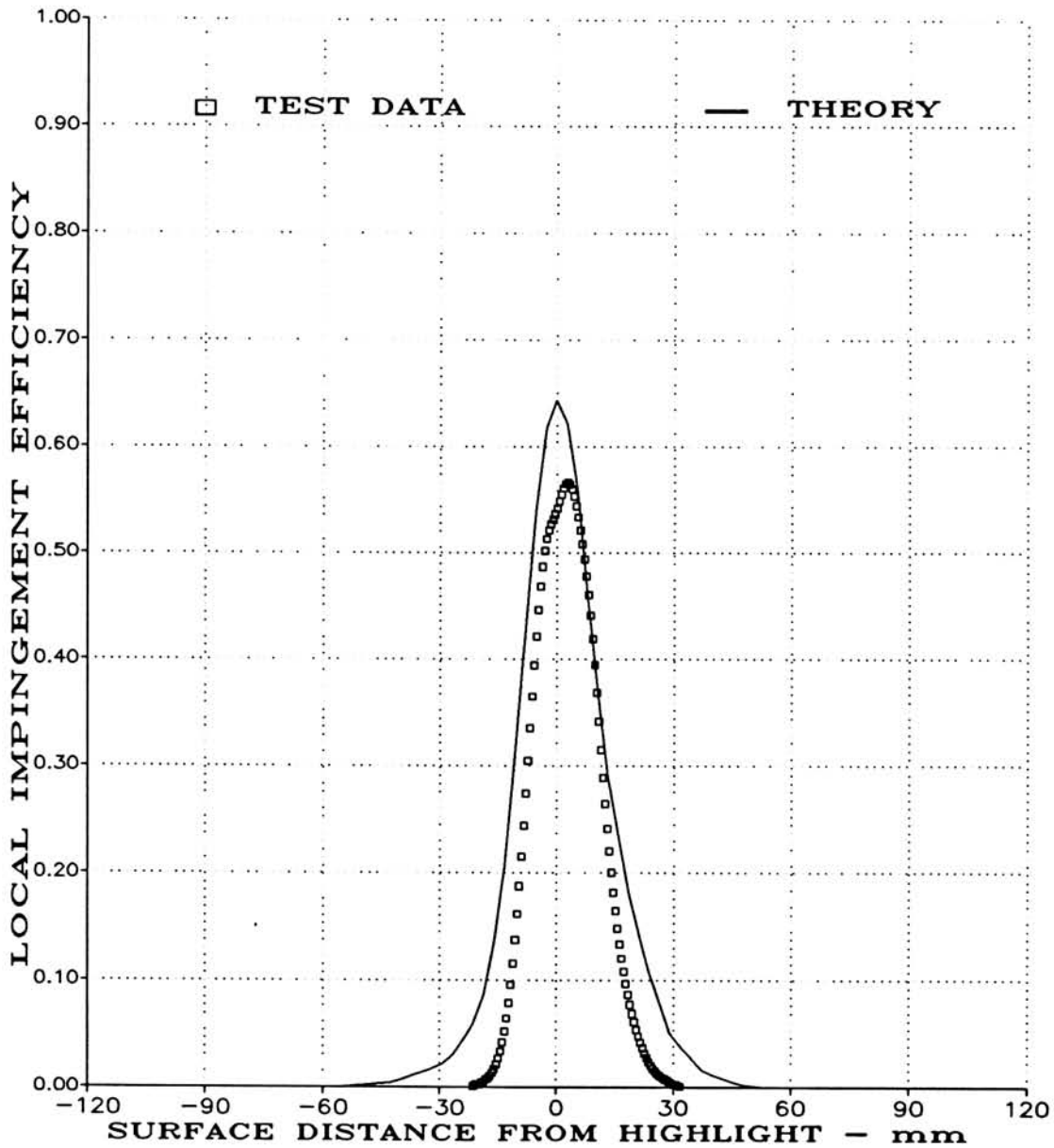
(Positive Surface Distance, S, on Inner Surface)

$$\bar{\beta}_{max} = 0.620, S_{O_{max}} = -21mm, S_{I_{max}} = 23mm \text{ (Experiment)}$$

(B2) STRIPS B,H, $\theta = 45^\circ$, MVD = 16 MICRONS, MASS FLOW = 17 LBM/SEC

FIGURE 7.29

AVERAGED LOCAL WATER IMPINGEMENT EFFICIENCY DATA
 FOR BOEING 737-300 INLET AT $\alpha = 0^\circ$ ($V_\infty = 173$ mph, $K_{0_{mvd}} = 0.062$)
 (PAGE 7 OF 10).



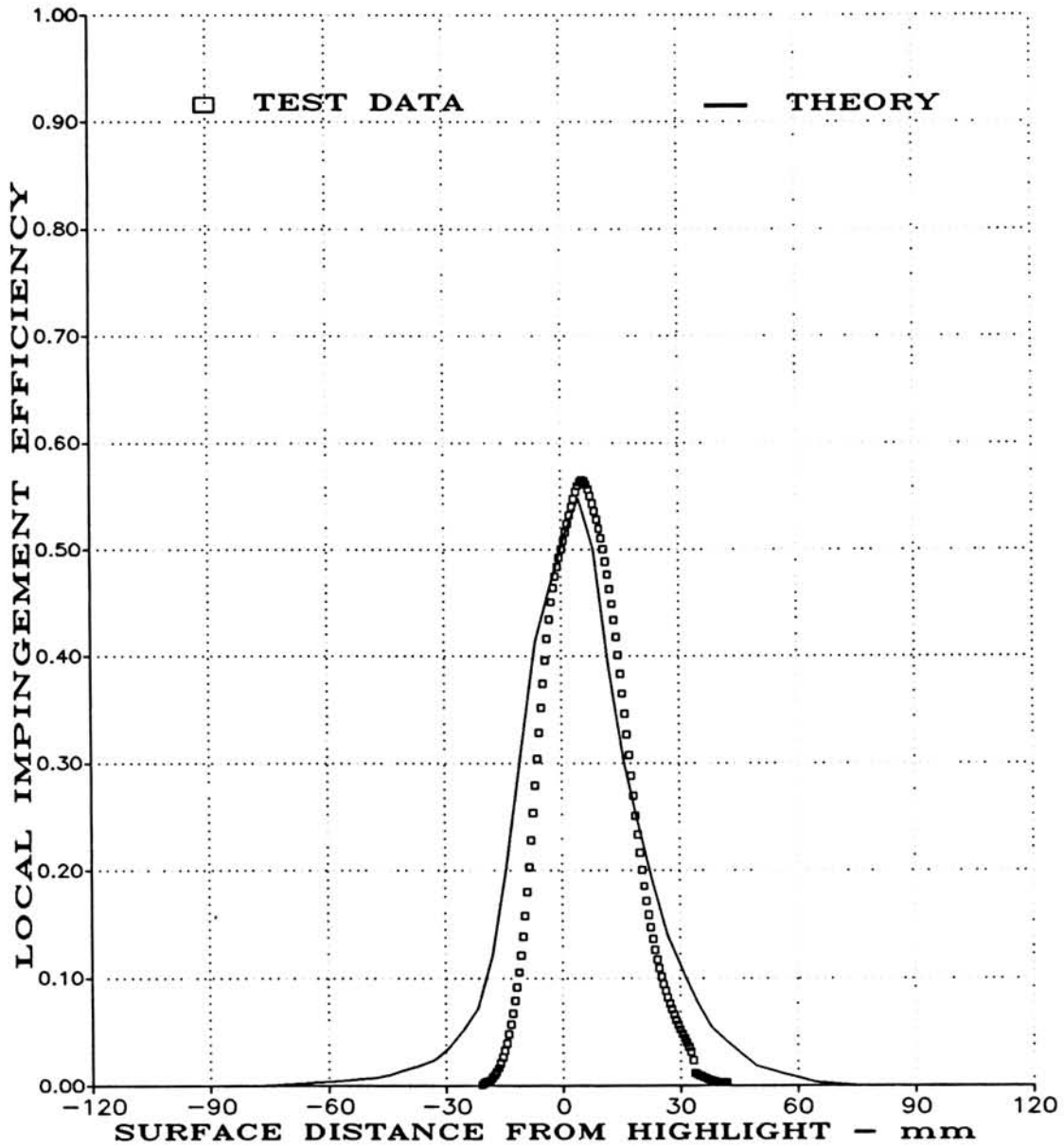
(Positive Surface Distance, S, on Inner Surface)

$$\bar{\beta}_{max} = 0.570, S_{O_{max}} = -16mm, S_{I_{max}} = 29mm \text{ (Experiment)}$$

(B3) STRIPS C,G, $\theta = 90^\circ$, MVD = 16 MICRONS, MASS FLOW = 17 LBM/SEC

FIGURE 7.29

AVERAGED LOCAL WATER IMPINGEMENT EFFICIENCY DATA
 FOR BOEING 737-300 INLET AT $\alpha = 0^\circ$ ($V_\infty = 173$ mph, $K_{0_{mvd}} = 0.062$)
 (PAGE 8 OF 10).



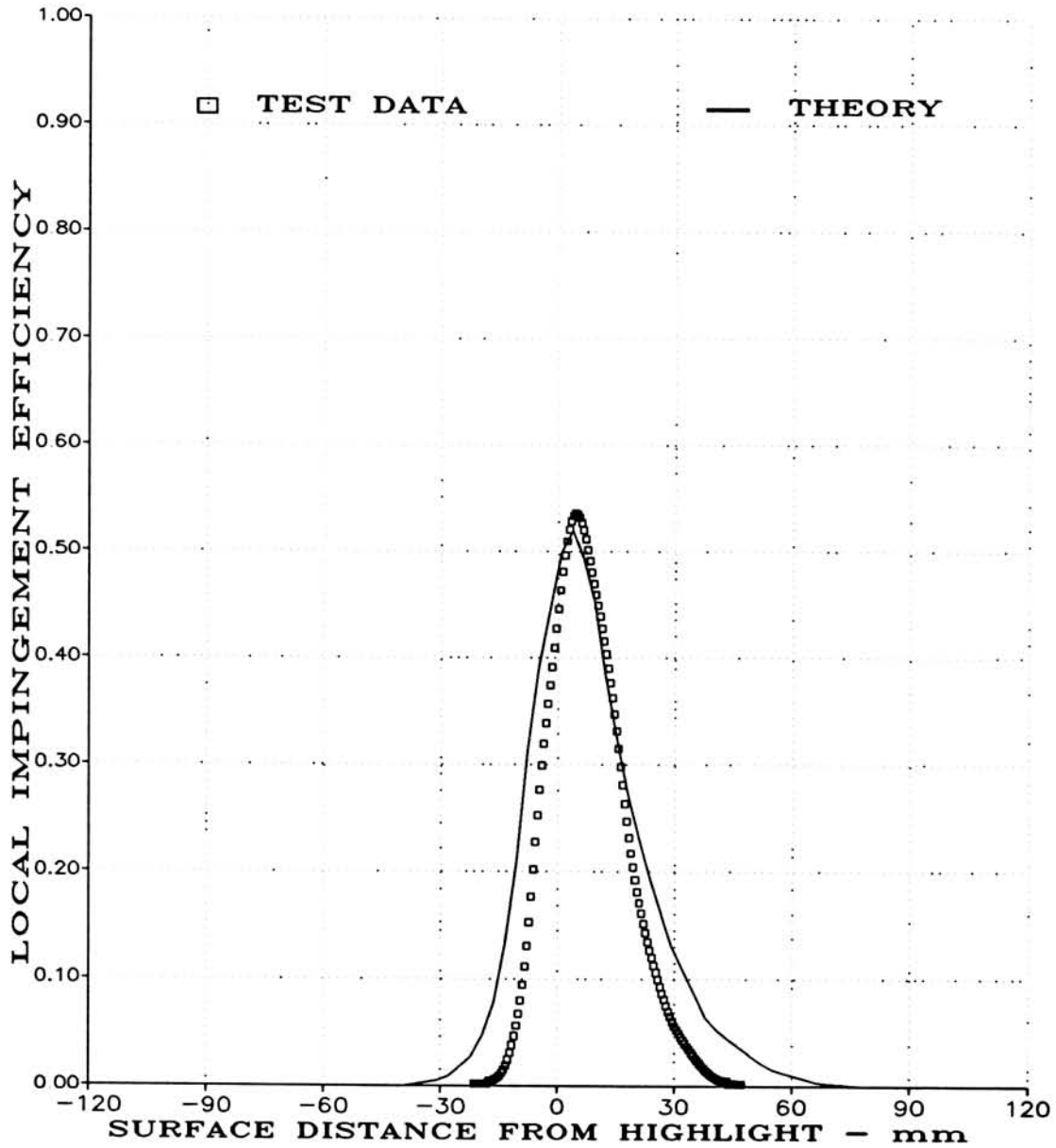
(Positive Surface Distance, S, on Inner Surface)

$$\bar{\beta}_{max} = 0.570, S_{O_{max}} = -20mm, S_{I_{max}} = 36mm \text{ (Experiment)}$$

(B4) STRIPS D,F, $\theta = 135^\circ$, MVD = 16 MICRONS, MASS FLOW = 17 LBM/SEC

FIGURE 7.29

AVERAGED LOCAL WATER IMPINGEMENT EFFICIENCY DATA
FOR BOEING 737-300 INLET AT $\alpha = 0^\circ$ ($V_\infty = 173$ mph, $K_{O_{mvd}} = 0.062$)
(PAGE 9 OF 10).



(Positive Surface Distance, S, on Inner Surface)

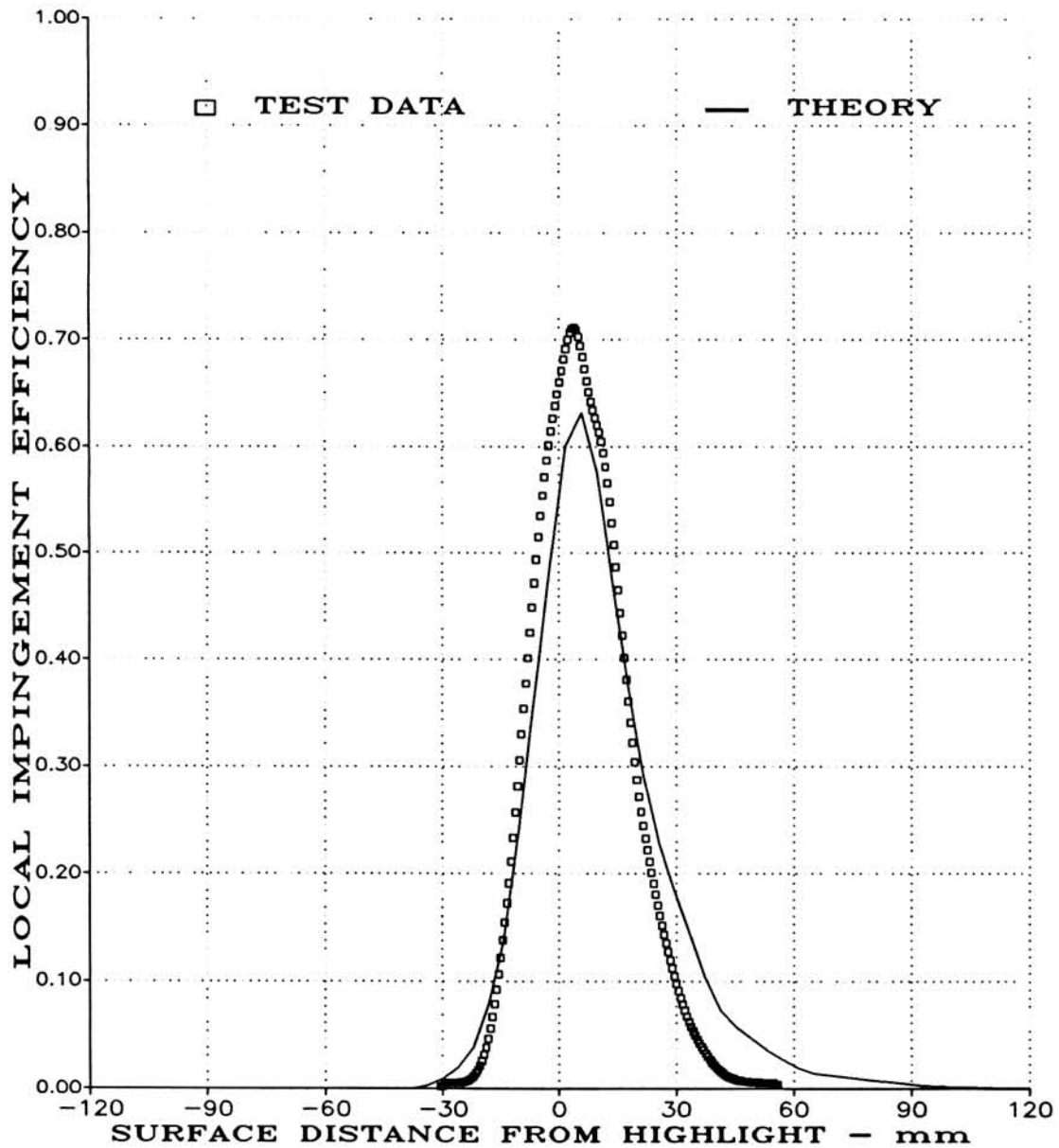
$$\bar{\beta}_{max} = 0.540, S_{O_{max}} = -15mm, S_{I_{max}} = 40mm \text{ (Experiment)}$$

(B5) STRIP E, $\theta = 180^\circ$, MVD = 16 MICRONS, MASS FLOW = 17 LBM/SEC

FIGURE 7.29

AVERAGED LOCAL WATER IMPINGEMENT EFFICIENCY DATA
 FOR BOEING 737-300 INLET AT $\alpha = 0^\circ$ ($V_\infty = 173$ mph, $K_{0_{mvd}} = 0.062$)
 (PAGE 10 OF 10).

TEST RUN ID: 1743915A, 1753915A, 1763915A



(Positive Surface Distance, S, on Inner Surface)

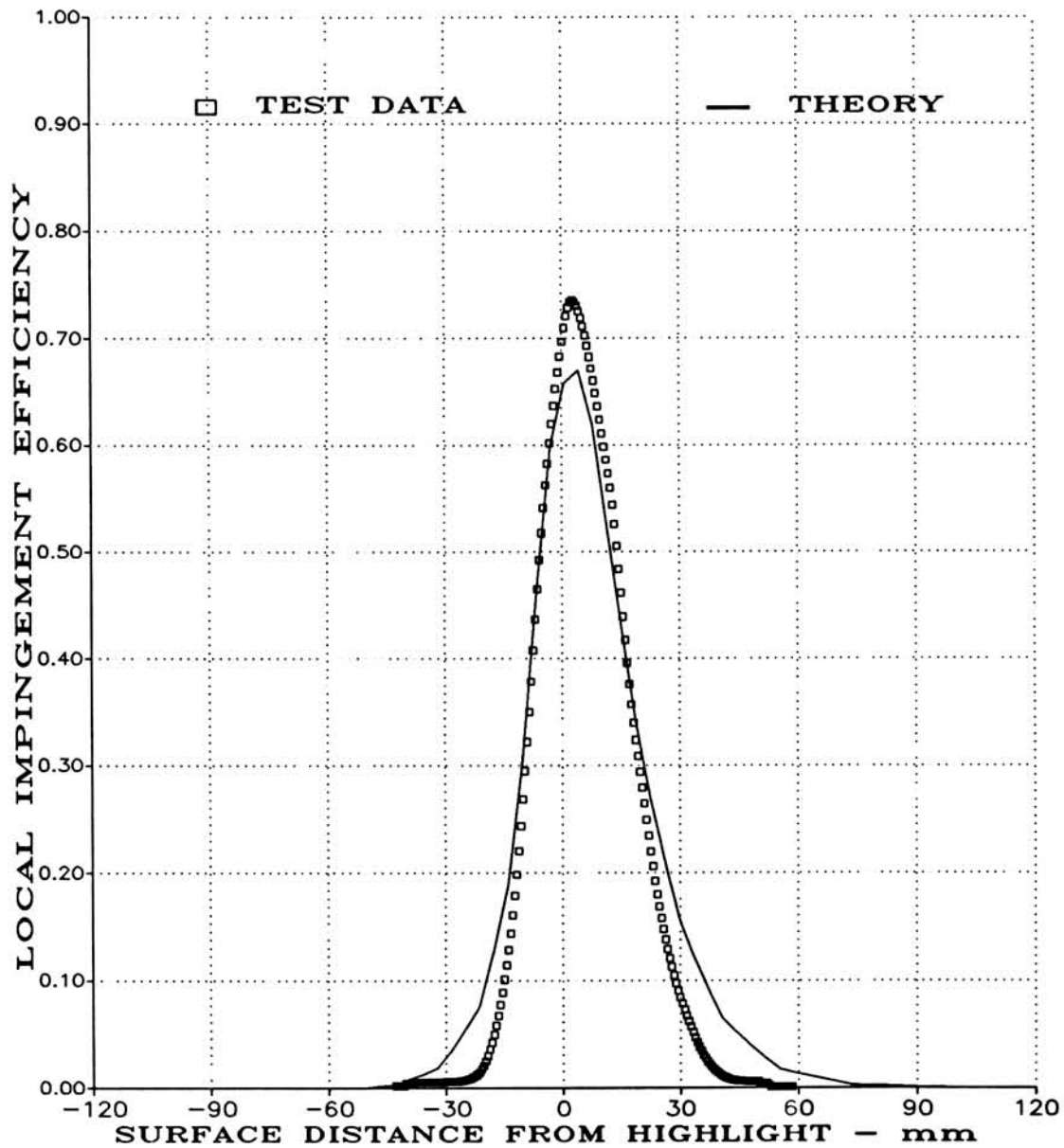
$$\bar{\beta}_{max} = 0.710, S_{O_{max}} = -22mm, S_{I_{max}} = 43mm \text{ (Experiment)}$$

(A1) STRIP A, $\theta = 0^\circ$, MVD = 20 MICRONS, MASS FLOW = 23 LBM/SEC

FIGURE 7.30

AVERAGED LOCAL WATER IMPINGEMENT EFFICIENCY DATA
FOR BOEING 737-300 INLET AT $\alpha = 15^\circ$ ($V_\infty = 171$ mph, $K_{0_{mvd}} = 0.089$)
(PAGE 1 OF 10).

TEST RUN ID: 1743915BH, 1753915BH, 1763915BH



(Positive Surface Distance, S, on Inner Surface)

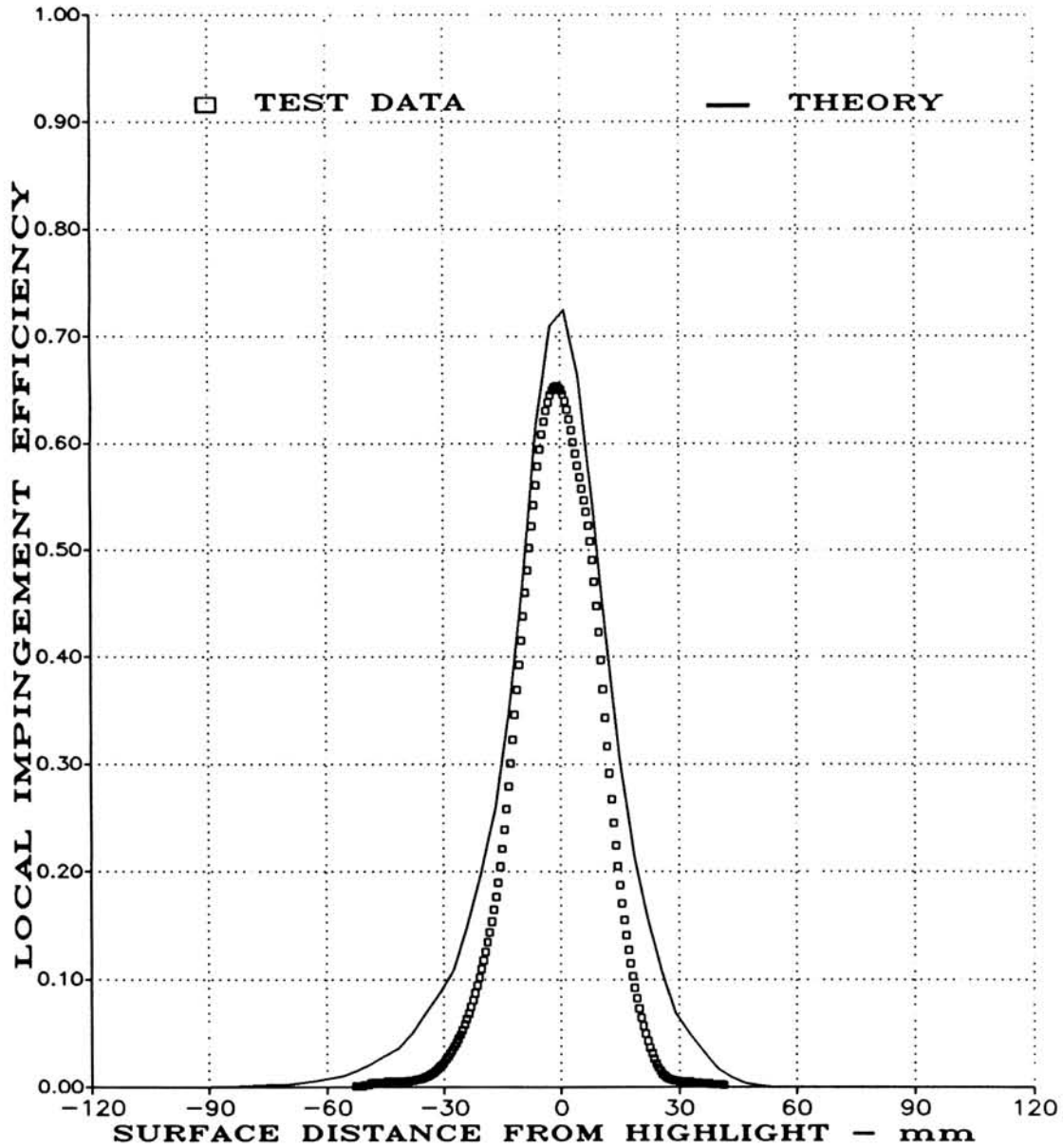
$$\bar{\beta}_{max} = 0.740, S_{O_{max}} = -25mm, S_{I_{max}} = 39mm \text{ (Experiment)}$$

(A2) STRIPS B,H, $\theta = 45^\circ$, MVD = 20 MICRONS, MASS FLOW = 23 LBM/SEC

FIGURE 7.30

AVERAGED LOCAL WATER IMPINGEMENT EFFICIENCY DATA
FOR BOEING 737-300 INLET AT $\alpha = 15^\circ$ ($V_\infty = 171$ mph, $K_{0_{mvd}} = 0.089$)
(PAGE 2 OF 10).

TEST RUN ID: 1743915CG, 1753915CG, 1763915CG



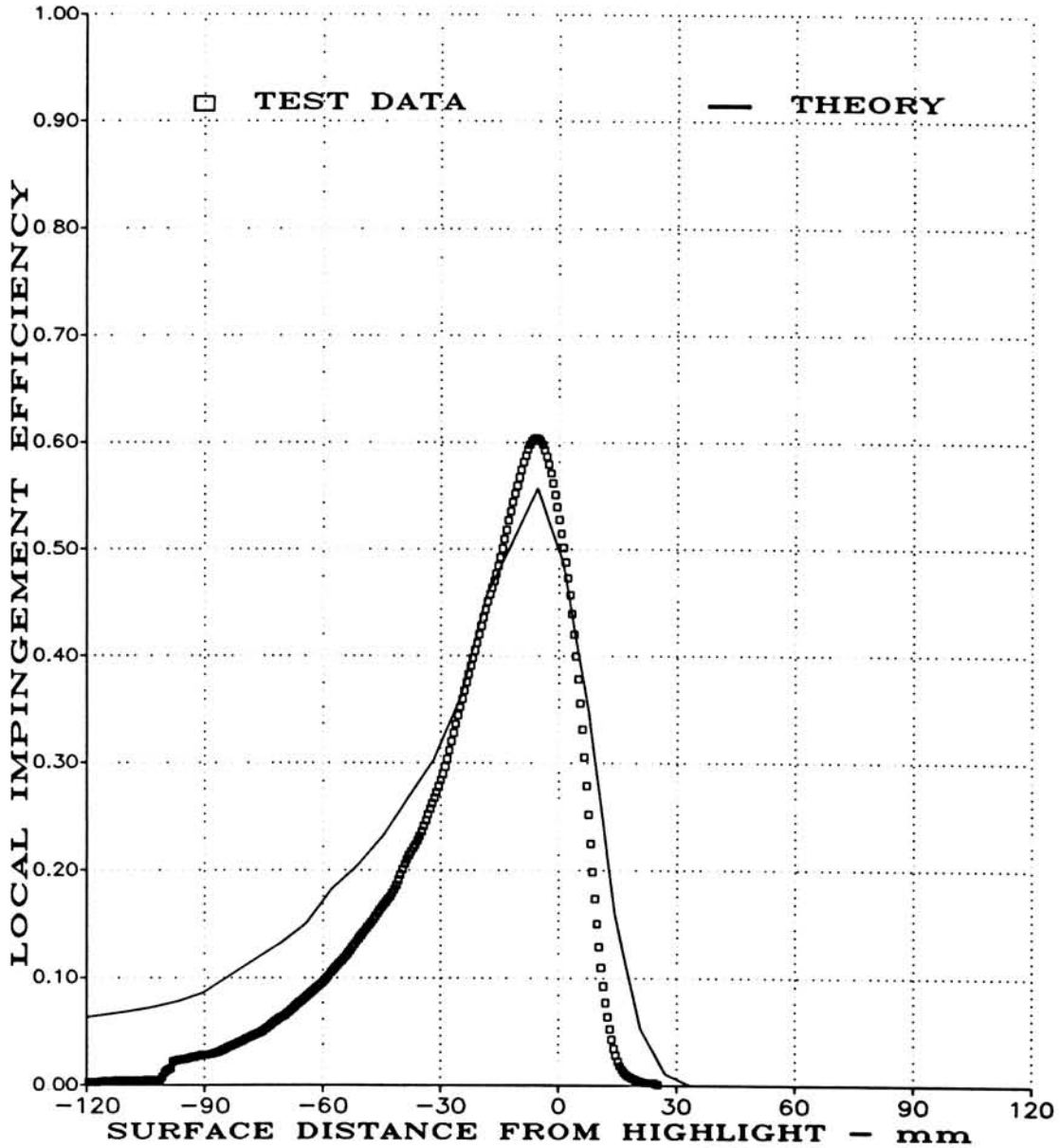
(Positive Surface Distance, S, on Inner Surface)

$$\bar{\beta}_{max} = 0.650, S_{O_{max}} = -39mm, S_{I_{max}} = 28mm \text{ (Experiment)}$$

(A3) STRIPS C,G, $\theta = 90^\circ$, MVD = 20 MICRONS, MASS FLOW = 23 LBM/SEC

FIGURE 7.30

AVERAGED LOCAL WATER IMPINGEMENT EFFICIENCY DATA
FOR BOEING 737-300 INLET AT $\alpha = 15^\circ$ ($V_\infty = 171$ mph, $K_{0_{mvd}} = 0.089$)
(PAGE 3 OF 10).



(Positive Surface Distance, S, on Inner Surface)

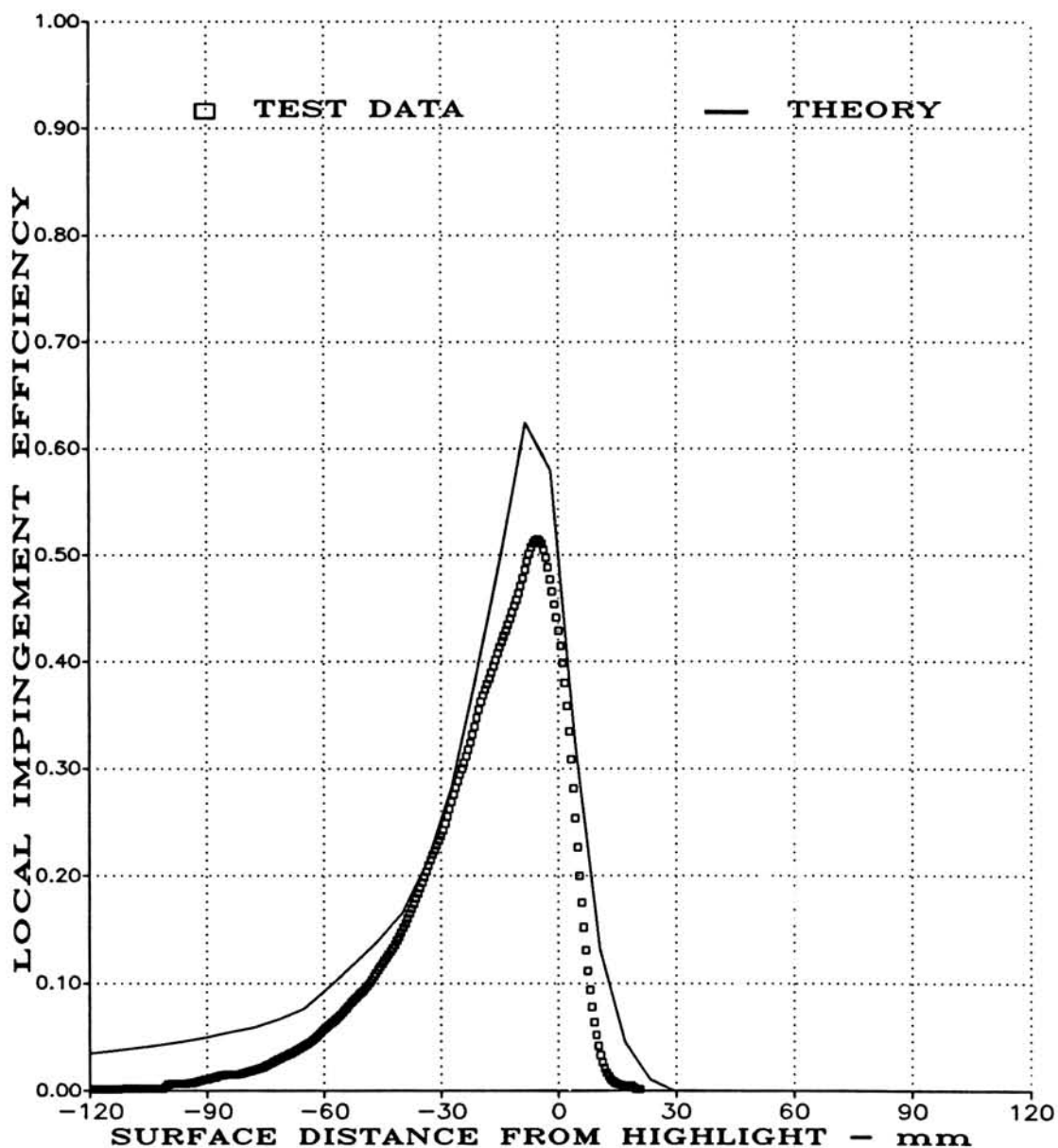
$$\bar{\beta}_{max} = 0.600, S_{O_{max}} = -190mm, S_{I_{max}} = 15mm \text{ (Experiment)}$$

(A4) STRIPS D,F, $\theta = 135^\circ$, MVD = 20 MICRONS, MASS FLOW = 23 LBM/SEC

FIGURE 7.30

AVERAGED LOCAL WATER IMPINGEMENT EFFICIENCY DATA
 FOR BOEING 737-300 INLET AT $\alpha = 15^\circ$ ($V_\infty = 171$ mph, $K_{O_{mvd}} = 0.089$)
 (PAGE 4 OF 10).

TEST RUN ID: 1743915E, 1753915E, 1763915E



(Positive Surface Distance, S, on Inner Surface)

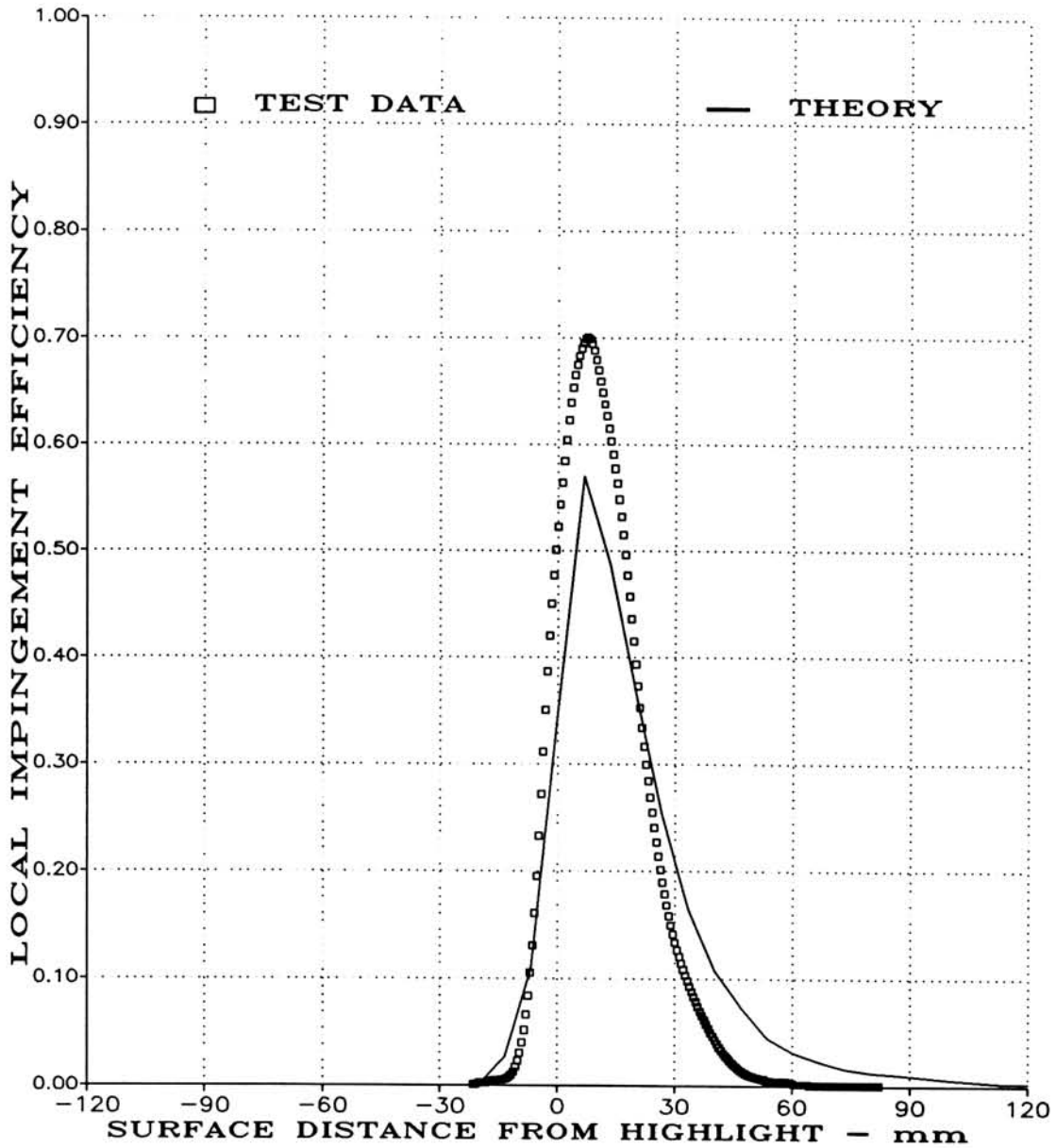
$$\bar{\beta}_{max} = 0.510, S_{O_{max}} = -187mm, S_{I_{max}} = 13mm \text{ (Experiment)}$$

(A5) STRIP E, $\theta = 180^\circ$, MVD = 20 MICRONS, MASS FLOW = 23 LBM/SEC

FIGURE 7.30

AVERAGED LOCAL WATER IMPINGEMENT EFFICIENCY DATA
FOR BOEING 737-300 INLET AT $\alpha = 15^\circ$ ($V_\infty = 171$ mph, $K_{0_{mvd}} = 0.089$)
(PAGE 5 OF 10).

TEST RUN ID: 1683615A, 1693615A, 1703615A, 1713615A, 1723615A, 1733615A



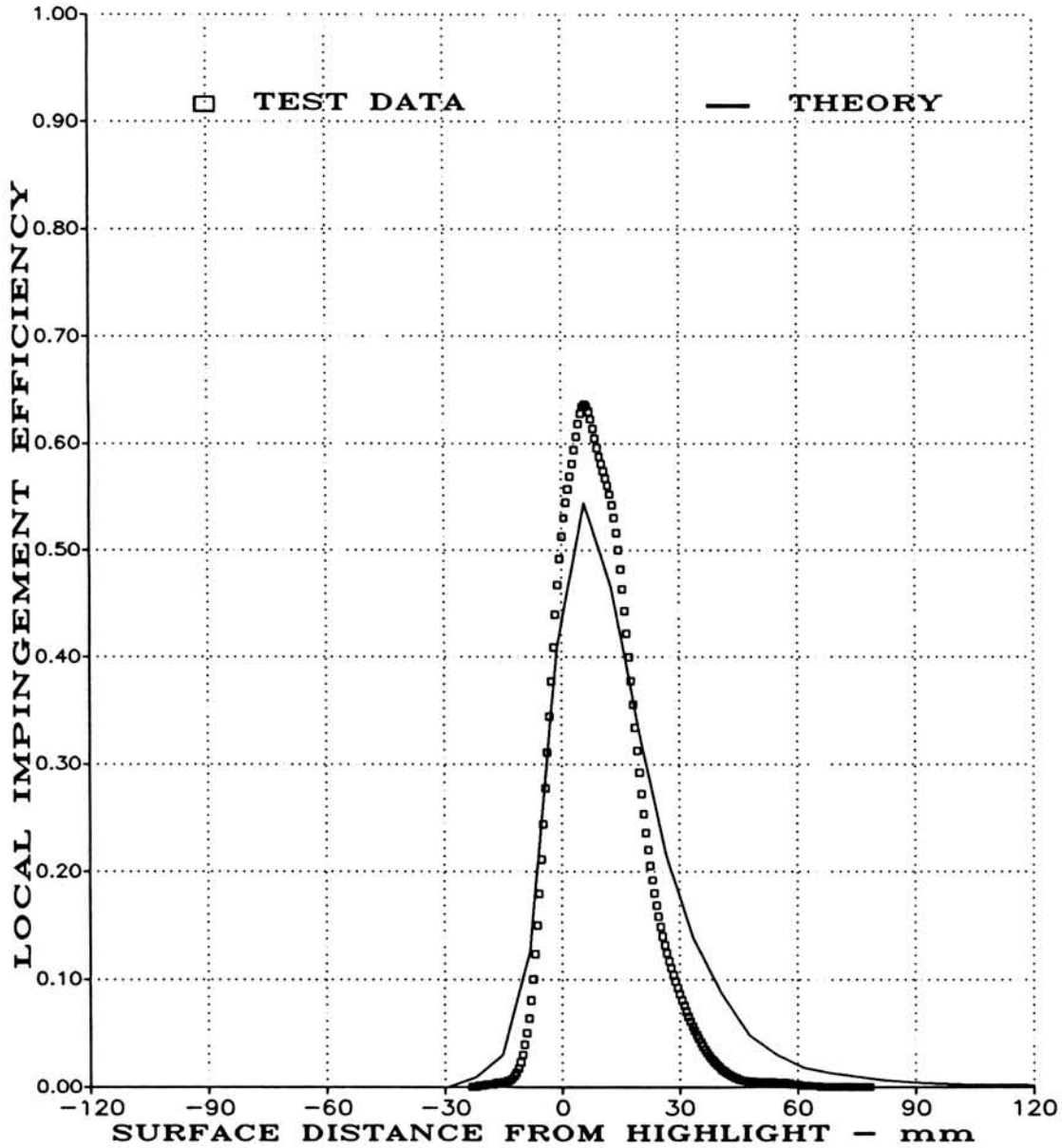
(Positive Surface Distance, S, on Inner Surface)

$$\bar{\beta}_{max} = 0.700, S_{O_{max}} = -10mm, S_{I_{max}} = 48mm \text{ (Experiment)}$$

(B1) STRIP A, $\theta = 0^\circ$, MVD = 16 MICRONS, MASS FLOW = 17 LBM/SEC

FIGURE 7.30

AVERAGED LOCAL WATER IMPINGEMENT EFFICIENCY DATA
FOR BOEING 737-300 INLET AT $\alpha = 15^\circ$ ($V_\infty = 171$ mph, $K_{0_{mvd}} = 0.062$)
(PAGE 6 OF 10).



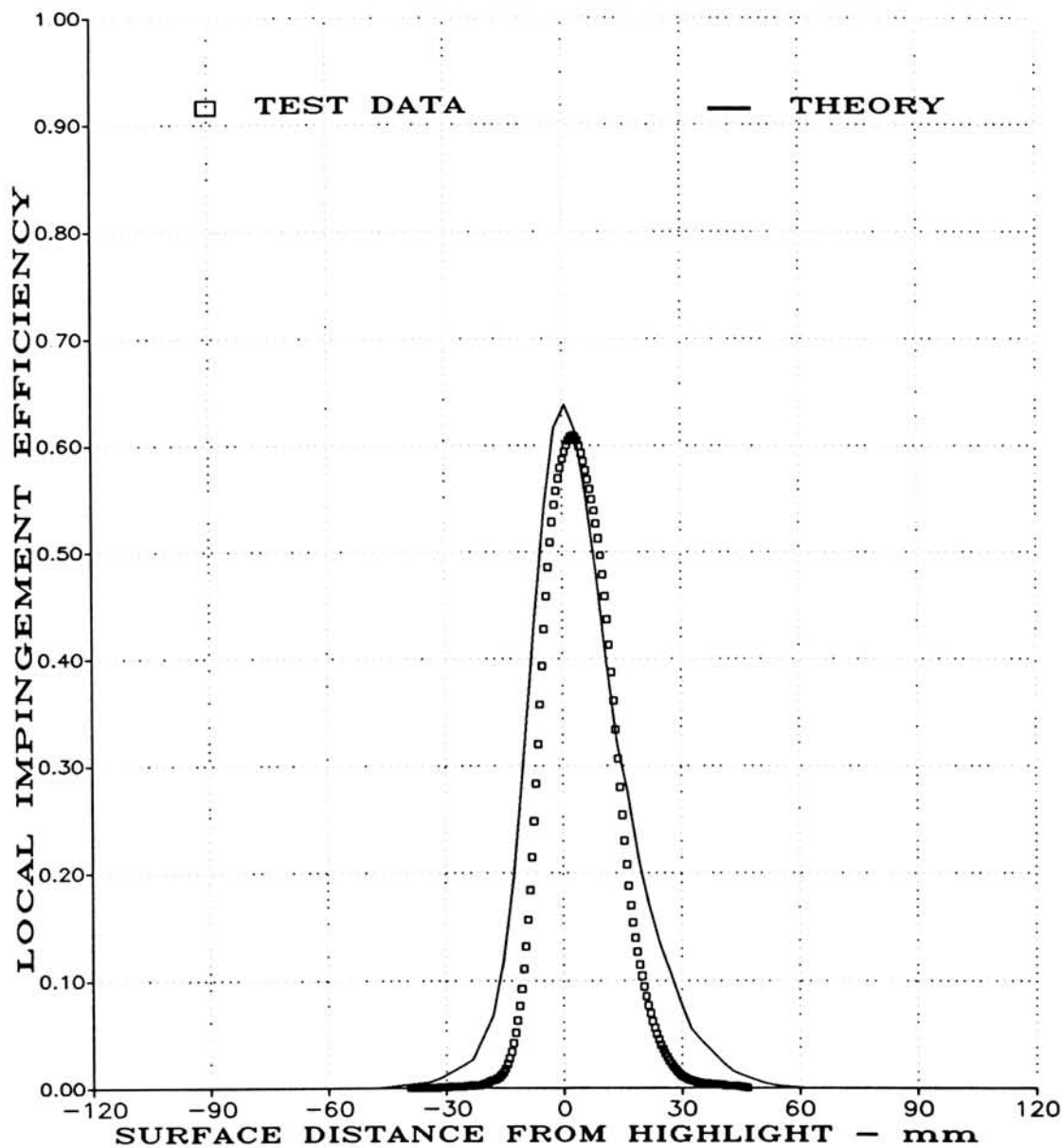
(Positive Surface Distance, S, on Inner Surface)

$$\bar{\beta}_{max} = 0.640, S_{O_{max}} = -11mm, S_{I_{max}} = 44mm \text{ (Experiment)}$$

(B2) STRIPS B,H, $\theta = 45^\circ$, MVD = 16 MICRONS, MASS FLOW = 17 LBM/SEC

FIGURE 7.30

AVERAGED LOCAL WATER IMPINGEMENT EFFICIENCY DATA
FOR BOEING 737-300 INLET AT $\alpha = 15^\circ$ ($V_\infty = 171$ mph, $K_{0_{mvd}} = 0.062$)
(PAGE 7 OF 10).



(Positive Surface Distance, S, on Inner Surface)

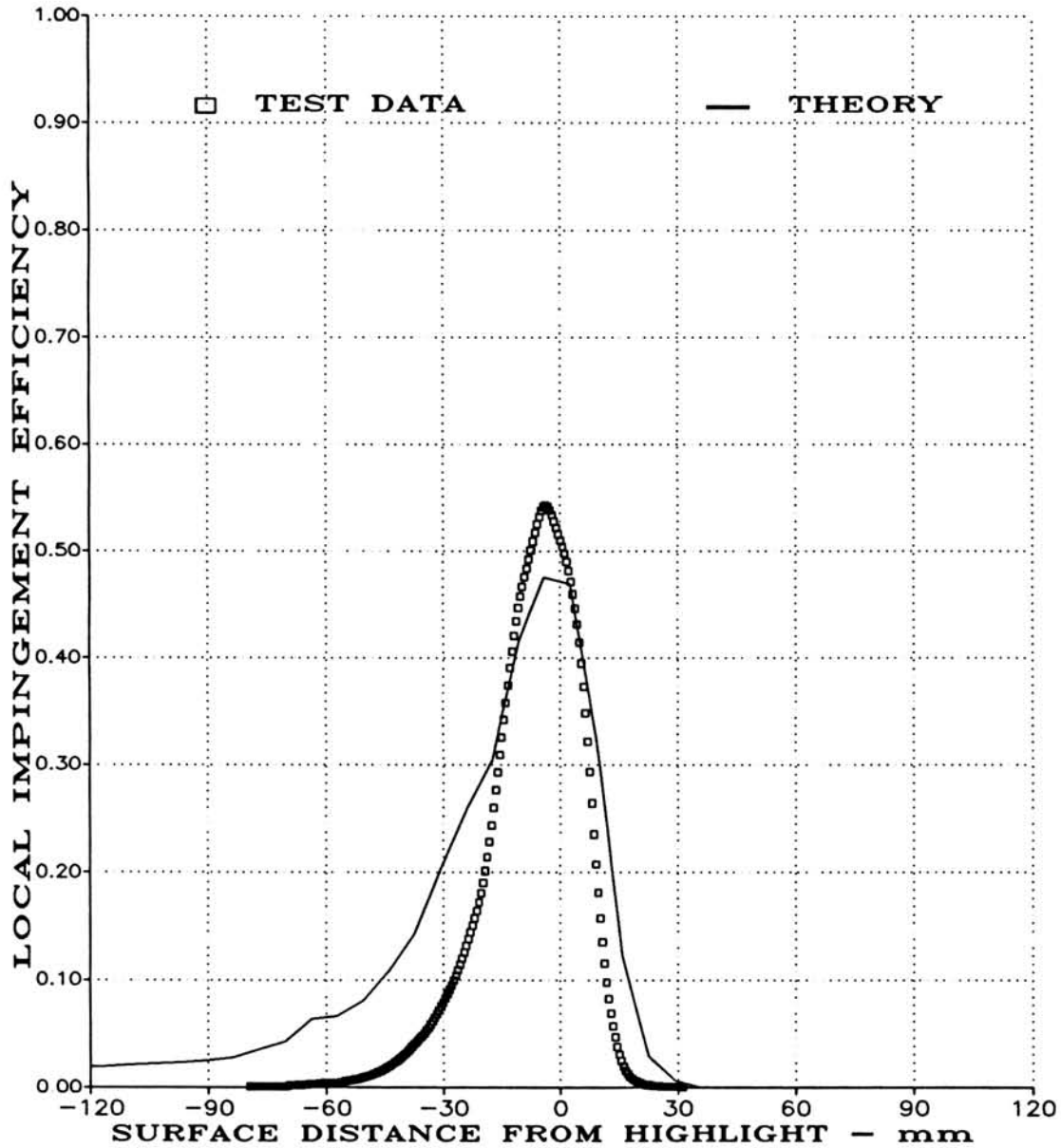
$$\bar{\beta}_{max} = 0.610, S_{O_{max}} = -16mm, S_{I_{max}} = 30mm \text{ (Experiment)}$$

(B3) STRIPS C,G, $\theta = 90^\circ$, MVD = 16 MICRONS, MASS FLOW = 17 LBM/SEC

FIGURE 7.30

AVERAGED LOCAL WATER IMPINGEMENT EFFICIENCY DATA
 FOR BOEING 737-300 INLET AT $\alpha = 15^\circ$ ($V_\infty = 171$ mph, $K_{0_{mvd}} = 0.062$)
 (PAGE 8 OF 10).

TEST RUN ID: 1683615DF, 1693615DF, 1703615DF, 1713615DF, 1723615DF, 1733615DF



(Positive Surface Distance, S, on Inner Surface)

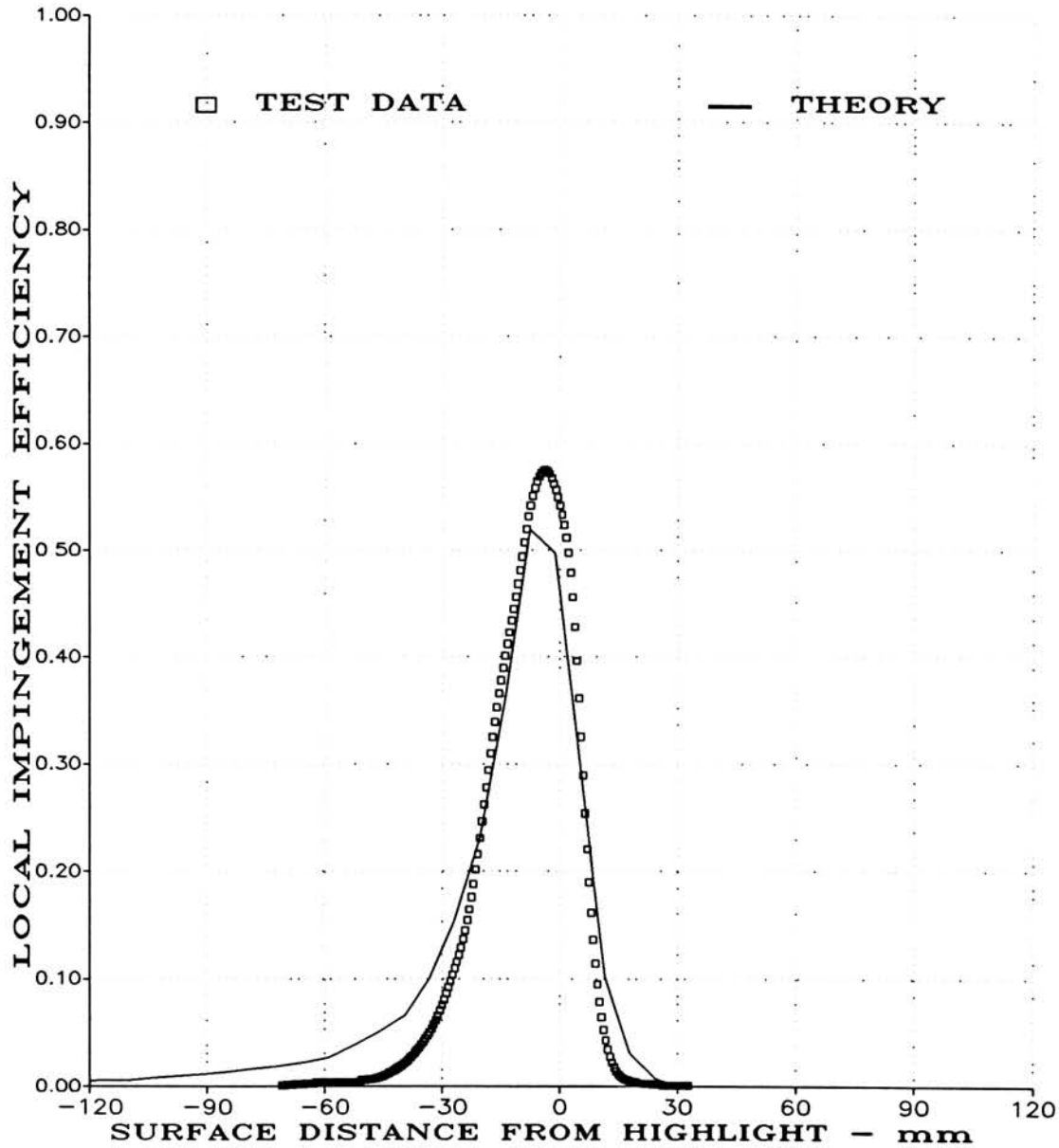
$$\bar{\beta}_{max} = 0.540, S_{O_{max}} = -55mm, S_{I_{max}} = 23mm \text{ (Experiment)}$$

(B4) STRIPS D,F, $\theta = 135^\circ$, MVD = 16 MICRONS, MASS FLOW = 17 LBM/SEC

FIGURE 7.30

AVERAGED LOCAL WATER IMPINGEMENT EFFICIENCY DATA
FOR BOEING 737-300 INLET AT $\alpha = 15^\circ$ ($V_\infty = 171$ mph, $K_{O_{mvd}} = 0.062$)
(PAGE 9 OF 10).

TEST RUN ID: 1683615E, 1693615E, 1703615E, 1713615E, 1723615E, 1733615E



(Positive Surface Distance, S, on Inner Surface)

$$\bar{\beta}_{max} = 0.580, S_{O_{max}} = -50mm, S_{I_{max}} = 16mm \text{ (Experiment)}$$

(B5) STRIP E, $\theta = 180^\circ$, MVD = 16 MICRONS, MASS FLOW = 17 LBM/SEC

FIGURE 7.30

AVERAGED LOCAL WATER IMPINGEMENT EFFICIENCY DATA
FOR BOEING 737-300 INLET AT $\alpha = 0^\circ$ ($V_\infty = 171$ mph, $K_{0_{mvd}} = 0.062$)
(PAGE 10 OF 10).

8.0 CONCLUSIONS

Water droplet impingement data were presented for several modern aircraft geometries: a Natural Laminar Flow airfoil NLF(1)-0414, two simulated glaze ice shapes, a medium speed 30 degrees swept MS-0317 airfoil, a 30 degrees NACA 0012 swept wing tip and a Boeing 737-300 engine inlet.

The work presented in this report is the conclusion of an extensive experimental investigation initiated in 1984 to provide experimental water droplet impingement data for the validation of computer codes used in icing analyses. The main objectives were to develop experimental and data reduction methods for obtaining water droplet impingement characteristics on aircraft surfaces and to provide experimental impingement data for a range of geometries, flow and spray cloud conditions.

The following conclusions are based on the results obtained during this research program:

1. The experimental investigation conducted has resulted in an extensive data base of water droplet impingement data for several aircraft geometries including engine inlets for which very little data existed prior to this work.
2. The experimental and data reduction methods are accurate and repeatable. The quality of the experimental results depends on careful monitoring of all test variables particularly those affecting spray cloud properties. Cloud uniformity and MVD size are difficult to control and measure. To improve the accuracy of the results each test condition must be repeated several times and the results must be averaged to produce the final impingement curves. The data reduction method is very efficient compared to colorimetric analysis and allows extraction of data without destroying the blotter strips. It is important that the laser calibration curve used in the data reduction process be checked periodically since the laser characteristics can change over long periods.
3. In water droplet impingement tests accurate LWC measurements are essential in obtaining impingement efficiency results. It is important that local LWC measurements be made in order to eliminate errors due to variations in cloud uniformity. The collector mechanism used in the 1985 tests and the improved design used in the 1989 tests proved useful in measuring local LWC.
4. In most cases the uncertainty in the experimental results obtained was less than 20%. The maximum uncertainty was in $\bar{\beta}_{max}$.
5. Correlation between experimental and computational results was good for the majority of cases presented.

APPENDIX A - DATA REDUCTION FOR CURVED STRIPS

Test blotter strips used in the April 1989 droplet impingement tests were of different shapes and sizes depending on test geometry. The various blotter strip shapes used are shown in Figures A.1, A.2 and A.3. The shape of a blotter strip is important in that it affects the data reduction process. The laser reflectometer was designed for straight blotter strips only. To scan curved blotter strips each strip had to be divided into straight segments and each segment had to be scanned separately. In most cases each curved blotter strip was divided into two straight segment.

Straight blotter strips (Fig. A.1) were the easiest to reduce. These strips were attached to the reflectometer drum and the data was extracted by scanning the strip at three different horizontal locations as shown in Figure A.1. The three horizontal scans were stored in a single file and were averaged to produce a single droplet impingement curve. The surface distance along the strip was identical to the surface distance of the geometry to which the strip was attached.

Figure A.2 shows the type of strips used in the testing of the finite swept wing tip. These strips were V-shaped to fit the wing section in the streamwise direction. To extract the impingement data from the V-shaped strips the strips were scanned along their centerline (line A-B-C in Fig. A.2). Section AB of the strip was scanned first, by positioning section AB on the reflectometer drum. The results were stored in a data file. Next section BC was positioned on the reflectometer drum and was scanned from B to C. The impingement results from section BC were stored in a data file. The two data files (one for section AB and one for section BC) were combined to produce the final impingement curve. To simplify the data reduction process only one horizontal scan was performed for each V-shaped blotter strip.

Figure A.3 shows the type of curved strips used in all impingement tests of the infinite swept MS(1)-0317 airfoil. The strip centerline (A-B-C-D-E) is shown in Fig. A.3. The centerline is curved so a large number of straight segments were required to preserve the actual surface distance. This significantly complicates the data reduction process. A simpler and equally accurate method was to approximate the centerline of the strip with two straight line segments a-b-c whose total length was equal to the curved centerline A-B-C-D-E. The laser scan was performed along the scan line a-b-c using the same procedure as the one used for the V-shaped strips discussed above.

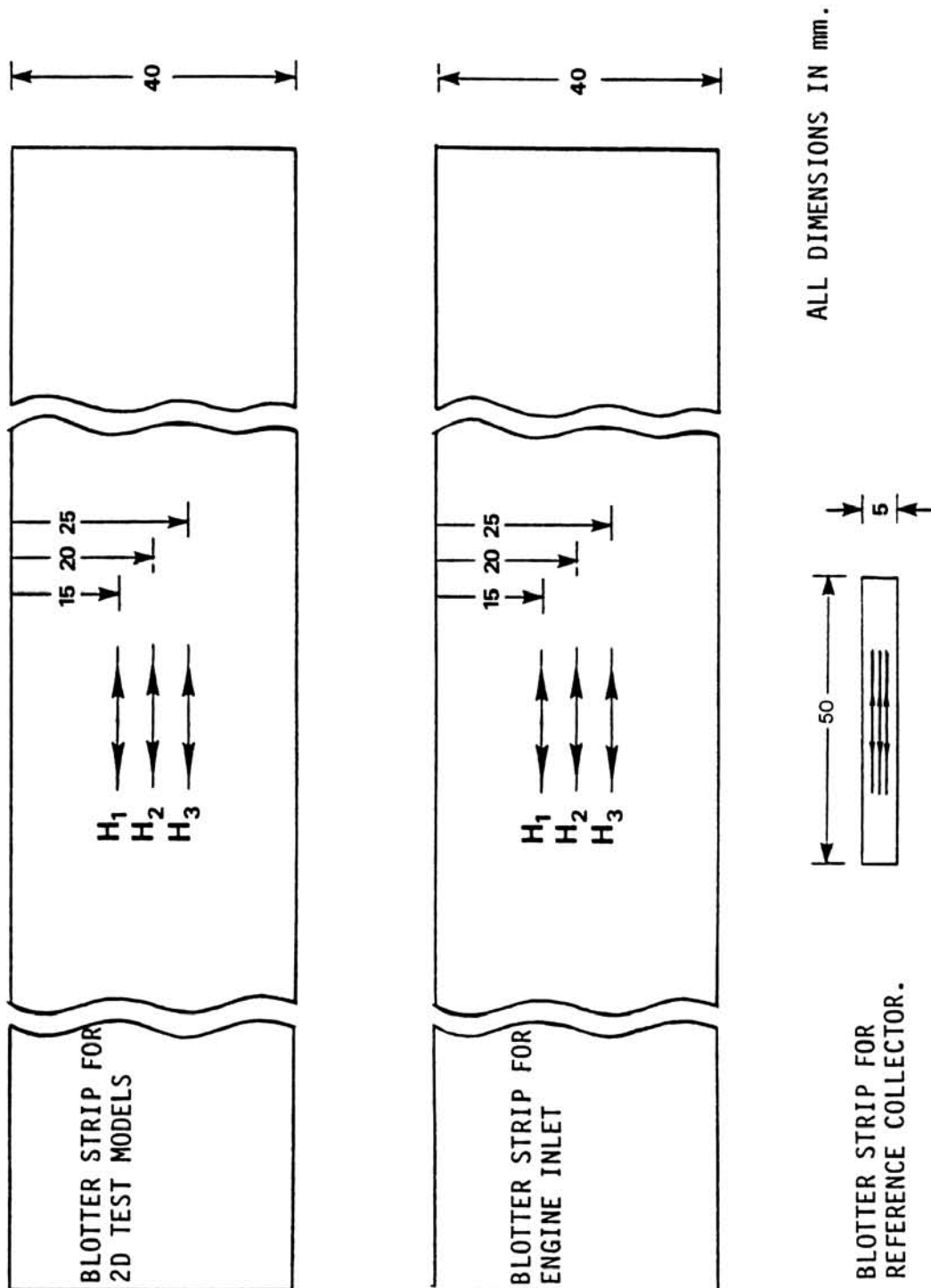


FIGURE A.1

STRAIGHT BLOTTER STRIPS USED ON NLF(1)-0414 AIRFOIL,
ICE SHAPES, BOEING 737-300 ENGINE INLET AND COLLECTOR.

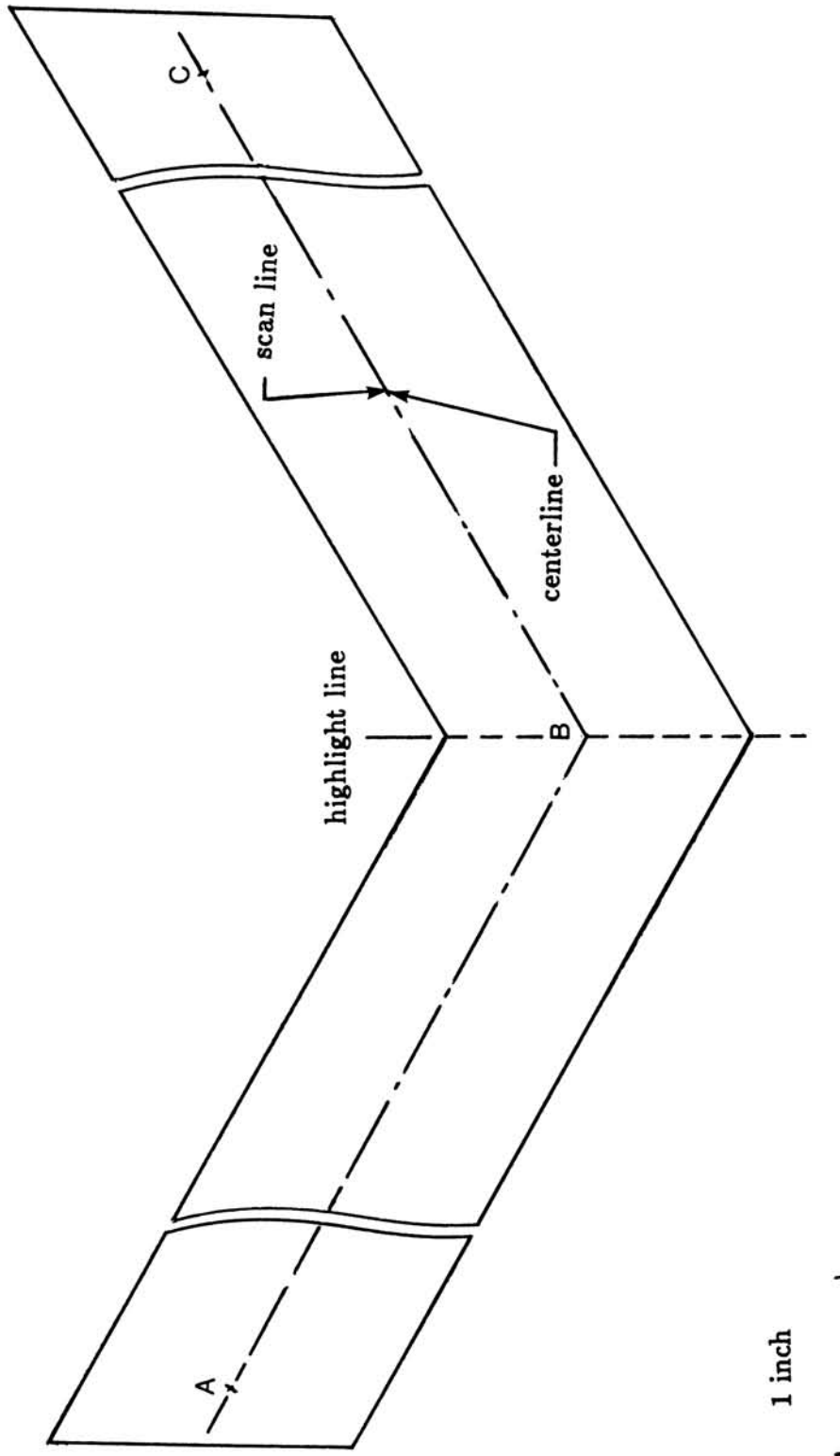


FIGURE A.2
 V-SHAPED BLOTTER STRIPS USED ON NACA 0012 SWEEP WING TIP.

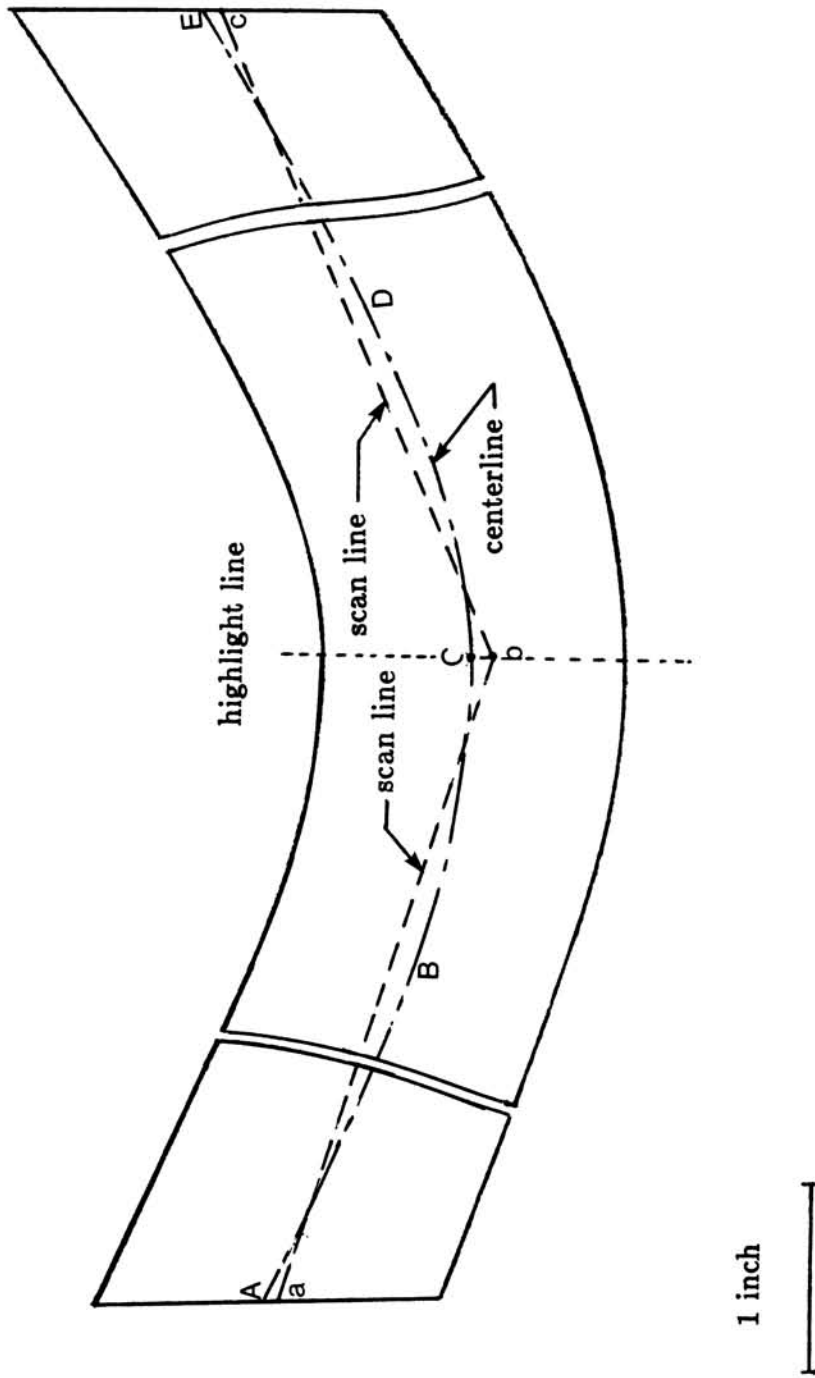


FIGURE A.3
 CURVED BLOTTER STRIPS USED ON MS(1)-0317 SWEEP AIRFOIL.

APPENDIX B - IMPINGEMENT TEST LOG SHEETS

Details of tunnel and spray system conditions for all impingement test runs performed in April of 1989 are given in this appendix. A total of 214 test runs were performed which are subdivided as follows:

- Uniformity tests- Runs 1 to 59 and 181 to 183
- Boeing 737-300 Inlet - Runs 60 to 71, 93 to 94 and 168 to 180. Runs 60 to 71 and 93 to 94 were discarded due to problems with the inlet mass flow system and the spray system air pressure.
- Reference Collector - Runs 95 to 115
- Ice Shapes - Runs 116 to 126
- NACA 0012 Swept Wing Tip - Runs 127 to 147
- MS(1)-0317 Swept Airfoil - Runs 148 to 167
- Laser Calibration - Runs 184 to 192
- NLF(1)-0414 Airfoil - Runs 215 to 236

B.1 - Test Variables Recorded

At the top left corner of each log sheet the test date and the dye concentration used are given. A dye concentration of 0.00025 was used for the first 59 (uniformity) runs. The concentration was then lowered to 0.0002 for the remaining tests. The higher concentration allowed easier detection of color variation on the blotter squares during the uniformity tests. The lower concentration was selected for the impingement tests to give optimum color intensity distribution on the blotter strips. A concentration of 0.0002 was typically obtained by combining 4 grams of blue dye powder with 20 liters (i.e., 20,000 grams) of distilled water.

B.1.1 - Run No and Run ID

Each test performed had a unique number assigned to it. The run number and the run ID which was used to identify each model, were placed on each blotter strip used in a test.

B.1.2 - Tunnel Conditions

Tunnel conditions, which were measured by the usual IRT instrumentation, were recorded for each test point. The tunnel total temperature was obtained from the average of eleven readings taken at different tunnel locations. The tunnel true air speed along with the freestream static and total pressures were also recorded. The air stream humidity level was monitored using the Dew Point temperature reading. A large difference between the dew point temperature reading and the air temperature reading indicates a low humidity level in the air stream (see table B.1). Two methods were employed to increase the humidity in the air stream. In one method moisture was added to the air stream by using the IRT spray system. A different approach was to decrease the tunnel air temperature by using the IRT refrigeration system.

B.1.3 - Spray System Conditions

Spray system conditions were monitored continuously at various locations in the spray system. The three columns under SUPPLY PRESSURE conditions in each log sheet give the desired settings for air and dyed water at the spray nozzle. The two columns under PLENUM PRESSURE show the spray system pressure settings prior to a test. These settings were adjusted manually using pressure regulators located in the tunnel plenum chamber. The dyed water pressure was controlled by adjusting the pressure in the tank containing the dye/water solution. This pressure was monitored by a pressure gauge attached to the dyed water supply tank. The tank pressure was set 6 psig higher than the value required at the nozzle to account for the hydrostatic pressure difference between the tank level and the nozzle level. The air pressure was set with air flowing through the nozzles and was monitored by a pressure gauge attached to the air pressure regulator. Both air and water pressure were checked PRIOR TO EACH TEST RUN. To monitor the system pressure fluctuations during test runs electronic transducers (Model 204E, Range: 0 to 250 psi, Setra Systems Inc, Natick, MASS., USA) were attached at various locations of the spray system and their readings were monitored from the tunnel control room. Variations in the readings of the transducers from their settings prior to each test were carefully monitored. The values given in the log sheets were the readings prior to the test. Transducers were attached to the supply tank containing the dye and water solution, to the dyed water supply line of nozzle 1, 3, 4, 6 and 7 and to the air line of nozzle 11.

B.1.4 - Mass Flow Conditions

Mass flow conditions were recorded for all inlet impingement tests. Output voltage from the Kurtz probe was recorded for each run. This voltage was converted into pounds mass per second using the following equation:

$$\text{Mass flow in lbm/sec} = (\text{Volts} - 0.11217)/0.13402$$

The equation above was obtained by a least squares fit to the mass flow data provided by NASA Lewis.

B.1.5 - Time Recordings

For each test point the spray duration in seconds was recorded along with the time of the day. Spray times of 2.6 and 4.5 seconds were used corresponding to spray clouds with MVD's of 20 and 16 μm respectively. The actual spray time duration is obtained by adding 0.33 seconds to the spray times shown in the log sheets. This was because the nozzles do not stop spraying immediately after the solenoid valves are closed (see Appendix G of Ref. 10).

DATE APRIL 6, 1969 (THURSDAY)

PBAR _____ PSIA

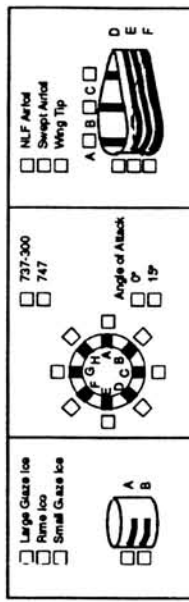
DYE CONCENTRATION 0.00025 GR/MCC

PSYCHROMETER READINGS _____ °F DB

_____ °F WB

RELATIVE HUMIDITY _____ PERCENT

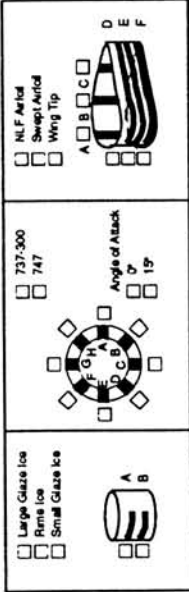
SPRAY UNIFORMITY TEST
 REFERENCE COLLECTOR TEST



| RUN NO | RUN ID | TUNNEL CONDITIONS | | | | | | | SPRAY CONDITIONS / MASS FLOW | | | | | | | | | | REMARKS | | | | |
|--------|---------------------------|-------------------|-----------|-----------------------|--------------------|----------------|-------------------------|------------------------------------|------------------------------|------------------------------------|---------------------|-----------|-----------|-----------|-----------|-----------|------------|---------|---------|------------|-------------|------------------|--|
| | | AIR TEMP (°F) | TAS (MPH) | P ₀ (PSIA) | PRESS TOTAL (PSIA) | DEW POINT (°F) | SUPPLY PRESSURE | | * PLenum PRESSURE | | TRANSDUCER READINGS | | | | | | MASS FLOW | | | TIME (SEC) | | | |
| | | | | | | | P _{AIR} (PSIG) | P _{H₂O} (PSIG) | P _{AIR} (PSIG) | P _{H₂O} (PSIG) | TANK PRES-SURE | NOZZLE #1 | NOZZLE #3 | NOZZLE #4 | NOZZLE #6 | NOZZLE #7 | NOZZLE #11 | (VOLTS) | | (LBS/SEC) | SPRAY (SEC) | SPRAY TIME (SEC) | |
| 1 | UNIFORMITY 1 NOZZLE #1 | 66 | 166 | 13.800 | 14.212 | 33.6 | 0.65 | 65 | 100 | 106 | 106 | 106 | 104 | 104 | 103 | 101 | 100 | | | 2.65 | 10.14P | NOZZLE #1 | ONE NOZZLE AT A TIME, APRIL 6, 1969 (THURSDAY) |
| 2 | UNIFORMITY 2 NOZZLE #2 | 64 | 166 | 13.8 | 14.200 | 33.5 | 0.65 | 65 | 100 | 106 | 106 | 104 | 104 | 103 | 102 | 100 | | | 2.65 | 10.28P | NOZZLE #2 | | |
| 3 | UNIFORMITY 3 NOZZLE #3 | 62 | 166 | 13.798 | 14.212 | 33.1 | 0.65 | 65 | 100 | 106 | 106 | 104 | 104 | 103 | 102 | 100 | | | 2.66 | 10.42P | NOZZLE #3 | | |
| 4 | UNIFORMITY 4 NOZZLE #4 | 60 | 166 | 13.797 | 14.200 | 33.6 | 0.65 | 65 | 100 | 106 | 106 | 104 | 104 | 103 | 102 | 100 | | | 2.66 | 10.55P | NOZZLE #4 | | |
| 5 | UNIFORMITY 5 NOZZLE #5 | 59 | 166 | 13.795 | 14.212 | 34.1 | 0.65 | 65 | 100 | 106 | 106 | 104 | 104 | 103 | 102 | 100 | | | 2.65 | 11.06P | NOZZLE #5 | | |
| 6 | UNIFORMITY 6 NOZZLE #6 | 59 | 166 | 13.791 | 14.200 | 34.4 | 0.65 | 65 | 100 | 106 | 106 | 104 | 104 | 104 | 102 | 100 | | | 2.66 | 11.19P | NOZZLE #6 | | |
| 7 | UNIFORMITY 7 NOZZLE #7 | 58 | 166 | 13.789 | 14.224 | 34.1 | 0.65 | 65 | 100 | 106 | 106 | 104 | 104 | 104 | 102 | 100 | | | 2.65 | 11.23P | NOZZLE #7 | | |
| 8 | UNIFORMITY 8 NOZZLE #8 | 58 | 166 | 13.789 | 14.200 | 34.2 | 0.65 | 65 | 100 | 106 | 106 | 104 | 104 | 104 | 102 | 99 | | | 2.65 | 11.24P | NOZZLE #8 | | |

* PRESSURE GAUGES ON WATER TANK AND NOZZLE AIR REGULATOR

SPRAY UNIFORMITY TEST
REFERENCE COLLECTOR TEST

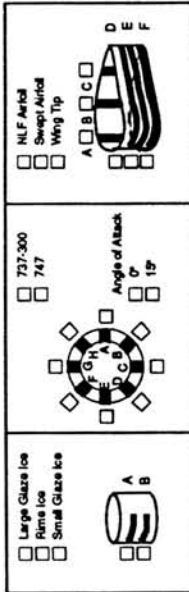


DATE APRIL 7, 1989 (FRIDAY)
 PSIA _____
 DYER CONCENTRATION = 0.00025 GR/MCC
 PSYCHROMETER READINGS = _____ °F DB
 = _____ °F WB
 RELATIVE HUMIDITY = _____ PERCENT

| RUN NO | RUN ID | TUNNEL CONDITIONS | | | | | SPRAY CONDITIONS / MASS FLOW | | | | | | | | | | | REMARKS | | | | | | |
|--------|------------------------------|-------------------|-----------|-------------------------|--------------------|----------------|------------------------------|------------------------------------|------------------------------------|-------------------|------------------------------------|---------------------|-----------|-----------|-----------|-----------|------------|---------|----------------|---------------------|------------------|------------------|---|---|
| | | AIR TEMP (°F) | TAS (MPH) | P _{atm} (PSIA) | PRESS TOTAL (PSIA) | DEW POINT (°F) | SUPPLY PRESSURE | | | * PREMIX PRESSURE | | TRANSDUCER READINGS | | | | | | | | | | | | |
| | | | | | | | PAIR (PSIG) | P _{H₂O} (PSIG) | PAIR / P _{H₂O} | PAIR (PSIG) | P _{H₂O} (PSIG) | NOZZLE #1 | NOZZLE #3 | NOZZLE #4 | NOZZLE #6 | NOZZLE #7 | NOZZLE #11 | | NOZZLE (VOLTS) | MASS FLOW (LBS/SEC) | SPRAY TIME (SEC) | SPRAY TIME (SEC) | | |
| 9 | UNIFORMITY 8A NOZZLE #8 | 61 | 165 | 13.801 | 14.212 | 33.7 | 65 | 100 | 0.65 | 65 | 106 | 107 | 106 | 105 | 105 | 104 | 103 | 101 | | | 2.65 | 1.41P | A REPEAT OF NOZZLE #8, APRIL 7, 1989 (FRIDAY) | |
| 10 | UNIFORMITY 9 NOZZLE #9 | 61 | 165 | 13.797 | 14.212 | 30.0 | 65 | 100 | 0.65 | 65 | 106 | 107 | 106 | 106 | 105 | 103 | 101 | | | | | 2.65 | 1.56P | NOZZLE #9 |
| 11 | UNIFORMITY 10 NOZZLE #10 | 59 | 165 | 13.794 | 14.212 | 31.2 | 65 | 100 | 0.65 | 65 | 106 | 106 | 105 | 104 | 103 | 102 | 100 | | | | | 2.65 | 2.11P | NOZZLE #10 |
| 12 | UNIFORMITY 11 ALL NOZZLES | 58 | 165 | 13.792 | 14.212 | 31.3 | 65 | 100 | 0.65 | 65 | 106 | 109 | 108 | 108 | 107 | 106 | 103 | | | | | 2.66 | 2.22P | ALL NOZZLES |
| 13 | UNIFORMITY 12 ALL NOZZLES | 57 | 165 | 13.776 | 14.200 | 30.5 | 65 | 100 | 0.65 | 65 | 106 | 111 | 110 | 110 | 109 | 108 | 105 | | | | | 2.65 | 4.38P | ALL NOZZLES |
| 14 | UNIFORMITY 13 NOZZLE #11 | 58 | 165 | 13.78 | 14.200 | 27.7 | 65 | 100 | 0.65 | 65 | 106 | 106 | 104 | 104 | 103 | 102 | 99 | | | | | 2.66 | 4.51P | NOZZLE #11 |
| 15 | UNIFORMITY 14 NOZZLE #12 | 57 | 165 | 13.779 | 14.212 | 27.2 | 65 | 100 | 0.65 | 65 | 106 | 106 | 104 | 104 | 104 | 102 | 100 | | | | | 2.64 | 5.13P | NOZZLE #12 |
| 16 | UNIFORMITY 15 NOZZLE #9 | 58 | 165 | 13.778 | 14.200 | 28.2 | 65 | 100 | 0.65 | 65 | 106 | 106 | 104 | 104 | 104 | 102 | 100 | | | | | 2.65 | 5.28P | NOZZLE #9, STOPPED AFTER RUN #18 TO REVIEW DATA |

* PRESSURE GAUGES ON WATER TANK AND NOZZLE AIR REGULATOR

SPRAY UNIFORMITY TEST
 REFERENCE COLLECTOR TEST

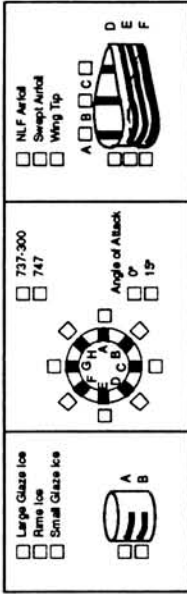


DATE APRIL 7, 1989 (FRIDAY) _____ PSIA
 PBAR _____ PSIA
 DYE CONCENTRATION = 0.00025 GRM/CC
 PSYCHROMETER READINGS _____ ° DB
 _____ ° WB
 RELATIVE HUMIDITY _____ PERCENT

| RUN NO | RUN ID | TUNNEL CONDITIONS | | | | | | | | | | SPRAY CONDITIONS / MASS FLOW | | | | | | | | | | REMARKS | | |
|--------|----------------|-------------------|-----------|-----------------------|--------------------|----------------|-----------------|------------------------------------|---------------------|------------------------------------|---------------------|------------------------------|-----------|-----------|-----------|------------|-----------|-----------|-------------|------------|------|---------|---|--|
| | | AIR TEMP (°F) | TAS (MPH) | P ₀ (PSIA) | PRESS TOTAL (PSIA) | DEW POINT (°F) | SUPPLY PRESSURE | | * BLENDING PRESSURE | | TRANSDUCER READINGS | | | | | | MASS FLOW | | TIME (SEC) | | | | | |
| | | | | | | | PAIR (PSIG) | P _{H₂O} (PSIG) | PAIR (PSIG) | P _{H₂O} (PSIG) | NOZZLE #1 | NOZZLE #3 | NOZZLE #4 | NOZZLE #6 | NOZZLE #7 | NOZZLE #11 | (VOLTS) | (LBS/SEC) | SPRAY (SEC) | SPRAY TIME | | | | |
| 17 | UNIFORMITY 16 | 56 | 165 | 13.779 | 14.188 | 26.0 | 0.65 | 65 | 100 | 65 | 106 | 107 | 106 | 106 | 105 | 106 | 105 | 103 | 101 | | | 2.65 | 6:47P | NOZZLES 1, 11 & 5 DISCONNECTED, APRIL 10, 1989 (MON) |
| 18 | UNIFORMITY 17 | 57 | 165 | 13.715 | 14.200 | 25.4 | 0.65 | 65 | 100 | 65 | 106 | 106 | 105 | 104 | 105 | 104 | 102 | 100 | | | 2.65 | 7:00P | NOZZLES 1, 11, 5 DISCON. REPEAT OF #17 | |
| 19 | UNIFORMITY 18 | 5.4 | 165 | 13.774 | 14.188 | 27.0 | 0.65 | 65 | 100 | 65 | 106 | 106 | 104 | 104 | 104 | 104 | 102 | 99 | | | 2.65 | 8:42P | MOVED NOZZLES #9 & #1 | |
| 20 | UNIFORMITY 19 | 5.4 | 165 | 13.774 | 14.18 | 26.8 | 0.65 | 65 | 100 | 65 | 106 | 107 | 105 | 105 | 104 | 104 | 103 | 100 | | | 2.65 | 8:55P | NOZZLE #1 ONLY AFTER MOVING IT TO NEW POSITION | |
| 21 | UNIFORMITY 20 | 5.4 | 165 | 13.778 | 14.188 | 26.6 | 0.65 | 65 | 100 | 65 | 106 | 105 | 103 | 103 | 102 | 101 | 99 | | | | 2.65 | 9:05P | NOZZLE #9 ONLY AFTER MOVING IT TO NEW POSITION | |
| 22A | UNIFORMITY 21A | 5.1 | 165 | 13.778 | 14.188 | 27.0 | 0.65 | 65 | 100 | 65 | 106 | 107 | 104 | 104 | 104 | 102 | 99 | | | | 2.65 | 10:20P | MOVED NOZZLES 1, 2, 3, 4, 5, 6, 7, 8, 9, 10, 12 | |
| 23 | UNIFORMITY 22 | 5.1 | 165 | 13.782 | 14.188 | 26.7 | 0.65 | 65 | 100 | 65 | 106 | 107 | 104 | 104 | 104 | 102 | 100 | | | | 2.65 | 10:30P | NOZZLE #3 | |
| 24 | UNIFORMITY 23 | 5.4 | 165 | 13.781 | 14.200 | 26.7 | 0.65 | 65 | 100 | 65 | 106 | 107 | 104 | 104 | 104 | 102 | 100 | | | | 2.65 | 10:54P | NOZZLE #4 | |
| 25 | UNIFORMITY 24 | 5.1 | 165 | 13.782 | 14.200 | 26.5 | 0.65 | 65 | 100 | 65 | 106 | 107 | 104 | 104 | 104 | 102 | 100 | | | | 2.65 | 11:05P | NOZZLE #3 | |
| 26 | UNIFORMITY 25 | 5.1 | 165 | 13.785 | 14.200 | 27.1 | 0.65 | 65 | 100 | 65 | 106 | 107 | 104 | 104 | 104 | 102 | 100 | | | | 2.65 | 11:20P | NOZZLES 1, 2, 3, 4, 5, 6, 7, 8, 9, 10, 12 | |

* PRESSURE GAUGES ON WATER TANK AND NOZZLE AIR REGULATOR

SPRAY UNIFORMITY TEST
 REFERENCE COLLECTOR TEST

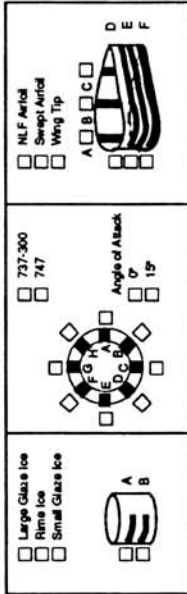


DATE APRIL 10, 1989 (MONDAY)
 P BAR _____ PSIA
 DYE CONCENTRATION = 0.00025 GR/MCC
 PSYCHROMETER READINGS = _____ °F DB
 = _____ °F WB
 RELATIVE HUMIDITY = _____ PERCENT

| RUN NO. | RUN ID | TUNNEL CONDITIONS | | | | | | | | | | SPRAY CONDITIONS / MASS FLOW | | | | | | | | | | REMARKS | | | | | | | | | |
|---------|------------|-------------------|-----------|-----------------------|------------------------|--------------------|----------------|-------------|-------------------------|-------------|-------------------------|------------------------------|-----------|-----------|-----------|-----------|-------------------|------------|---------|-----------|-------------|---------|---------------------|--|--|--|--|-----------|--|------------|--|
| | | AIR | | | | | PRESS | | | | | SUPPLY PRESSURE | | | | | * PLENUM PRESSURE | | | | | | TRANSDUCER READINGS | | | | | MASS FLOW | | TIME (SEC) | |
| | | TEMP (°F) | TAS (MPH) | P ₀ (PSIA) | P ₀₂ (PSIA) | PRESS TOTAL (PSIA) | DEW POINT (°F) | PAIR (PSIG) | P _{H2O} (PSIG) | PAIR (PSIG) | P _{H2O} (PSIG) | TANK PRES-SURE | NOZZLE #1 | NOZZLE #3 | NOZZLE #4 | NOZZLE #6 | NOZZLE #7 | NOZZLE #11 | (VOLTS) | (LBS/SEC) | SPRAY (SEC) | | SPRAY TIME | | | | | | | | |
| 27 | UNIFORMITY | 60 | 165 | 14.000 | 14.431 | 14.431 | 17.1 | 0.65 | 100 | 106 | 107 | 104 | 104 | 104 | 104 | 104 | 103 | | | 2.65 | 11:54 | | | | | | | | | | |
| 28 | UNIFORMITY | 57 | 165 | 13.997 | 14.431 | 14.431 | 16.1 | 0.65 | 100 | 106 | 106 | 104 | 104 | 104 | 104 | 102 | 102 | | | 2.67 | 11:37A | | | | | | | | | | |
| 29 | UNIFORMITY | 55 | 165 | 13.997 | 14.431 | 14.431 | 16.0 | 0.65 | 100 | 106 | 106 | 104 | 104 | 104 | 103 | 102 | 102 | | | 2.65 | 11:48A | | | | | | | | | | |
| 30 | UNIFORMITY | 54 | 165 | 13.999 | 14.431 | 14.431 | 16.1 | 0.65 | 100 | 106 | 107 | 104 | 104 | 104 | 104 | 102 | 102 | | | § | 11:58A | | | | | | | | | | |
| 31 | UNIFORMITY | 53 | 165 | 13.998 | 14.431 | 14.431 | 15.7 | 0.65 | 100 | 106 | 106 | 104 | 104 | 104 | 103 | 102 | 102 | | | § | 12:07P | | | | | | | | | | |
| 32 | UNIFORMITY | 53 | 165 | 13.996 | 14.431 | 14.431 | 15.3 | 0.65 | 100 | 106 | 106 | 104 | 104 | 104 | 103 | 102 | 102 | | | 2.66 | 12:15P | | | | | | | | | | |
| 33 | UNIFORMITY | 52 | 165 | 13.998 | 14.431 | 14.431 | 15.5 | 0.65 | 100 | 106 | 107 | 104 | 104 | 104 | 104 | 101 | 102 | | | 2.66 | 12:25P | | | | | | | | | | |
| 34 | UNIFORMITY | 51 | 165 | 13.994 | 14.431 | 14.431 | 15.3 | 0.65 | 100 | 106 | 107 | 104 | 104 | 104 | 104 | 101 | 102 | | | 2.66 | 12:37P | | | | | | | | | | |
| 35 | UNIFORMITY | 50 | 165 | 13.998 | 14.431 | 14.431 | 16.1 | 0.65 | 100 | 106 | 107 | 104 | 104 | 104 | 104 | 100 | 102 | | | 2.65 | 12:48P | | | | | | | | | | |
| 36 | UNIFORMITY | 50 | 165 | 13.998 | 14.431 | 14.431 | 16.8 | 0.65 | 100 | 106 | 107 | 104 | 104 | 104 | 104 | 101 | 102 | | | 2.67 | 12:59P | | | | | | | | | | |
| 37 | UNIFORMITY | 50 | 165 | 13.998 | 14.431 | 14.431 | 15.9 | 0.65 | 100 | 106 | 107 | 104 | 104 | 104 | 104 | 100 | 102 | | | 2.66 | 1:10P | | | | | | | | | | |
| 38 | UNIFORMITY | 50 | 165 | 13.989 | 14.400 | 14.400 | 16.5 | 0.65 | 100 | 106 | 107 | 104 | 104 | 104 | 104 | 100 | 102 | | | 2.67 | 1:22P | | | | | | | | | | |
| 39 | UNIFORMITY | 49 | 165 | 13.989 | 14.419 | 14.419 | 16.1 | 0.65 | 100 | 106 | 107 | 104 | 104 | 104 | 104 | 102 | 102 | | | 2.66 | 1:35P | | | | | | | | | | |
| 40 | UNIFORMITY | 49 | 165 | 13.981 | 14.407 | 14.407 | 18.5 | 0.65 | 100 | 106 | 107 | 104 | 104 | 104 | 104 | 102 | 102 | | | 2.66 | 6:15P | | | | | | | | | | |
| 41 | UNIFORMITY | 50 | 165 | 13.982 | 14.407 | 14.407 | 17.9 | 0.65 | 100 | 106 | 107 | 104 | 104 | 105 | 104 | 102 | 103 | | | 2.66 | 6:34P | | | | | | | | | | |
| 42 | UNIFORMITY | 49 | 165 | 13.975 | 14.407 | 14.407 | 17.5 | 0.65 | 100 | 106 | 105 | 102 | 102 | 102 | 100 | 100 | 100 | | | 2.65 | 6:49P | | | | | | | | | | |
| 43 | UNIFORMITY | 49 | 165 | -13.975 | 14.407 | 14.407 | 17.4 | 0.65 | 100 | 106 | 105 | 103 | 102 | 103 | 100 | 101 | 101 | | | 2.00 | 7:04P | | | | | | | | | | |
| 44 | UNIFORMITY | 48 | 165 | 13.973 | 14.407 | 14.407 | 18.2 | 0.60 | 80 | 106 | 107 | 104 | 104 | 104 | 104 | 102 | 102 | | | 2.65 | 7:16P | | | | | | | | | | |
| 45 | UNIFORMITY | 46 | 165 | 13.975 | 14.407 | 14.407 | 16.9 | 0.80 | 80 | 106 | 106 | 103 | 103 | 103 | 101 | 101 | 101 | | | 2.65 | 8:05P | | | | | | | | | | |

* PRESSURE GAUGES ON WATER TANK AND NOZZLE AIR REGULATOR

SPRAY UNIFORMITY TEST
 REFERENCE COLLECTOR TEST



DATE APRIL 11, 1988 (TUESDAY)
 PSIA _____
 PBAR _____
 DYE CONCENTRATION 0.0025 GR/MCC
 PSYCHROMETER READINGS _____ °F DB
 _____ °F WB
 RELATIVE HUMIDITY _____ PERCENT

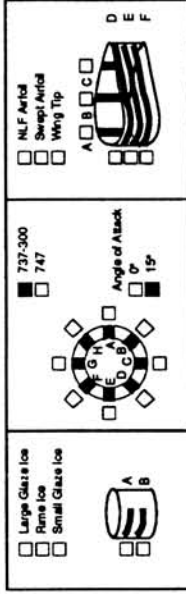
| RUN NO. | RUN ID. | TUNNEL CONDITIONS | | | | | SPRAY CONDITIONS / MASS FLOW | | | | | | | | | | REMARKS | | | | | | | | |
|---------|------------|-------------------|-----------|---------------------------|--------------------|----------------|------------------------------|------------------|-----------------|------------------|---------------------|------------------|----------------|-----------|-----------|-----------|-----------|------------|------------|---------|-------------|------------|------------|--|--|
| | | AIR TEMP (°F) | TAS (MPH) | P _{total} (PSIA) | PRESS TOTAL (PSIA) | DEW POINT (°F) | SUPPLY PRESSURE | | PLENUM PRESSURE | | TRANSDUCER READINGS | | | | | MASS FLOW | | TIME (SEC) | | | | | | | |
| | | | | | | | PAIR | P _{H2O} | PAIR | P _{H2O} | PAIR | P _{H2O} | TANK PRES-SURE | NOZZLE #1 | NOZZLE #3 | NOZZLE #4 | NOZZLE #6 | NOZZLE #7 | NOZZLE #11 | (VOLTS) | (LBS) (SEC) | SPRAY TIME | SPRAY TIME | | |
| 50 | UNIFORMITY | 58 | 165 | 13.802 | 14.392 | 25.8 | 0.65 | 100 | 65 | 106 | 65 | 106 | 108 | 105 | 105 | 106 | 105 | 106 | 106 | 61 | | | 2.66 | 7:15P | FULL STRIPS PLACED ALONG COLUMNS - ALL 12 NOZ. |
| 51 | UNIFORMITY | 57 | 165 | 13.800 | 14.382 | 21.8 | 0.65 | 100 | 65 | 106 | 65 | 106 | 106 | 103 | 103 | 104 | 102 | 101 | 61 | | | § | 7:35P | FULL STRIPS PLACED ALONG COLUMNS - ALL 12 NOZ. | |
| 52 | UNIFORMITY | 57 | 165 | 13.800 | 14.382 | 21.4 | 0.65 | 100 | 65 | 106 | 65 | 106 | 106 | 103 | 103 | 104 | 103 | 101 | 61 | | | 2.67 | 7:51P | FULL STRIPS PLACED ALONG COLUMNS - ALL 12 NOZ. | |
| 53 | UNIFORMITY | 57 | 165 | 13.807 | 14.382 | 21.3 | 0.80 | 80 | 80 | 106 | 80 | 106 | 106 | 103 | 103 | 104 | 102 | 101 | 7.4 | | | 2.67§ | 8:08P | FULL STRIPS PLACED ALONG COLUMNS - ALL 12 NOZ. | |
| 54 | UNIFORMITY | 56 | 165 | 13.806 | 14.382 | 21.5 | 0.80 | 80 | 80 | 106 | 80 | 106 | 106 | 103 | 103 | 104 | 103 | 101 | 7.4 | | | 3.16 | 8:25P | FULL STRIPS PLACED ALONG COLUMNS - ALL 12 NOZ. | |
| 55 | UNIFORMITY | 56 | 165 | 13.805 | 14.382 | 22.1 | 0.80 | 80 | 80 | 106 | 80 | 106 | 106 | 103 | 103 | 104 | 103 | 101 | 7.3 | | | 3.16 | 8:41P | FULL STRIPS PLACED ALONG COLUMNS - ALL 12 NOZ. | |
| 56 | UNIFORMITY | 55 | 165 | 13.802 | 14.395 | 23.1 | 0.80 | 80 | 80 | 106 | 80 | 106 | 106 | 103 | 103 | 104 | 103 | 101 | 7.4 | | | 3.15 | 9:00P | FULL STRIPS PLACED ALONG ROWS - ALL 12 NOZ. | |
| 57 | UNIFORMITY | 54 | 165 | 13.831 | 14.382 | 22.5 | 0.80 | 80 | 80 | 106 | 80 | 106 | 106 | 103 | 103 | 104 | 103 | 101 | 7.4 | | | 3.16 | 9:17P | FULL STRIPS PLACED ALONG ROWS - ALL 12 NOZ. | |
| 58 | UNIFORMITY | 53 | 165 | 13.834 | 14.382 | 22.5 | 0.65 | 65 | 65 | 106 | 65 | 106 | 106 | 103 | 103 | 104 | 103 | 101 | 60 | | | 2.65 | 9:33P | FULL STRIPS PLACED ALONG ROWS - ALL 12 NOZ. | |
| 59 | UNIFORMITY | 53 | 165 | 13.805 | 14.395 | 22.6 | 0.65 | 65 | 65 | 106 | 65 | 106 | 106 | 103 | 103 | 104 | 103 | 101 | 60 | | | 2.65 | 9:48P | FULL STRIPS PLACED ALONG ROWS - ALL 12 NOZ. | |

§ DISPLAY NOT WORKING

* PRESSURE GAUGES ON WATER TANK AND NOZZLE AIR REGULATOR

DATE APRIL 13, 1988 (THURSDAY)
 PBAR _____ PSIA
 DYE CONCENTRATION 0.0002 GRMCC
 PSYCHROMETER READINGS _____ °F DB
 _____ °F WB
 RELATIVE HUMIDITY _____ PERCENT

SPRAY UNIFORMITY TEST
 REFERENCE COLLECTOR TEST

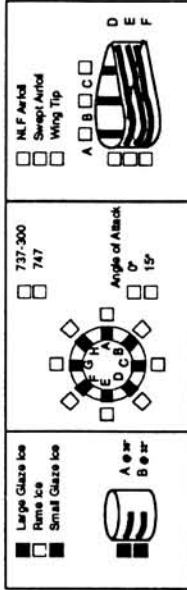


| RUN NO. | RUN ID | TUNNEL CONDITIONS | | | | | | | | | | SPRAY CONDITIONS / MASS FLOW | | | | | | | | | | REMARKS | | | |
|---------|--------|-------------------|-----------|-------------------------|--------------------|----------------|-------------|------------------------------------|-------------|------------------------------------|-------------------|------------------------------|-----|-----|-----|-----|-----|-----|-----|------|-------------|------------|-------|--------------------------|--|
| | | AIR TEMP (°F) | TAS (MPH) | P _{tot} (PSIA) | PRESS TOTAL (PSIA) | Dew POINT (°F) | PAIR (PSIG) | P _{H₂O} (PSIG) | PAIR (PSIG) | P _{H₂O} (PSIG) | FLUENIUM PRESSURE | TRANSDUCER READINGS | | | | | | | | | | | | | |
| | | | | | | | | | | | MASS FLOW | | | | | | | | | | TIME (SEC) | | | | |
| | | | | | | | | | | | | | | | | | | | | | SPRAY (SEC) | SPRAY TIME | | | |
| 65 | 737-15 | 60 | 165 | 13.970 | 14.407 | 26.2 | 0.80 | 80 | 100 | 80 | 106 | 80 | 106 | 106 | 104 | 104 | 105 | 104 | 102 | 77 | 2.18 | 17.20 | 3.20 | 2.05P | SPRAYTIME NOT SUFFICIENT FOR GOOD TRACE |
| 66 | 737-15 | 60 | 165 | 13.973 | 14.407 | 27.5 | 0.80 | 80 | 100 | 80 | 106 | 80 | 106 | 106 | 104 | 104 | 105 | 104 | 102 | 77 | 2.17 | 17.20 | 4.14 | 2.25P | SPRAYTIME NOT SUFFICIENT |
| 67 | 737-15 | 60 | 165 | 13.975 | 14.407 | 26.7 | 0.80 | 80 | 100 | 80 | 106 | 80 | 106 | 107 | 105 | 106 | 104 | 103 | 75 | 2.20 | 17.20 | 7.14 | 2.45P | SPRAYTIME NOT SUFFICIENT | |
| 68 | 737-15 | 60 | 165 | 13.976 | 14.407 | 27.2 | 0.80 | 80 | 100 | 80 | 106 | 80 | 106 | 107 | 105 | 106 | 104 | 103 | 74 | 2.17 | 17.20 | 9.73 | 3.06P |) | |
| 69 | 737-15 | 58 | 165 | 13.976 | 14.407 | 26.2 | 0.80 | 80 | 100 | 80 | 106 | 80 | 106 | 107 | 105 | 106 | 104 | 103 | 74 | 2.19 | 17.20 | 9.73 | 3.42P |) | |
| 70 | 737-15 | 60 | 165 | 13.975 | 14.407 | 25.6 | 0.80 | 80 | 100 | 80 | 106 | 80 | 106 | 107 | 115 | 106 | 104 | 103 | 74 | 2.16 | 17.20 | 9.72 | 4.05P |) 4 REPEATS | |
| 71 | 737-15 | 59 | 165 | 13.975 | 14.407 | 24.7 | 0.80 | 80 | 100 | 80 | 106 | 80 | 106 | 107 | 120 | 106 | 104 | 103 | 73 | 2.17 | 17.20 | 9.72 | 4.28P |) | |
| 83 | 737-15 | 67 | 165 | 13.847 | 14.249 | 28.3 | 0.65 | 65 | 100 | 65 | 106 | 65 | 106 | 106 | 104 | 103 | 106 | 104 | 103 | 60 | 2.88 | 22.94 | 2.87 | 7.45P | CHANGED INLET AND TOOK SOME MEASUREMENTS |
| 84 | 737-15 | 68 | 165 | 13.827 | 14.249 | 29.0 | 0.80 | 80 | 100 | 80 | 106 | 80 | 106 | 107 | 100 | 106 | 104 | 103 | 74 | 2.21 | 17.20 | 9.70 | 8.02P |) | |

* PRESSURE GAUGES ON WATER TANK AND NOZZLE AIR REGULATOR

☐ SPRAY UNIFORMITY TEST
 ■ REFERENCE COLLECTOR TEST

DATE APRIL 18, 1989 (TUESDAY)
 PBAR _____ PSIA
 DYE CONCENTRATION = 0.0002 GRMCC
 PSYCHROMETER READINGS = _____ °F DB
 = _____ °F WB
 RELATIVE HUMIDITY = _____ PERCENT

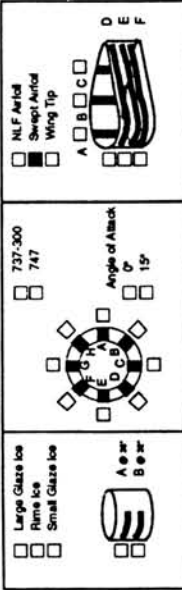


| RUN NO | RUN ID | TUNNEL CONDITIONS | | | | | SPRAY CONDITIONS / MASS FLOW | | | | | | | | | | | | REMARKS | | | | | | | |
|--------|---------------|-------------------|-----------|------------------------|--------------------|----------------|------------------------------|------------------------------------|-------------------------|------------------------------------|-------------------------|------------------------------------|---------------------|-----------|-----------|-----------|-----------|------------|---------|-----------|-----------|-------------|------------|--|---|---------------------------|
| | | AIR TEMP (°F) | TAS (MPH) | P _{st} (PSIA) | PRESS TOTAL (PSIA) | DEW POINT (°F) | SUPPLY PRESSURE | | | * PLENUM PRESSURE | | | TRANSDUCER READINGS | | | | | | | MASS FLOW | | TIME (SEC) | | | | |
| | | | | | | | P _{air} (PSIG) | P _{H₂O} (PSIG) | P _{air} (PSIG) | P _{H₂O} (PSIG) | P _{air} (PSIG) | P _{H₂O} (PSIG) | NOZZLE #1 | NOZZLE #3 | NOZZLE #4 | NOZZLE #6 | NOZZLE #7 | NOZZLE #11 | | (VOLTS) | (LBS/SEC) | SPRAY (SEC) | SPRAY TIME | | | |
| 111 | COLLECTOR α=0 | 57 | 165 | 13.904 | 14.309 | 35 | 0.65 | 65 | 100 | 65 | 106 | 65 | 106 | 104 | 105 | 103 | 102 | 60 | | | 2.66 | 2.42P | | | SPRAYED TUNNEL WALLS WITH WATER HOSE TO INCREASE HUMIDITY. MIDDLE BLADE TOP AND BOTTOM NOT MARKED | |
| 112 | COLLECTOR α=0 | 56 | 165 | 13.908 | 14.322 | 33 | 0.65 | 65 | 100 | 65 | 106 | 65 | 106 | 104 | 105 | 104 | 102 | 60 | | | 2.66 | 2.54P | | | | |
| 113 | COLLECTOR α=0 | 56 | 165 | 13.918 | 14.322 | 33 | 0.65 | 65 | 100 | 65 | 106 | 65 | 106 | 104 | 105 | 104 | 102 | 60 | | | 2.66 | 3.04P | | | | |
| 114 | COLLECTOR α=0 | 55 | 165 | 13.911 | 14.322 | 32.3 | 0.65 | 65 | 100 | 65 | 106 | 65 | 106 | 104 | 105 | 104 | 102 | 60 | | | 2.66 | 3.14P | | | | |
| 115 | COLLECTOR α=0 | 55 | 165 | 13.911 | 14.322 | 32.3 | 0.65 | 65 | 100 | 65 | 106 | 65 | 106 | 104 | 105 | 104 | 102 | 59 | | | 2.65 | 3.24P | | | | |
| 116 | LARGE GLAZE | 50 | 165 | 13.877 | 14.285 | 32.7 | 0.65 | 65 | 100 | 65 | 106 | 65 | 107 | 145 | 105 | 104 | 103 | 59 | | | 2.64 | 5.18P | | | INSTALLED ICE SHAPE | |
| 117 | SMALL GLAZE | 50 | 165 | 13.876 | 14.287 | 34 | 0.65 | 65 | 100 | 65 | 106 | 65 | 106 | 144 | 103 | 104 | 103 | 101 | 59 | | | 2.64 | 5.28P | | | |
| 118 | LARGE GLAZE | 52 | 165 | 13.874 | 14.297 | 33.6 | 0.65 | 65 | 100 | 65 | 106 | 65 | 106 | 144 | 103 | 104 | 103 | 101 | 59 | | | 2.66 | 5.37P | | | |
| 119 | SMALL GLAZE | 52 | 165 | 13.872 | 14.297 | 33.3 | 0.65 | 65 | 100 | 65 | 106 | 65 | 106 | 141 | 103 | 104 | 103 | 101 | 59 | | | 2.65 | 5.47P | | | |
| 120 | LARGE GLAZE | 52 | 165 | 13.878 | 14.297 | 33.2 | 0.65 | 65 | 100 | 65 | 106 | 65 | 106 | 138 | 103 | 104 | 103 | 101 | 59 | | | 2.65 | 5.58P | | | ICE SHAPE WAS UPSIDE DOWN |

* PRESSURE GAUGES ON WATER TANK AND NOZZLE AIR REGULATOR

DATE APRIL 19 1989 (WEDNESDAY)
 P BAR _____ PSIA _____
 DYE CONCENTRATION - 0.0002 GR/MCC
 PSYCHROMETER READINGS - _____ °F DB
 - _____ °F WB
 RELATIVE HUMIDITY - _____ PERCENT

SPRAY UNIFORMITY TEST
 REFERENCE COLLECTOR TEST

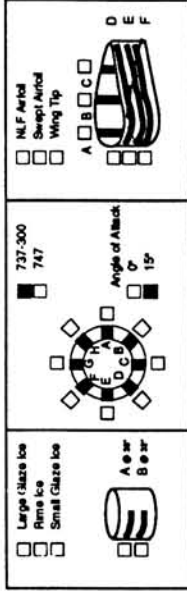


| RUN NO | RUN ID | TUNNEL CONDITIONS | | | | | | | | | | SPRAY CONDITIONS / MASS FLOW | | | | | | | | | | REMARKS | | | | | | | |
|--------|----------------|-------------------|-----------|------------------------|-------------------------|----------------|-------------------------|------------------------------------|-------------------------|------------------------------------|----------------|------------------------------|-----------|-----------|-----------|-----------|------------------|----------------|------------|-------------|------------|---------|---------------------|--|--|--|--|------------|--|
| | | AIR | | | | | PRESS | | | | | SUPPLY PRESSURE | | | | | * PLDMM PRESSURE | | | | | | TRANSDUCER READINGS | | | | | TIME (SEC) | |
| | | TEMP (°F) | TAS (MPH) | P _{st} (PSIA) | P _{tot} (PSIA) | DEW POINT (°F) | P _{air} (PSIG) | P _{H₂O} (PSIG) | P _{air} (PSIG) | P _{H₂O} (PSIG) | TANK PRES-SURE | NOZZLE #1 | NOZZLE #3 | NOZZLE #4 | NOZZLE #6 | NOZZLE #7 | NOZZLE #11 | NOZZLE (VOLTS) | ABSS (SEC) | SPRAY (SEC) | SPRAY TIME | | | | | | | | |
| 148 | SWEPT WING α=0 | 4.5 | 166 | 13.901 | 14.322 | 20.8 | 0.80 | 80 | 100 | 100 | 80 | 106 | 107 | 126 | 105 | 106 | 104 | 103 | 72 | | | 4.50 | 6.33 | | | | | | |
| 149 | SWEPT WING α=0 | 4.9 | 166 | 13.868 | 14.309 | 18.7 | 0.65 | 65 | 100 | 100 | 65 | 106 | 106 | 126 | 103 | 104 | 103 | 101 | 60 | | | 2.65 | 6.49 | | | | | | |
| 150 | SWEPT WING α=0 | 4.5 | 166 | 13.900 | 14.322 | 21.8 | 0.65 | 65 | 100 | 100 | 65 | 106 | 106 | 128 | 103 | 104 | 103 | 101 | 58 | | | 2.64 | 6.59 | | | | | | |
| 151 | SWEPT WING α=0 | 4.5 | 166 | 13.900 | 14.309 | 21.1 | 0.65 | 65 | 100 | 100 | 65 | 106 | 106 | 128 | 103 | 104 | 103 | 101 | 60 | | | 2.65 | 7.09 | | | | | | |
| 152 | SWEPT WING α=0 | 4.7 | 166 | 13.897 | 14.309 | 24.3 | 0.65 | 65 | 100 | 100 | 65 | 106 | 106 | 127 | 103 | 104 | 103 | 101 | 59 | | | 2.65 | 7.18 | | | | | | |
| 153 | SWEPT WING α=0 | 5.1 | 166 | 13.899 | 14.322 | 31.5 | 0.65 | 65 | 100 | 100 | 65 | 106 | 106 | 127 | 103 | 104 | 103 | 101 | 59 | | | 2.65 | 7.28 | | | | | | |
| 154 | SWEPT WING α=0 | 4.8 | 166 | 13.899 | 14.322 | 20.4 | 0.80 | 80 | 100 | 100 | 80 | 106 | 106 | 126 | 103 | 104 | 103 | 101 | 73 | | | 4.54 | 7.40 | | | | | | |
| 155 | SWEPT WING α=0 | 4.6 | 166 | 13.901 | 14.309 | 27.5 | 0.80 | 80 | 100 | 100 | 80 | 106 | 106 | 126 | 103 | 104 | 103 | 101 | 72 | | | 4.55 | 7.50 | | | | | | |
| 156 | SWEPT WING α=0 | 4.6 | 166 | 13.898 | 14.309 | 22.0 | 0.80 | 80 | 100 | 100 | 80 | 106 | 106 | 126 | 103 | 104 | 103 | 101 | 72 | | | 4.55 | 7.59 | | | | | | |
| 157 | SWEPT WING α=0 | 4.7 | 166 | 13.903 | 14.322 | 25.1 | 0.80 | 80 | 100 | 100 | 80 | 106 | 106 | 127 | 103 | 104 | 103 | 101 | 72 | | | 4.55 | 8.07 | | | | | | |

* PRESSURE GAUGES ON WATER TANK AND NOZZLE AIR REGULATOR

SPRAY UNIFORMITY TEST
 REFERENCE COLLECTOR TEST

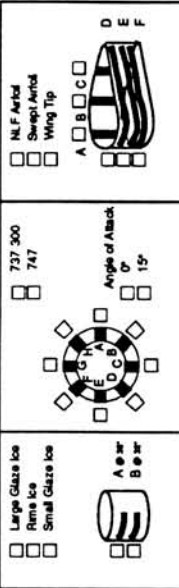
DATE APRIL 20 1989 (THURSDAY)
 PBAR = 14.507 PSIA
 DYE CONCENTRATION = 0.0002 GR/MCC
 PSYCHROMETER READINGS = ° DB
 = ° WB
 RELATIVE HUMIDITY = PERCENT



| RUN NO | RUN ID | TUNNEL CONDITIONS | | | | | | | | | | SPRAY CONDITIONS / MASS FLOW | | | | | | | | | | REMARKS |
|--------|-----------|-------------------|-----------|-------------------------|--------------------|----------------|-------------------------|------------------------------------|-------------------------|------------------------------------|---------------------|------------------------------|-----------|-----------|-----------|-----------|------------|----------------|---------------------|------------------|------------------|-------------------------|
| | | AIR TEMP (°F) | TAS (MPH) | P _{tot} (PSIA) | PRESS TOTAL (PSIA) | DEW POINT (°F) | P _{air} (PSIG) | P _{H₂O} (PSIG) | * PLENUM PRESSURE | | TRANSDUCER READINGS | | | | | | | | | | | |
| | | | | | | | | | P _{air} (PSIG) | P _{H₂O} (PSIG) | TANK PRES-SURE | NOZZLE #1 | NOZZLE #3 | NOZZLE #4 | NOZZLE #6 | NOZZLE #7 | NOZZLE #11 | NOZZLE (VOLTS) | MASS FLOW (LBS/SEC) | SPRAY TIME (SEC) | SPRAY TIME (SEC) | |
| 168 | 737 aa-15 | 4.5 | 171 | 13.821 | 14.297 | 8.1 | 80 | 100 | 80 | 106-7 | 106 | 132 | 103 | 104 | 103 | 101 | 72 | 2.42 | 17.2 | 4.51 | 6.15 | HIGHLIGHTS NOT MARKED |
| 169 | 737 aa-15 | 4.6 | 171 | 13.826 | 14.297 | 8.6 | 80 | 100 | 80 | 106-7 | 106 | 132 | 103 | 104 | 103 | 101 | 72 | 2.42 | 17.2 | 4.51 | 6.31 | |
| 170 | 737 aa-15 | 4.5 | 171 | 13.821 | 14.285 | 14.3 | 80 | 100 | 80 | 106-7 | 106 | 135 | 103 | 104 | 103 | 101 | 72 | 2.42 | 17.2 | 4.51 | 6.47 | |
| 171 | 737 aa-15 | 4.7 | 171 | 13.828 | 14.285 | 21.8 | 80 | 100 | 80 | 106-7 | 106 | 136 | 103 | 104 | 102 | 101 | 72 | 2.42 | 17.2 | 4.51 | 6.58 | |
| 172 | 737 aa-15 | 4.4 | 171 | 13.823 | 14.297 | 17.2 | 80 | 100 | 80 | 106-7 | 106 | 136 | 103 | 104 | 102 | 101 | 72 | 2.42 | 17.2 | 4.51 | 7.12 | |
| 173 | 737 aa-15 | 4.6 | 171 | 13.821 | 14.285 | 21.8 | 80 | 100 | 80 | 106-7 | 106 | 136 | 103 | 104 | 103 | 101 | 72 | 2.44 | 17.2 | 4.51 | 7.25 | |
| 174 | 737 aa-15 | 4.5 | 171 | 13.815 | 14.285 | 20.7 | 65 | 100 | 65 | 106-7 | 106 | 138 | 103 | 104 | 102 | 101 | 60 | 3.89 | 22.96 | 2.67 | 7.38 | |
| 175 | 737 aa-15 | 4.3 | 171 | 13.816 | 11.285 | 16.3 | 65 | 100 | 65 | 106-7 | 106 | 137 | 102 | 104 | 102 | 101 | 60 | 3.22 | 22.96 | 2.67 | 7.52 | |
| 176 | 737 aa-15 | 4.7 | 171 | 13.821 | 14.285 | 23.7 | 65 | 100 | 65 | 106-7 | 106 | 137 | 102 | 104 | 102 | 101 | 60 | 3.19 | 22.96 | 2.66 | 8.04 | |
| 177 | 737 aa-0 | 4.4 | 173 | 13.830 | 11.297 | 10.1 | 65 | 100 | 65 | 106-7 | 106 | 134 | 103 | 104 | 103 | 101 | 60 | 3.20 | 22.96 | 2.66 | 8.27 | CHANGED ANGLE OF ATTACK |

* PRESSURE GAUGES ON WATER TANK AND NOZZLE AIR REGULATOR

SPRAY UNIFORMITY TEST
REFERENCE COLLECTOR TEST

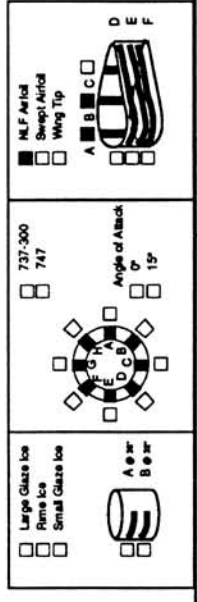


DATE APRIL 21 1989 (EVIDENT)
 P BAR 14.375 PSIA
 DYE CONCENTRATION 0.0002 GRMCC
 PSYCHROMETER READINGS °F DB
 °F WB
 RELATIVE HUMIDITY PERCENT

| RUN NO | RUN ID | TUNNEL CONDITIONS | | | | | | | | | | SPRAY CONDITIONS / MASS FLOW | | | | | | | | | | REMARKS | |
|--------|-------------|-------------------|--------------------------|-------------|--------------------------|-------------|--------------------------|----------------|-----------|-----------|-----------|------------------------------|-----------|------------|----------------|-----------------------|------------------|------------------|--|--|------|---------|----------------------|
| | | SUPPLY PRESSURE | | | | | * PLENUM PRESSURE | | | | | TRANSDUCER READINGS | | | | | | | | | | | |
| | | PAIR (PSIG) | PH ₂ O (PSIG) | PAIR (PSIG) | PH ₂ O (PSIG) | PAIR (PSIG) | PH ₂ O (PSIG) | TANK PRES-SURE | NOZZLE #1 | NOZZLE #3 | NOZZLE #4 | NOZZLE #6 | NOZZLE #7 | NOZZLE #11 | NOZZLE (VOLTS) | MASS FLOW (LBS) (SEC) | SPRAY TIME (SEC) | SPRAY TIME (SEC) | | | | | |
| 181 | UNIFORMITY | 87 | 165 | 13.872 | 14.322 | 33.1 | 0.80 | 80 | 100 | 80 | 106 | 106 | 83 | 104 | 106 | 103 | 102 | 73 | | | 4.52 | 6.22P | |
| 182 | UNIFORMITY | | 165 | 13.857 | 14.322 | 21.3 | 0.65 | 65 | 100 | 65 | 106 | 106 | 96 | 104 | 103 | 104 | 102 | 60 | | | 2.65 | 6.37P | PHOTO FILM 7 PHOTO 2 |
| 183 | UNIFORMITY | | 80 | 14.274 | 14.322 | 9.8 | 0.65 | 65 | 100 | 65 | 106 | 106 | 103 | 104 | 103 | 101 | - | 60 | | | 2.64 | 7.02P | MARLINS SPECIAL |
| 184 | CALIBRATION | | 165 | 13.867 | 14.322 | 16.4 | 0.65 | 65 | 100 | 65 | 106 | 106 | 103 | 103 | 105 | 103 | 102 | 59 | | | 2.65 | 7.18P | |
| 185 | CALIBRATION | | 165 | 13.871 | - | 18.4 | 0.65 | 65 | 100 | 65 | 106 | 106 | 108 | 103 | 104 | 103 | 101 | 60 | | | 1.01 | 7.30P | |
| 186 | CALIBRATION | | 165 | 13.878 | - | 21.3 | 0.65 | 65 | 100 | 65 | 106 | 106 | 108 | 103 | 104 | 103 | 101 | 60 | | | 0.52 | 7.40P | |
| 187 | CALIBRATION | | 165 | 13.867 | - | 23.8 | 0.65 | 65 | 100 | 65 | 106 | 106 | 108 | 103 | 104 | 103 | 101 | 60 | | | 1.51 | 7.48P | |
| 188 | CALIBRATION | | 165 | 13.876 | - | 24.4 | 0.65 | 65 | 100 | 65 | 106 | 106 | 110 | 103 | 104 | 103 | 101 | 60 | | | 2.01 | 7.57P | |
| 189 | CALIBRATION | | 165 | 13.875 | - | 23.9 | 0.65 | 65 | 100 | 65 | 106 | 106 | 114 | 103 | 104 | 103 | 101 | 60 | | | 2.51 | 8.06P | |
| 190 | CALIBRATION | | 165 | 13.878 | 14.220 | 16.0 | 0.65 | 65 | 100 | 65 | 106 | 106 | 118 | 103 | 104 | 103 | 101 | 60 | | | 3.00 | 8.19P | |
| 191 | CALIBRATION | | 165 | 13.862 | - | 20.0 | 0.65 | 65 | 100 | 65 | 106 | 106 | 114 | 103 | 104 | 103 | 101 | 60 | | | 3.52 | 8.26P | |
| 192 | CALIBRATION | | 165 | 13.865 | - | 22.0 | 0.65 | 65 | 100 | 65 | 106 | 106 | 117 | 103 | 104 | 103 | 101 | 60 | | | 4.00 | 8.33P | |

* PRESSURE GAUGES ON WATER TANK AND NOZZLE AIR REGULATOR

SPRAY UNIFORMITY TEST
 REFERENCE COLLECTOR TEST



DATE APRIL 25, 1988 (TUESDAY)
 P BAR = 14.285 PSIA
 DYE CONCENTRATION = 0.0002 GR/MCC
 PSYCHROMETER READINGS = °F DB
 = °F WB
 RELATIVE HUMIDITY = PERCENT

| RUN NO | RUN ID | TUNNEL CONDITIONS | | | | | | | | | | SPRAY CONDITIONS / MASS FLOW | | | | | | | | | | REMARKS |
|--------|-----------|-------------------|-----------|-------------------------|--------------------|----------------|-----------------|------------------------------------|-----------------|------------------------------------|---------------------|------------------------------|-----------|-----------|-----------|-----------|------------|----------------|---------------------|-------------------|------------------|--|
| | | AIR TEMP (°F) | TAS (MPH) | P _{tot} (PSIA) | PRESS TOTAL (PSIA) | DEW POINT (°F) | SUPPLY PRESSURE | | PLENUM PRESSURE | | TRANSDUCER READINGS | | | | | | | | | | | |
| | | | | | | | PAIR (PSIG) | P _{H₂O} (PSIG) | PAIR (PSIG) | P _{H₂O} (PSIG) | TANK PRES-SURE | NOZZLE #1 | NOZZLE #3 | NOZZLE #4 | NOZZLE #6 | NOZZLE #7 | NOZZLE #11 | NOZZLE (VOLTS) | MASS FLOW (LBS/SEC) | SPRAY TIME (SEC.) | SPRAY TIME (SEC) | |
| 215 | NLF 000-8 | 4.9 | 165 | 13.801 | 14.188 | 34.3 | 0.65 | 100 | 65 | 106 | 106 | 120 | 104 | 105 | 104 | 102 | 60 | | | 2.67 | 4.52P | |
| 216 | NLF 000-8 | 4.5 | 165 | 13.797 | 14.188 | 32.8 | 0.65 | 100 | 65 | 106 | 106 | 122 | 104 | 105 | 104 | 102 | 60 | | | 2.67 | 5.02P | |
| 217 | NLF 000-8 | 3.7 | 80 | 13.797 | 14.188 | 21.5 | 0.65 | 100 | 65 | 106 | 106 | 121 | 103 | 104 | 103 | 101 | 58 | | | 2.66 | 5.21P | |
| 218 | NLF 000-8 | 4.0 | 165 | 13.797 | 14.188 | 17.5 | 0.65 | 100 | 65 | 106 | 106 | 117 | 103 | 104 | 103 | 101 | 58 | | | 2.67 | 5.29P | |
| 219 | NLF 000-8 | 4.3 | 165 | 13.800 | 14.188 | 19.5 | 0.65 | 100 | 65 | 106 | 106 | 112 | 103 | 104 | 103 | 101 | 58 | | | 2.67 | 5.39P | |
| 220 | NLF 000-0 | 3.9 | 165 | 13.760 | 14.188 | 19.1 | 0.65 | 100 | 65 | 106 | 105 | 104 | 102 | 103 | 102 | 100 | 58 | | | 2.67 | 5.51P | |
| 221 | NLF 000-0 | 4.0 | 165 | 13.784 | 14.188 | 17.4 | 0.65 | 100 | 65 | 106 | 105 | 95 | 102 | 103 | 102 | 100 | 58 | | | 2.67 | 5.59P | |
| 222 | NLF 000-0 | 3.4 | 165 | 13.782 | 14.188 | 17.3 | 0.65 | 100 | 65 | 106 | 105 | 86 | 101 | 103 | 102 | 100 | 60 | | | 2.66 | 6.15P | STRIP LOOKS DIFFERENT THAN 220 AND 221 |
| 223 | NLF 000-0 | 3.9 | 165 | 13.784 | 14.188 | 15.9 | 0.65 | 100 | 65 | 106 | 105 | 85 | 102 | 103 | 102 | 100 | 59 | | | 2.66 | 6.23P | |
| 224 | NLF 000-0 | 4.3 | 165 | 13.787 | 14.200 | 16.8 | 0.65 | 100 | 65 | 106 | 104 | 86 | 101 | 103 | 101 | 100 | 59 | | | 2.66 | 6.32P | |

* PRESSURE GAUGES ON WATER TANK AND NOZZLE AIR REGULATOR

APPENDIX C - NOMENCLATURE

| | |
|-----------------------------|---|
| A_f | front area of a body, projected parallel to freestream velocity direction |
| A_{inlet} | area of inlet |
| $A_{\infty,m}$ | area, perpendicular to freestream direction, defined by tangent trajectories |
| c | chord length |
| C_D | droplet drag coefficient |
| C_{Dinc} | incompressible sphere drag coefficient |
| C | dye concentration |
| d | droplet diameter |
| d_i | droplet diameter, group i |
| dA_s | infinitesimal impingement area on body surface, Figure 2.2 |
| dA_{∞} | infinitesimal freestream area corresponding to dA_s , Figure 2.2 |
| \bar{E} | total impingement efficiency in clouds of nonuniform droplet size |
| $He - Ne$ | Helium - Neon gas-type laser |
| IRT | Icing Research Tunnel |
| $\bar{i}, \bar{j}, \bar{k}$ | unit vectors \parallel to x, y, z axis |
| K | inertia parameter, Equation (2-1) |
| $K_{0,mvd}$ | modified inertia parameter based on mean volumetric diameter, $\lambda K/\lambda_s$, dimensionless |
| L | characteristic dimension of body |
| LWC_s | liquid water content at body surface |
| LWC_{∞} | liquid water content of droplet cloud at freestream |
| M | Mach number of air flow relative to droplet |
| MVD | Mean Volumetric Diameter of the droplet cloud |
| N | number of droplet groups available in a discrete droplet distribution |
| $n(x)$ | number of droplets for droplet diameter x (or d) |
| \bar{n}_s | unit normal vector at body surface (pointing outward) |
| \bar{n}_{∞} | unit vector parallel to \bar{V}_{∞} |
| P_{AIR} | spray system air pressure |
| P_{st} | static pressure of air |
| P_t | total pressure of air |
| P_{WATER} | spray system water pressure |
| P_{WS} | wall static air pressure |
| Q | freestream dynamic pressure |
| q | velocity head experienced by a droplet in the flow field, Equation (D-2) |
| R | reflectivity |
| Re_{∞} | free stream Reynolds number with respect to droplet diameter |
| Re_v | Reynolds number of air flow relative to droplet |

| | |
|-------------------|--|
| s | distance along surface from point of reference |
| s_m | distance along surface from point of reference to impingement limit (p), Figure 2.2 |
| TAS | True Air Speed |
| T_{st} | static air temperature |
| T_t | total air temperature |
| t | time, dimensionless with L/V_∞ |
| \bar{t} | time |
| U | droplet velocity, dimensionless with V_∞ |
| \bar{U} | droplet velocity |
| V | potential flow velocity dimensionless with V_∞ |
| \bar{V}_{inlet} | air velocity at inlet plane |
| V_1 | photodetector voltage output (reflected beam) |
| V_2 | photodetector voltage output (optical feedback) |
| V_∞ | freestream airspeed |
| \bar{V}_∞ | freestream air velocity |
| W | engine inlet mass flow |
| \bar{w}_β | weighted local impingement rate |
| w_t | total liquid water content of droplet cloud |
| X | thickness of specimen, Equation (5-3) |
| x, r, θ | cylindrical coordinates |
| x, y, z | Cartesian coordinates |
| y_∞ | ordinate of coordinate system perpendicular to freestream velocity direction at $x = -\infty$, Figure 2.3 |
| $y_{\infty, m}$ | y_∞ corresponding to tangent trajectory, Figure 2.3 |
| α | angle of attack |
| β | local impingement efficiency for uniform droplets distribution |
| $\bar{\beta}$ | local impingement efficiency for clouds with non-uniform droplet size, Equation (2-4, 2-5) |
| γ | ratio of specific heats of air = 1.4 |
| ΔP_{sv} | static pressure difference, Figure 3.7 |
| $\delta_{i,j}$ | Kronecker delta |
| θ | central angle of cylinder measured from x-axis |
| θ_m | θ for tangent trajectory |
| λ | true range of droplet as projectile injected into still air |
| λ_s | range of droplet as projectile following Stoke's law |
| μ | absolute air viscosity |
| ρ | density of air |
| ρ_P | particle (droplet) density |
| ρ | density of water |
| σ | density ratio |

REFERENCES

1. Kim, J.J., "Particle Trajectory Computation on a 3-Dimensional Engine Inlet", NASA Contractor Report 175023, DOD-FAA-CT-86-1, Prepared for NASA/Lewis Research Center under Grant NAG 3-566, January 1986.
2. Norment H.J., "Calculation of Water Drop Trajectories to and About Arbitrary Three-Dimensional Bodies in Potential Airflow," NASA CR-3291, 1980.
3. Bragg, M.B. and Gregorek, G.M., "An Analytical Approach to Airfoil Icing", paper no. AIAA-81-0403, AIAA 19th Aerospace Sciences Meeting, St. Louis, Mo., January 12-15, 1981.
4. Breer, M.D. and Seibel, W., "Particle Trajectory Computer Program - User Manual", Boeing Document D3-9655-1, December 1974.
5. Stock, H.W., "Water Droplet Trajectory Computation Around an Air Intake," Zeitschrift fur Flugwissenschaften und Weltraumforschung, Band 8, Heft 3, pp. 200-208, 1984.
6. Von Glahn, U., Gelder, T.F., and Smyers, W.H. Jr., "A Dye Tracer Technique for Experimentally Obtaining Impingement Characteristics of Arbitrary Bodies and a Method for Determining Droplet Size Distribution," NACA TN 3338, March 1955.
7. Gelder, T.P., Smyers, W.H. Jr., and von Glahn, U., "Experimental Droplet Impingement on Several 2-dimensional Airfoils with Thickness Ratios of 6 to 16 Percent," NACA TN 3839, December 1956.
8. Lewis, J.P. and Ruggeri, R.S., "Experimental Droplet Impingement on Four Bodies of Revolution," NACA TN 4092, December 1957.
9. Gelder, T.F., "Droplet Impingement and Ingestion by Supersonic Nose Inlet in Subsonic Tunnel Conditions," NACA TN 4268, May 1958.
10. Papadakis, M., Elangovan, R., Freund Jr., G.A., Breer, M.D., Zumwalt, G.W., and Whitmer, L., "An Experimental Method for Measuring Water Droplet Impingement Efficiency on Two- and Three-Dimensional Bodies," NASA Contractor Report 4257, DOT/FAA/CT-87/22, Prepared for NASA-Lewis Research Center under Grant NAG-3-566, November, 1989.
11. Federal Aviation Regulation Part 25, Appendix C, 1974.
12. Langmuir, I and Blodgett, K.B., "A Mathematical Investigation of Water Droplet Trajectories", Army Air Forces Technical Report No. 5418, 1946.
13. McGhee, R.J., Viken, J.K., Pfenninger, W., Beasley, W.D., and Harvey, W.D., "Experimental Results For a Flapped Natural-Laminar-Flow Airfoil", NASA TM 85788, 1984.

14. McGhee, R.J., and Beasley, W.D., "Low-Speed Aerodynamic Characteristics of a 17-Percent-Thick Medium-Speed Airfoil Designed for General Aviation Application", NASA TP 1786, 1980.
15. Breer, M.D., Seibel, W., and Lewis-Smith, F.A., "Potential Flow and Data Preparation Programs, Users Manual," Boeing Document D3-982 1, July 1976.
16. Gibson, S.G., "User's Manual for MASTER: Modeling of Aerodynamic Surfaces by Three-Dimensional Explicit Representation," Boeing Document D6-51088, January 1983.
17. Reyhner, T.A., "Program P582 Transonic Potential Flow about Complex 3-dimensional Configurations," Boeing Coordination Sheet Prop-B8411-C86-022, July, 1986.
18. Schmidt, W.F., "Water Droplet Impingement Prediction for Engine Inlets by Trajectory Analysis in a Potential Flow Field," Boeing Document D3-6961, Final Report, 1965.

REPORT DOCUMENTATION PAGEForm Approved
OMB No. 0704-0188

Public reporting burden for this collection of information is estimated to average 1 hour per response, including the time for reviewing instructions, searching existing data sources, gathering and maintaining the data needed, and completing and reviewing the collection of information. Send comments regarding this burden estimate or any other aspect of this collection of information, including suggestions for reducing this burden, to Washington Headquarters Services, Directorate for Information Operations and Reports, 1215 Jefferson Davis Highway, Suite 1204, Arlington, VA 22202-4302, and to the Office of Management and Budget, Paperwork Reduction Project (0704-0188), Washington, DC 20503.

| | | | | |
|---|---|--|---|--|
| 1. AGENCY USE ONLY (Leave blank) | | 2. REPORT DATE December 1994 | 3. REPORT TYPE AND DATES COVERED Final Contractor Report | |
| 4. TITLE AND SUBTITLE Experimental Water Droplet Impingement Data on Airfoils, Simulated Ice Shapes, an Engine Inlet and a Finite Wing | | | 5. FUNDING NUMBERS WU-505-68-11 G-NAG3-566 | |
| 6. AUTHOR(S) M. Papadakis, M. Breer, N. Craig, and X. Liu | | | | |
| 7. PERFORMING ORGANIZATION NAME(S) AND ADDRESS(ES) Wichita State University Aerospace Engineering Department Wichita, Kansas 67260-0044 | | | 8. PERFORMING ORGANIZATION REPORT NUMBER E-9254 | |
| 9. SPONSORING/MONITORING AGENCY NAME(S) AND ADDRESS(ES) National Aeronautics and Space Administration Lewis Research Center Cleveland, Ohio 44135-3191 and Federal Aviation Administration, Technical Center Atlantic City International Airport, New Jersey 08405 | | | 10. SPONSORING/MONITORING AGENCY REPORT NUMBER NASA CR-4636 DOT/FAA/CT-TN93/18 | |
| 11. SUPPLEMENTARY NOTES Prepared under Interagency Agreement DTFA-03-81-A-00209 with the FAA Technical Center. M. Papadakis and X. Liu, Wichita State University, Wichita, Kansas 67260-0044 (work funded by NASA Grant NAG3-566); M. Breer and N. Craig, Boeing Military Airplanes, Wichita, Kansas. Project Managers, Colin S. Bidwell and Robert J. Shaw, Turbomachinery and Propulsion Systems Division, organization code RTI, 216-433-3947; and James T. Riley, Federal Aviation Administration, Technical Center, 609-485-4144. | | | | |
| 12a. DISTRIBUTION/AVAILABILITY STATEMENT Document Availability Change Notice This document was published in December 1994 with a restriction. It was changed March 2005 to Unclassified/Unlimited per DAA modified March 30, 2005. RESTRICTED DISTRIBUTION DOCUMENT Distribution limited to U.S. Government agencies and U.S. Government agency contractors only. Unclassified - Unlimited Subject Category 03 Available electronically at http://gltrs.grc.nasa.gov This publication is available from the NASA Center for Aerospace Information, (301) 621-0390. | | | 12b. DISTRIBUTION CODE | |
| 13. ABSTRACT (Maximum 200 words) An experimental method has been developed to determine the water droplet impingement characteristics on two- and three-dimensional aircraft surfaces. The experimental water droplet impingement data are used to validate particle trajectory analysis codes that are used in aircraft icing analyses and engine inlet particle separator analyses. The aircraft surface is covered with thin strips of blotter paper in areas of interest. The surface is then exposed to an airstream that contains a dyed-water spray cloud. The water droplet impingement data are extracted from the dyed blotter paper strips by measuring the optical reflectance of each strip with an automated reflectometer. Experimental impingement efficiency data are presented for an NLF (1)-0414 airfoil, a swept MS (1)-0317 airfoil, a Boeing 737-300 engine inlet model, two simulated ice shapes and a swept NACA 0012 wingtip. Analytical impingement efficiency data are also presented for the NLF (1)-0414 airfoil and the Boeing 737-300 engine inlet model. | | | | |
| 14. SUBJECT TERMS Trajectory code validation; Water droplet trajectories; Impingement characteristics; Impingement data; Experimental impingement data; Trajectory codes | | | 15. NUMBER OF PAGES 179 | |
| | | | 16. PRICE CODE | |
| 17. SECURITY CLASSIFICATION OF REPORT Unclassified | 18. SECURITY CLASSIFICATION OF THIS PAGE Unclassified | 19. SECURITY CLASSIFICATION OF ABSTRACT Unclassified | 20. LIMITATION OF ABSTRACT | |